Report No. 84
DOE/ET/53016-75
UC-20f9

Columbia University
in the City of New York

A NUMERICAL STUDY OF THE COLUMBIA HIGH-BETA DEVICE: TORUS-II

Ralph Izzo

1981

Research Supported by an NSF Fellowship
and DOE Contract DE-AS02-76ET-53016

Plasma Physics Laboratory
School of Engineering and Applied Science
Columbia University
New York, N.Y. 10027

DISCLAIMER

DOE/ET/53016--75

DE82 007363

Report No. 84
DOE/ET/53016-75
UC-20f
g

A NUMERICAL STUDY OF THE COLUMBIA HIGH BETA DEVICE: TORUS-II

Ralph Izzo

1981

Research Supported by an NSF Fellowship
and DOE Contract DE-AS02-76ET-53016

Plasma Physics Laboratory

School of Engineering and Applied Science

Columbia University

New York, N.Y. 10027

Report No. 84
DOE/ET/53016-75
UC-20f

A NUMERICAL STUDY OF THE COLUMBIA HIGH BETA DEVICE: TORUS-II

Ralph Izzo

Submitted in partial fulfillment of the

requirements for the degree

of Doctor of Philosophy

in the Faculty of Pure Science

COLUMBIA UNIVERSITY

1981

ABSTRACT

A NUMERICAL STUDY OF THE COLUMBIA HIGH BETA DEVICE:TORUS-II

Ralph Izzo

The ionization, heating and subsequent long-time-scale behavior of the helium plasma in the Columbia fusion device, Torus-II, is studied. The purpose of this work is to perform numerical simulations while maintaining a high level of interaction with experimentalists.

The device is operated as a toroidal z-pinch to prepare the gas for heating. This ionization of helium is studied using a zero-dimensional, two-fluid code. It is essentially an energy balance calculation that follows the development of the various charge states of the helium and any impurities (primarily silicon and oxygen) that are present. The code is an atomic physics model of Torus-II. In addition to ionization, we include three-body and radiative recombination processes.

The plasma is heated by turbulent poloidal skin currents, induced by a fast reversal of the toroidal magnetic field which converts the toroidal z-pinch into a high beta tokamak. The heating dynamics are simulated by solving single-fluid resistive magnetohydrodynamic equations numerically in one- and two-dimensions. Inertia terms are kept to capture the fast-time-scale plasma dynamics. The equations are driven by prescribed boundary conditions for the poloidal flux and

current functions. Since the plasma containment vessel is a non-conductor, specification of poloidal flux on the boundary is difficult. Inductance codes are used to describe the flux distribution realistically.[36]

Using heating results as initial conditions, a one-dimensional MHD diffusion code, complete with resistivity, thermal conductivity, and radiation losses, is used to simulate the high beta phase.[37]

The zero-dimensional code contains more than ionization and recombination modeling. We also include bremsstrahlung and line radiation, ohmic heating of electrons, wave heating of ions, electron-ion energy transfer and other effects. Therefore, the code is useful in linking the above MHD computations.[38]

We present results for charge state evolution of all species, as well as, ion and electron temperatures during the z-pinch phase. For the heating phase, profiles of currents, magnetic fields, density, temperature, plasma beta, and safety factor, q, have been obtained. We also identify maximum impurity levels for successful operation as a high beta tokamak.

We conclude that Torus-II is an excellent vehicle for high beta research. Some problems associated with the device and how they may be corrected to allow for better operation are discussed.

ACKNOWLEDGEMENTS

The nature of this dissertation was such as to require a group effort throughout. For this reason, the list of people to thank is long, but each has played a significant role in the work.

My sincerest and warmest gratitude is extended to my advisor, Prof. C.K. Chu. His scientific expertise requires no further acknowledgement. Here I wish to bring attention to his special talents of understanding and guidance through the sometimes painful periods of growth that accompany independent research; for this I will always be grateful.

A very special thank you to Gordon Erlebacher for his indispensable help in all phases of the research; for the many lunch-time conversations ranging from variational methods in plasma physics to winter skiing escapades. But most of all, for beginning with me, what promises to be a truly great friendship.

To the entire Torus-II experimental group. Especially, Prof. G.A. Navratil for hours of discussion in the lab, his office, or anywhere else I could annoy him. To Prof. T.C. Marshall for excellent advice on how to model the plasma. To Prof. R.A. Gross for constant moral support.

To Aaron Auslander, Edl Schamiloglou and David Elkin, for their friendship and making the time spent at Columbia more pleasant. Also, thank you to David for doing most of the EFFI work.

Two dear friends can not go without mention. Thank you, to Karen Danowski, for her love and the patience that has come with it; for sharing the many triumphs and disasters that accompanied the research. To Joseph Brudno, a very special type of teacher who has helped me to understand a little better what life is about. I thank these two people for teaching me a kind of caring rarely seen, by the best of all possible methods, by example.

I extend the simplest but most meaningful "thank you" to my father, mother, sister and brother, for their support throughout my educational career, I dedicate this work to them.

TABLE OF CONTENTS

I. INTRODUCTION

The economic feasibility of fusion energy is greatly enhanced by increasing the ratio of plasma pressure to magnetic field pressure. This ratio is the plasma parameter, β . A common definition for average beta is

$$\langle\beta\rangle \equiv \frac{\langle P \rangle}{\{ B_{\Phi o}^2/8\pi \}}^{1}$$

where $\langle P \rangle$ is the volume averaged thermodynamic pressure and $B_{\Phi o}$ is the vacuum toroidal magnetic field at the geometric center of the plasma.

High beta values are desirable for two principal reasons.[2] First, a higher beta due to large thermodynamic pressure results in a higher fusion energy density. Secondly, small magnetic fields are cheaper to produce than large fields. Thus, a strong emphasis has been placed on the need to increase beta to the limits imposed by stability considerations. It was thought that the beta of tokamak devices was limited by a critical value, above which plasma pressure driven ballooning modes appear. Recent numerical[3] and analytical work[4] indicate that a second critical beta exists above which the plasma is again stable. The result has been increased interest in high beta research.

Several methods can be used to produce high beta plasmas. Researchers at Columbia employ a pinch technique with a unique heating scheme[5] to generate such plasmas. The device is known as Torus-II. It is particularly well suited for research into the proposed

second stability regime. Torus-II is basically a belt pinch geometry with large poloidal ohmic heating currents. The major radius is 22.5 cm. The height to width ratio is 25.4 cm. to 12.6 cm. Its operation is described in four separate stages. (See Figure I.1) For completeness we give a brief description of each phase of operation and some general comments on how the phases are simulated.

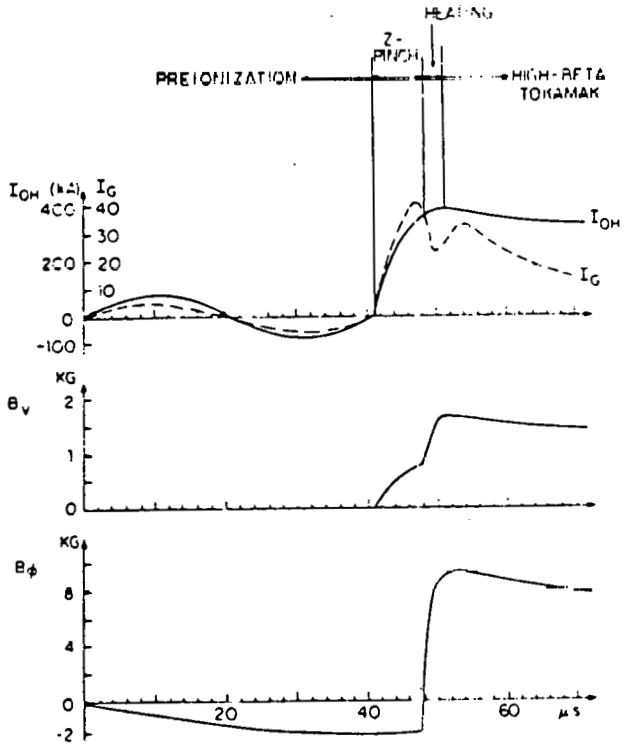

Figure I.1. Applied fields and currents in Torus-II. I_{oh} is the ohmic heating coil current for pre-ionization and z-pinch. B_v is the vertical magnetic field. B_ϕ is the toroidal (bias and maximum heating) field. Experimental toroidal gas current is I_G.

The primary objective of this research has been to use existing codes and also new codes to obtain a clear and comprehensive picture of the operation of Torus-II. We draw from different areas

of physics to achieve our desired result. These areas are MHD theory, electromagnetic theory and atomic physics. Figure I.2 illustrates the experimental phases and the key phenomena occuring at that time. Also depicted is the manner in which numerical calculations are used to help understand and explain these phenomena.

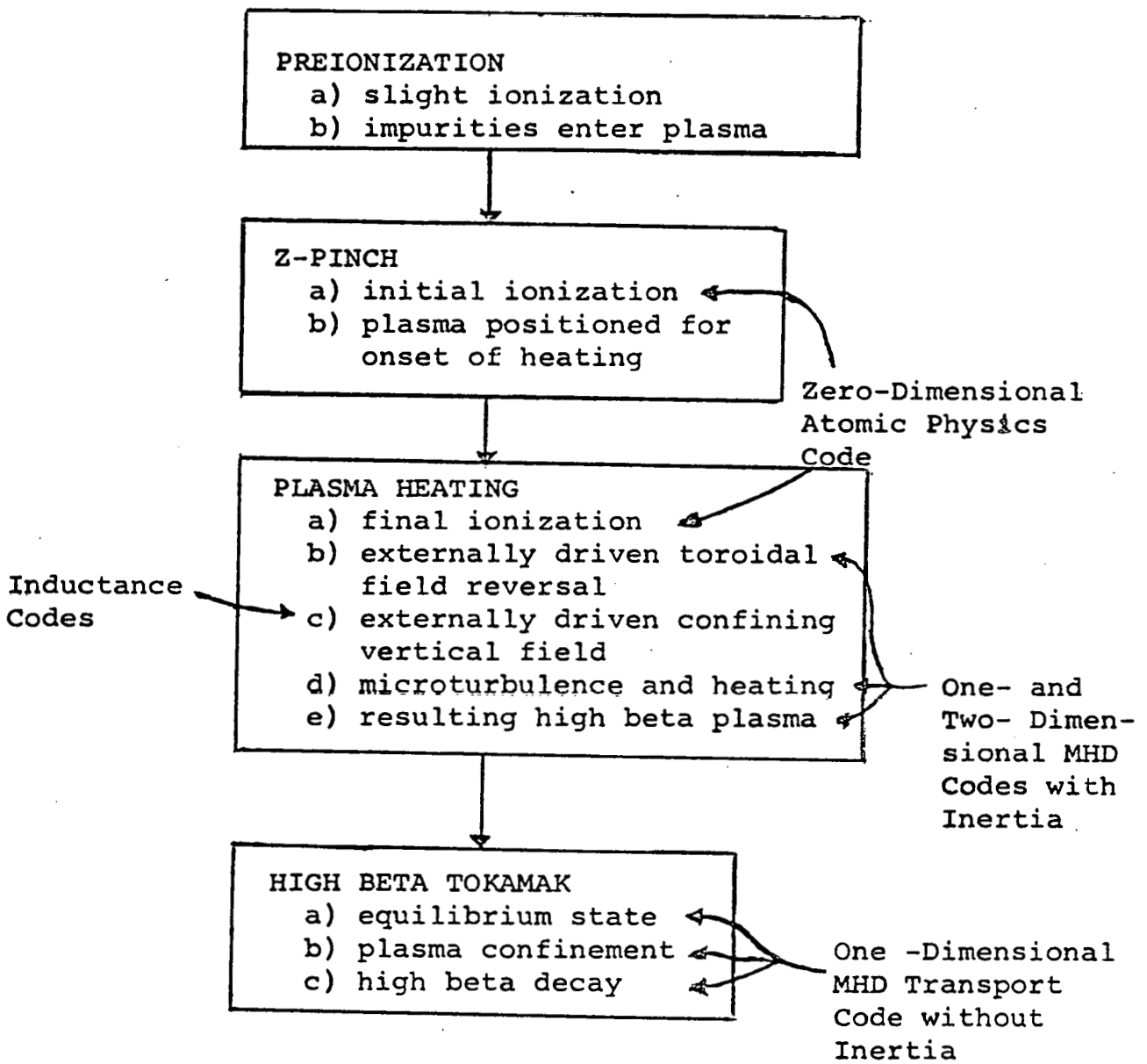

Figure I.2. Flow chart depicting interfacing of numerical simulations and Torus-II experiment.

This is the chief objective of the research. Emphasis is placed on constant interaction with experimentalists. We are simulating an active device with the intention of interpreting experimental results already obtained and guiding future efforts to produce desirable high beta plasmas.

Experimentally, during the pre-ionization phase a sinusoidal current form with amplitude on the order of 50 ka. is driven through the inner toroidal coils (referred to as ohmic heating coils in Figure I.3). The helium gas is heated to initiate the ionization. No

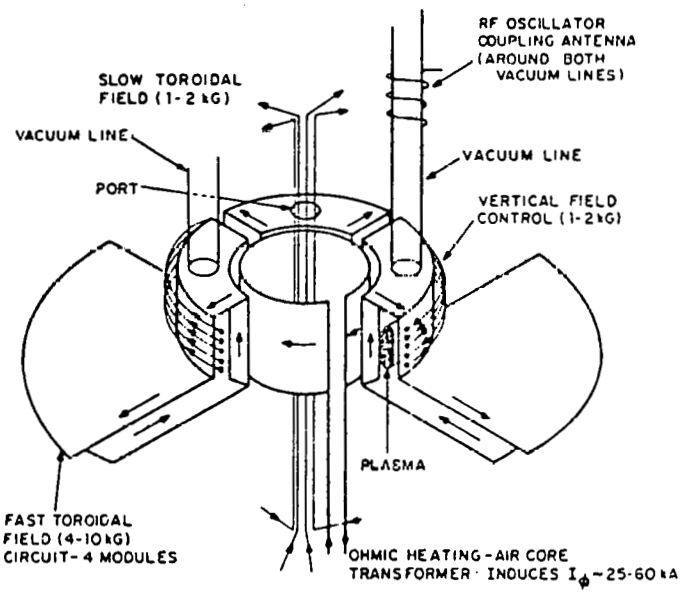

Figure I.3. General description of Torus-II. Arrows indicate direction of current flow in external conductors.

current is programmed in the outer toroidal coils (referred to as the vertical field coils) at this time, thus no vertical field is present and the gas bounces off the vacuum vessel wall. This has

the important adverse effect of polluting the plasma. A toroidal bias field ($\simeq$ 1 kG) is embedded in the plasma. We do not simulate this phase, however, it is important to note that most of the impurities enter the plasma region at this time.

The z-pinch phase continues the ionization process while positioning the plasma. Currents are programmed in both sets of toroidal coils thereby setting up a vertical field to keep the plasma away from the chamber walls. The external currents are $\sim$ 100 ka. during this phase. The net resulting vacuum vertical field is $\sim$ 600-800 G. Recent experimental work indicates there is a strongly non-uniform vacuum vertical field profile.[6] This is contrary to earlier theoretical predictions of a uniform B_{vt} profile[7]. Experimentalists report a post-z-pinch plasma temperature of $\sim$5 eV with a peak electron density of $\sim 3 \times 10^{14}$ cm^{-3}. The toroidal plasma current is $\sim$40 ka. The ionization of helium is not complete.

The z-pinch is simulated using a zero-dimensional code. It is essentially a two fluid, energy balance calculation complete with the atomic physics that dominates this phase. The ionization of the main gas (helium) and impurities (oxygen and silicon) is calculated by coupling species equations with electron and ion energy equations. Effects due to line radiation, recombination, bremsstrahlung, ohmic heating, energy confinement, electron-ion equilibration and other phenomena are also simulated. The results of the computation are in excellent agreement with available experimental data.

The phase of greatest importance is the heating phase, during which the most interesting physics takes place. There are two

heating modes in Torus-II, parallel and anti-parallel. In both cases the toroidal field is ramped from its initial bias value to its final value in 1.7 μsec. For the parallel case, a positive bias field is increased to a larger positive value. For anti-parallel heating, a negative bias field is reversed. The final toroidal field is 4-10 kG. The original design philosophy[8] was to use the rapid field reversal to generate large poloidal electric fields ($\lesssim$ 1 kV/cm). This leads to microturbulence and an anomalously high resistivity. The result is enhanced ohmic heating of the electrons. The ions are heated through scattering with ion-acoustic waves thereby obtaining some of the wave energy. Experimental evidence indicates that this is indeed the heating mechanism for Torus-II. These results are presented in (9). The rapid heating scheme generates a high beta plasma ($\langle\beta\rangle \simeq 10\%$) which is greatly elongated ($\sim$4-5:1).

The major portion of this work is devoted to the simulation of the heating phase. Several different codes are used. The heart and soul of the calculation is performed using a two-dimensional, single fluid, dissipative MHD code. Inertial terms are included to capture all fast time scale effects. Additional details of the calculation are given later. The basic idea is to specify boundary conditions for poloidal magnetic flux and toroidal field which accurately represent the effects of externally driven currents on the actual device. The boundary conditions are responsible for forming the post-heating plasma configuration. The spatial dependence of the poloidal flux along the boundary is not a simple problem to

solve since the vessel is a non-conducting shell (pyrex). We determine the realistic boundary conditions with inductance codes. Essentially, the plasma is modeled as a toroidal current carrying conductor. With knowledge of the total plasma current and externally applied currents we calculate the poloidal field and flux profiles. This information is fed into the heating code as a boundary condition. Using the value for plasma current obtained in the heating calculation we again run the inductance codes to generate a corrected value of the boundary condition. The iterations are continued until the plasma current used in the inductance calculation agrees with that value resulting from the MHD heating simulation. In this manner, the geometry of the device is accurately modeled.

Precise modeling of transport physics is also important for accurate simulation of the experiment. A one-dimensional, single fluid, dissipative MHD code with inertial terms included is used to study different regimes of parameter space. The one-dimensional code requires much less computing time than the two-dimensional code and is therefore the logical choice for extensive numerical experiments. The key plasma parameters are electrical conductivity, thermal conductivity and low density behavior. Testing of different numerical schemes is also much more easily accomplished with the 1-D code.

Finally, the zero-dimensional code is also applied to the heating phase so as to gauge the dominant atomic processes during this stage. A trade-off is made between complex physics modeling and

complex geometric effects in the simulations. Detailed energy studies are performed in the zero-dimensional code loaded with atomic physics. Detailed transport studies are performed in one-dimensional MHD codes. Detailed external-coil-geometry effects are studied using two-dimensional MHD and inductance codes.

The result of heating is the high beta tokamak state. At this time all external currents are crowbarred. Experimental results vary depending on the plasma set-up phase. A dirty plasma quickly ($\sim$10 μsec) cools. A warm plasma (100 eV) has been maintained for as long as 30 μsec. There is experimental evidence of an axially shrinking plasma throughout this phase. Recent work indicates possible poloidal rotations of the plasma.

A one-dimensional, single fluid, resistive MHD code without inertia terms is used to simulate the high beta tokamak phase. The code includes radiative losses and more sophisticated modeling of the thermal and electrical conductivities. Plasma evolution in time is followed through successive equilibria thereby allowing for efficient, inexpensive, long-time-scale simulations. Post-heating phase plasma conditions are used as initial conditions. The plasma is no longer driven by prescribed boundary conditions at this time. Rather, the physics of the transport and loss parameters respond to the specified initial conditions to yield the decay of the high beta state and the eventual loss of plasma confinement. This portion of the overall simulation has been extremely important in obtaining operating limits due to radiative losses. Maximum tolerable

impurity levels for different high beta cases are calculated. The code has been written so as to be easily adaptable to different post-heating phase plasma states.

The time dependent zero-dimensional calculation has again proved useful as a check on the plasma temperature versus time behavior during the high beta tokamak phase of the device.

The format for the remainder of the thesis is as follows. In chapter II, we derive the equations that make up the mathematical model. No reference is made to Torus-II since the equations are general. We sketch the derivation of the two-dimensional start-up equations since it has been given in detail elsewhere.[10] The complete one-dimensional transport equations are developed as well as the derivation of the inductance equations and the atomic physics relations.

In chapter III, we discuss the numerical methods used in each code. Here we return to the specifics of Torus-II when discussing the types of modifications made on the general model described in chapter II. We also discuss how each code is run, what information is extracted from it and how this couples with other phases of the simulation.

The results of the Torus-II simulation are presented in chapter IV. An overview of the plasma state and device operation is given. Its significance for high beta research is also discussed.

For completeness, a listing of each code has been included in the appendix.

II. MATHEMATICAL MODEL

1.A) One- and Two-Dimensional MHD Equations With Inertia

For completeness we present the equations* of magnetohydrodynamics for a single fluid with finite electrical and thermal conductivity. In vector form, the continuity equation is

$$\frac{\partial \rho}{\partial t} + \nabla\cdot(\rho \underline{v}) = 0 \qquad \text{II.1.1}$$

The momentum equation is

$$\rho \frac{D\underline{v}}{Dt} = -\nabla p + \frac{\underline{J} \times \underline{B}}{c} \qquad \text{II.1.2}$$

The energy equation is

$$\rho C_v \frac{DT}{Dt} = -p\nabla\cdot\underline{v} + \frac{\underline{J}\cdot\underline{J}}{\sigma} + \nabla\cdot\kappa\nabla T - P_r \qquad \text{II.1.3}$$

Faraday's law is

$$\frac{1}{c}\frac{\partial \underline{B}}{\partial t} = -\nabla \times \underline{E} \qquad \text{II.1.4}$$

Neglecting the displacement current as usual, Ampere's law is given by

$$\underline{J} = \frac{c}{4\pi} \nabla \times \underline{B} \qquad \text{II.1.5}$$

---

*All units are c.g.s-Gaussian unless otherwise specified.

For finite electrical conductivity, Ohm's law is

$$\underline{E} = \frac{\underline{J}}{\sigma} - \frac{\underline{v} \times \underline{B}}{c} \qquad \text{II.1.6}$$

The magnetic field is everywhere divergence free.

$$\nabla \cdot \underline{B} = 0 \qquad \text{II.1.7}$$

The above variables are: ρ = mass density

T = fluid temperature

$\underline{v}$ = fluid velocity

$\underline{J}$ = current density

$\underline{E}$ = electric field

$\underline{B}$ = magnetic field

C_v = specific heat at constant volume

σ = electrical conductivity

κ = thermal conductivity

p = thermodynamic pressure

c = speed of light in vacuum

P_r = radiated power loss term

$\frac{D}{Dt}$ = Stokes' derivative = $\frac{\partial}{\partial t} + (\underline{v} \cdot \nabla)$

The equations are written for the cylindrical coordinate system shown in Figure II.1, with axisymmetry about the z-axis (ϕ is an ignorable coordinate).

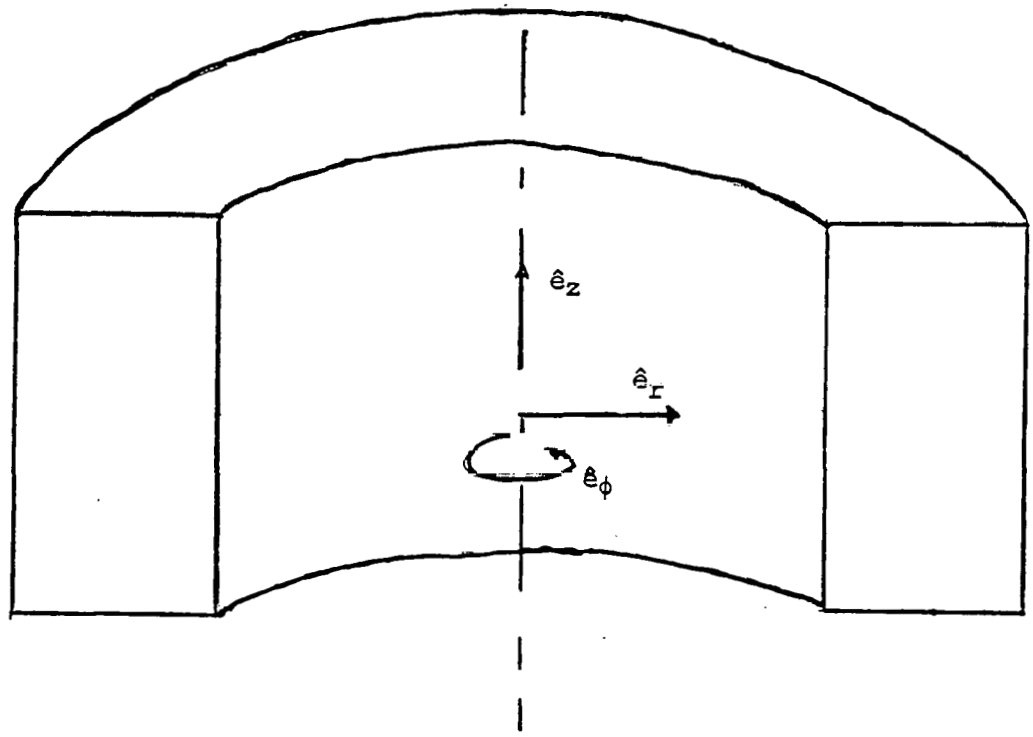

Figure II.1. Coordinate system for which the MHD equations are written.

Define the two functions $\Psi(r,z,t)$ and $\chi(r,z,t)$ such that

$$\underline{B} = -\frac{1}{r}\frac{\partial \Psi}{\partial z}\hat{e}_r + \frac{\chi}{r}\hat{e}_\phi + \frac{1}{r}\frac{\partial \Psi}{\partial r}\hat{e}_z \qquad \text{II.1.8}$$

We omit the details of the usual derivation, see for example (11). A brief sketch is given here. Clearly equation II.1.8 automatically satisfies II.1.7. This is one of the two reasons for specifying $\underline{B}$ as above. The other is the ease with which boundary conditions may be expressed in terms of Ψ and χ.

From Ampere's law we write $\underline{J}$ in terms of Ψ and χ. Substituting $\underline{J}$ into Ohm's law yields the electric field in terms of Ψ, χ and the fluid velocity, $\underline{v}$. This expression for $\underline{E}$ is then used in Faraday's law. Of the three resulting scalar equations, two are not

identical. They are the two governing equations for psi and xi.

$$\frac{D\Psi}{Dt} = \frac{c^2}{4\pi\sigma}\left(r\frac{\partial}{\partial r}\frac{1}{r}\frac{\partial \Psi}{\partial r} + \frac{\partial^2 \Psi}{\partial z^2}\right) \qquad \text{II.1.9}$$

$$\begin{aligned}\frac{\partial \chi}{\partial t} = \frac{c^2}{4\pi}\Bigg(&r\frac{\partial}{\partial r}\frac{1}{\sigma r}\frac{\partial \chi}{\partial r} + \frac{\partial}{\partial z}\frac{1}{\sigma}\frac{\partial \chi}{\partial z}\Bigg) \\ &-r\frac{\partial}{\partial r}\left(\frac{v_r \chi}{r} - \frac{1}{r}\frac{\partial \Psi}{\partial z}\right) \\ &+\frac{\partial}{\partial z}\left(v_\phi \frac{\partial \Psi}{\partial r} - v_z \chi\right)\end{aligned} \qquad \text{II.1.10}$$

Equations II.1.1-3,9,10 form a system of seven equations for the eight unknowns $\underline{v}$, ρ, T, Ψ, χ and p. To close the system, the ideal gas law is used as an equation of state.

$$p = \rho C_v (\gamma - 1) T \qquad \text{II.1.11}$$

where γ is the ratio of specific heats for the gas. Equations II.1.1-3,9-11 when coupled to a proper set of initial-boundary conditions completely determine the plasma state in two dimensions.

From this point it is trivial to derive the one-dimensional equations. Simply set $\frac{\partial}{\partial z} = 0$ in the above equations. We omit the details and present only the results.

$$\underline{B} = \frac{\chi}{r}\hat{e}_\phi + \frac{1}{r}\frac{\partial \Psi}{\partial r}\hat{e}_z \qquad \text{II.1.12}$$

$$\frac{\partial \Psi}{\partial t} + v_r \frac{\partial \Psi}{\partial r} = \frac{c^2}{4\pi\sigma} \left(r \frac{\partial}{\partial r} \frac{1}{r} \frac{\partial \Psi}{\partial r} \right) \qquad \text{II.1.13}$$

$$\frac{\partial \chi}{\partial t} + r \frac{\partial}{\partial r} \left(\frac{v_r \chi}{r} \right) = \frac{c^2}{4\pi} r \frac{\partial}{\partial r} \left(\frac{1}{\sigma r} \frac{\partial \chi}{\partial r} \right) \qquad \text{II.1.14}$$

$$\frac{\partial \rho}{\partial t} + \frac{1}{r} \frac{\partial}{\partial r} (\rho v_r r) = 0 \qquad \text{II.1.15}$$

$$\frac{\partial}{\partial t} (\rho v_r) + \frac{1}{r} \frac{\partial}{\partial r} (r\rho v_r^2 + (\gamma-1) r\rho C_v T) = \frac{C_v T(\gamma-1)}{r} + \frac{J_\phi B_z - J_z B_\phi}{c} \qquad \text{II.1.16}$$

$$\frac{\partial T}{\partial t} + v_r \frac{\partial T}{\partial r} + (\gamma-1) \frac{T}{r} \frac{\partial}{\partial r} (r v_r) = \frac{1}{\rho C_v r} \frac{\partial}{\partial r} \left(r\kappa \frac{\partial T}{\partial r} \right) + \frac{J_\phi^2 + J_z^2}{\rho\sigma C_v} - \frac{P_r}{\rho C_v} \qquad \text{II.1.17}$$

For the fluid formulation to be valid we must have

$$L \gg \lambda_d$$
$$\left| \frac{P}{\nabla P} \right| \gg r_g \qquad \text{II.1.18}$$

where L is a characteristic length of the plasma (typically on the same order as $p/\nabla p$), λ_d is the Debye length of the plasma and r_g is the Larmor radius of the particle.

1.B) Initial and Boundary Conditions for the MHD Equations With Inertia

The equations form a parabolic system although the continuity and momentum equations look formally hyperbolic. A complete discussion of appropriate initial and boundary conditions is given in (10,11). Briefly, initial values of ρ, T, Ψ, χ and $\underline{v}$ are needed everywhere. Boundary values of Ψ, χ, T and one component of velocity are needed.

It is easy to show that the functions Ψ and χ have physical meaning. In particular, Ψ is related to the poloidal flux and χ to the total poloidal current. Following (11) we state

$$\Psi = \frac{\text{poloidal flux}}{2\pi}$$

$$\chi = \frac{2 \times I_z}{c}$$

Therefore, it is important that the boundary values prescribed for Ψ and χ accurately represent the effects of the currents both external to and inside the plasma. Our approach for specifying these conditions is more careful and realistic than earlier studies since the previous work was related to experimental design while we are concerned with an experimental simulation. Two complementary inductance calculations are performed making use of elementary circuit theory and electromagnetic theory.

1.B.i) Coils[12] and EFFI[13]

The problem to be solved is as follows. Given a set of toroidal current carrying conductors with known total current, calculate the magnetic field everywhere in the poloidal plane. The solution is carried out in two parts. First we obtain the current distribution within the conductors (Coils) and then solve for $\underline{B}$ (EFFI). Consider the geometry in Figure II.2.A. Suppose the total current in each of the conductors is known and given as I_1, I_2 and I_3. To calculate how the currents are distributed we proceed as follows. (Note: In the general case this may seem to be an exercise of little interest, however, our ultimate goal is to calculate poloidal flux along the boundary of a toroidal fusion device. Such boundaries are always close to external current windings. Thus, the current distribution can be important.) Break each conductor into many smaller conductors choosing the shape of the smaller conductor to match the larger one. See Fiqure II.2.B. Conductor 1 is broken into M smaller conductors, 2 into N-M and 3 into K-N. The choice of N, M and K depends upon the desired accuracy of the current distribution. For each conductor

$$I_1 = \sum_{1}^{M} I_j \qquad \text{II.1.19}$$

$$I_2 = \sum_{M+1}^{N} I_j \qquad \text{II.1.20}$$

$$I_3 = \sum_{N+1}^{K} I_j \qquad \text{II.1.21}$$

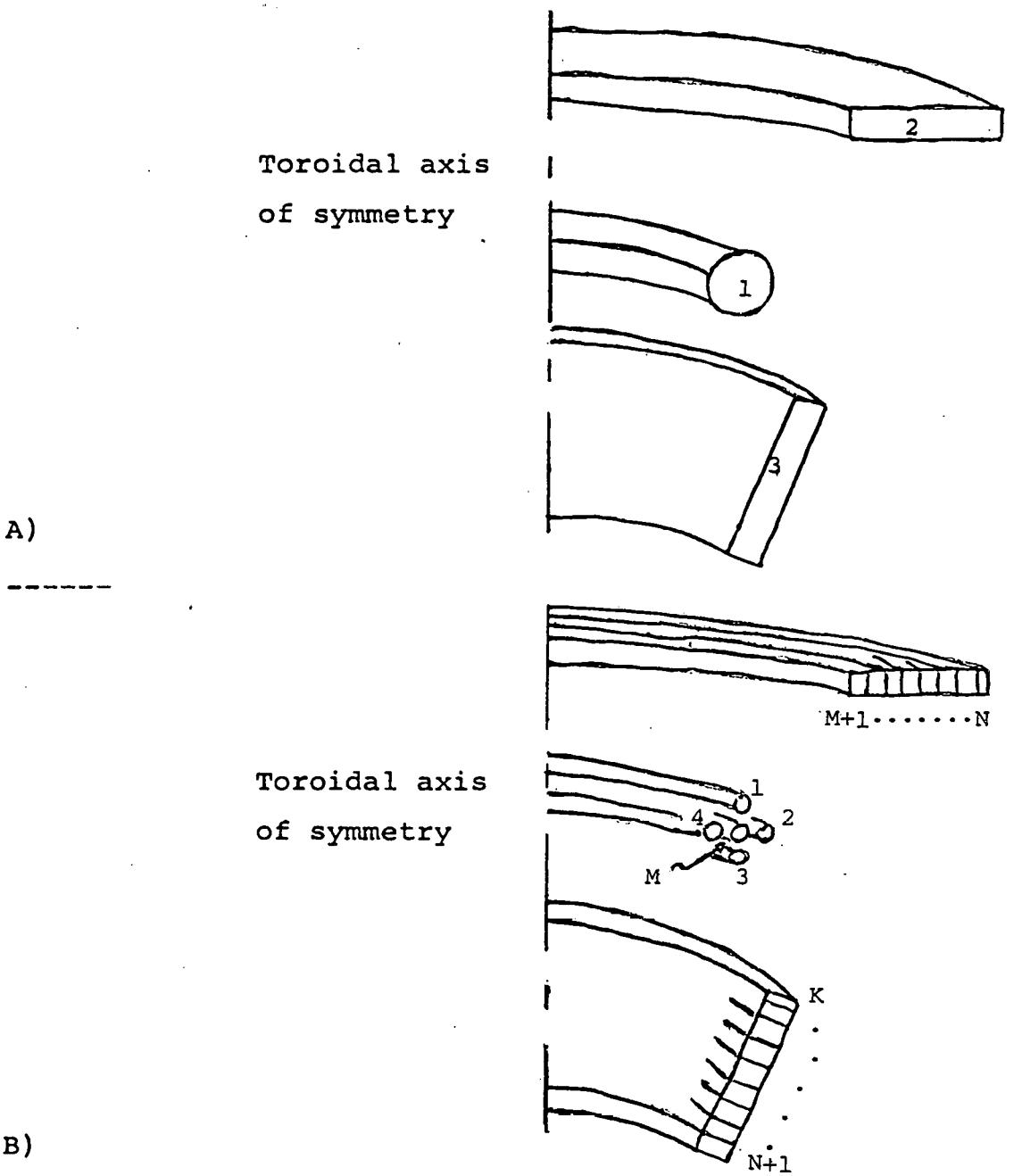

Figure II.2 A) Three toroidal current windings of arbitrary poloidal cross-section.
B) Filament-splitting model of same three conductors.

The flux enclosed by any one of the smaller current loops is

$$\Phi_j = \sum_{1}^{K} L_{js} I_s$$

$$j=1.2,..K \qquad \text{II.1.22}$$

where L_{js} is the mutual inductance of loops j and s. For the case j=s we have a self inductance. To this point we have 2K unknowns (Φ_j, I_j j=1,...K) and only K+3 equations. The following constraint is imposed on the system. Each of the original conductors 1, 2, 3, must be a flux surface. This is only rigorously true if $\underline{J} = 0$ inside the conductor, i.e. perfect conductors. Thus,

$$\Phi_1 = \Phi_j \quad j=1,2,..M \qquad \text{II.1.23}$$

$$\Phi_2 = \Phi_j \quad j=M+1,..N \qquad \text{II.1.24}$$

$$\Phi_3 = \Phi_j \quad j=N+1,..K \qquad \text{II.1.25}$$

where Φ_1, Φ_2, Φ_3 are three additional unknowns. The above constraint generates K new equations. It is easy to extrapolate the above for a system of C large conductors each with a known total current. A system of (K+C) equations is produced by breaking the C large conductors into K smaller conductors. The equations are solved for the K (I_j: j=1,2...K) plus C (Φ_j: j=1,...C) unknowns, thereby obtain-

ing the current distribution to the desired accuracy. The code that performs this calculation is referred to as Coils. Next, consider the second half of the problem. Given the current distribution, compute the magnetic field everywhere. Basically, a volume integration of the Biot-Savart law generates the desired field pattern. The method is completely explained in (13). The code used, known as EFFI, calculates the vector potential and electromagnetic field for coil systems of arbitrary geometry. The coils are constructed from circular arcs and/or straight segments of rectangular cross sectional conductors. The code is also capable of calculating magnetic flux surfaces, magnetic force and inductance. A combination of analytical and numerical integration of the Biot-Savart law for a volume distribution of current is performed. In this manner, field values inside and outside the conductors are obtained. Thus, Coils and EFFI are instrumental in determining boundary values of poloidal flux to be used in the two-dimensional MHD start-up calculation.

2.A) One-Dimensional MHD Transport Equations[14]

The equations are identical to II.1.1-7 except that the momentum equation is simplified by dropping the inertial term.

$$\nabla p = \frac{\underline{J} \times \underline{B}}{c} \qquad \text{II.2.1}$$

The plasma motion is one of diffusion through states of successive

equilibria. The spirit of the calculation is as follows. March the equations for density, temperature and magnetic field forward in time such that II.2.1 is always true. The details of the derivation are given. First, we non-dimensionalize all variables such that a subscript "o" denotes a fixed reference value.

$$\tilde{\rho} = \frac{\rho}{\rho_o} \qquad \tilde{t} = \frac{t}{t_o} \qquad \tilde{r} = \frac{r}{r_o}$$

$$\tilde{u} = \frac{u}{(r_o/t_o)} \qquad \tilde{T} = \frac{T}{T_o} \qquad \tilde{\underline{B}} = \frac{\underline{B}}{B_o}$$

$$\tilde{p} = \frac{p}{\rho_o R T_o} \qquad \tilde{\underline{J}} = \frac{\underline{J}}{(B_o c/4\pi r_o)} \qquad \tilde{\underline{E}} = \frac{\underline{E}}{(B_o r_o/c t_o)}$$

$$\tilde{\kappa} = \frac{\kappa}{\kappa_o} \qquad \tilde{\sigma} = \frac{\sigma}{\sigma_o} \qquad \tilde{\nabla} = r_o \nabla$$

$$\tilde{P}_r = \frac{P_r}{(\rho_o C_v T_o/t_o)}$$

where R is the ideal gas constant and u is the radial component of velocity, previously written v_r. Substitution of the above variables into the continuity, momentum and energy equation yield (dropping the tilde notation)

$$\frac{\partial \rho}{\partial t} + \frac{1}{r}\frac{\partial}{\partial r}(\rho u r) = 0 \qquad \text{II.2.2}$$

$$(\underline{J} \times \underline{B})_r = C_1 \frac{\partial p}{\partial r}$$

$$C_1 = \frac{4\pi\rho_o R T_o}{B_o^2} \qquad \text{II.2.3}$$

$$\rho \frac{\partial T}{\partial t} + \rho u \frac{\partial T}{\partial r} = -C_2 p \frac{\partial u}{\partial r} + C_3 \frac{\underline{J}\cdot\underline{J}}{\sigma} + C_4 \nabla\cdot\kappa\nabla T - P_r$$

$$C_2 = \frac{R}{C_v} \; ; \quad C_3 = \frac{C_2}{C_1} \frac{c^2 t_o}{4\pi r_o^2 \sigma_o} \; ; \quad C_4 = \frac{C_2 \kappa_o t_o}{r_o^2 \rho_o C_v} \qquad \text{II.2.4}$$

Similar algebraic manipulations with Faraday's law, Ampere's law and Ohm's law yield

$$\frac{\partial \underline{B}}{\partial t} = -\nabla \times \underline{E} \qquad \text{II.2.5}$$

$$\underline{J} = \nabla \times \underline{B} \qquad \text{II.2.6}$$

$$\underline{E} = C_5 \frac{\underline{J}}{\sigma} - \underline{u} \times \underline{B}$$

$$C_5 = \left(\frac{c}{r_o}\right)^2 \frac{t_o}{4\pi\sigma_o} \qquad \text{II.2.7}$$

The ideal gas law simplifies to

$$p = \rho T \qquad \text{II.2.8}$$

Note the physical significance of the dimensionless constants. We can think of C_4 and C_5 as time scale ratios.

$$C_4 = \frac{R}{C_v} \frac{\kappa_o}{r_o^2 \rho_o R} t_o \equiv \frac{t_o}{\tau_h} \qquad \text{II.2.9}$$

where $$\tau_h = \frac{\rho_o C_v r_o^2}{\kappa_o}$$

is a thermal conduction time scale. Similarly,

$$C_5 \equiv \frac{t_o}{\tau_b} \qquad \text{II.2.10}$$

where $$\tau_b = \frac{4\pi\sigma_o r_o^2}{c^2}$$

is a field diffusion time scale.

The constant, C_1, can be written as the square of the ratio of the thermal speed to the Alfven speed.

$$C_1 = \left(\frac{(4\pi\rho_o)^{.5}}{Bo}\right)^2 ((RT)_o^{.5})^2 \qquad \text{II.2.11}$$

$$= \frac{v_{th}^2}{v_a^2}$$

The constant, C_2, is the ratio of thermal to internal energy.

$$C_2 = \frac{R}{C_v}\frac{T_o}{T_o} = \frac{v_{th}^2}{C_v T_o} \qquad \text{II.2.12}$$

Continuing with the derivation, combine II.2.5-7 to get

$$\frac{\partial \underline{B}}{\partial t} = \nabla \times (\underline{u} \times \underline{B}) - C_5 \nabla \times \{\frac{\nabla \times \underline{B}}{\sigma}\} \qquad \text{II.2.13}$$

Combining II.2.3 and II.2.6 with a well known vector identity yields

$$\nabla\{ C_1 p + \frac{B^2}{2}\} = (\underline{B}\cdot\nabla)\,\underline{B} \qquad \text{II.2.14}$$

For convenience, we collect our results to this point and present them in scalar form. The one-dimensional continuity equation is

$$\frac{\partial \rho}{\partial t} + \frac{1}{r}\frac{\partial}{\partial r}(\rho u r) = 0 \qquad \text{II.2.15}$$

The momentum equation is

$$\frac{\partial}{\partial r}\{C_1 p + \frac{B^2}{2}\} = -\frac{B_\phi^2}{r} \qquad \text{II.2.16}$$

The energy equation is

$$\frac{\partial T}{\partial t} + u\frac{\partial T}{\partial r} = \frac{C_2 T}{r}\frac{\partial}{\partial r}(ur) + C_3\frac{(J_\phi^2 + J_z^2)}{\rho\sigma} + \frac{C_4}{\rho r}\frac{\partial}{\partial r}(\kappa r \frac{\partial T}{\partial r}) - \frac{P_r}{\rho} \qquad \text{II.2.17}$$

The field equations have been combined to give

$$\frac{\partial B_\phi}{\partial t} = C_5 \frac{\partial}{\partial r}\left(\frac{1}{\sigma r} \frac{\partial}{\partial r}(rB_\phi) \right) - \frac{\partial}{\partial r}(uB_\phi) \qquad \text{II.2.18}$$

$$\frac{\partial B_z}{\partial t} = \frac{C_5}{r} \frac{\partial}{\partial r}\left(\frac{r}{\sigma} \frac{\partial B_z}{\partial r} \right) - \frac{1}{r} \frac{\partial}{\partial r}(uB_z r) \qquad \text{II.2.19}$$

The equations are not yet in their final form. By differentiating the momentum equation with respect to time and substituting the above expressions for $\frac{\partial \rho}{\partial t}$, $\frac{\partial T}{\partial t}$ and $\frac{\partial B}{\partial t}$ we will generate a single ordinary differential equation for the plasma velocity. We show only the first few steps of this procedure. Taking a time derivative of II.2.16 and using II.2.8 yields

$$C_1 \frac{\partial}{\partial r}\left(\rho \frac{\partial T}{\partial t} + T \frac{\partial \rho}{\partial t}\right) + \frac{\partial}{\partial r}\left(B_z \frac{\partial B_z}{\partial t} + B_\phi \frac{\partial B_\phi}{\partial t}\right) = -\frac{2B_\phi}{r} \frac{\partial B_\phi}{\partial t}$$

Substituting II.2.15,17,18 and 19 gives

$$C_1 \frac{\partial}{\partial r}\{Mu + Z \frac{\partial u}{\partial r} + N\} + \frac{\partial}{\partial r}\{B_z(-B_z \frac{\partial u}{\partial r} - \frac{u}{r} \frac{\partial}{\partial r}(rB_z) + S)$$

$$+ B_\phi(-B_\phi \frac{\partial u}{\partial r} - u \frac{\partial B_\phi}{\partial r} + Q)\}$$

$$= -\frac{2B_\phi}{r}\{-B_\phi \frac{\partial u}{\partial r} - u \frac{\partial B_\phi}{\partial r} + Q\} \qquad \text{II.2.20}$$

where

$$M \equiv -\frac{T}{r}\frac{\partial}{\partial r}(\rho r) - \rho\frac{\partial T}{\partial r} - \frac{\rho C_2 T}{r} \qquad \text{II.2.21}$$

$$N \equiv \frac{C_3}{\sigma}(J_\phi^2 + J_z^2) + \frac{C_4}{r}\frac{\partial}{\partial r}\left(\kappa r \frac{\partial T}{\partial r}\right) - P_r \qquad \text{II.2.22}$$

$$Z \equiv -(C_2 + 1)\, p \qquad \text{II.2.23}$$

$$Q \equiv C_5 \frac{\partial}{\partial r}\left(\frac{1}{\sigma r}\frac{\partial}{\partial r}(rB_\phi)\right) \qquad \text{II.2.24}$$

$$S \equiv \frac{C_5}{r}\frac{\partial}{\partial r}\left(\frac{r}{\sigma}\frac{\partial B_z}{\partial r}\right) \qquad \text{II.2.25}$$

Omitting several pages of algebraic manipulation we now write II.2.20 in its final form.

$$A\,\xi_{,rr} + B\,\xi_{,r} + D\,\xi + E = 0 \qquad \text{II.2.26}$$

where

$$\xi \equiv ur$$

$$A \equiv -C_1 Z + (B_\phi^2 + B_z^2) \qquad \text{II.2.27}$$

$$B \equiv \frac{\partial A}{\partial r} - \frac{A}{r} \qquad \text{II.2.28}$$

$$D \equiv -r \frac{\partial}{\partial r}(B_\phi/r)^2 \qquad \text{II.2.29}$$

$$E \equiv -r \{C_1 \frac{\partial N}{\partial r} + \frac{\partial}{\partial r}(SB_z)\} - \frac{1}{r}\frac{\partial}{\partial r}(B_\phi Q r^2) \qquad \text{II.2.30}$$

with N, Z, Q and S given by equations II.2.22-25 respectively.

2.B) Initial and Boundary Conditions for the One-Dimensional Transport Equations

Equations II.2.15, 17, 18, 19 and 26, when combined with proper initial and boundary values are solved for ρ, T, $\underline{B}$ and u for all time and space. The field and energy equations form a parabolic system. The continuity equation is formally hyperbolic while the momentum equation is an ordinary differential equation with a two point boundary condition. Initial values of ρ, T, and $\underline{B}$ are needed for all radial positions. Boundary values to be specified as functions of time are written for temperature (or $\frac{\partial T}{\partial r}$), magnetic field (or $\frac{\partial \underline{B}}{\partial r}$) and plasma velocity. Since the momentum equation does not contain inertial terms, there should be no need to prescribe the velocity on the boundary. However, in our derivation, a time derivative of the momentum equation is taken, thereby re-introducing the need for specification of u on the boundary.

The purpose of the calculation is to follow the plasma evolution after it has been heated. This is a long time scale problem in which plasma behavior is dictated by dissipative processes that respond to specified initial conditions. The plasma is no longer driven by external currents as in the start-up calculation. Therefore, boundary conditions play a passive role in the transport computation. Equation II.2.19 for the time evolution of B_z is rewritten for the case

$$B_z = \frac{1}{r}\frac{\partial \Psi}{\partial r}$$

where Ψ is the poloidal flux function described earlier. Substituting the above into II.2.19 yields

$$\frac{\partial \Psi}{\partial t} + \frac{\xi}{r}\frac{\partial \psi}{\partial r} - C_5 \frac{r}{\sigma}\frac{\partial}{\partial r}\left(\frac{1}{r}\frac{\partial \psi}{\partial r}\right) = 0$$

Physical arguments are then used to appropriately prescribe $\psi(t)$ on the boundary.

Since detailed spatially resolved experimental data is not always available, some assumptions must be made when specifying initial conditions. These assumptions are based on experimental data known with certainty. The physical arguments and assumptions made specifically for Torus-II are presented in chapter III section 2.

3.) Zero-Dimensional Atomic Physics Model[15]

This is primarily an atomic physics picture of the evolution of all ionic species while maintaining energy balance. The basic equations can be split into three groups. Firstly, there are species equations to be solved. These equations follow the ionization and recombination processes of the main filling gas and all impurity elements through all charge states. Secondly, we consider energy equations for two fluids, i.e. electrons and ions. Thirdly, ohmic heating power supplied into the plasma must be modeled. We forgo any detailed circuit modeling of externally programmed currents and the coupling to the plasma current. Instead, the plasma current is prescribed as a known function of time. Emphasis is placed on including all the necessary physics in the energy and species equations.

Consider first the species equations. Let n_x^z denote the number density of element x with a charge of z. The rate equation is

$$\frac{dn_x^z}{dt} = n_e \{n_x^{z-1} S_x^{z-1} - n_x^z (S_x^z + \alpha_x^z) + n_x^{z+1} \alpha_x^{z+1}\} \quad \text{II.3.1}$$

where n_e = electron number density (cm^{-3})

S_x^z = collisional ionization rate coefficient for atom x with a charge state of z (cm^3/sec)

α_x^z = total recombination rate coefficient for atom x with a charge state of z (cm^3/sec)

The ionization and recombination coefficients can be obtained from various sources.[16,17,18] While each source presents the same functional dependence of S_x^z and α_x^z on temperature and density, they each warn that no simple analytical formula is exact. For convenience, the formulation of (16) is used. The ionization coefficient is

$$S_x^z = \frac{10^{-5}(T_e/E_x^z)^{.5}}{(E_x^z)^{1.5}(6. + T_e/E_x^z)} \exp(-E_x^z/T_e) \qquad \text{II.3.2}$$

where T_e = electron temperature (eV)

E_x^z = the ionization energy required to produce charge state (z + 1) of atom x (eV)

The recombination rate coefficient includes both radiative recombination and three-body recombination.

$$\alpha_x^z = \alpha_{x,r}^z + n_e \alpha_{x,3}^z \qquad \text{II.3.3}$$

The radiative recombination rate coefficient is

$$\alpha_{x,r}^z = 5.2 \times 10^{-14} Z (E_x^z/T_e)^{.5}\{.43 + .5 \ln(E_x^z/T_e) + .469 (T_e/E_x^z)^{.33}\} \qquad \text{II.3.4}$$

The three-body recombination rate coefficient is

$$\alpha^{z}_{x,3} = 1.4 \times 10^{-3} \left(\frac{z+1}{z} \right)^{6} (E^{z}_{x}/T_e)^{2} \exp\left(\frac{E^{z}_{x}}{(z+2)^{2} T_e} \right) \qquad \text{II.3.5}$$

For an element of atomic number Z_x, we note that equation II.3.1 is only true for $z=1,..,(Z_x-1)$. The rate equation for the neutral species is

$$\frac{dn^{0}_{x}}{dt} = n_e \{-n^{0}_{x} S^{0}_{x} + n^{1}_{x} \alpha^{1}_{x}\} \qquad \text{II.3.6}$$

The rate equation for the Z_x charge state is

$$\frac{dn^{Z_x}_{x}}{dt} = n_e \{n^{Z_x-1}_{x} S^{Z_x-1}_{x} - n^{Z_x}_{x} \alpha^{Z_x}_{x}\} \qquad \text{II.3.7}$$

The equations as written, conserve the total number of particles for a given species, x. Consider any species, then the total number density of x is given by

$$n_x = \sum_{z=0}^{Z_x} n^{z}_{x} \qquad \text{II.3.8}$$

This number must remain constant. To show that this is true, we sum the rate equations for $z=0,1,...Z_x$ to get

$$\frac{dn_x}{dt} = \frac{dn_x^0}{dt} + \ldots + \frac{dn_x^{Z_x}}{dt} =$$

$$n_e \{-n_x^0 S_x^0 + n_x^1 \alpha_x^1 + n_x^0 S_x^0 - n_x^1 (S_x^1 + \alpha_x^1) + n_x^2 \alpha_x^2 + \ldots$$

$$+ n_x^{Z_x - 1} S_x^{Z_x - 1} - n_x^{Z_x} \alpha_x^{Z_x}\} = 0$$

The contribution to the right hand side due to $\frac{dn_x^{z-1}}{dt}$ is almost entirely canceled by the contribution due to $\frac{dn_x^z}{dt}$. The remaining terms are $(-n_x^z S_x^z + n_x^{z+1} \alpha_x^{z+1})$ which are ultimately canceled by the contribution from $\frac{dn_x^{Z_x}}{dt}$. This implies that n_x is independent of time as desired.

The electron number density is

$$n_e = \sum_x \sum_{z=1}^{Z_x} z n_x^z \qquad \text{II.3.9}$$

where the inner summation gives the contribution to the total number of electrons from any given species, x, and the outer summation is the contribution from all the species. Similarly, the ion number density is

$$n_i = \sum_x \sum_{z=1}^{Z_x} n_x^z \qquad \text{II.3.10}$$

Next we consider the energy equations (actually a power balance). For the electron temperature,

$$\frac{d}{dt}\left(\frac{3}{2} n_e T_e\right) = P_{ohm} - P_{eq,ei} - P_{brem} - P_{ion} - P_{rec} - P_{lr} - P_{cdiff} - P_{tdiff} - P_{add,e} \qquad \text{II.3.11}$$

For the ion temperature,

$$\frac{d}{dt}\left(\frac{3}{2}n_i T_i\right) = P_{heat} + P_{eq,ei} - P_{add,i} \qquad \text{II.3.12}$$

where each term on the right hand side of both energy equations has units of $eV/cm^3/sec$. These terms represent various power gains and losses. They are,

P_{ohm} = ohmic heating power input to the plasma

$P_{eq,ei}$ = electron-ion energy exchange rate

P_{brem} = continuum radiated power due to bremsstrahlung radiation

P_{ion} = power associated with ionization of all species

P_{rec} = power associated with electron-ion recombination processes

P_{lr} = power associated with line radiation of all species

P_{cdiff} = power associated with transport losses for a steady state classical plasma

P_{tdiff} = power associated with enhanced transport losses due to field fluctuations

P_{add,e_i} = phenomenological power terms for electron and/or ion equation specifically for experiment being simulated

P_{heat} = power associated with heating of ions

Analytic formulae are used to model each power term. The ohmic heating power delivered to the electrons is

$$P_{ohm} = 6.25 \times 10^{12}\ \eta J^2 \qquad \text{II.3.13}$$

where η is the plasma resistivity in units of ohm-m and J is the total plasma current density in amps/m^2. The electron-ion energy exchange rate is given by (19) as

$$P_{eq,ei} = 7.95 \times 10^{-33} \, n_e \frac{(T_e - T_i)}{T_e^{1.5}} \ln\Lambda \left\{ \sum_x \frac{1}{M_x} \left(\sum_{z=1}^{Z_x} n_x^z z^2 \right) \right\} \qquad \text{II.3.14}$$

where $\Lambda = 1.55 \times 10^{10} \, (T_e^3/n_e)^{.5}$ $\quad T_e \leq 36.2$ eV

$\qquad\quad 5.61 \times 10^{11} \, (T_e/n_e)^{.5}$ $\quad T_e > 36.2$ eV

M_x is the mass (grams) of one particle of species x. The power due to bremsstrahlung radiation is given by (20) as

$$P_{brem} = 1.06 \times 10^{-13} T_e^{.5} n_e \sum_x \left(\sum_{z=1}^{Z_x} n_x^z z^2 \right) \qquad \text{II.3.15}$$

The power lost due to the ionization of all species is

$$P_{ion} = n_e \sum_x \left(\sum_{z=0}^{Z_x - 1} E_x^z n_x^z S_x^z \right) \qquad \text{II.3.16}$$

The power lost through recombination processes is

$$P_{rec} = \frac{3 n_e T_e}{2} \sum_x \left(\sum_{z=1}^{Z_x} \alpha_x^z n_x^z \right) \qquad \text{II.3.17}$$

Assuming that all line radiation results from radiative decay following collisional excitation of the ground state of the various ionization levels, we use an expression for the radiated power loss

due to the resonance line of an ion in a corona model plasma. From (21),

$$P_{lr} = \frac{3.16 \times 10^{-6} n_e}{T_e^{.5}} \sum_x \{ \sum_{z=0}^{Z_x - 1} n_x^z f_x^z \exp(-\Delta E_x^z / T_e) \} \qquad \text{II.3.18}$$

where f_x^z is an averaged oscillator strength for the resonance lines of species x in charge state z. The term ΔE_x^z is an averaged excitation potential (eV).

The classical transport power loss term is

$$P_{cdiff} = \frac{3}{2} \frac{n_e T_e}{\tau_c} \qquad \text{II.3.19}$$

where τ_c is an energy confinement time based upon classical arguments. The enhanced transport power loss term is

$$P_{tdiff} = \frac{3}{2} \frac{n_e T_e}{\tau_t} \qquad \text{II.3.20}$$

where τ_t is an energy confinement time modified due to field fluctuations. Similarly, the phenomenological power losses are given by

$$P_{add,\substack{e \\ i}} = \frac{3}{2} n_{\substack{e \\ i}} T_{\substack{e \\ i}} / \tau_{\substack{e \\ i}} \qquad \text{II.3.21}$$

where the subscript "e" denotes electron and "i" denotes ion. Such a term is used to compensate for any additional arbitrary

loss not explicitly taken into account above. The power associated with the heating of ions is given in (9). Ions gain energy by scattering ion-acoustic fluctuations thereby obtaining some of the wave energy.

$$P_{heat} = \frac{n_i}{I\bar{U}} \left\{\frac{\langle \tilde{E}^2 \rangle / 8\pi}{n_e T_e}\right\} T_e \omega_{pi} \qquad \text{II.3.22}$$

where the bracketed term is the ratio of the energy content of the plasma waves relative to the plasma energy. This is a good measure of the turbulence associated with the excitation of longitudinal plasma waves.

The two energy equations together with the (Z_x+1) ion rate equations for each species, x, form a coupled system of non-linear ordinary differential equations. To solve for ion temperature, electron temperature, ion densities and neutral atom densities, all as functions of time, we must prescribe initial values for T_e, T_i, n_x^z (for all x and z) as well as plasma current density as a function of time.

III. NUMERICAL METHODS

1.A) Solution of the MHD Equations With Inertia

The solution of the equations is similar to that of Lui and Chu.[10] Here we sketch the solution and discuss the significance for this new work, i.e. how the equations are modified to represent Torus-II.

We non-dimensionalize all variables discussed in chapter II, section 1. Let

$$\tilde{r} = \frac{r}{a} \qquad \tilde{z} = \frac{z}{a} \qquad \tilde{\rho} = \frac{\rho}{\rho_o}$$

$$\tilde{t} = \frac{t}{t_o} \qquad \tilde{\kappa} = \frac{\kappa}{\kappa_o} \qquad \tilde{\sigma} = \frac{\sigma}{\sigma_o}$$

$$\tilde{v} = \frac{v}{v_a} \qquad \tilde{\Psi} = \frac{\Psi}{B_o a^2} \qquad \tilde{T} = \frac{T}{v_a^2/C_v}$$

$$\tilde{\chi} = \frac{\chi}{B_o a} \qquad t_o = \frac{a}{v_a} \qquad v_a = \frac{B_o}{(4\pi\rho_o)^{.5}}$$

$$\tilde{J} = \frac{J}{B_o c/4\pi a} \qquad \tilde{B} = \frac{B}{B_o}$$

where σ_o, ρ_o and κ_o are the initial electrical conductivity, plasma mass density and thermal conductivity respectively. B_o is a characteristic value of magnetic field and "a" is the plasma chamber half-width. First we write the parabolic equations for Ψ, χ and T in the form (dropping tilde notation)

$$A^n_{i+1,j}\xi^{n+1}_{i+1,j} + B^n_{i,j}\xi^{n+1}_{i,j} + C^n_{i-1,j}\xi^{n+1}_{i-1,j} =$$

$$D^n_{i,j-1}\xi^n_{i,j-1} + E_{i,j}\xi^n_{i,j} + F^n_{i,j+1}\xi^n_{i,j+1}$$

III.1.1

where $\underline{\xi} = \begin{bmatrix} \Psi \\ \chi \\ T \end{bmatrix}$. The scheme is implicit in alternating directions (ADI). Thus, for one time step, subscript "i" refers to the radial coordinate and the next time step it refers to the vertical coordinate. The hyperbolic equations are written in conservation law form.

$$\frac{\partial \underline{W}}{\partial t} + \frac{1}{r}\frac{\partial}{\partial r} r\underline{M}(\underline{W},T) + \frac{\partial}{\partial z}\underline{N}(\underline{W},T) = \underline{S}(\underline{W},T) + \underline{F}(\underline{J},\underline{B})$$

with

$$\underline{W} = \begin{bmatrix} \rho \\ \rho v_r \\ \rho v_z \\ \rho v_\phi \end{bmatrix} \qquad \underline{M} = \begin{bmatrix} \rho v_r \\ \rho v_r^2 + (\gamma-1)\rho T \\ \rho v_r v_z \\ \rho v_r v_\phi \end{bmatrix}$$

$$\underline{N} = \begin{bmatrix} \rho v_z \\ \rho v_r v_z \\ \rho v_z^2 + (\gamma-1)\rho T \\ \rho v_z v_\phi \end{bmatrix} \qquad \underline{S} = \begin{bmatrix} 0 \\ (\gamma-1)\rho T/r + \rho v_\phi^2/r \\ 0 \\ -\rho v_r v_\phi / r \end{bmatrix}$$

$$\underline{F} = \begin{bmatrix} 0 \\ J_\phi B_z - J_z B_\phi \\ J_r B_\phi - J_\phi B_r \\ J_z B_r - J_r B_z \end{bmatrix} \qquad \text{III.1.2}$$

$\underline{M}$, $\underline{N}$, $\underline{S}$ and $\underline{F}$ represent radial and axial fluxes of mass and momentum, the lower order source terms representing curvature effects and the forcing terms due to $\underline{J} \times \underline{B}$. To solve the set of equations, we write

$$\underline{M} = \underset{\sim}{A}\,\underline{W} \qquad \underline{N} = \underset{\sim}{B}\,\underline{W} \qquad \text{III.1.3}$$

where $\underset{\sim}{A}$ and $\underset{\sim}{B}$ are non-unique, 4 x 4 matrices. We use

$$\underset{\sim}{A} = \begin{bmatrix} 0 & 1 & 0 & 0 \\ (\gamma-1)T - v_r^2 & 2v_r & 0 & 0 \\ -v_r v_z & v_z & v_r & 0 \\ -v_r v_\phi & v_\phi & 0 & v_r \end{bmatrix}$$

$$\underset{\sim}{B} = \begin{bmatrix} 0 & 0 & 1 & 0 \\ -v_r v_z & v_z & v_r & 0 \\ (\gamma-1)T - v_z^2 & 0 & 2v_z & 0 \\ -v_z v_\phi & 0 & v_\phi & v_z \end{bmatrix} \qquad \text{III.1.4}$$

An ADI method is also used for the hyperbolic equations. A predictor value, $\underline{W}^*$, is calculated by an explicit Lax-Friedrichs[22] scheme using known values at the old time step. This $\underline{W}^*$ is used for nonlinear terms in the parabolic equations. We then calculate $\Psi_{i,j}^{n+1}$, $\chi_{i,j}^{n+1}$ and $T_{i,j}^{n+1}$. Then $\underline{W}^{n+1}$ is obtained by solving the hyperbolic equations with $\underline{S}$ given by $.5(\underline{S}^n + \underline{S}^*)$, $\underline{F}$ by $.5(\underline{F}^n + \underline{F}^{n+1})$, $\underset{\sim}{A}\underline{W}$ by $.5(\underset{\sim}{A}^n\underline{W}^n + \underset{\sim}{A}^*\underline{W}^*)$ and $\underset{\sim}{B}\underline{W}$ by $.5(\underset{\sim}{B}^n\underline{W}^n + \underset{\sim}{B}^*\underline{W}^*)$.

To improve numerical stability, a Lapidus-type pseudo viscosity is included.[11] Now we proceed to the modifications made for Torus-II. (Note: For Torus-II operating ranges we can easily show that $L >> \lambda_d$ and $|P/\nabla p| >> r_g$ as is necessary for the fluid theory to be applicable.)

1.B) Modification of the MHD Equations With Inertia

For the simulation of Torus-II, emphasis is placed on transport modeling, a new low density treatment, more realistic boundary conditions and radiation losses.

(i) Transport Modeling

We consider kinematic viscosity, thermal conductivity, electrical conductivity, radiative losses and incomplete ionization effects.

The ion kinematic viscosity coefficient scales as

$$\nu_i \sim T_i \tau_i / M_i$$

where τ_i is the ion collision time, M_i is the ion mass and T_i is the ion temperature. The corresponding dissipation time scale is on the order of 1 msec. This is much longer than the heating time of 4 μsec. Thus, no kinematic viscous effects are included in the equations.

We are principally concerned with cross field thermal conduction. Using classical perpendicular ion thermal conductivity, two cases were studied. A realistic time and space dependent conductivity and a constant conductivity model. It was found that any non-smooth behavior in κ during the heating phase leads to temperature singularities and eventual code failure. This occurs quite readily since

$$\kappa \sim n^2/(T^{\cdot 5} B^2)$$

Our treatment of energy losses is not exact in other more important respects-radiation, ionization, impurity transport.Thus, the second model has been adopted where the thermal conductivity is maintained at an appropriate fixed value.

Field and mass diffusion are controlled by the electrical resistivity. Field soak-in times scale as

$$\tau_f \sim L^2/c^2\eta$$

Classical Spitzer values of η for temperatures of 100 eV yield $\tau_f \sim 1$ msec. Experimental results cited earlier indicate the existence of an anomalously high resistivity resulting from plasma turbulence. Physically, the fast toroidal field reversal drives large poloidal electric fields. When the electron drift velocity greatly exceeds the ion acoustic speed, unstable plasma ion waves drive microturbulence on the plasma edge. The turbulence "digs" into the plasma resulting in the rapid soak-in of the field observed experimentally (∿5 μsec). Typically, η_{anom} is two orders of magnitude greater than η_{class}. The resistivity is scaled linearly with the electric field as in (8).

$$\eta = \eta_o \frac{J}{J_o} \qquad \text{III.1.5}$$

where J_o is the maximum computed current density and

$$\eta_o = (8m_e/M_i)^{.33}\omega_{pe}^{-1} \qquad \text{III.1.6}$$

is the empirical Buneman resistivity. To avoid numerical difficulty in regions of low current density, a cutoff value is set for η such that

$$\frac{\eta_o}{166.} \leq \eta \leq \eta_o$$

The anomalous resistivity is used for the initial 4 μsec of the toroidal field reversal. We then switch over (within 2 μsec) to a Spitzer resistivity for the remainder of the simulation. The above model has proven quite effective in simulating Torus-II as shall be shown in the next chapter.

Two different radiation models are used in the heating phase calculations. The first method is quite simple. Energy losses not accounted for otherwise, are lumped into a zero-dimensional confinement time parameter (τ_{loss}) in the energy equation. It is chosen ($\sim$15 μsec) to match experimental results for the ion temperature decay as obtained from spectroscopic measurements. It has the advantage of simplicity while generating realistic plasma behavior. In particular, as temperature decreases, there is an increase in the classical resistivity ($\sim T^{-1.5}$) resulting in a decay of plasma current. In the second case, power loss is calculated from radiation curves given in (23) for different elements. The dominant impurities in Torus-II are silicon and oxygen. They are

prescribed as a fixed percentage of the plasma density. The fundamental assumption of this model is that the plasma is in coronal equilibrium. This is not a good assumption during the heating phase of Torus-II. Its primary advantage over the first method, (zero-dimensional loss term), is its spatial dependence. Since it is rather cumbersome to use and computationally time consuming we've opted for the zero-dimensional loss model during the heating phase.

Ionization losses are accounted for by deliberately programming less poloidal flux through the hole in the torus than the external coils are capable of delivering. This automatically stipulates that not all energy is available for heating.

(ii) A New Low Density Treatment

As in earlier works (e.g. (10)) a low density cutoff value is prescribed for two reasons. First, we wish to avoid treatment of a vacuum region and a vacuum-plasma boundary. Secondly, for extremely low density, the Alfven speed becomes large. The Courant-Lewy-Friedrichs number grows such that explicit schemes become unstable and implicit schemes lose accuracy. Typically, 1-10% of the initial fill density is used.

Inaccuracies may still creep into the calculation. Thus, every $\sim$100 time steps each point is tested to see if it is in a low density region. This is done by simpling calculating an average density based upon neighboring points. For example,

$$\bar{\rho}_{i,j} = \frac{1}{9}\left(\rho_{i+2,j} + \rho_{i+1,j} + \rho_{i,j} + \rho_{i-2,j} + \rho_{i-1,j} + \rho_{i,j+2} + \rho_{i,j+1} + \rho_{i,j-2} + \rho_{i,j-1}\right)$$

If this average density is significantly less than the peak plasma density, it is considered to be in a low density region. If that is the case, we proceed to smooth out any large grdients in Ψ and χ by a simple averaging process. For the poloidal flux,

$$\Psi_{i,j})_{smooth} = \frac{\Psi_{i+1,j} + \Psi_{i,j} + \Psi_{i-1,j} + \Psi_{i,j+1} + \Psi_{i,j-1}}{5}$$

A similar expression is written for $\chi_{i,j})_{smooth}$. This simple method has helped tremendously to squash numerical fluctuations. It has also been useful in simulating the physics of Torus-II. Recall that the vacuum vessel of the torus is an insulator. Thus, any open field lines that intersect it must carry zero current. Invariably, simulations have shown that these field lines exist in regions of low plasma density. Since $\underline{J}$ is obtained by differentiating Ψ and χ we are closer to the condition $\underline{J} \equiv 0$ by smoothening out these two variables in such regions.

Another phenomena to be modeled is that the low density region is probably loaded with all kinds of neutral species. To account for this the resistivity is artificially fixed at η_0, thereby maintaining a large resistivity even when $\underline{J}$ is small. This is quite different from our treatment of the resistivity in the turbulent

high density plasma region. (See eqn. III.1.5) Augmenting the resistivity serves to kill off any remaining currents not taken care of by the filtering described above.

Another characteristic worth simulating is that while the impurity levels may be ∿1-2% in the bulk of the plasma, they are probably quite high in the low density region. When the average ion model is used for radiation losses, the impurity levels in the low density region are fixed at 50% oxygen and 50% silicon.

(iii) Torus-II Initial and Boundary Conditions

For this heating simulation we start from post z-pinch conditions. Initial conditions play a passive role in determining the final plasma state, whereas, the boundary specifications for Ψ and χ are directly responsible for plasma formation and heating. Most of our attention has been directed towards realistic modeling of boundary conditions. Only a brief statement regarding initial conditions is necessary.

The initial density profile is specified in accordance with the total mass of plasma expected after heating. The original height to width ratio is taken to be 2:1. A uniform temperature of 1 eV is prescribed everywhere. Pressure is readily calculated from the ideal gas law. The fluid is initially at rest. Complete experimental data for the negative toroidal bias field is available along the horizontal midplane. (Figure III.1) The depth of the

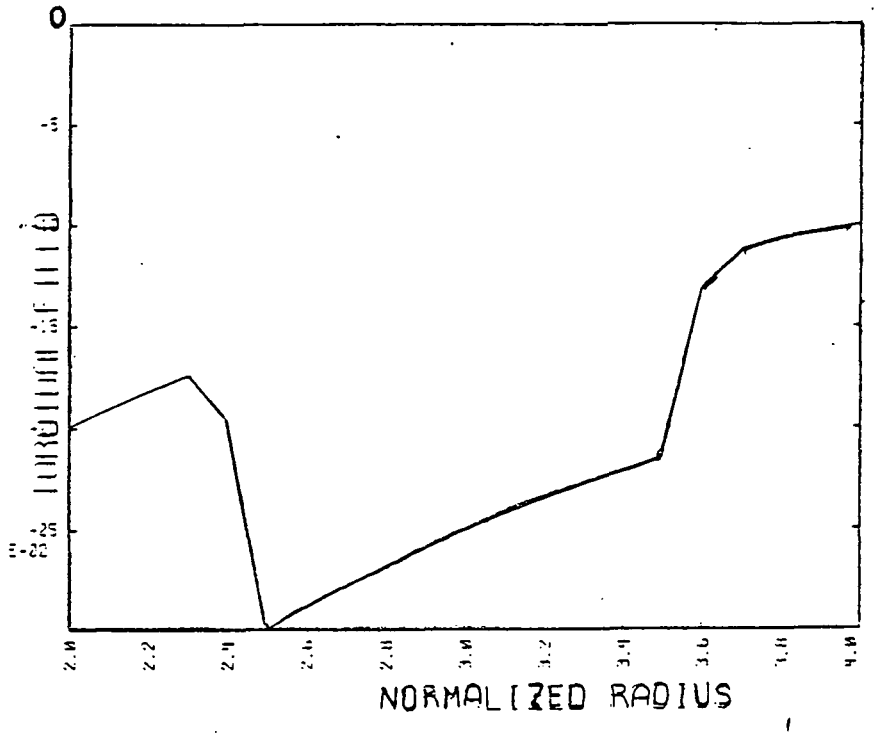

UNITS· GAUSS
TIME· INITIAL CONDITIONS
VESSEL HALF-WIDTH·7.5 CM

Figure III.1. Initial toroidal magnetic field profile along horizontal midplane for Torus-II heating phase simulation.

well decreases with distance away from the midplane. A perfect 1/r dependence is prescribed everywhere above the plasma. A toroidal plasma current of 35 kA is assumed. This is integrated once to give the z-component of magnetic field and integrated again to give the poloidal flux everywhere.

We have already discussed the boundary conditions required by the differential equations (Chapter II Section 1.B). However, the difference schemes require additional boundary specifications for plasma density and the remaining components of velocity. Thus, for boundary conditions, the temperature is held at 1 eV, the normal

component of velocity is zero and all other velocity components as well as plasma density are extrapolated at the wall. Since the simulation is performed for the upper half plane only, symmetry conditions are used on the horizontal midplane. The even variables are

$$\Psi(+z) = \Psi(-z)$$

$$\chi(+z) = \chi(-z)$$

$$\rho(+z) = \rho(-z)$$

$$T(+z) = T(-z)$$

$$v_r(+z) = v_r(-z)$$

while v_ϕ and v_z are taken to be odd about z=0. Since the plasma chamber wall is non-conducting, Ψ and χ must be prescribed as functions of both space and time. Figure III.2 shows the coil geometry of Torus-II in detail.

From Ampere's law, χ is given in terms of coil currents through the hole in the vertical direction. For a circular path around the torus we obtained

$$\chi_{wall}(t) = \frac{2\ I(t)}{c}$$

We specify $\chi_{wall}(t)$ independent of position since poloidal currents can not leak into or out of the device. A simple linear time dependence is used which preserves continuity of $\chi_{wall}(t=0)$ and the initial condition described earlier.

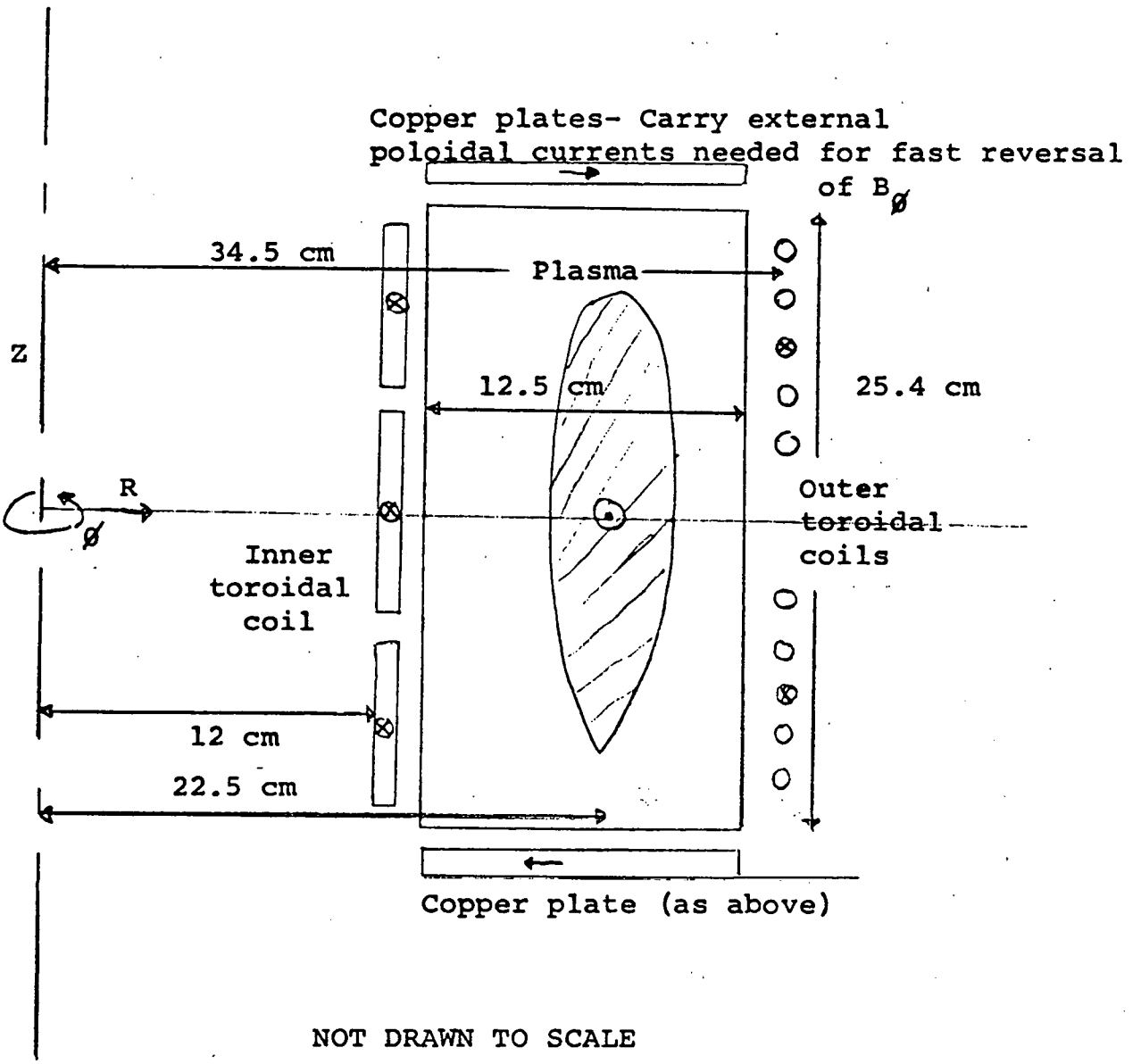

NOT DRAWN TO SCALE

Figure III.2. Torus-II coil geometry.

$$\chi_{wall}(t) = \begin{cases} \chi_{init} + (\chi_{final} - \chi_{init})\ t/t_p & t \leq t_p \\ \chi_{final} & t > t_p \end{cases}$$

where t_p is 1.7 μsec for Torus-II and χ_{init} is a measure of the initial toroidal bias field. It is crucial to the amount of heating performed by the turbulent poloidal currents generated upon the reversal of the bias field. The experiment can be operated at different heating power levels. The parameter χ_{final} is adjusted to give the proper final vacuum toroidal field which is directly related to the heating power used in the lab. We simulate two heating schemes, the so called quarter power (12 GW) and half power (25 GW) cases. For the quarter power calculation χ_{final} is set equal to 6×10^4 G-cm while for the half power case we use 8.3×10^4 G-cm. Such conditions yield a vacuum toroidal field of 2700 G and 3700 G respectively at the major radius of the device.

The poloidal flux function, Ψ, is related to the primary transformer flux, the external vertical field flux and the flux due to toroidal plasma currents. In the one dimensional analysis, given a value of poloidal flux passing through the center of the device (Ψ_{hole}), we integrate various vertical field profiles to get Ψ at the outer wall. This is similar to the earlier work of H.C. Lui. In the two dimensional analysis we consider the effects of the non-conducting side walls, the conducting copper plates on the top and bottom of the device and the toroidal plasma current. For both analyses, realistic values for Ψ are obtained using inductance codes. This is a major deviation from the Lui formulation.

The region of computation is 15 cm $\leq r \leq$ 30 cm and 0 cm $\leq z \leq$ 15.75cm. This is larger than the plasma chamber. Such a domain is convenient because of the natural boundary conditions along the endlines of z. Specifically, at z=0 exists the horizontal plane of symmetry. The reflection condition $\Psi(-z)=\Psi(+z)$ discussed above is invoked here. The boundary along z=15.75 cm coincides with the location of the upper copper plate. These copper plates carry poloidal currents causing the rapid reversal in toroidal magnetic field. For the time scales of the simulation, the plates are modeled as flux surfaces.

$$\Psi(r,z=15.75,t) = \Psi_{top}(t)$$

Along the inner and outer walls the flux is prescribed as a function of time and height.

$$\Psi(r=15,z,t) = \Psi_i(z,t)$$
$$\Psi(r=30,z,t) = \Psi_o(z,t)$$

The boundary values of Ψ are obtained from EFFI and Coils. The torus is approximated by 40 toroidal windings (Figure III.3) all of dimensions comparable to the windings on the device itself. Various combinations are run to simulate different times in the experiment

$$I_{inner} = \sum_{1}^{12} I_j = \begin{cases} 300 \text{ kA} \\ 200 \text{ kA} \\ 100 \text{ kA} \end{cases}$$

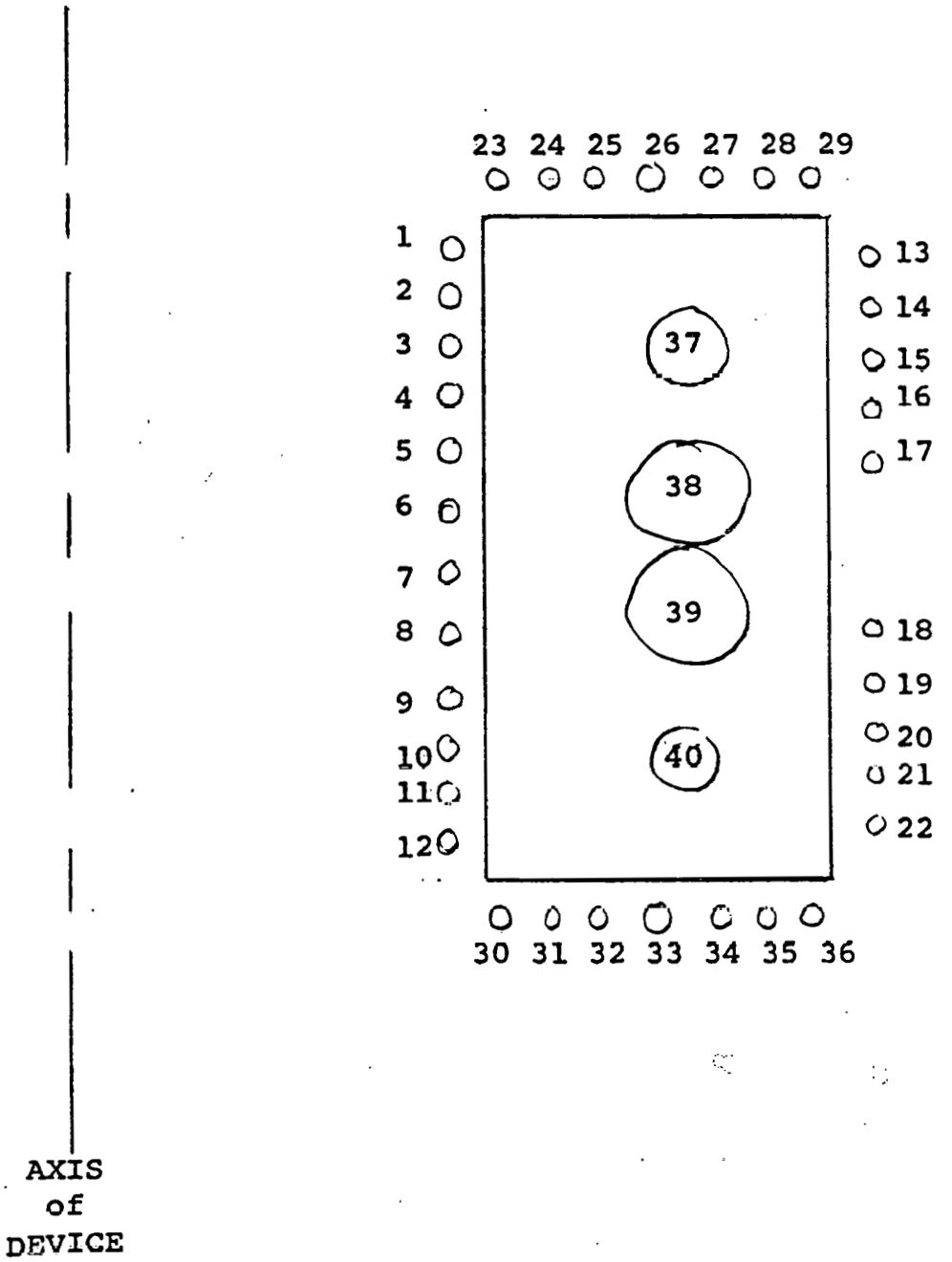

Figure III.3. Current winding distribution used in COILS computation of leakage pattern.

$$I_{outer} = \sum_{13}^{22} I_j = \begin{cases} 150 \text{ kA} \\ 100 \text{ kA} \end{cases}$$

$$I_{plasma} = \sum_{37}^{40} I_j = \begin{cases} -30 \text{ kA} \\ -50 \text{ kA} \\ -80 \text{ kA} \end{cases}$$

$$I_{plates} = \sum_{23}^{29} I_j = \sum_{30}^{36} I_j = 0$$

The results from Coils were surprising. Depending upon the combination of currents used, the flux through the hole (i.e. Ψ at any of coil positions 1-12) was 3-8x10^6 G-cm^2 (.03-.08 V-sec) which is remarkably close to experimental values of .08 V-sec deliverable by the inner transformer. Also from Coils, we consistently found that $\Psi_{top} \sim .85\ \Psi_{hole}$. This implies that 15% of the flux in the hole leaks back into the vacuum vessel. Another surprising result from Coils was that $\Psi_{outside} \sim 1.25\Psi_{hole}$ which implies that the flux due to the outer toroidal windings is almost as important as that due to the inner transformer. Thus it is indeed not appropriate to refer to these windings as "vertical field-ohmic heating" coils. The final startling result was that the copper plates have a current of 12-25 kA induced flowing opposite to the outer coil currents on the outside of the device and returning on the inside of the device. These results are summarized in Table III.1. Equipped with the current distributions supplied by the Coils code, we then use EFFI to obtain more detailed information on the magnetic field distribution. Results are shown in Figure III.4 for a plasma current of 35 kA,

Table III.1

Summary of Coils Results

I_{outer}	90 - 190 kA
I_{inner}	100 - 330 kA
I_{plasma}	30 - 80 kA
Ψ_{hole}	.03 - .08 V-sec
$\Psi_{outside}$	.05 - .10 V-sec
Ψ_{top}	.03 - .07 V-sec
I_{plates}	12 - 25 kA
Average B_z on left	-60 to -600 G
Average B_z on right	+2 to +3 kG

inner winding current of 220 kA and an outer winding current of 90 kA. For comparison, two cases are shown, with and without copper plates. EFFI clearly shows the leakage effects due to the geometry of the external windings. Note that while EFFI also gives $\Psi_{hole} \simeq .03$ V-sec, the purpose of these codes is not to extract exact numerical values for Ψ along the boundary. Rather, the codes are used to answer the following questions. How do Ψ_{top}, Ψ_{hole} and $\Psi_{outside}$ compare with eachother? What are the leakage patterns? Where is the leakage most important? What is the approximate numerical value of Ψ_{hole}? Are the external toroidal currents performing the tasks for which

Figure III.4.A

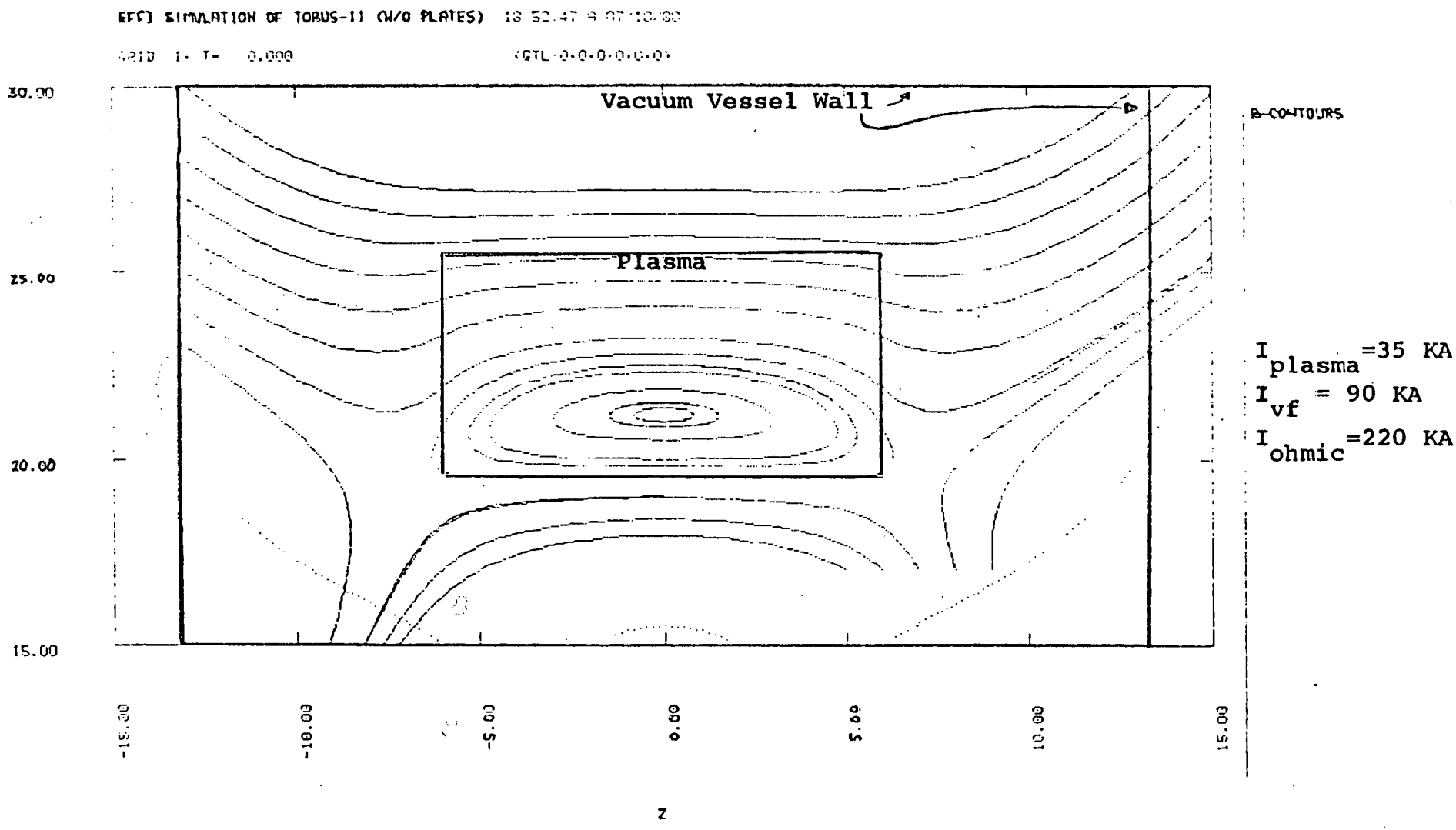

Figure III.4.B

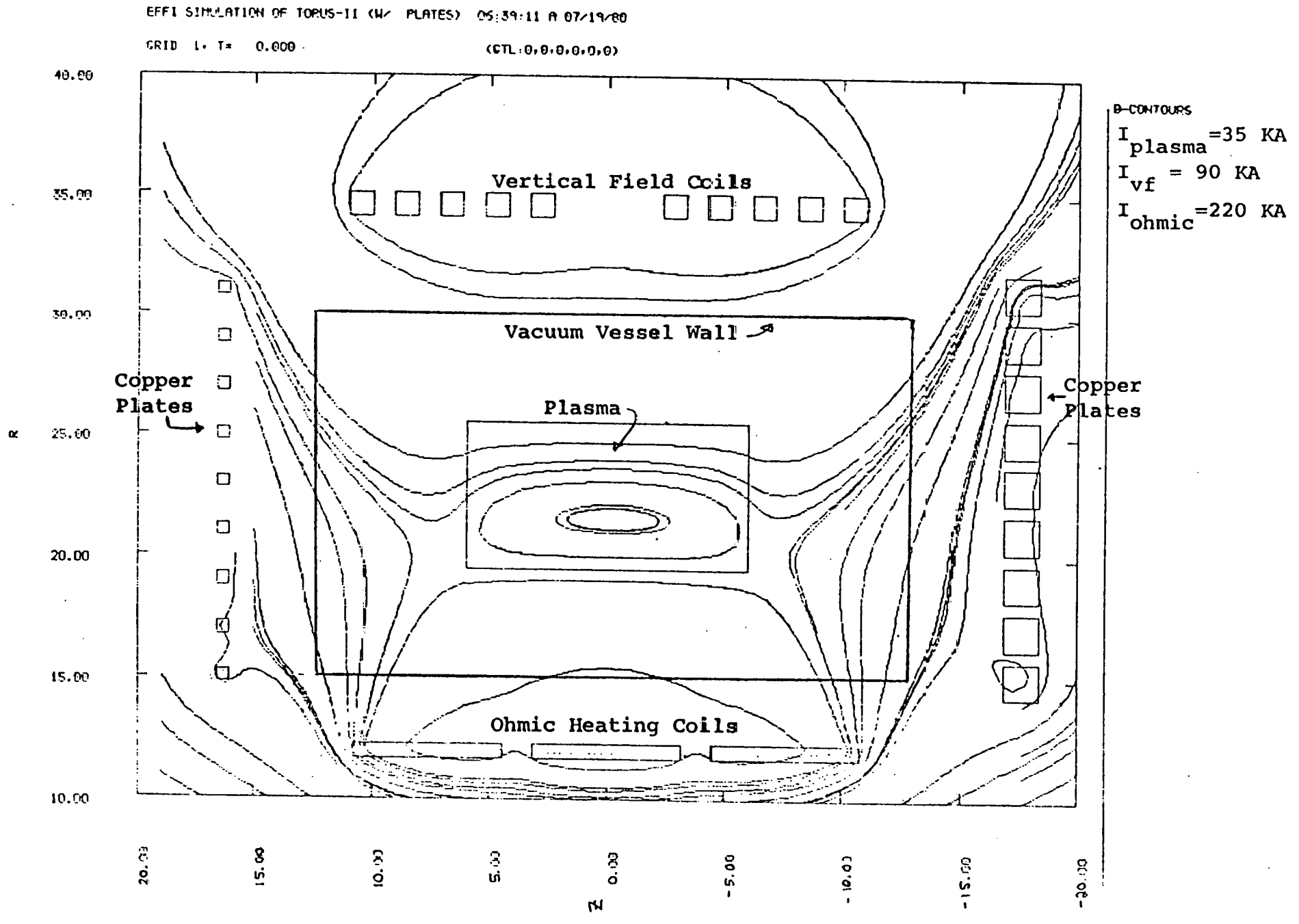

they were originally designed? All of these questions have been satisfactorally answered. Indeed the prescribed boundary conditions for Ψ in the heating calculation were given a form that produces the same leakage pattern as that obtained through the inductance calculations.

By using the inductance codes as described above we accurately simulate the heating phase of the experiment. The questions raised and answered by the inductance calculations are listed above. From the heating simulation we wish to answer the following set of questions. What are the effects of anomalous transport? How does it compare with classical transport? What is the plasma current? What do the flux surfaces look like? What is the magnetic field profile? How is the plasma confined? What are the plasma temperature and pressure profiles? What is the heating mechanism? Can we form a high beta equilibrium?

2.A) Solution of the MHD Equations Without Inertia (1-D Diffusion)

The discretized forms ofequations II.2.15, 17, 18, 19 and 26 are omitted. Fully implicit, space centered difference schemes are used. However, we do wish to point out that when each of these equations is discretized they are all of the same form. Symbolically,

$$A_\rho(\xi^n)\ \rho_{j-1}^{n+1} + B_\rho(\xi^n)\ \rho_j^{n+1} + C_\rho(\xi^n)\ \rho_{j+1}^{n+1} = D_\rho(\rho^n,\xi^n) \qquad \text{III.2.1}$$

$$A_{B\phi}(\xi^n,\rho^{n+1})\ B_{\phi_{j-1}}^{n+1} + B_{B\phi}(\xi^n,\rho^{n+1})\ B_{\phi_j}^{n+1} + C_{B\phi}(\xi^n,\rho^{n+1})\ B_{\phi_{j+1}}^{n+1} = D_{B\phi}(\zeta^n,\rho^{n+1},B_\phi^n) \qquad \text{III.2.2}$$

$$A_{B_z}(\xi^n,\rho^{n+1})\ B_{z_{j-1}}^{n+1} + B_{B_z}(\xi^n,\rho^{n+1})\ B_{z_j}^{n+1} + C_{B_z}(\xi^n,\rho^{n+1})\ B_{z_{j+1}}^{n+1} = D_{B_z}(\xi^n,\rho^{n+1},B_z^n) \qquad \text{III.2.3}$$

$$A_T(\xi^n,\underline{J}^{n+1},\rho^{n+1})\ T_{j-1}^{n+1} + B_T(\xi^n,\underline{J}^{n+1},\rho^{n+1})\ T_j^{n+1} + C_T(\xi^n,\underline{J}^{n+1},\rho^{n+1})\ T_{j+1}^{n+1} = D_T(\xi^n,\underline{J}^{n+1},\rho^{n+1},T^n) \qquad \text{III.2.4}$$

$$A_\xi(\xi^n,\underline{B}^{n+1},\underline{J}^{n+1},T^{n+1},\rho^{n+1})\xi_{j-1}^{n+1} + B_\xi(\xi^n,\underline{B}^{n+1},\underline{J}^{n+1},T^{n+1},\rho^{n+1})\ \xi_j^{n+1} + C_\xi(\xi^n,\underline{B}^{n+1},\underline{J}^{n+1},T^{n+1},\rho^{n+1})\ \xi_{j+1}^{n+1} = D_\xi(\xi^n,\underline{B}^{n+1},\underline{J}^{n+1},T^{n+1},\rho^{n+1}) \qquad \text{III.2.5}$$

A doublesweep[24] method is used to solve each equation thereby generating ξ^{n+1}, T^{n+1}, $\underline{B}^{n+1}$ and ρ^{n+1} for all positions. Given initial values for density, temperature and magnetic field, we solve III.2.5 to obtain the appropriate velocity distribution. This is kept as the old velocity, ξ_j^n. Equations III.2.1-4 are then solved in succession for the new density, temperature and magnetic field profiles. All new currents may then be computed by Ampere's law and the new field information. This information is used when solving for the new temperature profile. The final step is to calculate the new transport coefficients σ_j^{n+1} and κ_j^{n+1}. We then solve equation III.2.5 for the new diffusion velocity. The solution for the new time step is then complete. The entire procedure is then repeated.

B) The MHD Equations Without Inertia and Torus-II

Once again, for Torus-II the emphasis is placed upon transport modeling, the low density treatment and radiation losses. For this phase of our work we stress initial conditions over boundary conditions. Recall that the thrust of this work is to simulate the high beta tokamak state.

(i) Transport Modeling

Once again kinematic viscous effects are ignored since the duration of the experiment is $\leq$ 40 μsec.

Since we are no longer driving the plasma on a fast time scale one would expect that some of the fluctuations which forced us to use a constant thermal conductivity would no longer be important.

Indeed this is partially true. Since B_ϕ is no longer rapidly reversed and the plasma temperature profile is smoother than during the heating phase, we can set

$$\kappa \sim \frac{1}{T^{.5}B^2} \qquad \text{III.2.6}$$

However, the code can not handle the n^2 dependence in the thermal conductivity. The reason is simple. The Torus-II plasma is narrow ($a \simeq 3$ cm) and dense ($n_{peak} \sim 10^{15} cm^{-3}$). If κ is allowed to be proportional to n^2 we found that the thermal conductivity drops drastically in the low density regions resulting in unrealistic heat concentrations and temperature spikes. Thus, we use III.2.6 thereby allowing κ to vary somewhat both in space and time.

The plasma turbulence discussed earlier is not a factor during the high beta tokamak phase. Therefore, the electrical resistivity is modeled classically. Its value is given by (in seconds)

$$\eta_{perpendicular} = \frac{3.3x10^{-14} \ln \Lambda}{T^{1.5}} \qquad \text{III.2.7}$$

for T in eV and a $Z_{effective}$ of 2, where $\ln \Lambda$ is the usual Coulomb logarithm. We do not use a constant value for the Coulomb logarithmbut rather let

$$\Lambda \sim (T^3/\rho)^{.5}$$

This is done since for Torus-II operating parameters, the Coulomb

logarithm can vary by as much as a factor of three. We get,

$$5 \leq \ln \Lambda \leq 15$$

This can make the difference between a 20 μsec diffusion time scale and a 60 μsec diffusion time scale. For a device with a total pulse length of 50 μsec, such discrepancies are important.

The radiation losses are simulated exclusively by using the average ion model of (23). Briefly, when the electron collisional ionization rate is exactly balanced by the total recombination rate, a "coronal equilibrium" exists. Radiation is caused by bremsstrahlung, radiative decay due to $\Delta n=0$ and $\Delta n\neq 0$ line transitions following electron collisional excitation, radiative recombination and dielectronic recombination. Post gives results for the ("coronal equilibrium") radiation obtained by solving the time dependent, atomic physics, rate equations (similar to those presented in Chapter II Section 3) until a steady state is reached. Radiation power levels for silicon and oxygen as functions of temperature are given in Figure III.5. The Torus-II plasma does not exactly satisfy the condition for coronal equilibrium given by (25) as

$$\frac{10^{12}}{\tau_i} < n_e < 10^{16} T(\text{eV})^{3.5}$$

It should be a fairly good approximation since, for Torus-II, the above will read (for oxygen and silicon at 100 eV)

Figure III.5.A

A)
Oxygen
Power
Radiated
(ergs-
cm^3/sec)

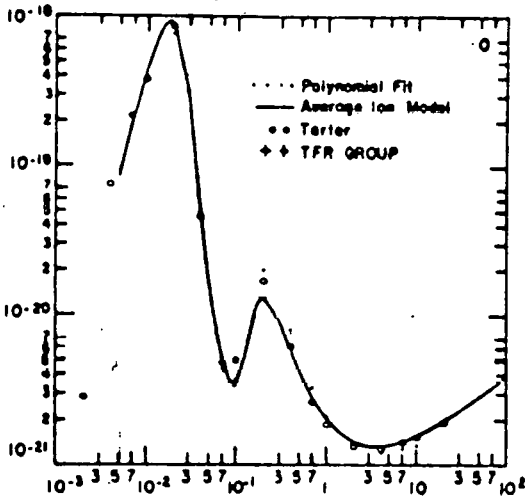

Figure III.5.B

B)
Silicon
Power
Radiated
(ergs-
cm^3/sec)

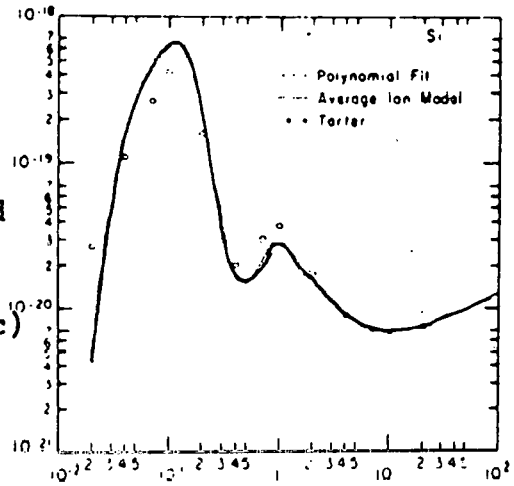

$$\frac{10^{12}}{\tau_i} \simeq 10^{16}$$

$$n_e \simeq 10^{15} \quad \Big\} \rightarrow\rightarrow\rightarrow\rightarrow\rightarrow \quad 10^{16} \not< 10^{15} < 10^{23}$$

$$10^{16}\, T^{3.5} \simeq 10^{23}$$

However, since it does provide us with useful information on time and spatially varying cooling rates it has been included in the calculation.

(ii) Low Density Treatment

To repeat, for the high beta tokamak phase, we solve an elliptic momentum equation. This was not the case in the heating calculation. There is no need for the detailed smoothening of the field quantities as described in Chapter II Section 1.B.ii. The resistivity is still artificially increased in the low density regions. The impurity levels are again fixed at high levels in the low density regions.

The major difference from the low density treatment of the heating simulation is that the total current is now set equal to zero before computing the temperature in these regions. This is to insure that no fictitious ohmic heating arises from numerically generated plasma currents in the high resistivity areas.

(iii) Torus-II Initial and Boundary Conditions

During the high beta phase of Torus-II, all external currents are crowbarred. The decay time of these currents without plasma

present has been experimentally determined to be in excess of 100 μsec.[26] However, in the presence of plasma, the outer windings exhibit a rapid decay (∿30 μsec) while the inner winding decay time is not affected.[27] Obviously the decay of plasma current is the controlling factor in the above observations. Therefore, boundary conditions should always reflect the effects of plasma current decay and must not be used to drive the plasma to any particular state. This is fundamentally different from our treatment of boundary conditions in the heating computation. Now, plasma evolution is determined solely by prescribed initial conditions and the modeling of transport parameters.

We are dealing with a one-dimensional calculation. Temperature is held fixed at 3 eV at each radial endpoint. The radial velocity is set equal to zero on the boundary. A perfect crowbar is prescribed for B_ϕ. Experimental results indicate that this is true for the time scale of interest. One must be careful in prescribing the poloidal flux function. It was observed that by specifying a decay rate for flux through the hole and flux in the plasma chamber, large toroidal currents are induced in the low density regions. The reason for this is as follows. Plasma responds through dissipative processes to initially prescribed parameters. If the boundary condition does not exactly match the plasma decay rates it will drive the plasma to some other state, but not necessarily the one to which it would evolve if left unguided. The solution decided upon was to extrapolate the value of the poloidal FIELD at both boundary points.

The results are astounding. The plasma decay is determined solely by the physics of the dissipative processes as desired. There is further justification for choosing such boundary conditions. The region of computation is 15 cm $\leq$ r $\leq$ 30 cm. The inner windings are located at r $\approx$ 12 cm. Recall the earlier inductance calculations which indicate a large amount of flux leakage into the vacuum vessel. The result was that the plasma does not see all the flux in the hole but somewhat less. When the system is crowbarred, the current in the inner coil slowly decays thereby decreasing the flux in the hole. Simultaneously there must be a decrease in the flux leakage into the plasma chamber. The net result is that the flux on the inner vessel boundary is relatively constant. Thus, any specified decay in Ψ would be in error. By extrapolating B_z at this wall we can still insure that the flux remains constant. Another reason for extrapolating B_z will become evident as we discuss the somewhat different physics at work along the outer wall. Here we must consider the poloidal flux contributed by the toroidal plasma current as well as external currents. The decay rate of the flux from the plasma current is determined both by the resistivity and plasma position. A large resistivity causes a rapid decay in plasma current. The decay rate of the poloidal flux then depends upon the radial position of the plasma since for plasma at large r there is a very small positive contribution to the poloidal flux and a large negative contribution. So a rapid decay in the plasma current would not lead to a rapid decay in the flux. Another view is that for plasma with a small

major radius there is a large vertical component of magnetic field beyond the plasma. As the plasma current decays, this field collapses (Ψ now does decrease rapidly) resulting in a loss of confinement. The critical point here is that Ψ on the outer wall depends on several different factors. By simpling extrapolating B_z we avoid having to predict the flux decay but rather can observe it as a result of the dissipative processes at work. Note that, in one dimension, extrapolating B_z implies

$$\frac{\partial B_z}{\partial r} = 0$$

which implies $\rightarrow\rightarrow\rightarrow\rightarrow$ $J_\phi \equiv 0$

This is very sensible. Recall our initial difficulty in specifying Ψ was the resulting induced toroidal current in the low density region. Now we avoid such a problem with the above boundary condition.

Once again, the numerical scheme requires a boundary specification of plasma density. To avoid boundary layer effects due to an improperly specified ρ_{wall} (i.e. a condition which does not accurately reflect the dissipative processes of the system) we simply extrapolate its value there.

Next we turn our attention to the all important initial conditions. Values for density, temperature and magnetic field must be given for all r. Three related methods are used. First, results generated by the start-up calculation can be used as initial con-

ditions for the high beta tokamak state. Secondly, experimental data for this time can be used. Thirdly, arbitrary initial equilibrium profiles can be specified. Each has advantages and problems associated with it. The heating simulation, as we will see, yields important qualitative and quantitative information regarding the Torus-II plasma. However, to ask exact profiles of it is a bit too much. Detailed experimental information of pressure and $\underline{B}$ profiles is simply not available. In making arbitrary assumptions we run the risk of straying from Torus-II conditions. By combining the strengths of each method, an effective set of initial conditions for the high beta phase can be generated.

Consider "arbitrary" profile specification. Let w denote plasma width, r_p denote location of peak plasma density and n_p denote the peak plasma number density. Profiles symmetric about r_p are considered, such that

$$n(r) = \begin{cases} n_{min} & r < r_p - \frac{w}{2} \; ; \; r > r_p + \frac{w}{2} \\ n_{min} + n_p\left(1. - \left|\frac{r-r_p}{w/2}\right|^{x_n}\right) & r_p - \frac{w}{2} \leq r \leq r_p + \frac{w}{2} \end{cases}$$

where n_{min} is the cutoff plasma density discussed earlier and x_n is any positive real number.

Similarly, let r_T denote the location of peak plasma temperature and T_p denote the peak plasma temperature. Based upon heating simulations, we want a temperature profile such that

$$T \sim \begin{cases} k_L r & \text{for } r < r_{TL} \\ k_R r & \text{for } r > r_{TR} \end{cases} \qquad \text{III.2.9}$$

where k_L and k_R are slopes for those regions in which the temperature profile is prescribed as a linear function of r, namely, to the left (towards inner wall) and right (towards outer wall) of the peak temperature position. The positions where the linear profiles are no longer valid are specified as r_{TL} and r_{TR}. We require that the temperature and its first derivative be continuous at these points. Therefore, at r_{TL}

$$\frac{dT}{dr} = k_L \qquad \text{and} \qquad T = T_L \qquad \text{III.2.10.a}$$

and at r_{TR}

$$\frac{dT}{dr} = k_R \qquad \text{and} \qquad T = T_R \qquad \text{III.2.10.b}$$

with T_L and T_R unknown. For a wall temperature of T_w, we take

$$k_L = \frac{T_L - T_w}{r_{TL} - r_i} \quad , \quad k_R = \frac{T_w - T_R}{r_o - r_{TR}} \qquad \text{III.2.11}$$

where r_i and r_o are the usual boundaries for our calculation of 15 cm and 30 cm respectively. We choose to write

$$\frac{dT}{dr} = \begin{cases} k_L \left(\frac{r_T - r}{r_T - r_{TL}}\right)^{x_{TL}} & r_{TL} \leq r \leq r_T \\ k_R \left(\frac{r - r_T}{r_{TR} - r_T}\right)^{x_{TR}} & r_T \leq r \leq r_{TR} \end{cases} \qquad \text{III.2.12}$$

where x_{TL} and x_{TR} are positive real numbers. By such a choice we automatically satisfy the derivative conditions of II.2.10. The above also insures that $\frac{dT}{dr}$ is zero at r_T. Several parameters still have not been assigned values, they are, T_L, T_R, x_{TL} and x_{TR}. Without these numbers, k_L and k_R remain unknown. Consider an integration from the inner wall to r_T.

$$\int_{r_i}^{r_T} \frac{dT}{dr}\, dr = T_p - T_w$$

Substituting equations III.2.9,11 and 12, performing the integration and rearranging terms we get

$$T_L = \frac{T_o + \underline{R}_L T_w/(x_{TL}+1)}{1 + \underline{R}_L/(x_{TL}+1)} \qquad \text{III.2.13}$$

where

$$\underline{R}_L = \frac{r_T - r_{TL}}{r_{TL} - r_i}$$

A similar integration to the outer wall yields

$$T_R = \frac{T_o + \underline{R}_R T_w/(x_{TR}+1)}{1 + \underline{R}_R/(x_{TR}+1)} \qquad \text{III.2.14}$$

where

$$\underline{R}_R = \frac{r_{TR} - r_T}{r_o - r_{TR}}$$

Thus, by choosing x_{TR} and x_{TL} ("shape factors") we can calculate T_L

and T_R using III.2.13 and 14. Then we know dT/dr everywhere and can integrate to get T(r) initially. Such a temperature distribution is sketched in Figure III.6.

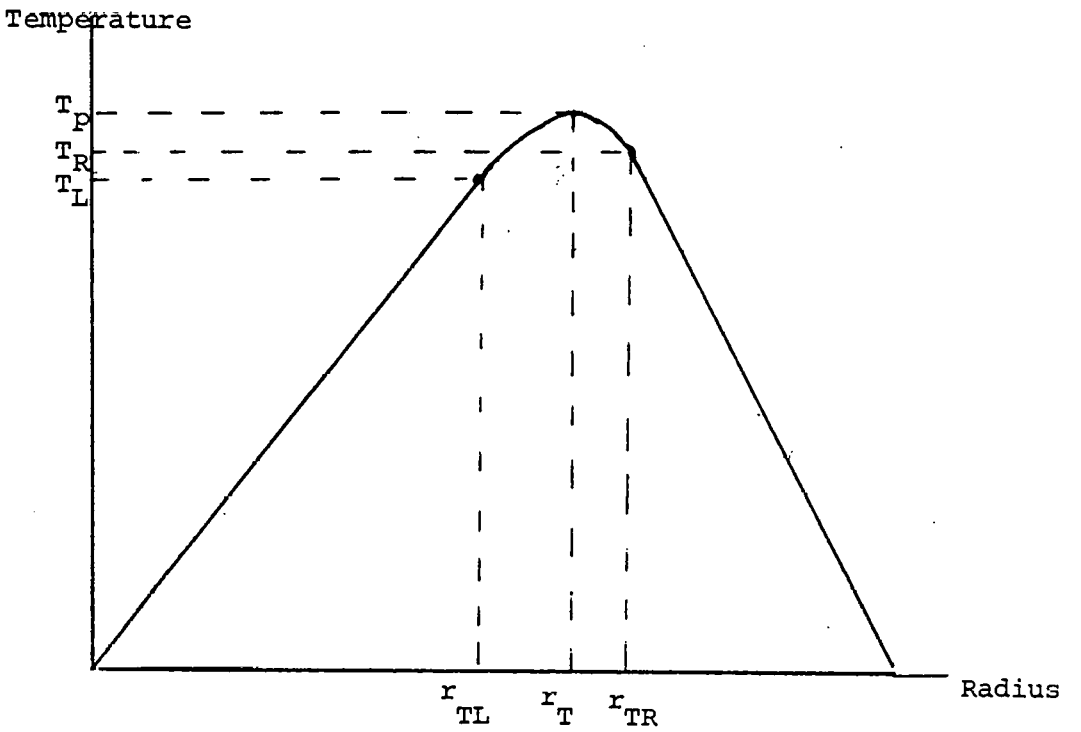

Figure III.6 Typical temperature profile used as initial condition for simulation of high beta tokamak state of Torus-II.

Rather than specify B_z, we prescribe J_ϕ and integrate to get the magnetic field. We specify I_p, the total toroidal plasma current and the plasma height, h. A continuous current density profile is prescribed

$$J_\phi = \begin{cases} J_o\left(\dfrac{r - r_{JL}}{r_J - r_{JL}}\right)^{x_{JL}} & r_{JL} \le r \le r_J \\ J_o\left(\dfrac{r_{JR} - r}{r_{JR} - r_J}\right)^{x_{JR}} & r_J \le r \le r_{JR} \end{cases} \qquad \text{III.2.15}$$

where r_{JR}, r_{JL}, x_{JL} and x_{JR} are given parameters in much the same way as for the previous temperature discussion. The peak plasma current density, J_o, must be computed. The average plasma current per unit height is

$$\frac{I_p}{h} = \int_{r_i}^{r_o} J_\phi \, dr$$

Substituting III.2.15 we can solve for J_o.

$$J_o = \frac{I_p/h}{\left\{\frac{r_J - r_{JL}}{x_{JL}+1} + \frac{r_{JR} - r_J}{x_{JR}+1}\right\}} \qquad \text{III.2.16}$$

Again, by specifying the "shape factors" x_{JL} and x_{JR} we can compute J_o above. We then have our initial $J_\phi(r)$ by using III.2.15.

The poloidal field is calculated from the one-dimensional relationship

$$J_\phi = \frac{-dB_z}{dr}$$

It is easy to experimentally obtain B_z at the outside wall of the plasma chamber. Therefore, our initial profile is specified as

$$B_z(r) = B_z(r_o) + \int_{r}^{r_o} J_\phi \, dr' \qquad \text{III.2.17}$$

Similarly, the poloidal flux is obtained by integrating the vertical component of the magnetic field.

$$\Psi(r) = \Psi_{hole} + \int_{r_i}^{r} r' B_z dr' \qquad \text{III.2.18}$$

where Ψ_{hole} is a known value for flux in the hole.

This leaves us with the toroidal magnetic field and poloidal current yet to be determined. As in the case of the MHD equations with inertia, we write

$$B_\phi = \frac{\chi(r)}{r} \qquad \text{III.2.19}$$

with χ representing the usual poloidal current function. For a vacuum, χ is independent of radius and we get $B_\phi \sim 1/r$ as expected. In the plasma region, a diamagnetic well or paramagnetic bump will exist. The heating simulations indicate that the high beta plasma of Torus-II exhibits a slight diamagnetism. Therefore, if we let r_B be the deepest point of the well, PW the decimal depth of the well and r_{BL}, r_{BR} the locations where B_ϕ deviates from 1/r behavior, then

$$\chi(r) = \begin{cases} \chi_o & r<r_{BL} \text{ and } r>r_{BR} \\ \chi_o\{1.-PW(\frac{r_{BR}-r}{r_{BR}-r_B})^{x_{BR}}\} & r_B \leq r \leq r_{BR} \\ \chi_o\{1.-PW(\frac{r-r_{BL}}{r_B-r_{BL}})^{x_{BL}}\} & r_{BL} \leq r \leq r_B \end{cases}$$

III.2.18

χ_o is the known vacuum value of the poloidal current function. Again, x_{BR} and x_{BL} are prescribed "shape factors". Note that III.2.18 assures us of the continuity of B_ϕ at r_B, r_{BL} and r_{BR}.

The initial poloidal current density is easily obtained from

$$J_z = \frac{1}{r}\frac{\partial \chi}{\partial r} \qquad \text{III.2.19}$$

In summation, from heating calculations and experimental data we know the plasma width, peak plasma density, location of peak density, peak temperature, location of peak temperature, plasma current, plasma height, poloidal flux in hole, vertical component of magnetic field on outer wall, vacuum toroidal field, and the depth and location of the toroidal field well. Using all the above in conjunction with assumed "shape factors" we generate all the necessary initial values.

The high beta tokamak simulation is performed to answer some very important questions. How long can the plasma be maintained in equilibrium? What are the important loss mechanisms? What are the typical profiles of density, temperature, pressure, current density and magnetic field? How quickly does the temperature decay? What are the maximum tolerable impurity levels? How quickly does beta decay? What are the most desirable states to reach through heating? That is, what are the optimum initial conditions to be used in order to maintain a high beta plasma for times of interest?

3.A) Solution of the Zero-Dimensional Atomic Physics Equations

A fourth order accurate Runge-Kutta scheme[28] is used to solve the equations. Formally, they are written

$$\frac{d\underline{x}(t)}{dt} = \underline{F}(\underline{x}) \qquad \text{III.3.1}$$

where $\underline{x}^T = (t, n_x^0, n_x^1, .., n_x^{Zx}, T_e, T_i)$

and $\underline{F}(\underline{x})$ represents the right hand side of the rate equations described in Chapter II Section 3. We prescribe $\underline{x}(0)$ and march the coupled system forward in time. Recall that the purpose of this calculation is to simulate the ionization processes during the z-pinch phase, the "burn through" during the heating phase and the cooling of the high beta tokamak phase.

3.B) Torus-II Parameters in Zero-Dimensional Simulation

The chief species present in Torus-II are helium (main filling gas), silicon and oxygen (impurities from pyrex wall). We can now quantify the number of equations to be solved. They are equations for $\dot{t}$, $\dot{n}^0_{He}$, $\dot{n}^{+1}_{He}$, $\dot{n}^{+2}_{He}$, $\dot{n}^0_{Ox}$,.., $\dot{n}^{+8}_{Ox}$, $\dot{n}^0_{Si}$,.., $\dot{n}^{+14}_{Si}$, $\dot{T}_e$ and $\dot{T}_i$ for a total of 30 equations.

To compute the ionization and recombination rates we need the ionization energies for helium, oxygen and silicon in each charge state. This information is given in Table III.2. For any temperature, we can solve the species equations for helium, oxygen and silicon. With these newly obtained number densities for each ionic species we can compute the new electron number density and proceed

to the energy equations.

Table III.2

Ionization Energies (eV)[29]

Charge State	Helium	Oxygen	Silicon
0	24.6	13.6	8.2
+1	54.4	35.1	16.3
+2	-	54.9	33.5
+3	-	77.4	45.1
+4	-	113.9	166.8
+5	-	138.1	205.1
+6	-	739.3	246.5
+7	-	871.4	303.2
+8	-	-	351.1
+9	-	-	401.4
+10	-	-	476.1
+11	-	-	523.5
+12	-	-	2437.7
+13	-	-	2673.1

The ohmic power in Torus-II varies drastically over the course of the various phases of operation. Since we begin from a post-preionization state, the plasma is only partially ionized ($\sim 10^{14}$ cm^{-3} He^{+1}). The toroidal plasma current is increased to ~ 200 A/cm^2 within

2 μsec and held at that value for an additional 2 μsec. The plasma resistivity is taken to be the classical (Spitzer) value. Instead of using a z_{eff} of 2 as before, we allow it to vary since we now can follow the ionization of all species in detail. This 4 μsec period is the z-pinch simulation. The toroidal field is reversed and heating begins. This is simulated by tripling the plasma current. More importantly, at this time, we switch to an anomalous resistivity. In Torus-II, since the heating is caused by poloidal edge currents which eventually dig into the plasma, the current density is actually much higher where $\nabla x\underline{B}$ is largest. Since we are dealing with a zero-dimensional model we must use an average or bulk plasma current density. The anomalous resistivity is modeled as described earlier. The current is ramped upwards over 2 μsec and then decays to its original value within $\sim$2 μsec. At the completion of the decay the anomalous resistivity is shut off. This marks the end of the heating phase. During the ensuing high beta tokamak state the resistivity is switched back to the classical form and the current density is kept at $\sim$200 A/cm^2. It is important to realize that as more is learned experimentally about Torus-II, these current/resistance-time profiles can be easily changed. The above is summarized in Figure III.7. Note that ohmic power plays the role of the plasma driving term just as boundary values for Ψ and χ did in the start-up calculation and initial conditions did in the one-dimensional diffusion calculation. The plasma response is described by the following loss terms.

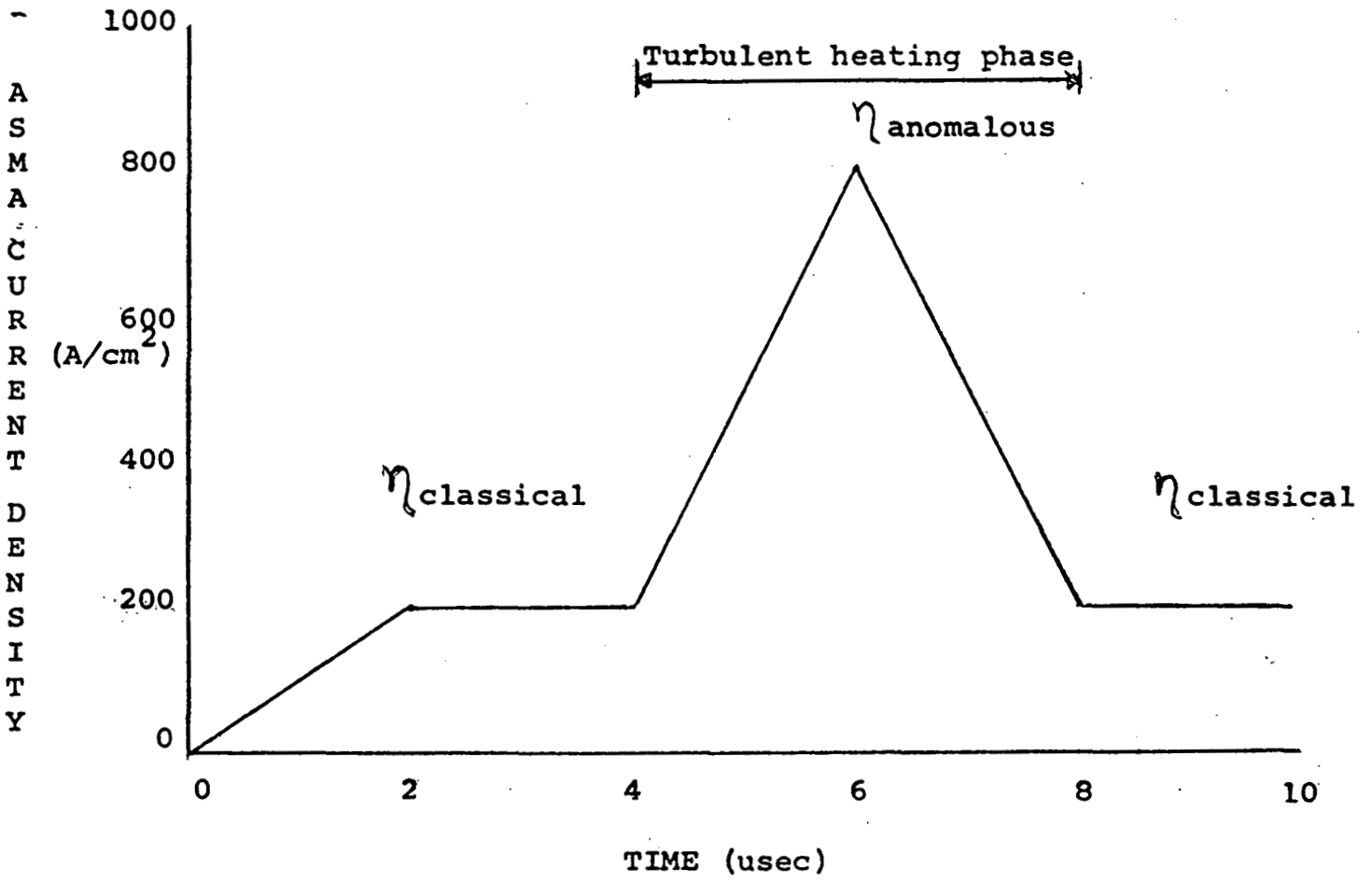

Figure III.7 **Typical plasma current programming for zero-dimensional simulation of Torus-II.**

The electron-ion energy exchange rate is computed using m_{He}, m_{Ox} and m_{Si} in equation II.3.14. This term alone is not sufficient to explain the ion heating observed in Torus-II. It has been included in the calculation since it can be important during the high beta state. Ion heating is modeled through equation II.3.22. Using experimental results[9], we can express this term as

$$P_{heat} = 2.5 \times 10^{-3} Z_{eff} T_e n_i^{3.5} \frac{eV}{cm^3\text{-sec}} \qquad \text{III.3.2}$$

This term is included in the ion energy equation only during the heating period. It is set equal to zero during the z-pinch and high beta phases. This is done simply because the above term represents heating from the scattering of ion-acoustic oscillations by the ions. This effect has been observed only during the turbulent heating phase.

In the electron energy equation, bremsstrahlung radiation is included. The crucial losses during the z-pinch and initial portion of the heating phase are due to the ionization of the helium, oxygen and silicon. At low temperatures recombination losses are important. The primary loss mechanism during the high beta state is the line radiation of the impurity elements, oxygen and silicon. For completeness, helium line radiation losses have also been included. In Table III.3 we list the line transitions considered, the transition energies and corresponding oscillator strengths.

Table III.3

Line Transition Data[30,31]

	ΔE (eV)	f
He^{0}	21.2	.276
He^{+1}	40.8	.416
Ox^{0}	10.7	.105
Ox^{+1}	15.9	.551
Ox^{+2}	16.0	.628
Ox^{+3}	14.7	.657
Ox^{+4}	12.6	.530
Ox^{+5}	12.0	.196
Ox^{+6}	561.0	.813
Ox^{+7}	653.0	.416

Table III.3 (continued)

	ΔE (eV)	f
Si^{0}	4.9	.625
Si_{+1}	9.8	3.620
Si_{+2}	9.6	3.956
Si_{+3}	8.9	1.605
Si_{+4}	104.6	.211
Si_{+5}	49.9	.330
Si_{+6}	44.9	.740
Si_{+7}	39.0	.443
Si_{+8}	35.8	.335
Si_{+9}	47.9	.539
Si_{+10}	33.7	.402
Si_{+11}	281.0	2.025
Si_{+12}	-	-
Si_{+13}	-	-
Si		

Other important effects in Torus-II are those due to transport losses. Long time constants (∿1 msec) are prescribed in equations II.3.19 and II.3.21 during the z-pinch and high beta tokamak states. However, a short time constant (∿10 μsec) is prescribed during the heating phase in equation II.3.20 due to the turbulence present at that time. These effects should not be written-off so readily. It is difficult to quantify the time constants properly. For this reason the accuracy of our calculations decreases over long times. We do not expect much difficulty over the early times.

The atomic physics calculations are very useful in solidifying earlier MHD work. The zero-dimensional code is the only one capable of describing the z-pinch phase. It has helped to answer the following questions. When is the helium fully ionized? How much power,

designed to heat the plasma, is lost in ionizing helium? How can this be corrected? What are the principal loss mechanisms? What are the time dependent (as opposed to steady-state, coronal model) radiation losses? What are the necessary ohmic power inputs to achieve high beta? Perhaps the most important question of all to be answered is, can we burn through the oxygen and silicon radiation barriers to get to interesting temperatures?

IV) RESULTS AND CONCLUSIONS

The results of the Torus-II simulation are presented here as follows. First we describe the z-pinch predictions of the zero-dimensional atomic physics code. Next, we discuss the heating phase results from the MHD codes with inertia and the zero-dimensional code. We then follow the plasma into the high beta state and give the results of the one-dimensional transport code. In each case, we relate the results to the important questions raised earlier. After describing the present machine operation, recommendations are made for an improved experiment.

1) The Torus-II Z-Pinch Phase

The initial conditions for this simulation are listed in Table IV.1.

Table IV.1

Initial Conditions for Z-Pinch Phase

Ion Temperature	.5 eV
Electron Temperature	.5 eV
Helium (neutral)	9×10^{14} cm^{-3}
Helium (+1)	1×10^{14} cm^{-3}
Oxygen (neutral)	2×10^{13} cm^{-3}
Silicon (neutral)	1×10^{13} cm^{-3}

The preionization phase does not heat the plasma appreciably, thus the low starting temperatures. Typical dirty impurity concentra-

tions of 1% silicon and 2% oxygen (SiO_2 from the pyrex wall) are used. Two cases are run. The current is increased to its maximum value within 2 μsec and held fixed for an additional 2 μsec. The current densities chosen correspond to z-pinch plasma currents of 20-40 kA. Figure IV.1 shows the slight heating of the electrons and ions. At a temperature of ∿5 eV, the ionization and recombination rates of helium are comparable. Therefore, we see no appreciable ionization of helium at this time. By the end of the 4 μsec period only 17% of the oxygen content is singly ionized while ∿80% of silicon is singly ionized. Radiative losses are not important during this phase. The primary limitation of this calculation is that no other code can help to supply the much needed ohmic power input as accurately as possible, thus, we depend upon some uncertain experimental results. It suffices to say that a significant number of neutrals are present as we begin the heating phase, a very undesirable condition. The above description of species evolution is illustrated in Figure IV.2.

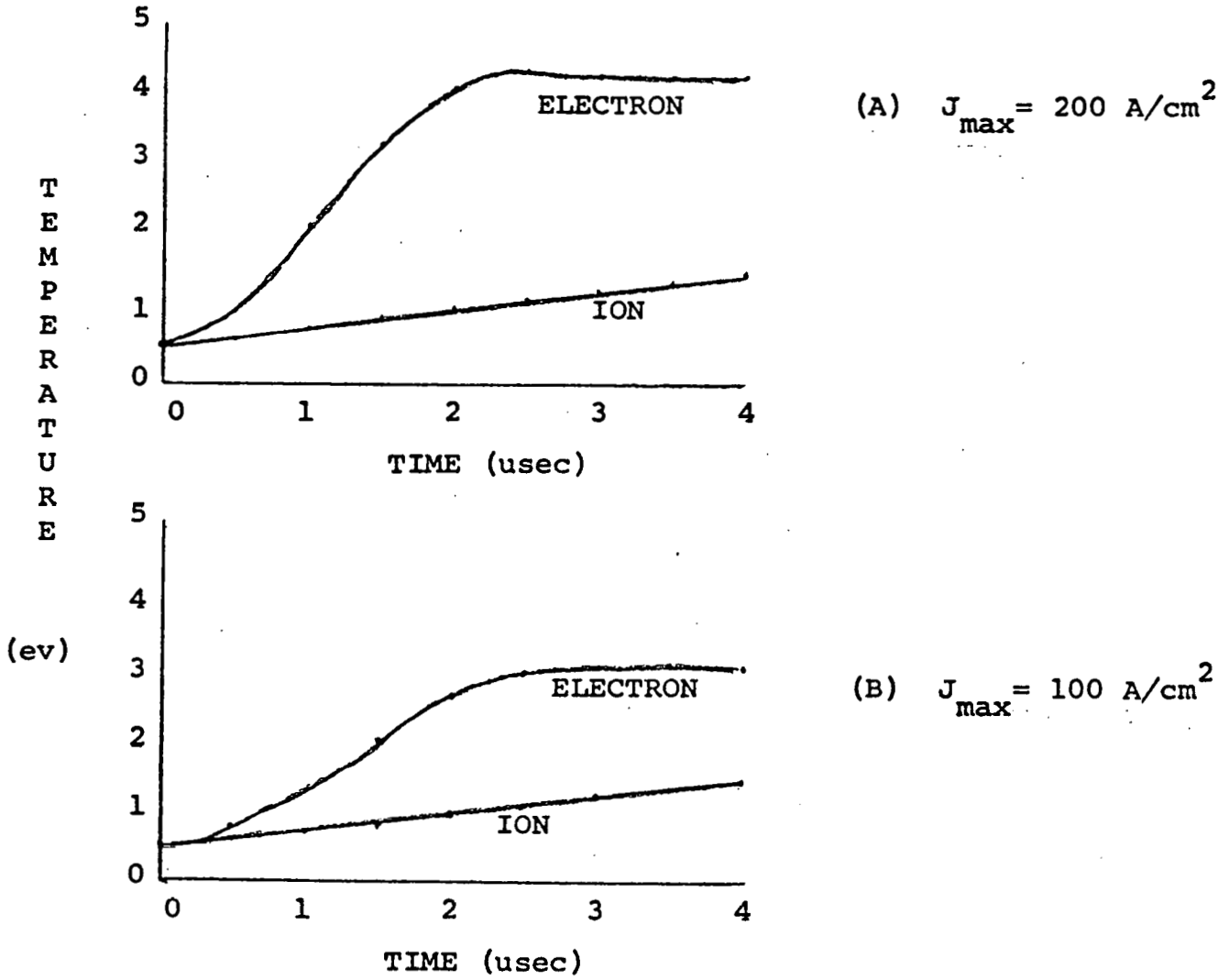

Figure IV.1
Computed electron and ion temperatures from zero-dimensional code for Torus-II z-pinch phase.

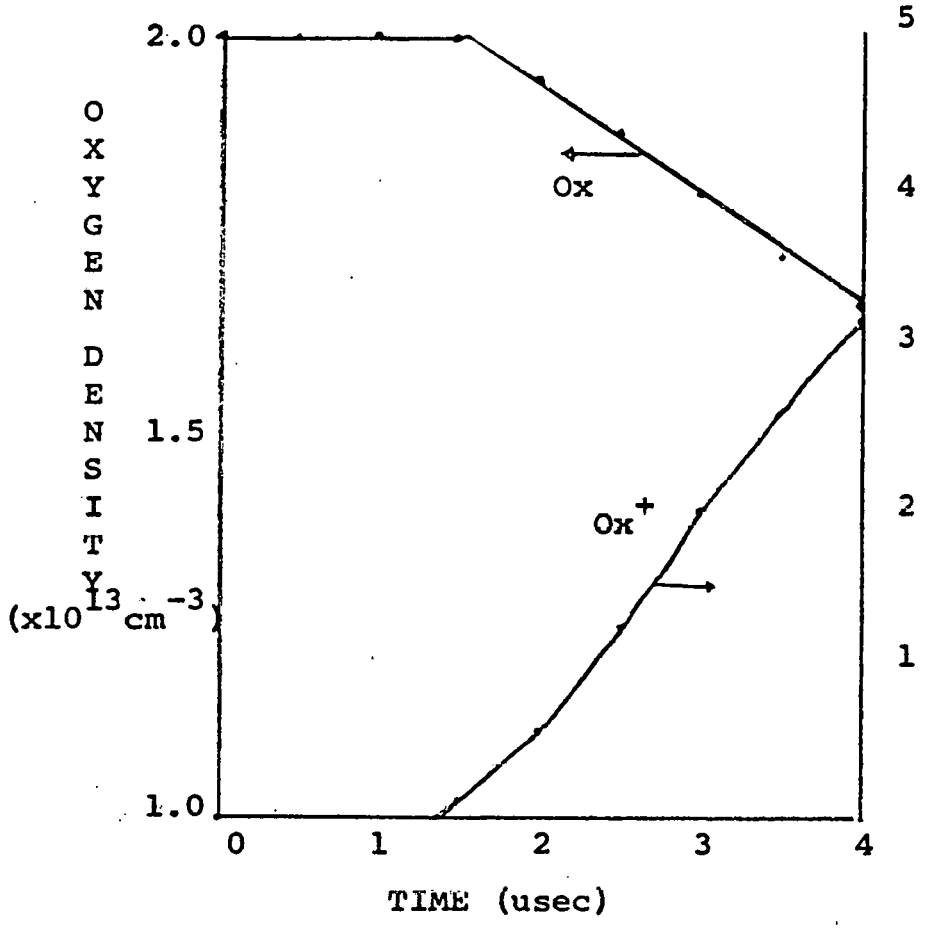

(A)

$(x10^{12}\ cm^{-3})$

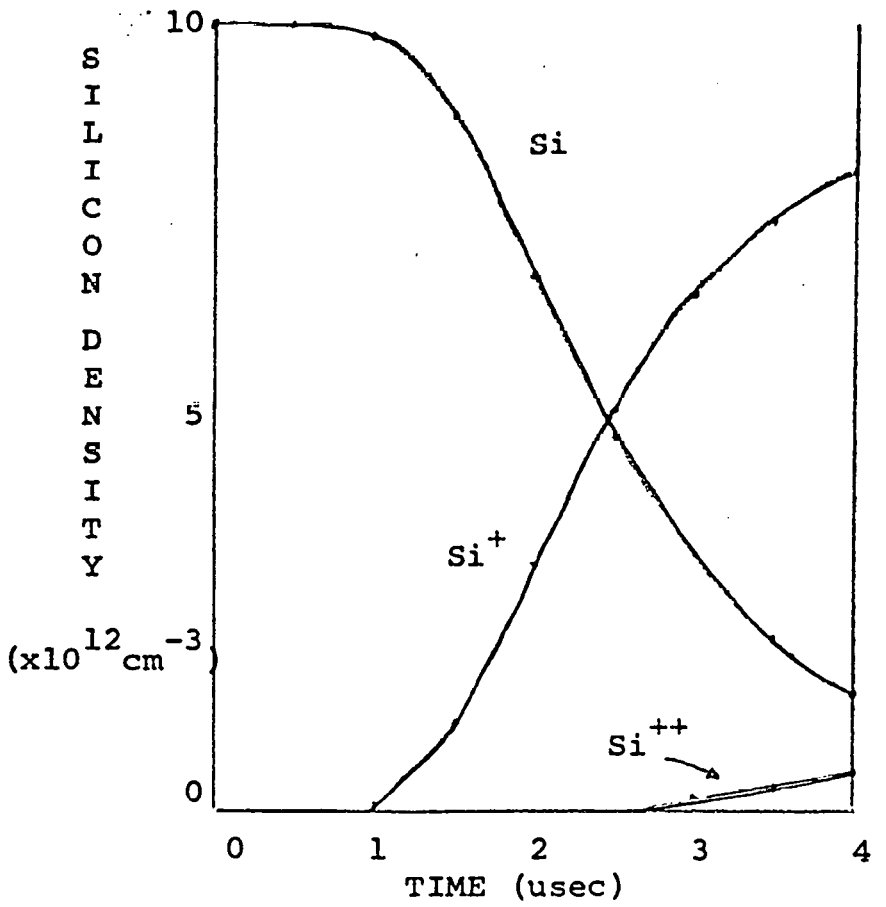

(B)

Figure IV.2
Ionization of impurity species during Torus-II z-pinch phase. Peak current density is 200 A/cm^2.

2) The Torus-II Heating Phase

2.A) One-Dimensional Heating Study

To this point little has been said of the one-dimensional MHD equations with inertia. This study is performed to define appropriate boundaries in parameter space for Torus-II. One of its many important results was that a high beta plasma with excellent radial equilibrium can be obtained using the heating scheme of Torus-II. The fast reversal of the toroidal magnetic field leads to poloidal electric fields consistent with the scaling of the anomalous resistivity. Typical inputs and results are given in Table IV.2.

Table IV.2

Heating Simulation (1-D)

Inputs:

B_ϕ (r=22.5 cm) = 2670 G

$B_{vertical}$ = 200 G in hole

Linear ramp to ∿1 kG in vacuum vessel

$\sigma_{anomalous} \sim 8 \times 10^{12} \{\frac{1.5 \times 10^{13}}{J_{total}}\}$ sec^{-1}

$\kappa = 2.8 \times 10^6$ erg/sec/K/cm

$\Psi_{hole}(t=0) \sim 4\pi \times 10^5$ G-cm^2

$\Psi_{hole}(t=5\ \mu sec) \sim 8\pi \times 10^5$ G-cm^2

Results:

Temperature	∿	70 - 150 eV	$I_{\phi,plasma}$ ∿40-50 kA
Density	∿	1 x 10^{15} cm^{-3}	$B_{\phi,well}$ ∿20-60%
$\langle\beta_\phi\rangle$	∿	40%	

The simplicity of solution of the MHD equations in one dimension allows for extensive probing of parameter space without consuming excessive computer time. Indeed, the various methods described in chapter III which are used to simulate the Torus-II heating phase are all direct results of exhaustive numerical experiments performed with the one-dimensional code. For example, different anomalous resistivity models, different switching on and off of the anomalous and classical resistivities, the effects of variable thermal conductivity, different filtering techniques of numerical oscillations in the low density regions, varying the flux in the hole and other effects were all tested using the one-dimensional calculation. Using the values for various plasma parameters obtained from the 1-D code, the two-dimensional simulation is performed with emphasis on the proper modeling of boundary conditions.

2.B) Two-Dimensional Heating Study

(i) Quarter Power Simulation

By coupling Coils, EFFI and the MHD equations, several important characteristics of the plasma state are understood. The coil geometry is directly responsible for the greatly elongated, high beta plasma and its subsequent evolution. Using the initial conditions described earlier we follow the plasma heating for 6 μsec. First consider the quarter power case. Important inputs are summarized in Table IV.3.

Table IV.3

Quarter Power Input Summary

Case number	1	2	3
Ψ_{hole}(V-sec)	.020	.020	.027
Ψ_{outer}(V-sec)	.014	.021	.025
Ψ_{top}	$.8\Psi_{hole}$	$.8\Psi_{hole}$	$.9\Psi_{hole}$
Variation in z	z^8	z^4	z^8
τ_{loss}	∞	∞	∞

The results of case 1 and case 2 differ in that the plasma currents at 6 μsec are 66 kA and 80 kA respectively. The magnetic axis of case 1 is shifted approximately 1 cm to the right of the magnetic axis obtained in case 2. All other results are identical. To maintain a manageable number of figures, no graphs of case 2 are included. The implications of the similarity of cases 1 and 2 are as follows. Since plasma current has increased substantially by changing the poloidal flux contributed by the outer toroidal windings, we can conclude that the coupling between the plasma and these windings is strong. Indeed it is absurd to refer to such windings as the "vertical field" coils since they play a significant role in inducing the toroidal plasma current. This effect is not as pronounced as expected since the flux variation along z is such that the flux (z^4) leakage is more spread out in case 2. This implies that the plasma as a whole does not see as much flux as it would if the leakage was restricted to the corners (z^8). Another important conclusion is

that the heating of the Torus-II plasma must be caused by poloidal plasma currents. This is obvious since the plasma temperature is the same for both cases eventhough the toroidal currents are quite different.

Now we compare case 1 with case 3 since these are noticeably different. Consider Figures IV.3 and IV.4. (Note: We will try to give details in our discussions and use graphs only to illustrate the key points. This is done to keep the number of graphs manageable.) At 1.5 μsec both cases exhibit some loss of plasma to the top of the vessel. By 2 μsec we observe a much broader plasma for case 3 while at 3 μsec the two are equally wide. At 4 μsec, note that a fairly well confined, hot plasma has formed in both cases. At 6 μsec a substantial loss of plasma to the outer corners of the device is observed for case 1 while case 3 has maintained excellent confinement. So the plasma of case 3 remains squatter and better confined than that of case 1. This effect is also easily observed in Figures IV.5 and IV.6. Note that at all times there is a greater amount of flux towards the inside of the device for case 1 than for case 3. This is caused by the prescribed leakage flux which is greater in case 1 (20%) than it is in case 3 (10%). The result is a squeezing and elongating of the plasma. The effect is most evident at 2.5 μsec. Note the resulting shift in magnetic axis of 1.5 cm. This is clearly caused by the sizeable increased amount of vertical field programmed in case 3. The toroidal plasma current is 88 kA at 6 μsec for this

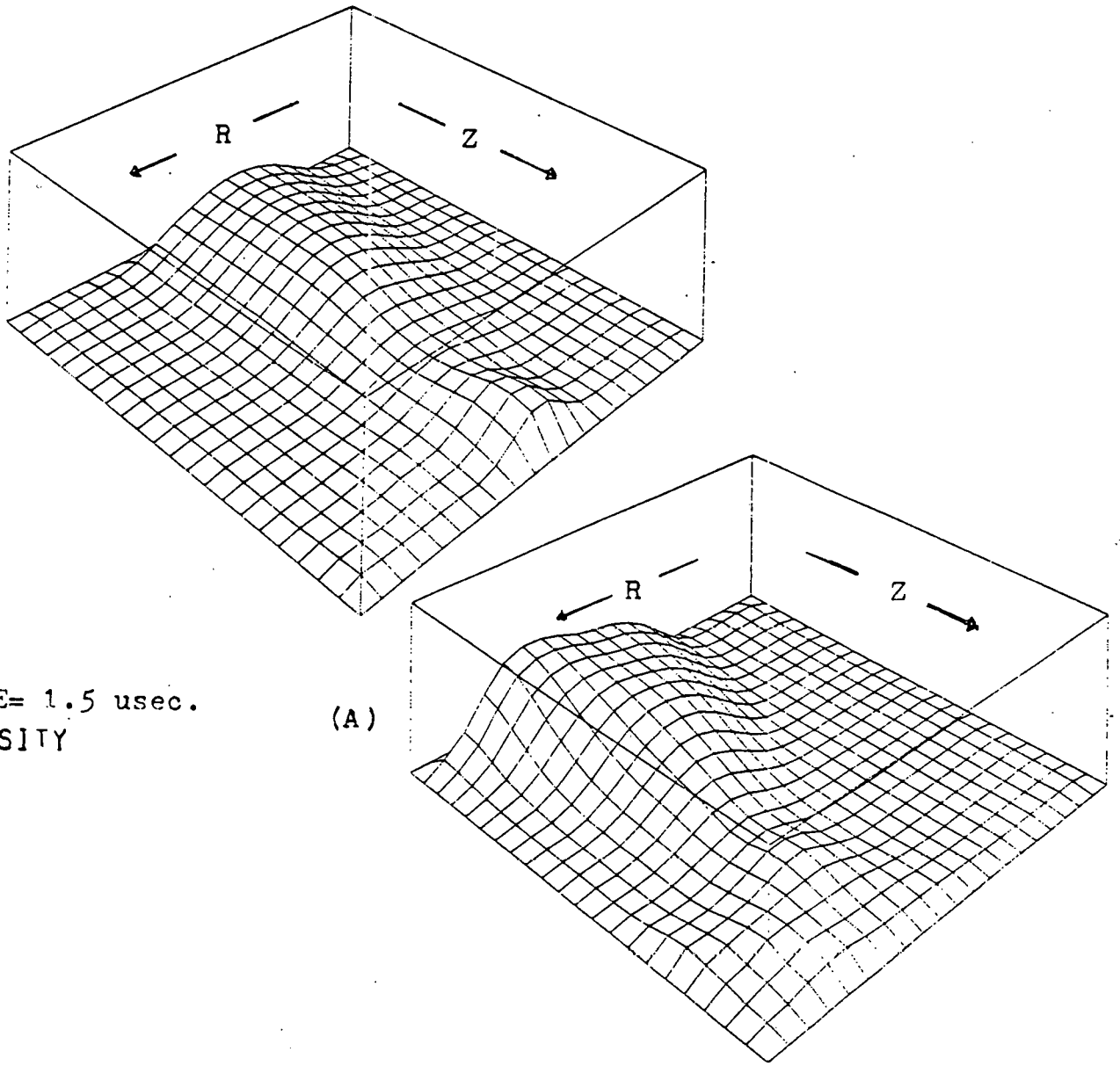

Figure IV.3. Density profile in upper half plane for heating case 1.

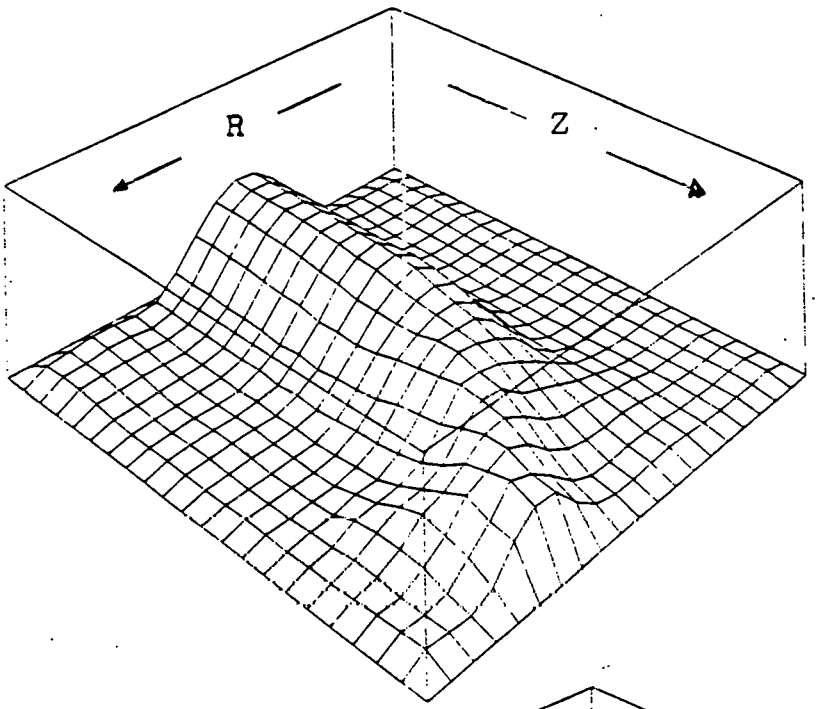

Figure IV.3.C

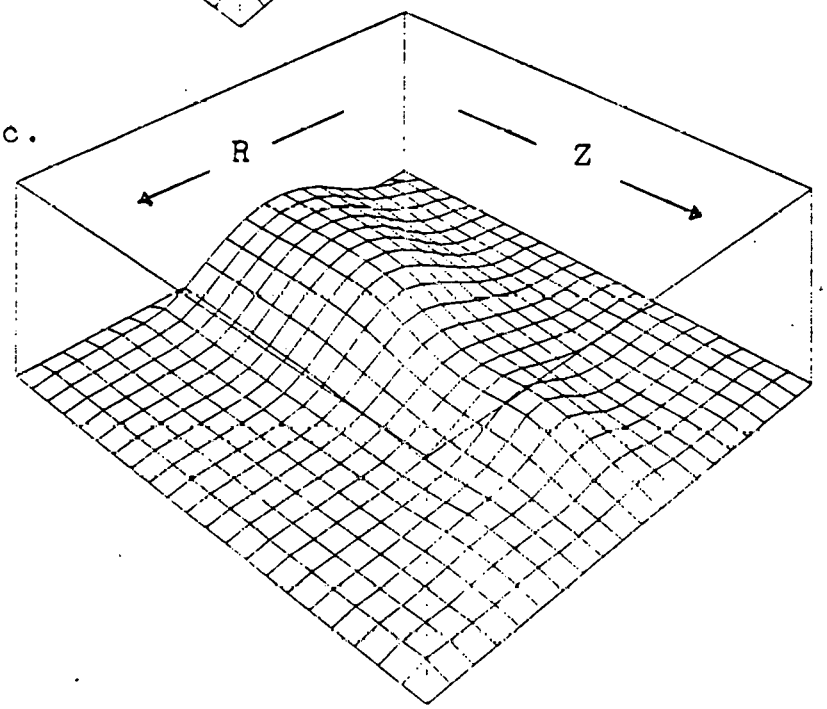

TIME=6.0 usec.
DENSITY

TIME=1.5 usec.
DENSITY

(A)

Figure IV.4. Density profile in upper half plane for heating case 3.

Figure IV.4.B

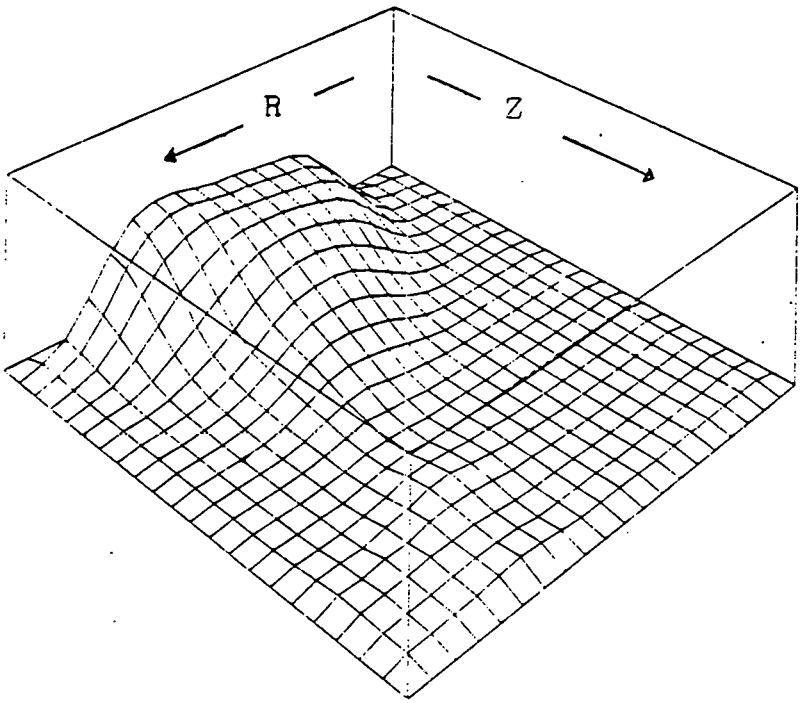

TIME=2.5 usec
DENSITY

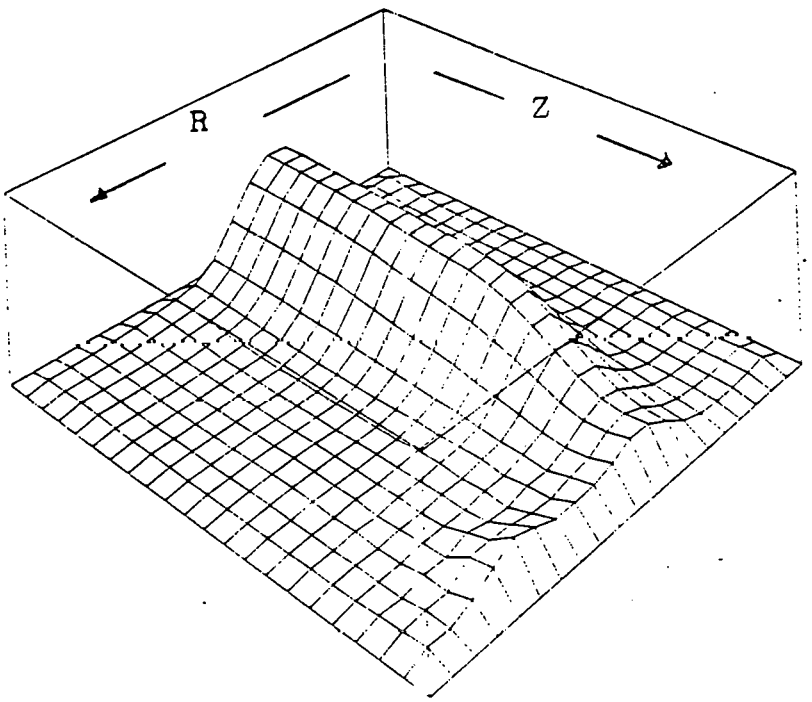

Figure IV.4.C

TIME=6.0 usec
DENSITY

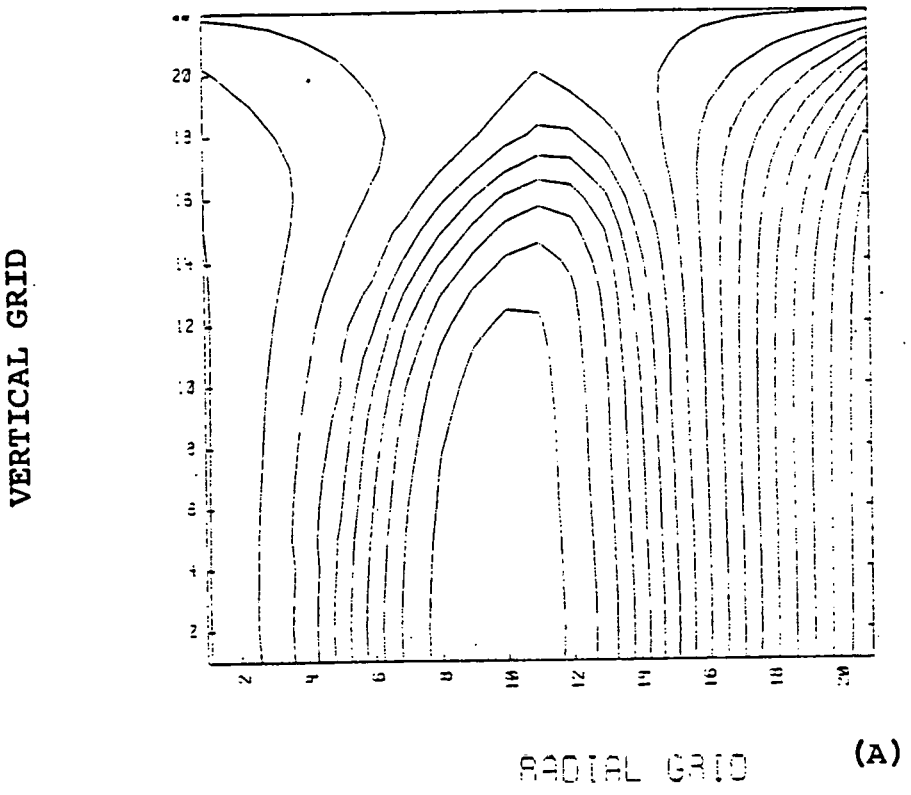

Figure IV.5

Poloidal flux contours in upper half plane for heating case 1.

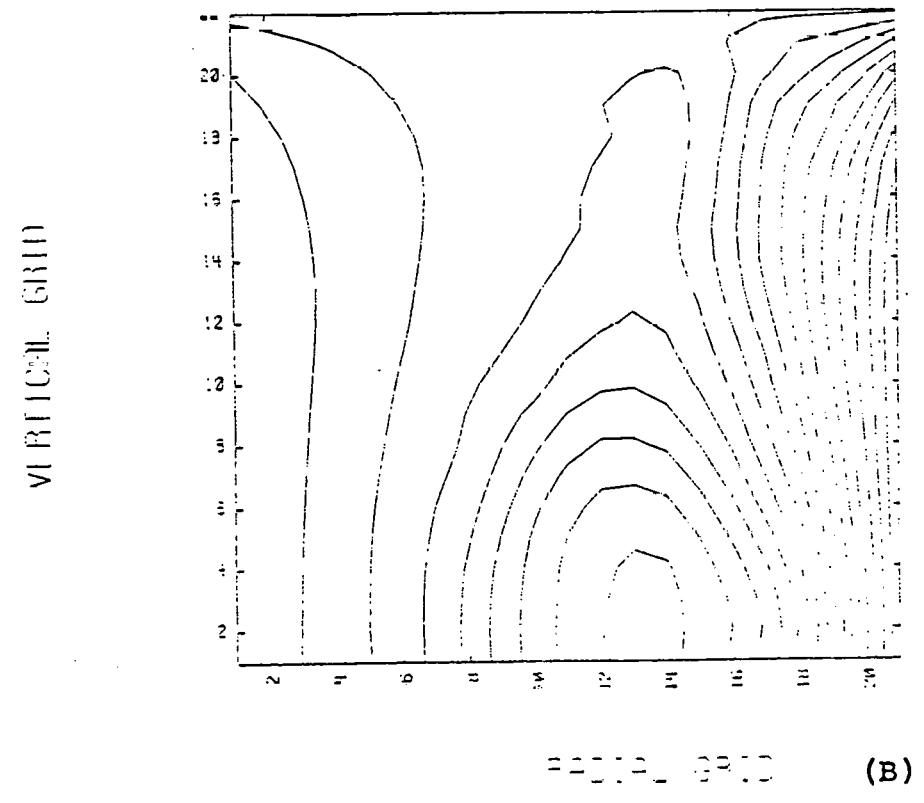

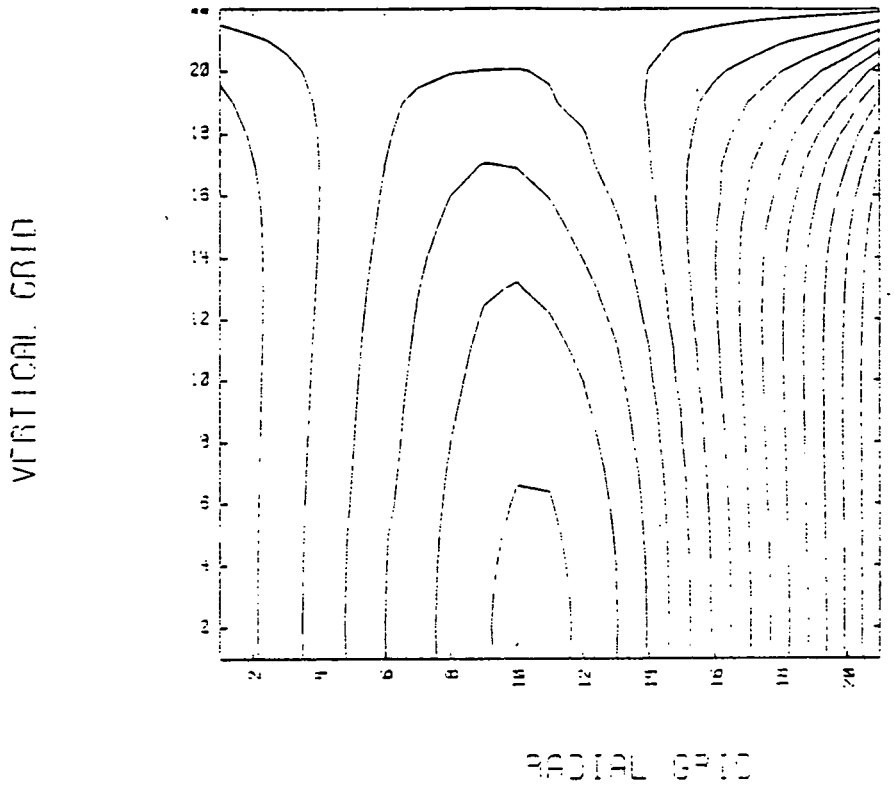

Figure IV.5.C

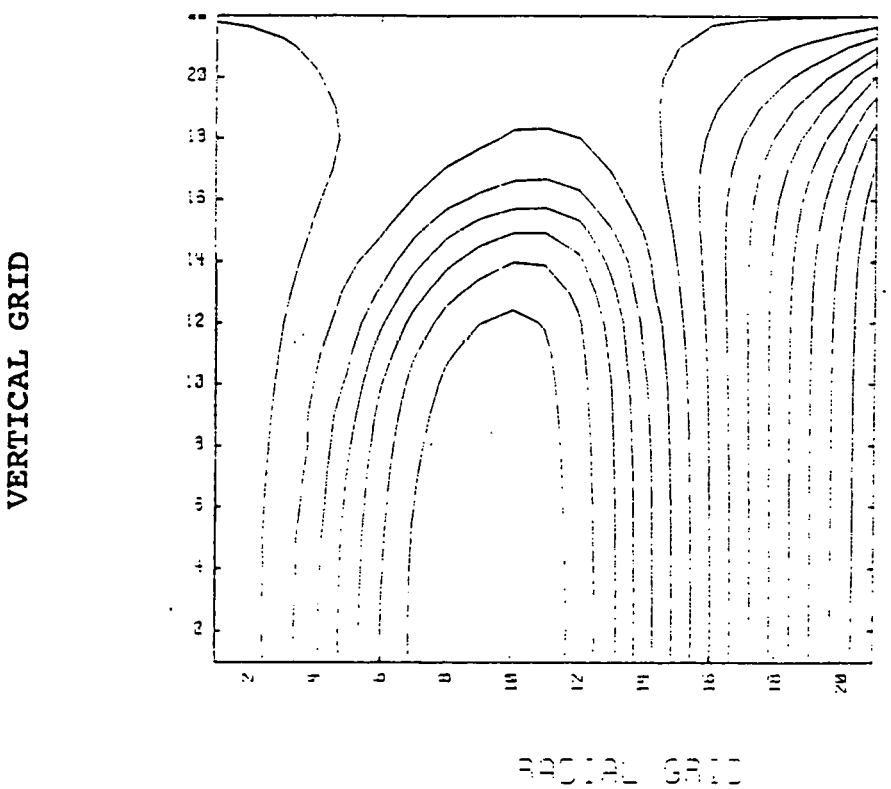

Figure IV.6

Poloidal flux contours in upper half plane for heating case 3.

(A)

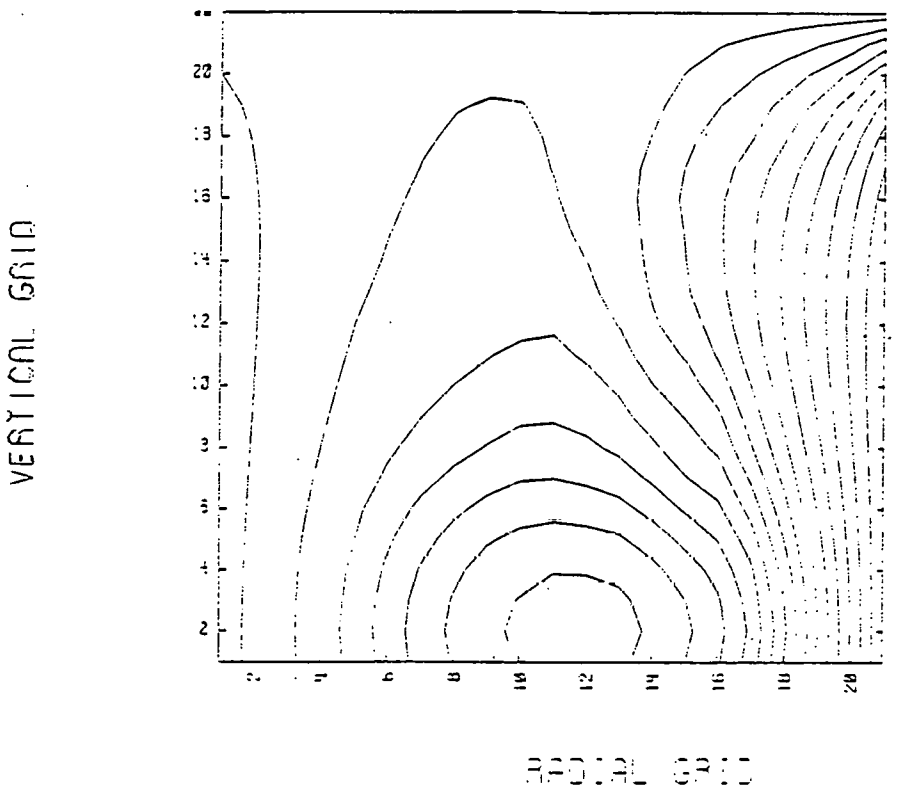

Figure IV.6.B

POLOIDAL FLUX
AVRG= 2.5 USED

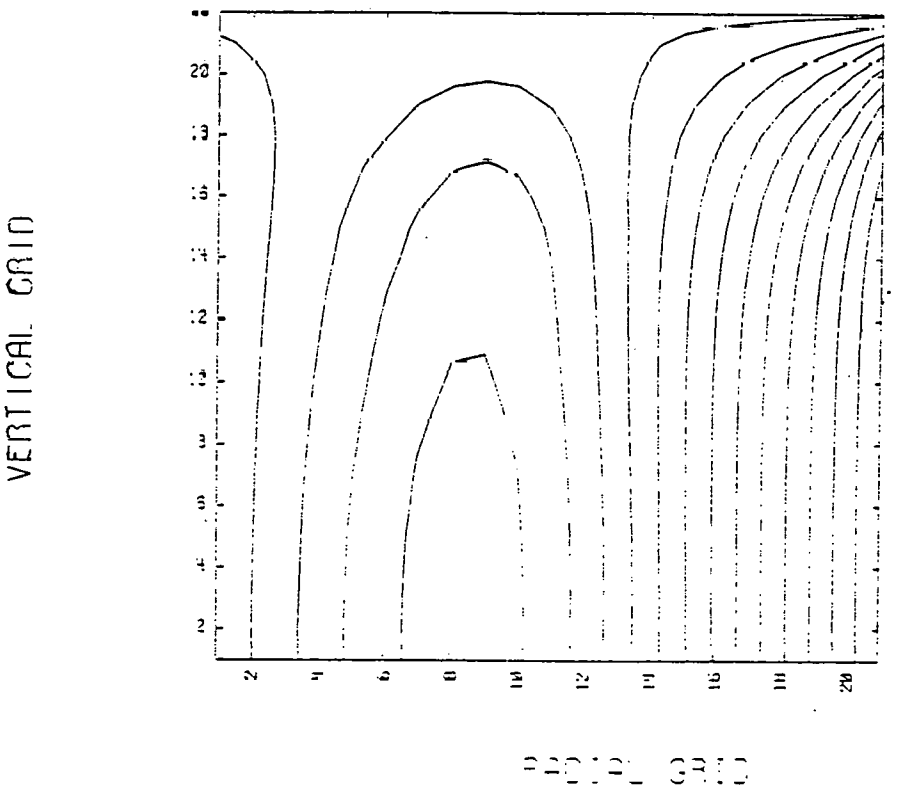

Figure IV.6.C

POLOIDAL FLUX
AVRG= 5.0 USED

same case. At the risk of over emphasizing a point, Figures IV.7 and IV.8 also point to a squatter, better confined current profile for case 3. Note the loss of current to the corners for both cases but the greater severity exists when the leakage is greater. To research this point further, simulations were performed with leakage fluxes of 40 - 60%. The result was that no plasma could be confined in such a system. Therefore, the leakage flux in Torus-II can be a problem if it gets too large.

Next, consider the plasma along the horizontal plane of symmetry, z=0. Figures IV.9 and IV.10 show that due to the better vertical confinement of case 3 it is always denser (and often broader) than the plasma of case 1. The usual plasma bouncing is also seen. Figures IV.11 and IV.12 indicate a slightly warmer plasma for case 3. At early times this is easily explained by the steeper gradients in B_ϕ which give rise to larger poloidal currents for case 3. Observe how the plasma edge is heated first and then the remainder of the plasma. These effects are due to the confinement scheme. Less leakage results in a greater plasma density along z=0. This in turn results in a deeper, more lasting $\partial B_\phi / \partial r$ which translates into a warmer plasma. Both cases have diamagnetic wells after the heating is completed. See Figures IV.13 and IV.14. The larger well for case 1 is expected since the plasma beta is higher than in case 3. (Same pressure but plasma is in lower B_ϕ region for case 1.) The toroidal field soak-in phenomena has been observed experimentally[9] on the same time scale as illustrated in Figures IV.13 and IV.14.

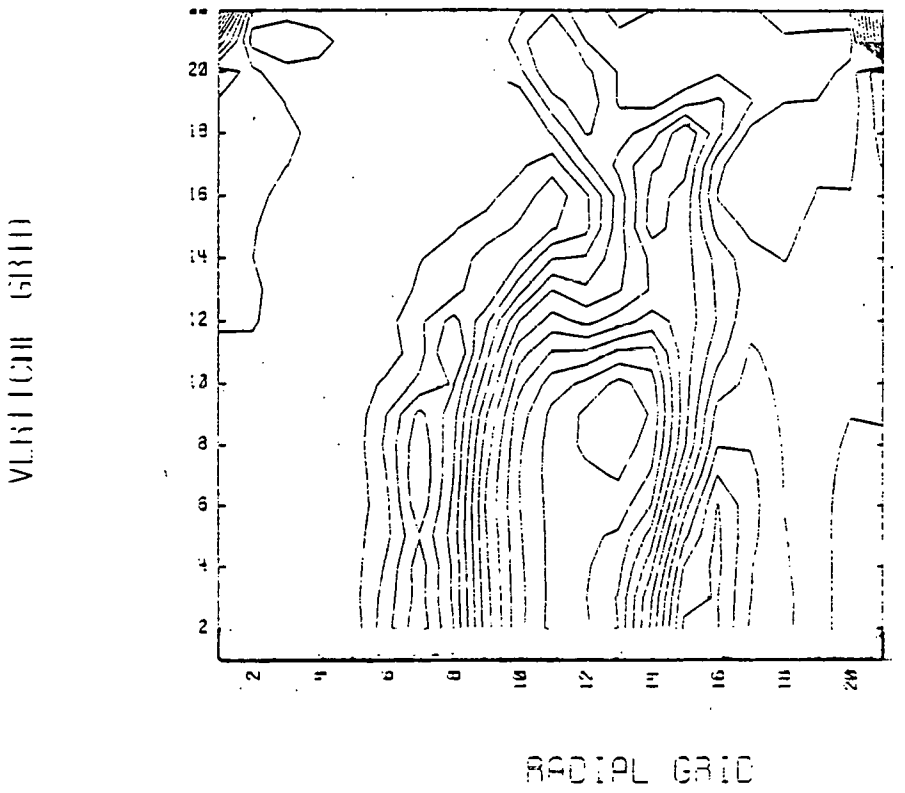

(A)

Figure IV.7

Toroidal current density contours in upper half plane for heating case 1.

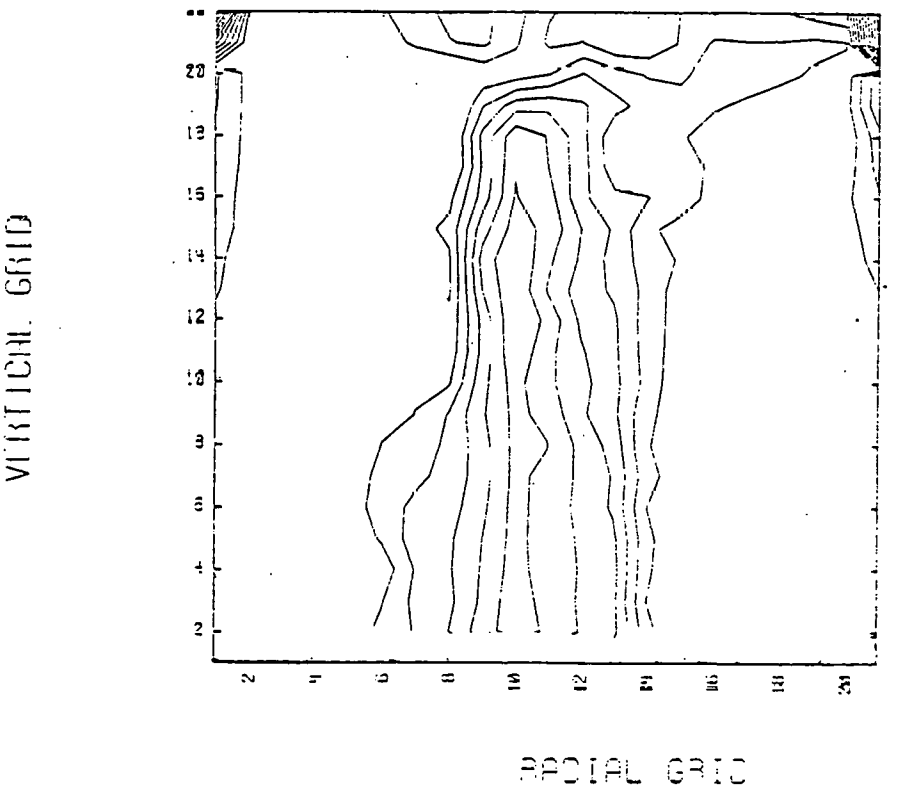

(B)

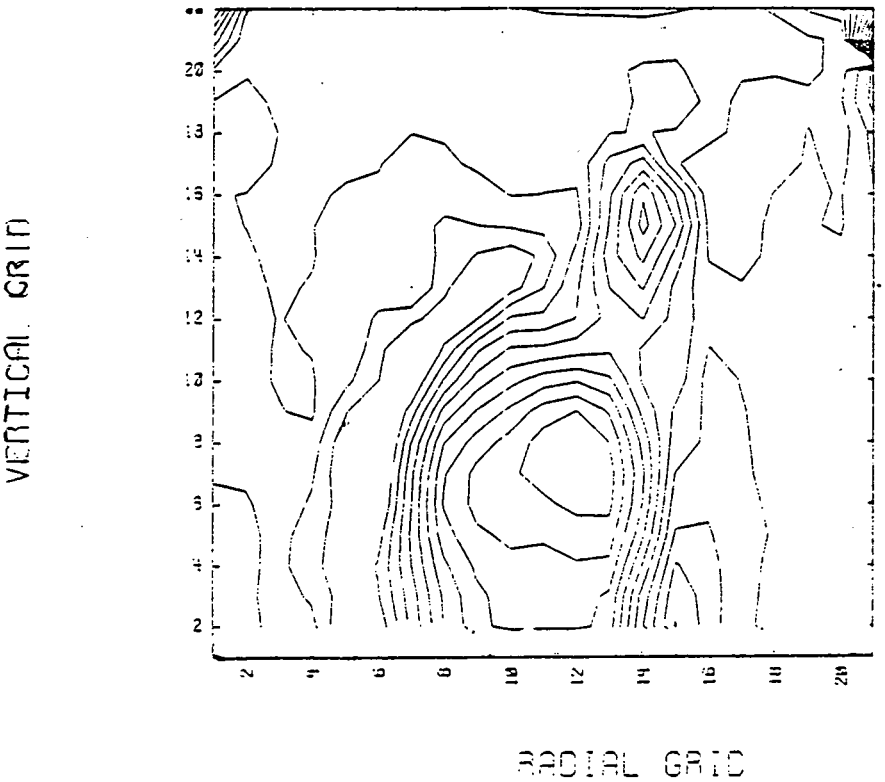

(A)

Figure IV.8

Toroidal current density contours in upper half plane for heating case 3.

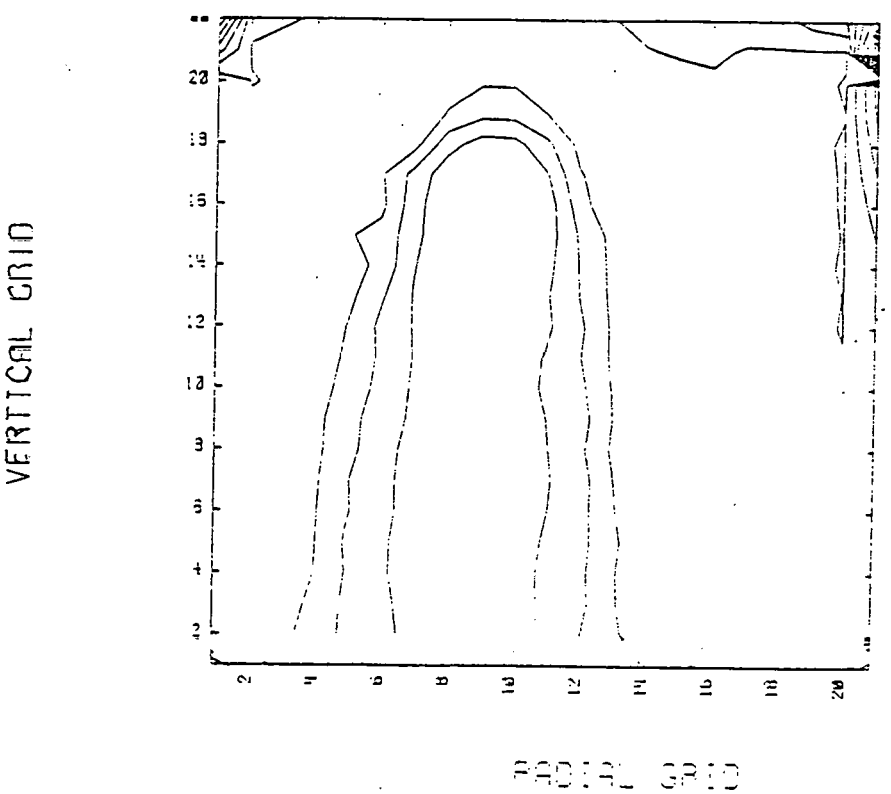

(B)

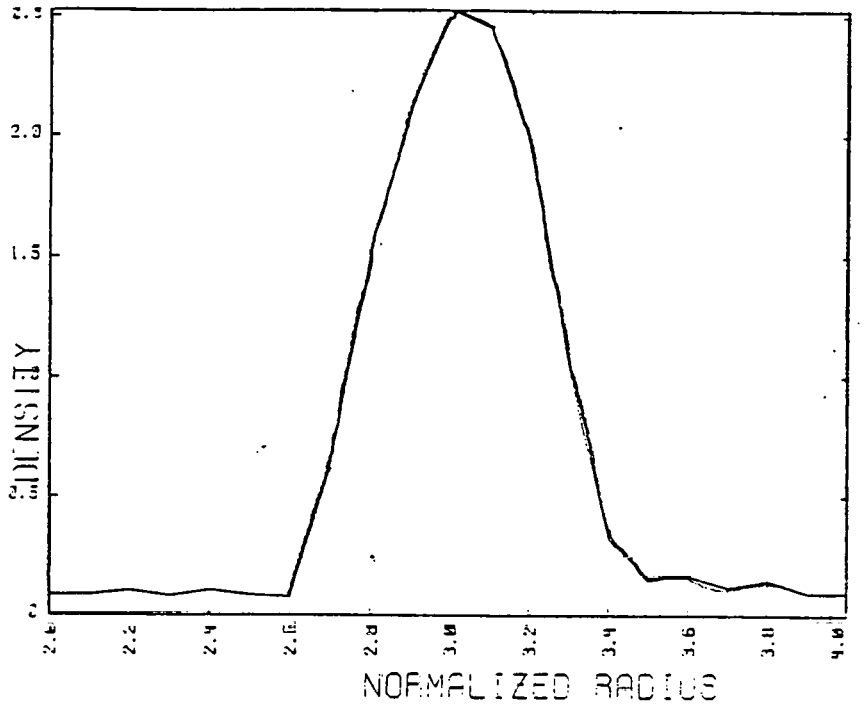

Figure IV.9

Plasma density profiles along horizontal mid-plane for heating case 1.

UNITS: NORMALIZED
TIME: 2.0 USED
VESSEL HALF-WIDTH=7.5 CM

(A)

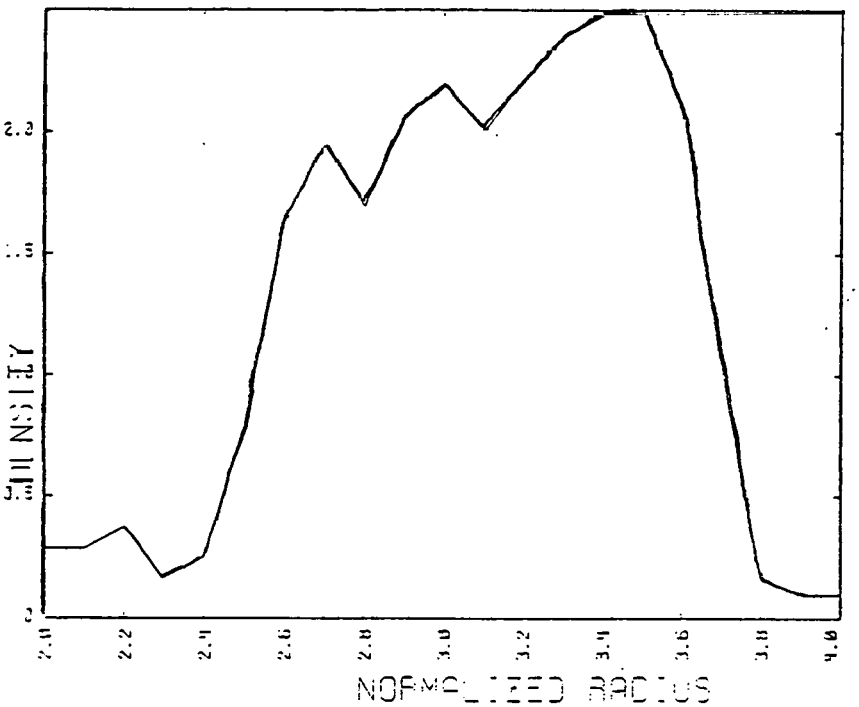

UNITS: NORMALIZED
TIME: 3.0 USED
VESSEL HALF-WIDTH=7.5 CM

(B)

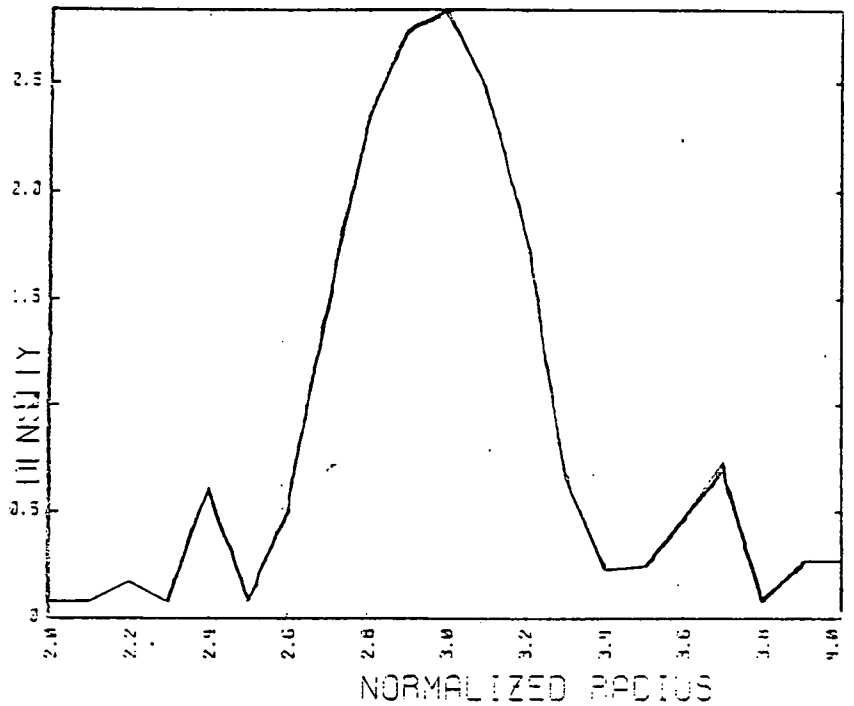

Figure IV.9.C

UNITS: NORMALIZED
TIME: 5.0 USEC
VESSEL HALF-WIDTH=7.5 CM

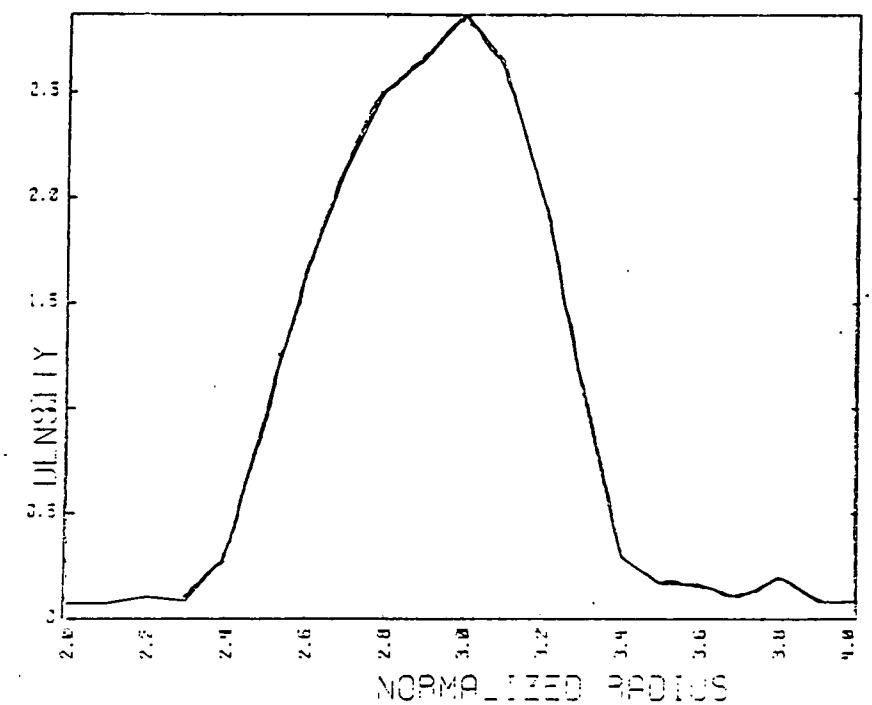

Figure IV.10

Plasma density profiles along horizontal mid-plane for heating case 3.

UNITS: NORMALIZED
TIME: 2.0 USEC
VESSEL HALF-WIDTH=7.5 CM

(A)

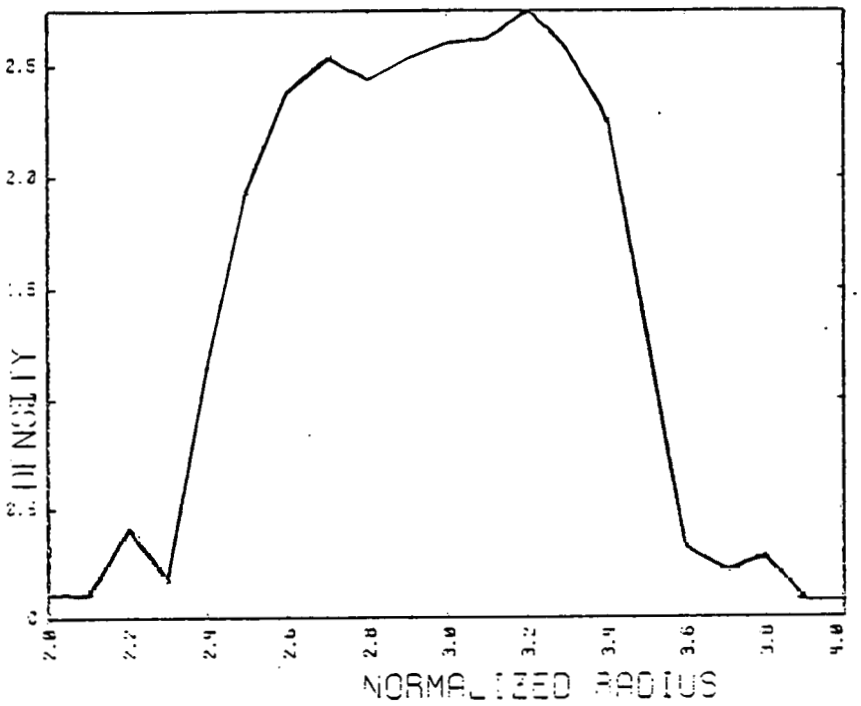

Figure IV.10.B

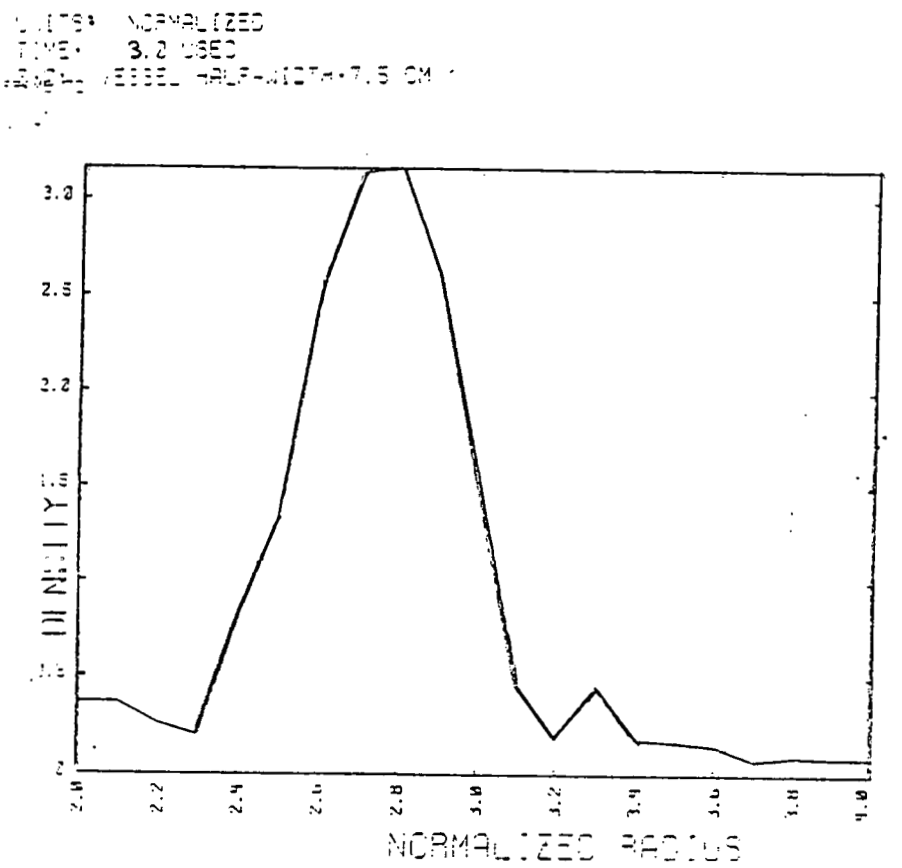

Figure IV.10.C

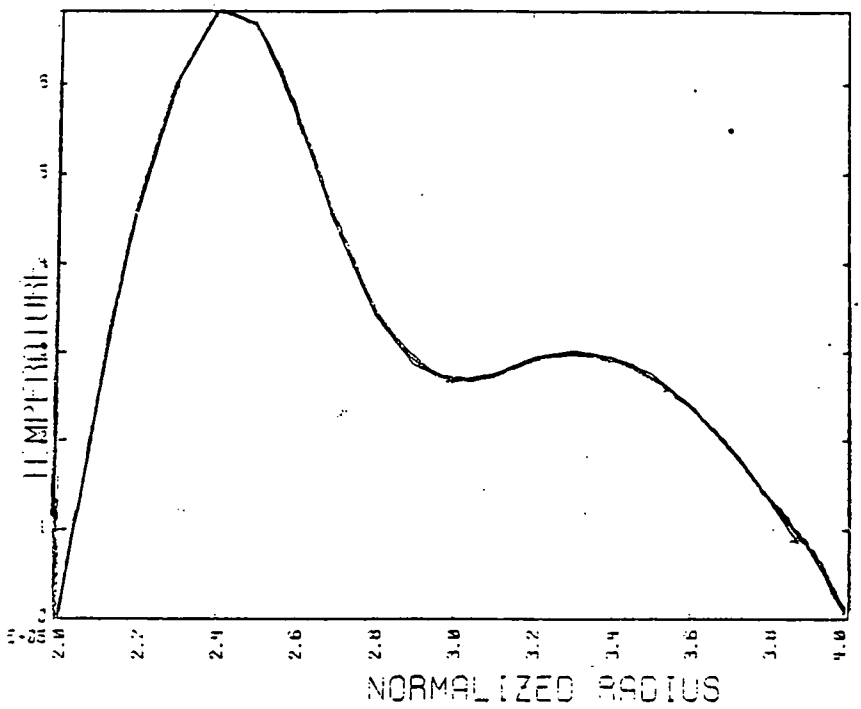

Figure IV.11

Plasma temperature profiles along horizontal mid-plane for heating case 1.

(A)

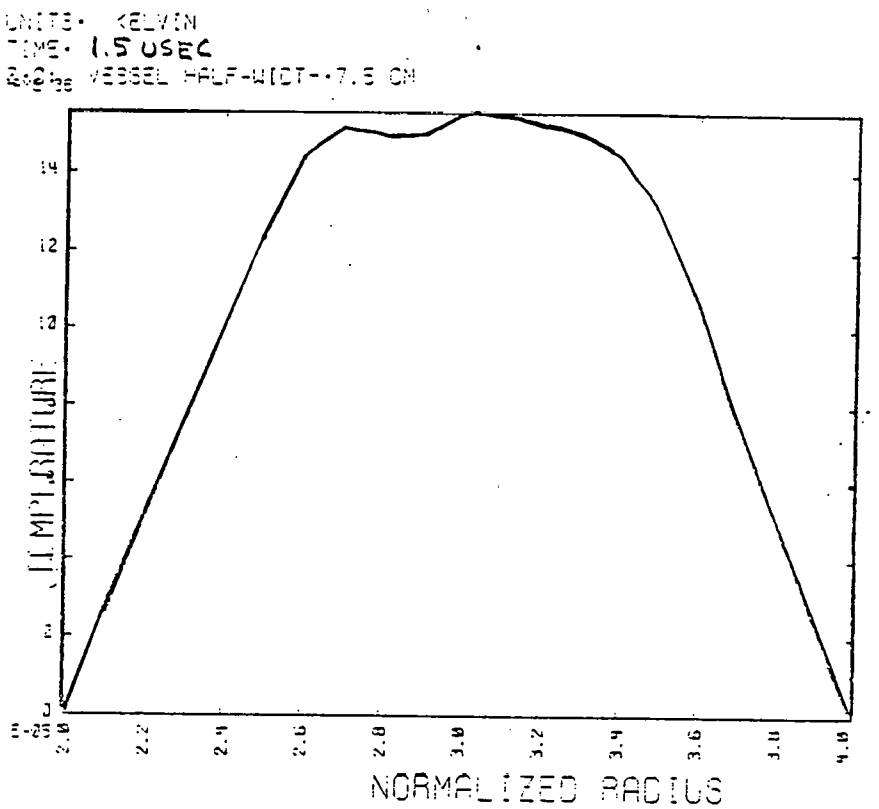

(B)

UNITS: KELVIN
TIME: 3.0 USEC

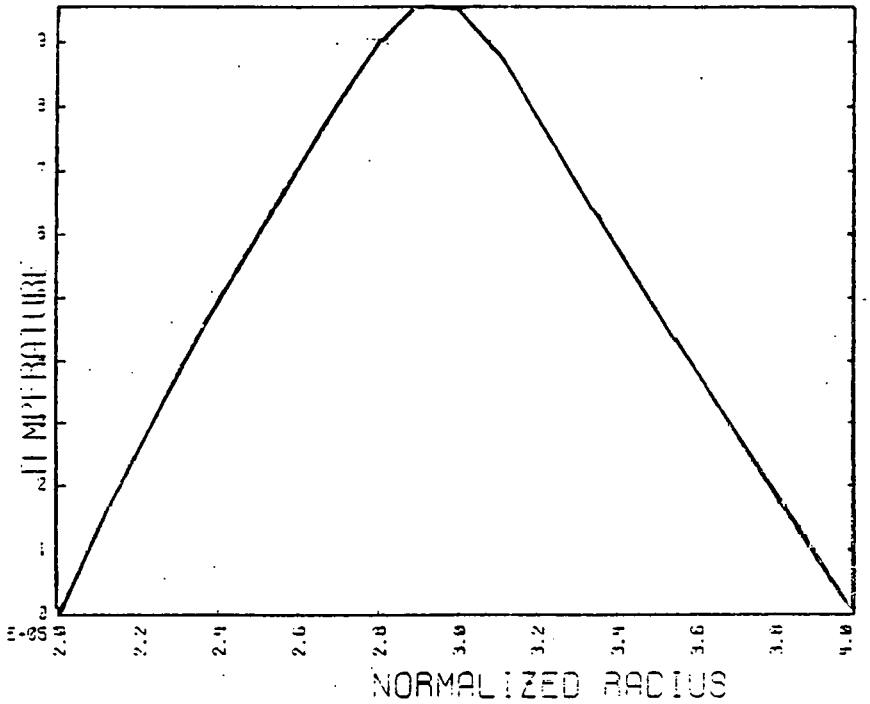

Figure IV.11.C

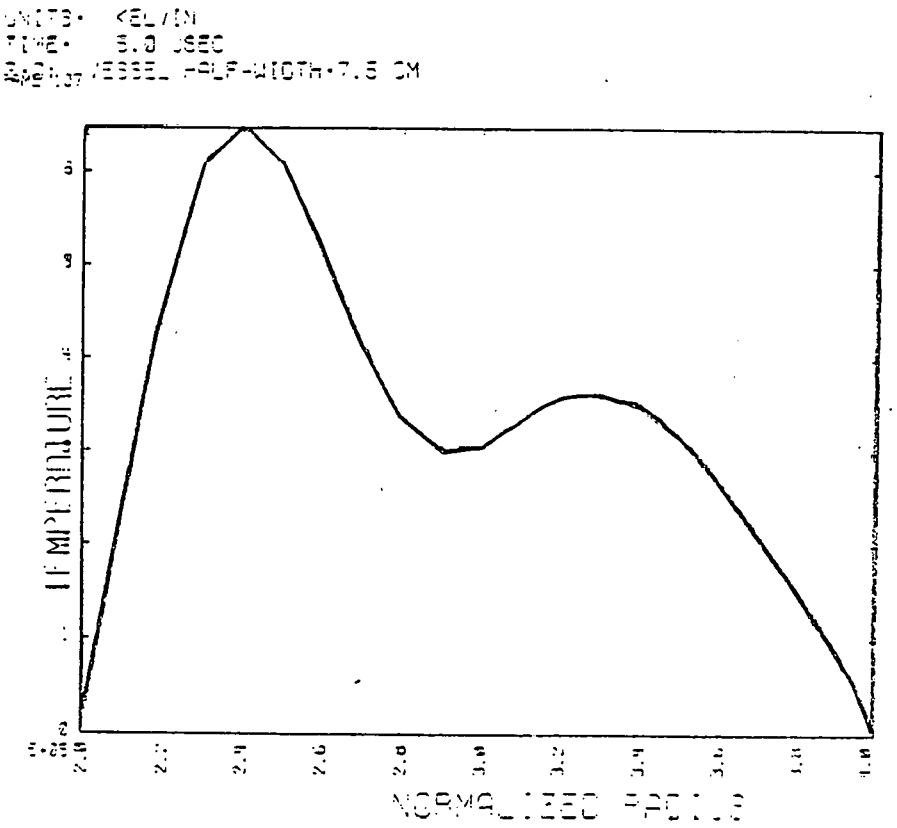

(A)

Figure IV.12

Plasma temperature profiles along horizontal mid-plane for heating case 3.

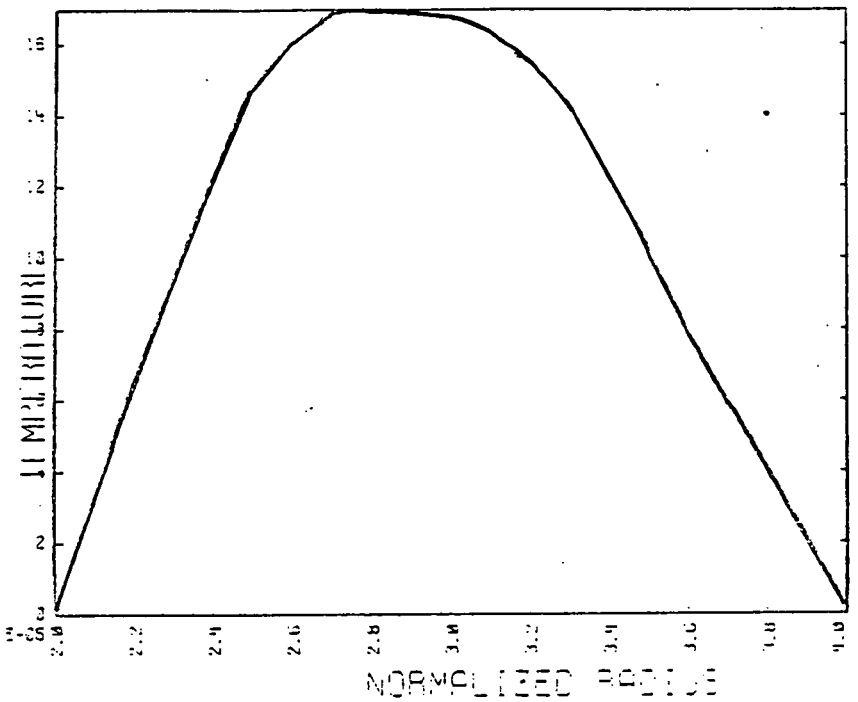

Figure IV.12.B

UNITS: KELVIN
TIME: 3.0 USEC
[illegible] VESSEL HALF-WIDTH=7.5 CM

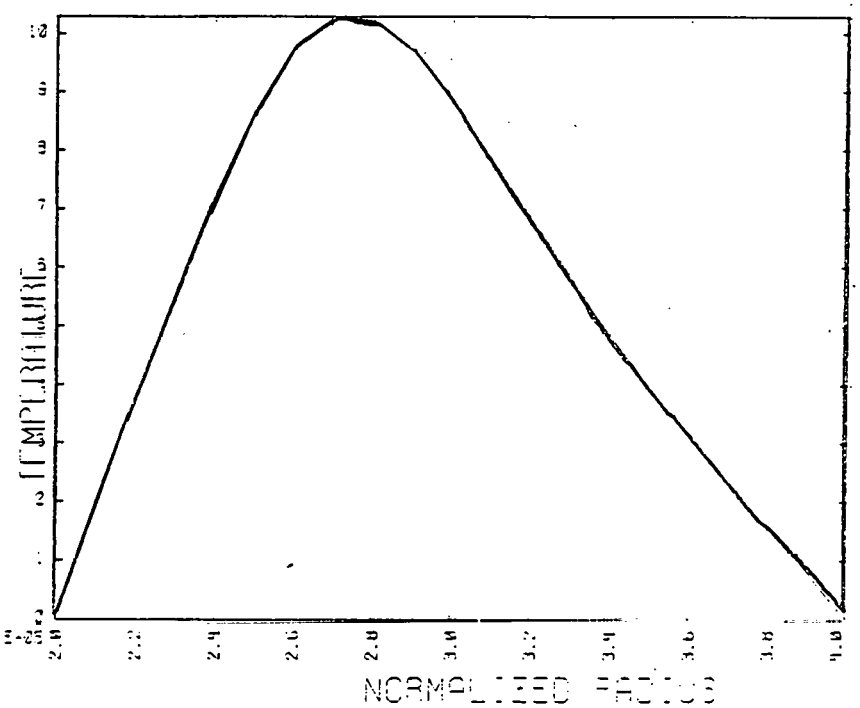

Figure IV.12.C

UNITS: KELVIN
TIME: 5.0 USEC
[illegible] VESSEL HALF-WIDTH=7.5 CM

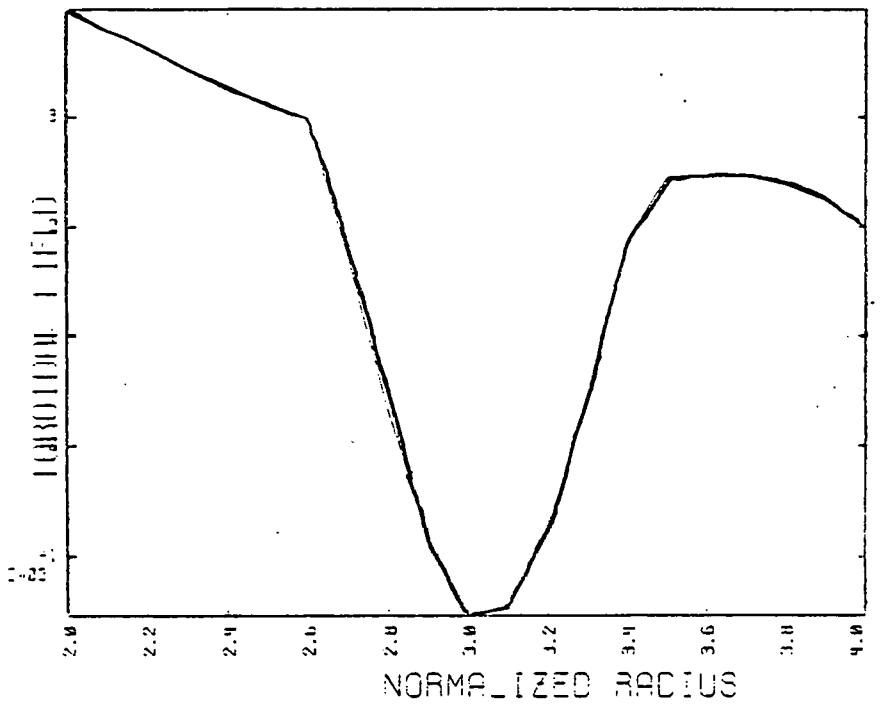

Figure IV.13

Toroidal field profiles along horizontal mid-plane for heating case 1.

(A)

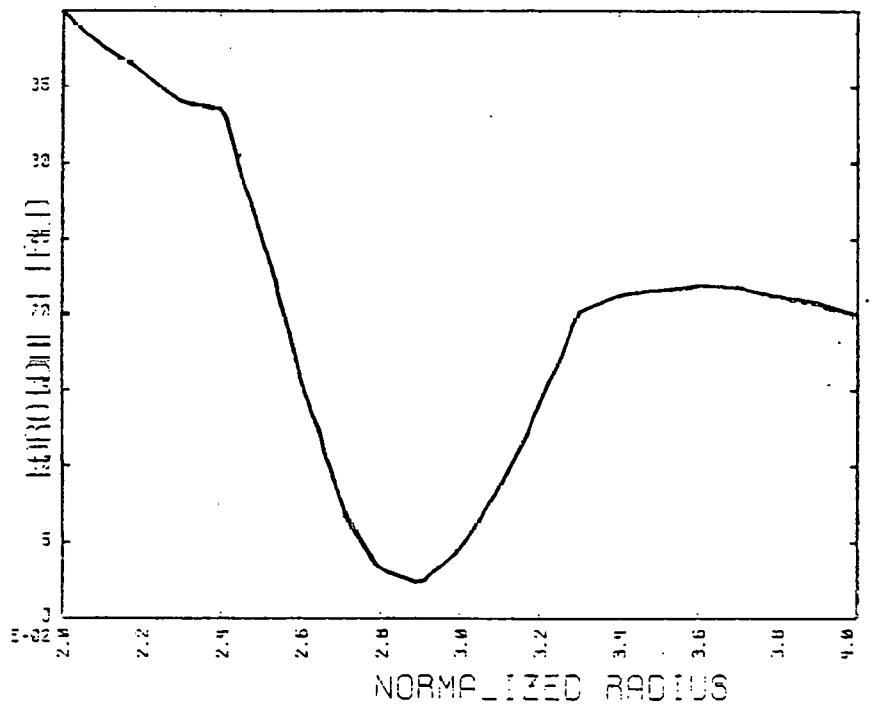

(B)

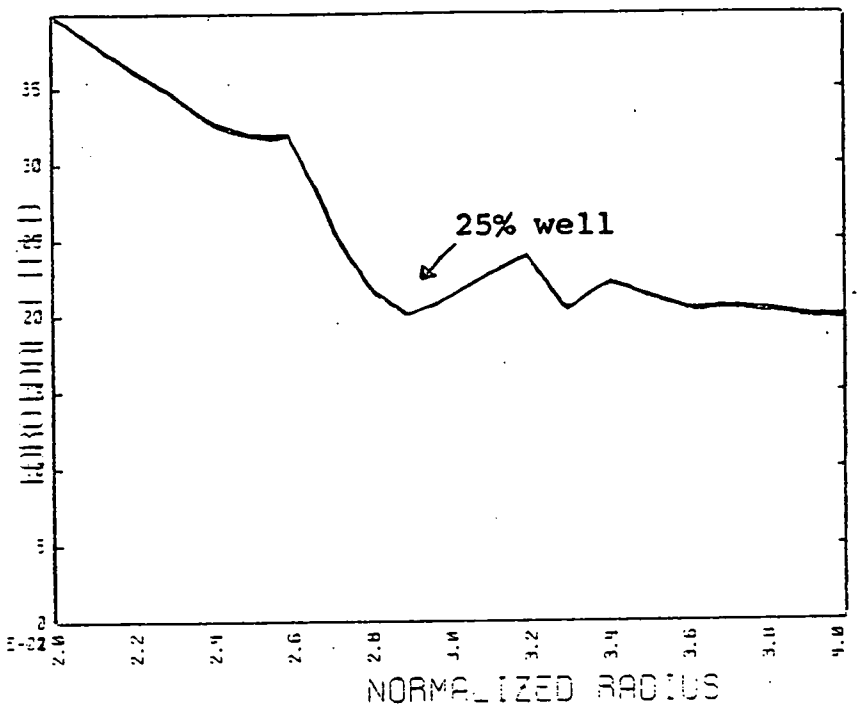

Figure IV.13.C

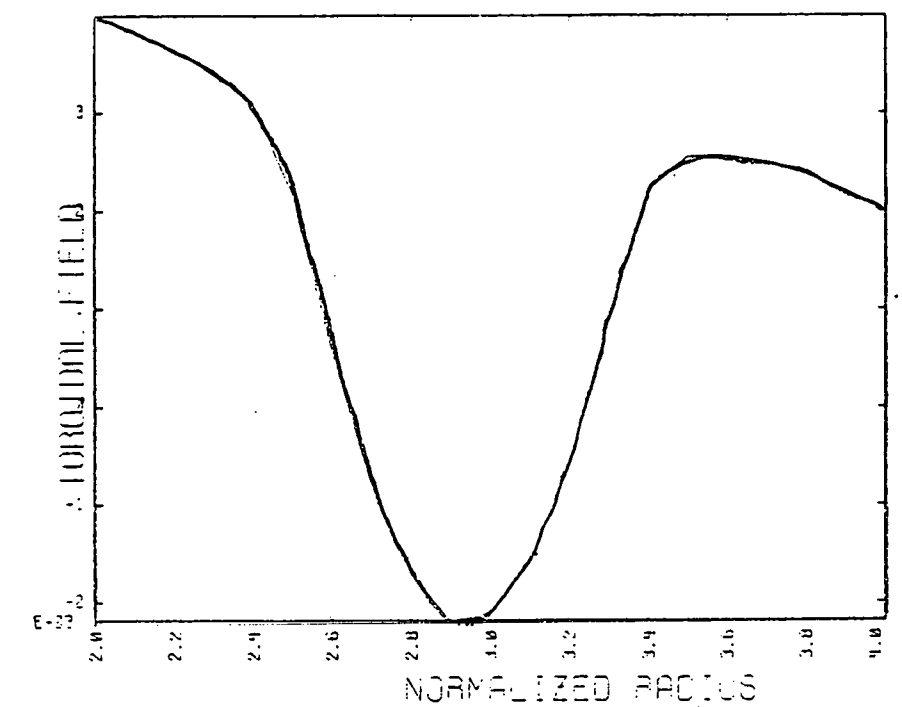

Figure IV.14

Toroidal field profiles along horizontal mid-plane for heating case 3.

(A)

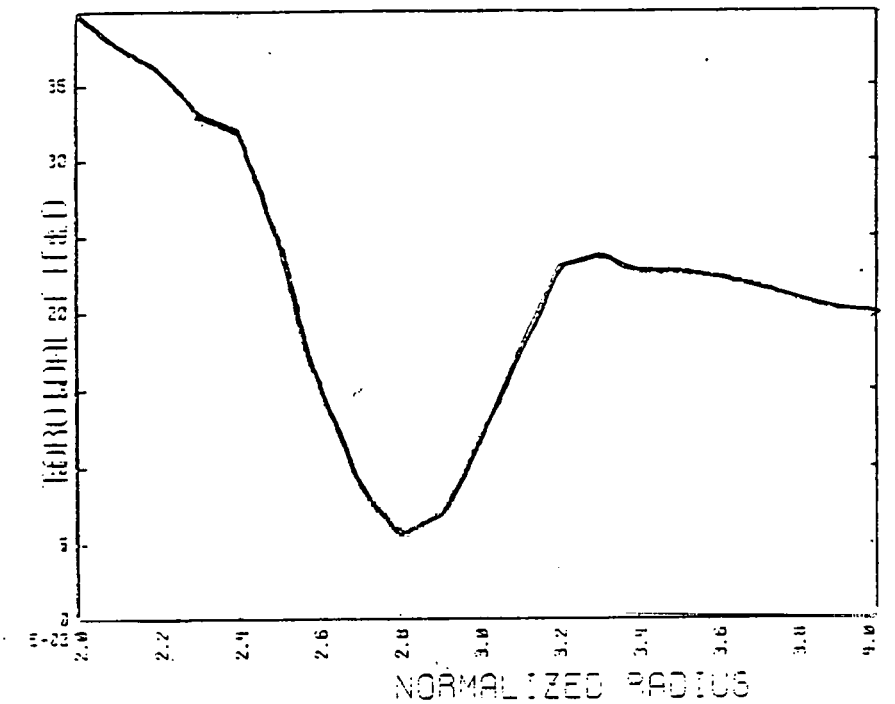

Figure IV.14.B

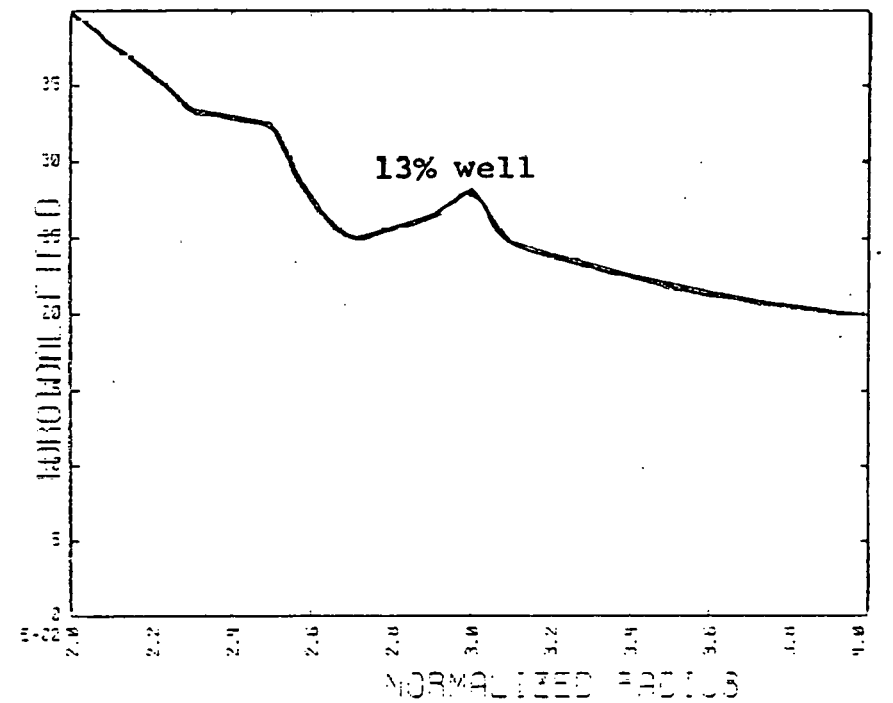

Figure IV.14.C

Analysis of Figures IV.15 and IV.16 indicates that the magnitudes of the toroidal current densities are the same for both cases, however, it is spread over a larger region in case 3 thereby resulting in a larger plasma current. Published experimental values of plasma current are ∿20 - 30 kA. At the time of this writing there was an expressed desire to obtain additional magnetic probe data to confirm such numbers. The most recent experimental data indicates that the plasma current may be as large as 90 kA during the heating phase. The 25 kA measurement was made 20 μsec after the toroidal field reversal. While lower values of plasma current have been simulated, we have never succeeded in heating to a plasma state with such low plasma currents. The codes do indicate a loss of current to the corners. Later we will discuss plasma flow patterns and "current shedding". Regardless of the magnitude of the plasma current obtained, its distribution along z=0 as a function of time is always characterized by an initial skin effect followed by a soak-in to a parabolic shape with marked current reversal on the plasma edge. The current then shifts and piles up on the outside. As the plasma returns and moves inward, the plasma current distributes itself parabollically again. Further detailed discussion will be presented in Chapter IV Section 2.B.ii. In Figures IV.17 and IV.18 we observe the compression of the poloidal magnetic field as the plasma moves towards the outside and its subsequent relaxation as the plasma returns inward. Note that the structure of B_z is the same in

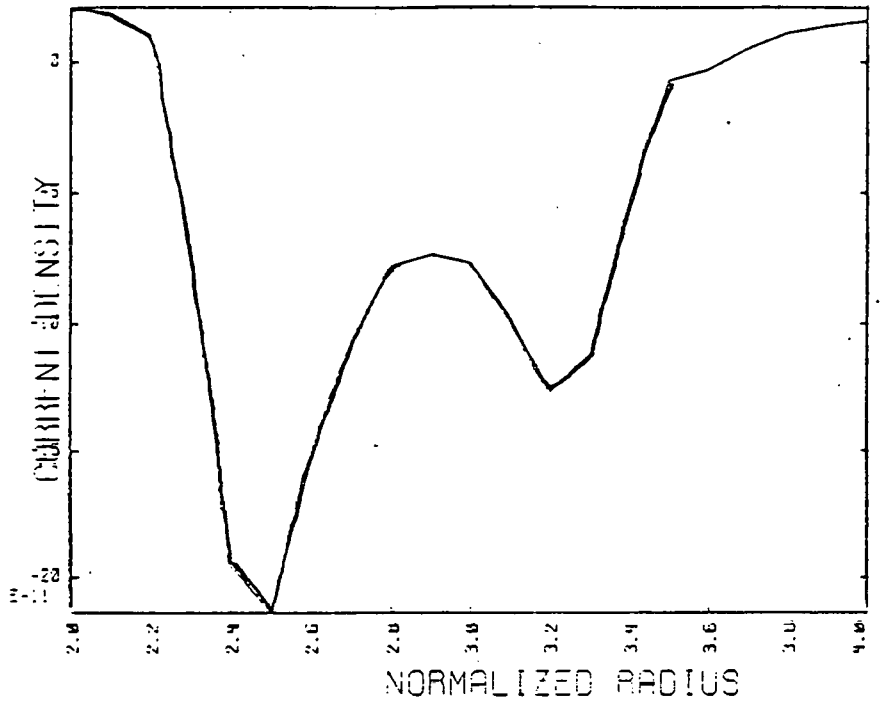

Figure IV.15

Plasma toroidal current density profiles along horizontal mid-plane for heating case 1.

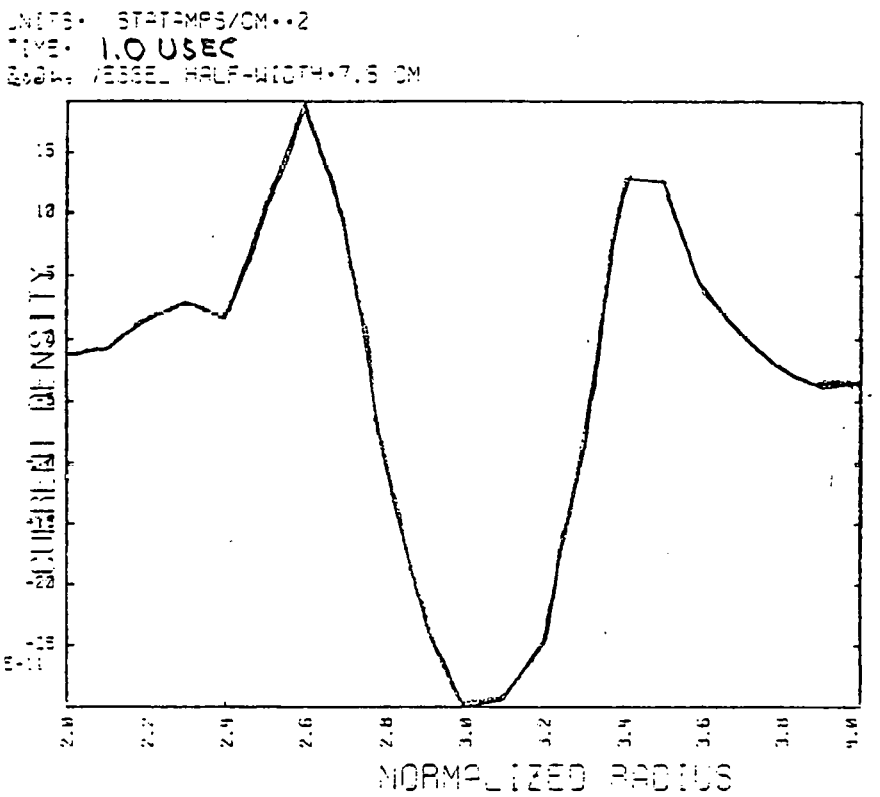

(A)

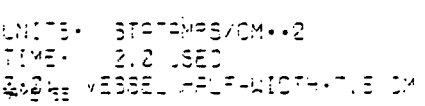

(B)

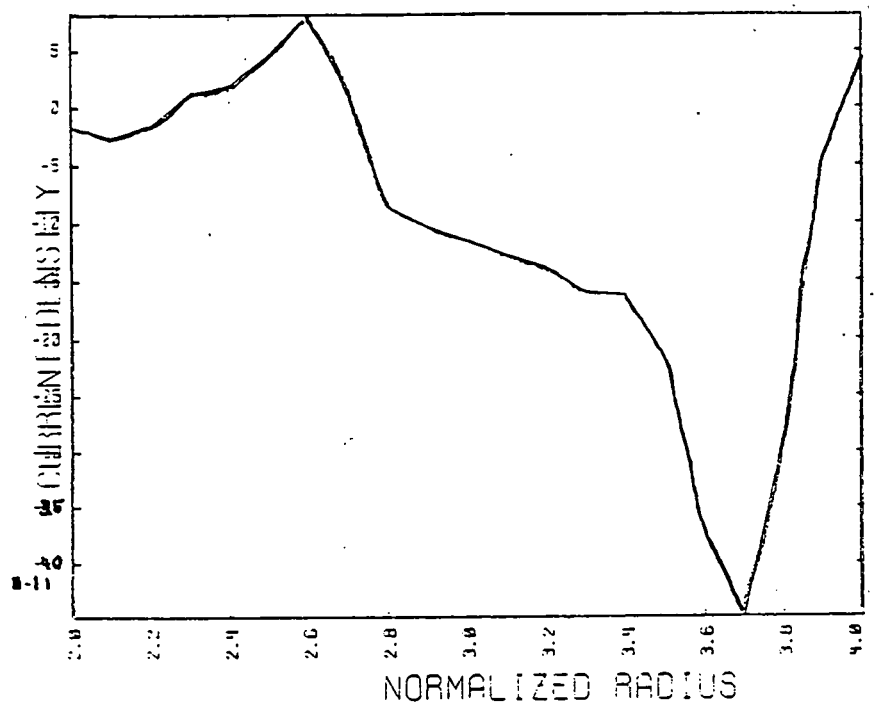

Figure IV.15.C

UNITS: STATAMPS/CM**2
TIME: 2.5 USED
VESSEL HALF-WIDTH=7.5 CM

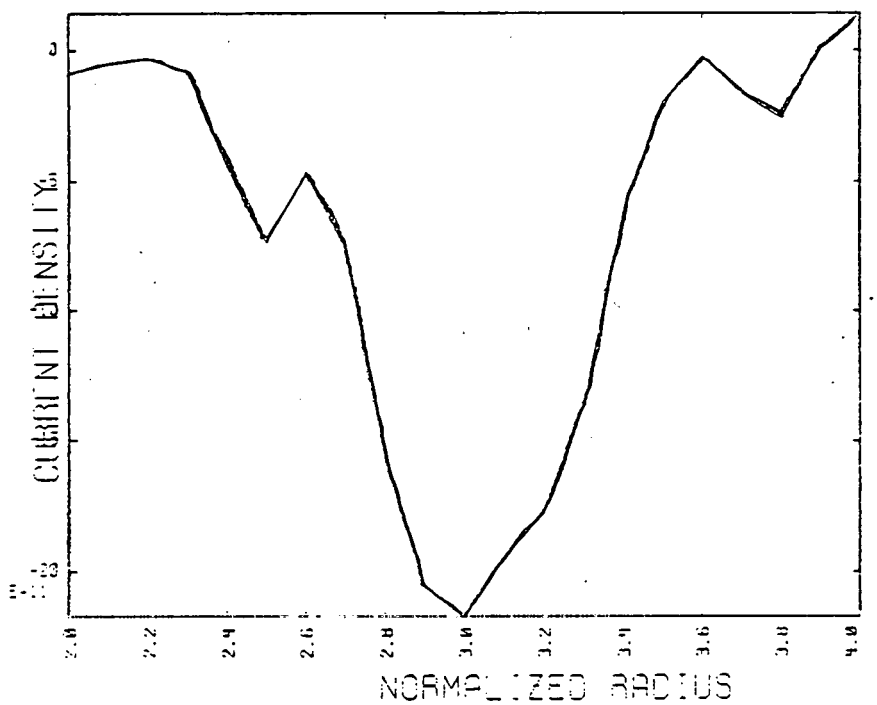

Figure IV.15.D

UNITS: STATAMPS/CM**2
TIME: 5.0 USED
VESSEL HALF-WIDTH=7.5 CM

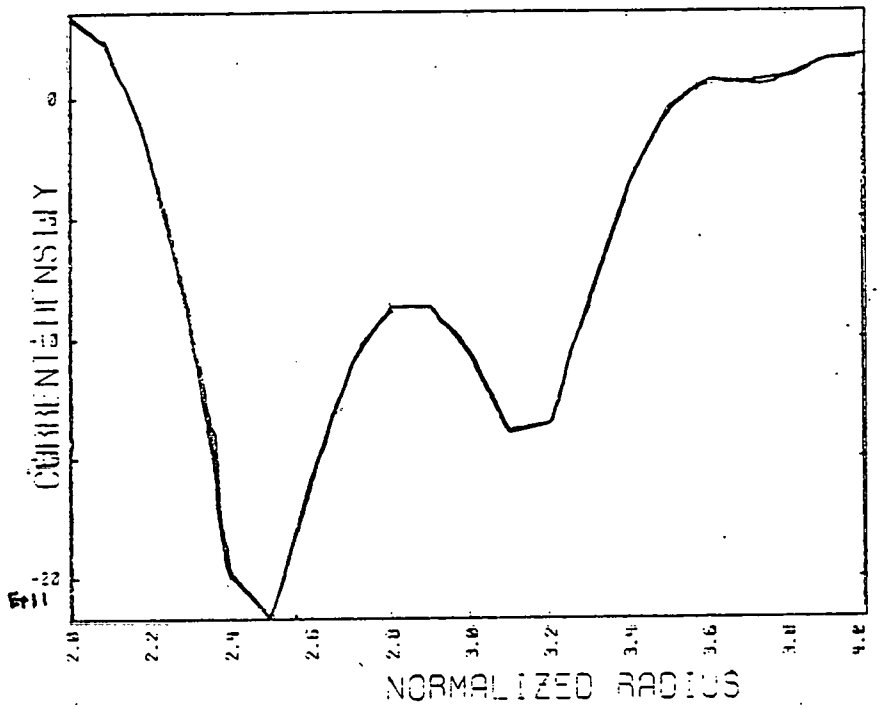

Figure IV.16

Plasma toroidal current density profiles along horizontal midplane for heating case 1.

(A)

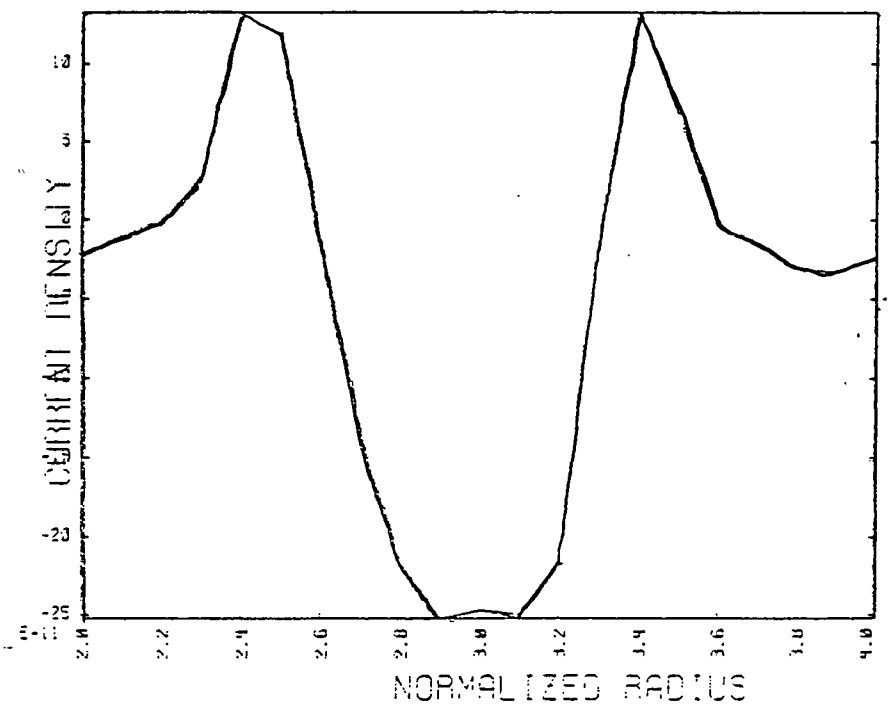

(B)

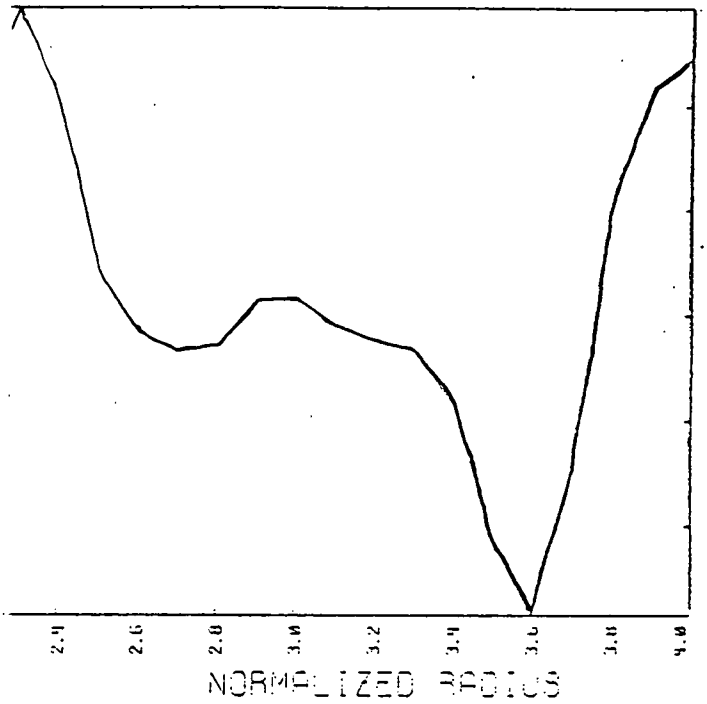

Figure IV.16.C

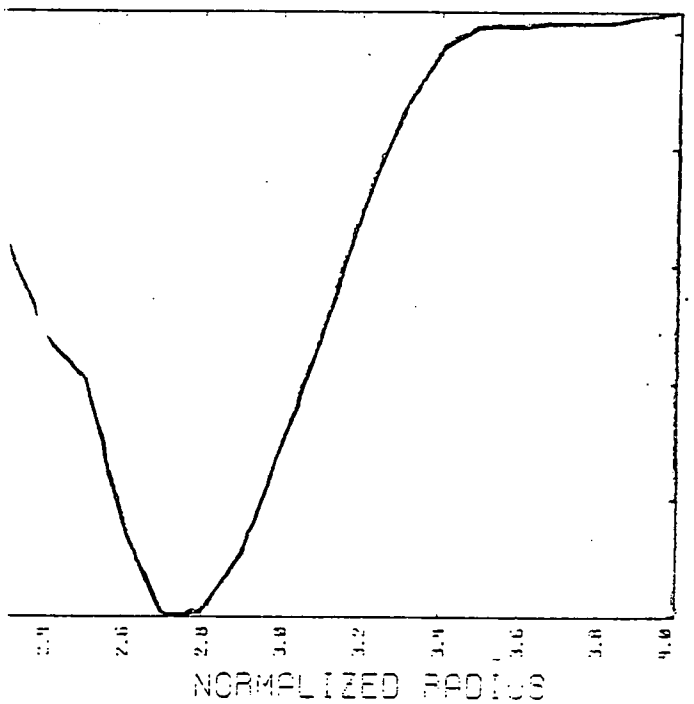

Figure IV.16.D

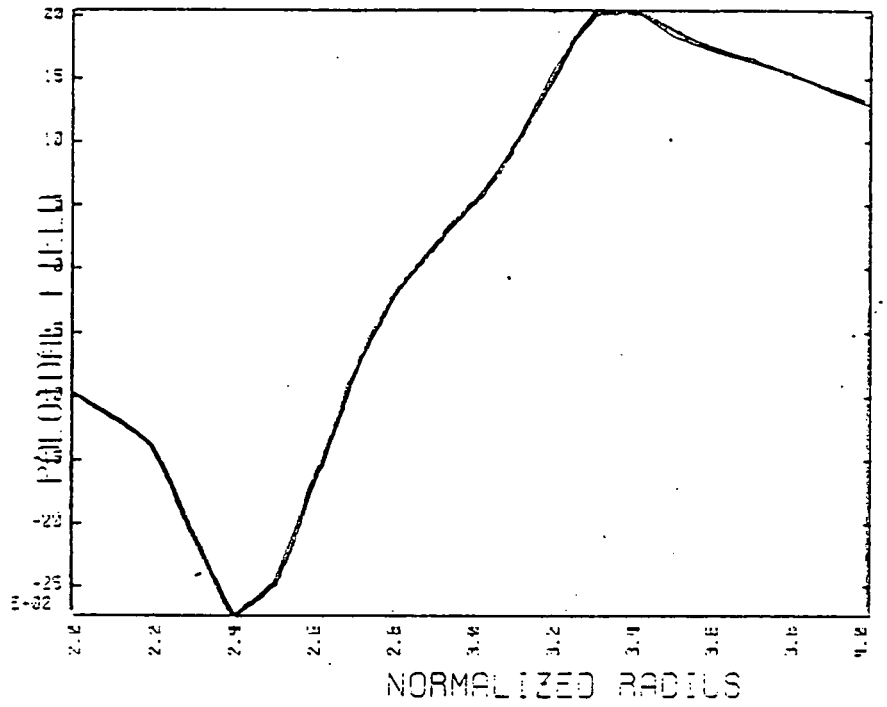

Figure IV.17

Poloidal field profiles along horizontal mid-plane for heating case 1.

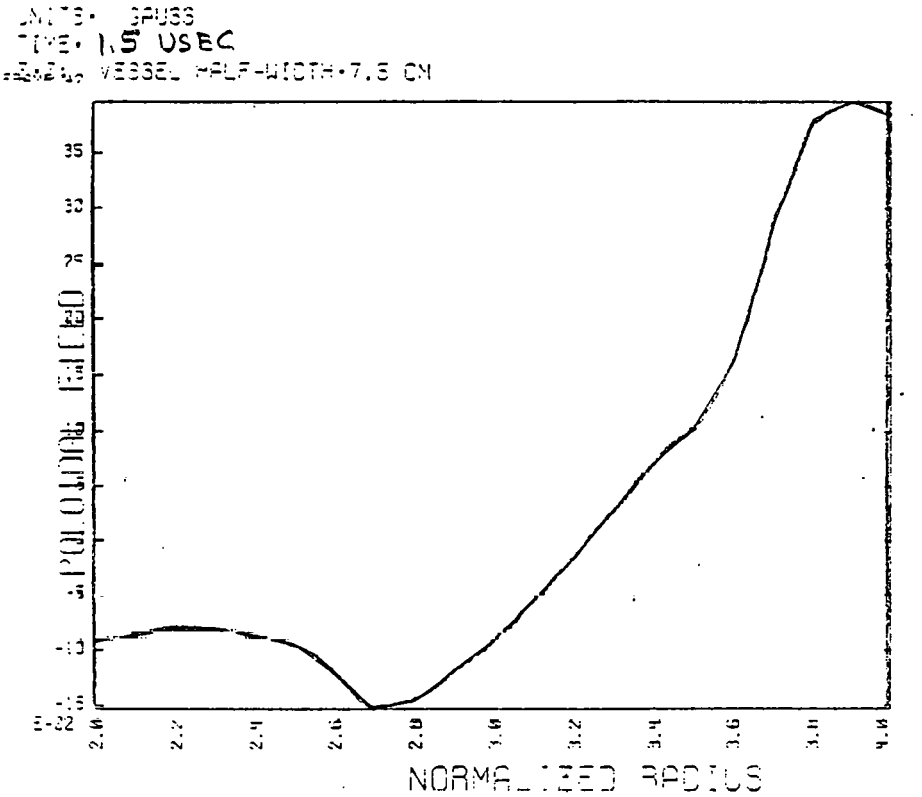

(A)

(B)

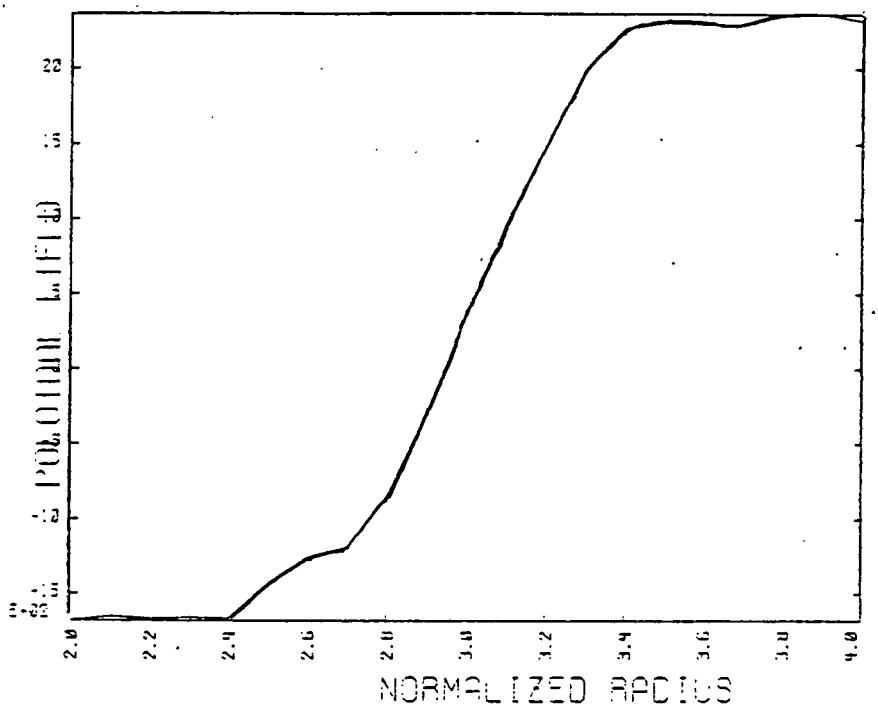

Figure IV.17.C

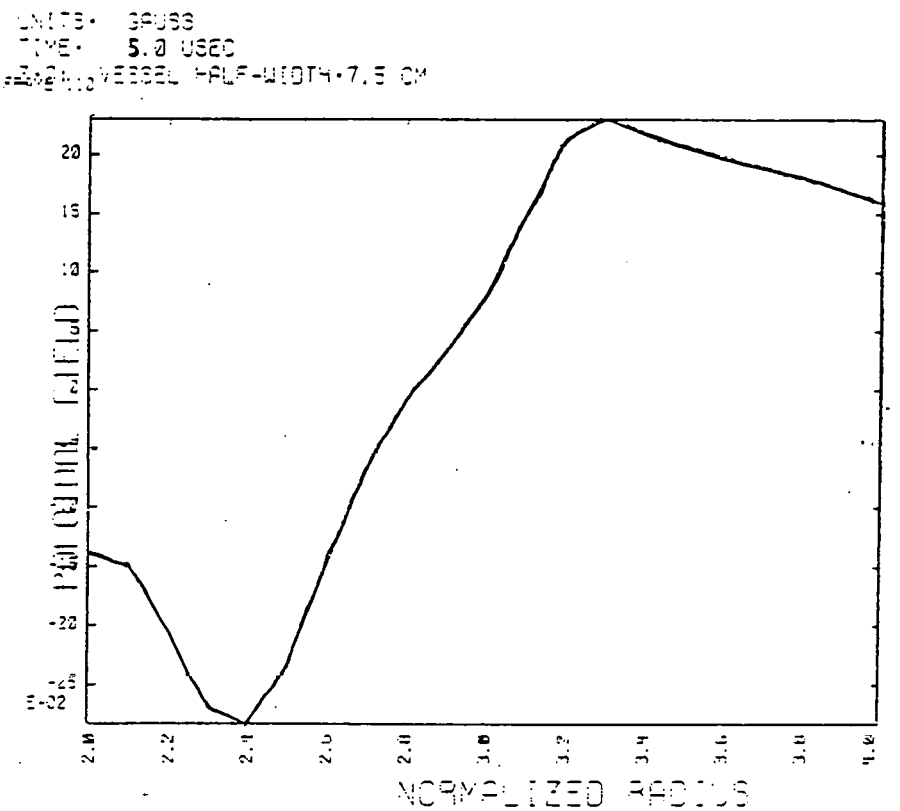

Figure IV.18

Poloidal field profiles along horizontal mid-plane for heating case 3.

(A)

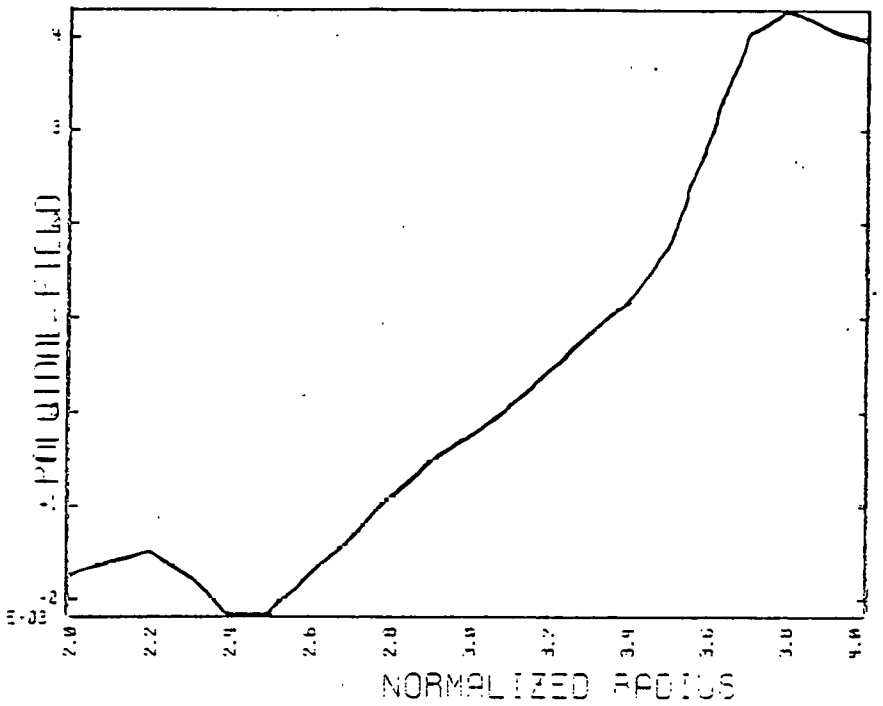

Figure IV.18.B

UNITS: GAUSS
TIME: 2.5 USED
VESSEL HALF-WIDTH=7.5 CM

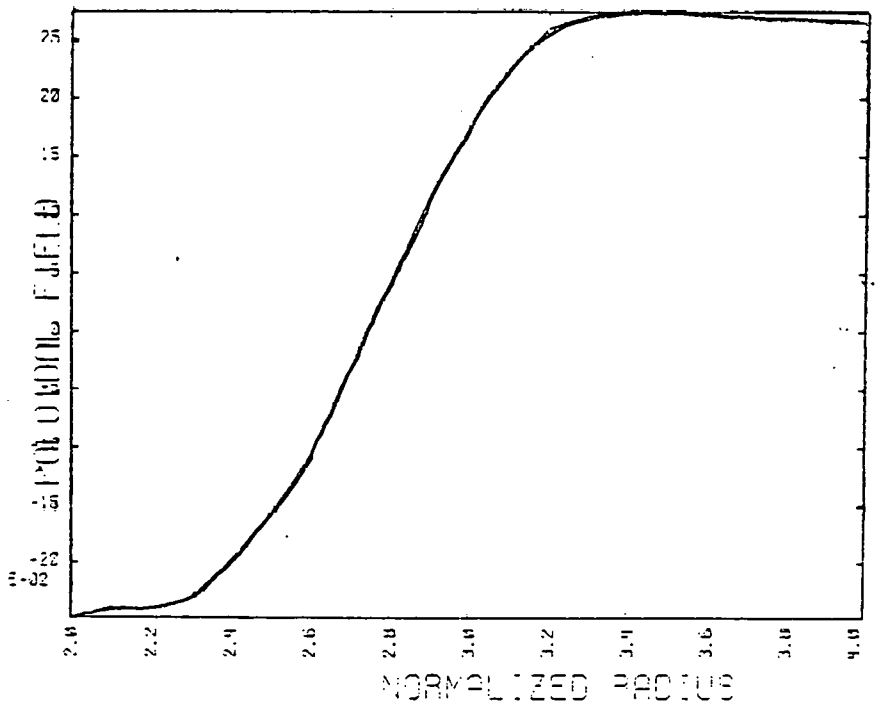

Figure IV.18.C

UNITS: GAUSS
TIME: 5.0 USED
VESSEL HALF-WIDTH=7.5 CM

both cases. This should be obvious from the similarity in the current density profiles. The important differences are the previously mentioned shift of the magnetic axis and the enhanced value of B_z on the outside. Both are caused by the additional vertical field programmed in case 3.

We omit graphs of plasma pressure since such information is easily extracted from the density and temperature profiles. At 6 μsec the peak beta is 85% for case 1 and 78% for case 3. There is no experimental data for these early times to check against. It is important to realize that no radiation or ionization losses are included in the above simulations. Modeling these effects would decrease the plasma beta.

Due to the elongation of the plasma, even at these large values of toroidal plasma current, for case 1 the safety factor has been computed to be .95 on the axis and 1.1 on the plasma edge.

(ii) Half Power Simulation

Next we consider three cases of half power heating. The results are sufficiently different from those of the previous section to warrant detailed explanation once more. Radiation and ionization losses are accounted for in these simulations. The principal inputs are listed in Table IV.4.

A post z-pinch configuration is the initial configuration. Again, rather than include all the graphs generated by the code, we state that

Table IV.4

Half Power Input Summary

Case number	4	5	6
Ψ_{hole} (V-sec)	.020	.020	.010
Ψ_{outer} (V-sec)	.019	.019	.013
Ψ_{top}	.8 Ψ_{hole}	.9 Ψ_{hole}	.9 Ψ_{hole}
Variation in z	z^8	z^8	z^8
τ_{loss} (μsec)	10	10	15
Ionization correction	Yes	No	No
Crowbar	Perfect	Perfect	Perfect
$\eta_{anomalous}$ (sec)	$\leftarrow\leftarrow\leftarrow$ $1.25 \times 10^{-9} \{\frac{J}{1.5 \times 10^{13}}\}$ $\rightarrow\rightarrow\rightarrow$		
κ (ergs/cm/sec/K)	3×10^6	3×10^6	3×10^6

cases 4 and 6 differ the most while case 5 has common characteristics with both of the others. For this reason we will describe case 5 without including an enormous number of graphs.

The toroidal plasma current of case 4 after 6 μsec (66 kA) is identical to that of case 5 at the same time. This is expected due to the specification of identical amounts of poloidal flux on the boundaries.

The peak temperature obtained in case 5 ($\simeq$215 eV at 2 μsec) is the same as that for case 6, however, it does cool less rapidly. This is related to the better confinement of plasma in case 5, that is, there is less plasma near the cold walls. The ionization

correction listed in Table IV.4 is simply an ad hoc correction to the gas constant. Since we are using a single fluid model,

$$P = P_e + P_i = k(n_e T_e + n_i T_i)$$

For $T_i \simeq T_e \equiv T$ we get,

$$P = (n_e + n_i)kT$$

Depending upon the degree of ionization of the helium we obtain,

$$n_i \leq n_e \leq 2n_i$$

Therefore, we program a time dependent electron number density such that the helium is completely ionized after 1.7 μsec. This lowers the pressure thereby affecting both the momentum and energy equations directly. The net effect was determined to be quite small. The programmed ionization case was found to be only slightly (∿2%) cooler. This indicates that compressional heating is not important in Torus-II. It does not imply that poor plasma preparation has no effect on heating as will be discussed when we present the results of the zero-dimensional computation. Another calculation lending support to this claim is that the computed values of $\rho C_v \partial T/\partial t$ are the same order of magnitude as the ohmic heating term, ηJ^2. Returning to the issue of confinement, we note that the only difference

between cases 4 and 5 is the leakage near the copper plates. Once again we conclude that more leakage yields poorer confinement. The flux contours for these two simulations indicate that a sizeable magnetic pressure due to the leakage will tend to elongate the plasma substantially.

Comparing cases 5 and 6 we find a major difference in the plasma current. The latter carries 44 kA at 6 μsec compared to the 66 kA of case 5. This is due to the reduced amount of flux used in the boundary conditions. Plasma confinement is quite similar due to the prescription of equal percentages of flux leakage. However, in case 6, plasma is lost to the outer wall. This does not happen in case 5. This is a result of the low vertical field specified in case 6. The effects of a large plasma current on the temperature is evident only at later times. We are referring to toroidal plasma current. We will discuss this matter below. It is best to now directly compare cases 4 and 6.

The principal difference in the inputs is the poloidal flux on the boundaries and the amount of leakage. Case 4 exceeds case 6 on both counts. The results of greatest interest are those relating to effectiveness of heating and confinement.

Plasma temperature is slightly higher for case 4 than case 6. Let us now finalize our ideas regarding the heating mechanism. For convenience, the toroidal plasma current for each case described in this chapter and the corresponding peak temperature are listed in Table IV.5 Bearing in mind that cases 4-6 contain the phenom-

Table IV.5

Plasma Heating Summary

Case		Toroidal Current (kA)	Temperature (eV)
1	Quartz Heater	66	140
2		80	140
3		88	145
4	Halfheater	66	215
5		66	210
6		44	210

enological loss time constant while cases 1-3 do not, we must conclude that the heating mechanism can only be ohmic poloidal currents. This must be true since the hotter plasmas are characteristic of larger B_ϕ and there is no correlation to the toroidal current. The role of J_ϕ in heating becomes evident as we return to our comparison of cases 4 and 6. Note that the loss constant for the latter is larger than for the former. Thus, we should expect more rapid cooling for case 4. However, this is not observed for two reasons. While poloidal currents are responsible for the initial heating of the plasma, any losses that are important over long times must be compensated for by ohmic heating from toroidal currents since these last much longer than the poloidal currents. Thus, a plasma with a larger J_ϕ will cool much less rapidly eventhough the initial heating is determined solely by the poloidal current. The second reason is related to plasma confinement. This will be discussed again later.

Briefly, the plasma of case 6 rests against the cold outer wall and looses energy by conduction. The slight discrepancy in the temperature of cases 4 and 6 (See Figure IV.19 and IV.20) can also be related to the way the resistivity is computed. Recall,

$$\eta \sim (J_\phi^2 + J_z^2)$$

Thus, larger toroidal currents will yield a higher resistivity and enhance the heating. It is important enough to repeat, that barring large scale plasma confinement difficulties, plasma temperature is directly related to the final reversed toroidal field. A large part of plasma cooling is caused by the zero-dimensional loss term. As more experimental data becomes available, this term can be adjusted to more closely follow the experiment. With respect to the plasma resistivity, several attempts were made to run the code without an enhanced value. For the known rise times of the external currents, the code bombed without exception. This implies that an enhanced resistivity must be present for successful operation of the codes and is probably a good representation of the experiment.

The difference in the larger toroidal current of case 4 over case 6 can not be quickly dismissed as simply due to the boundary values of poloidal flux, although such boundary values are important. Note that the current densities of the two cases are very similar (Figures IV.21 and IV.22) for the early times. Indeed, J_ϕ profiles for all the simulations are similar for $t \leq 4$ μsec. At the later times, depending upon the shape of the confining fields

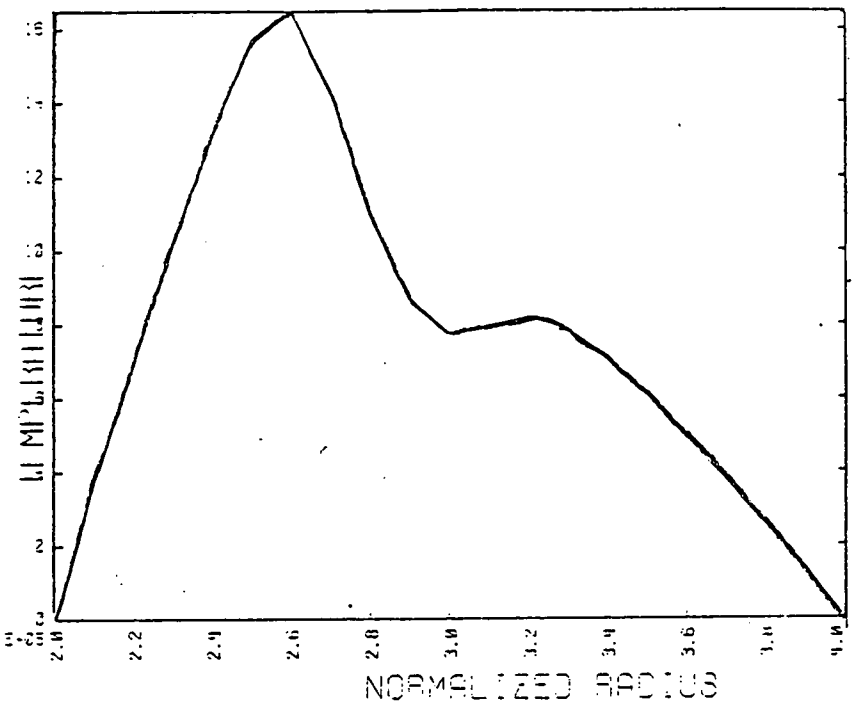

Figure IV.19

Plasma temperature profiles along the horizontal mid-plane for heating case 4.

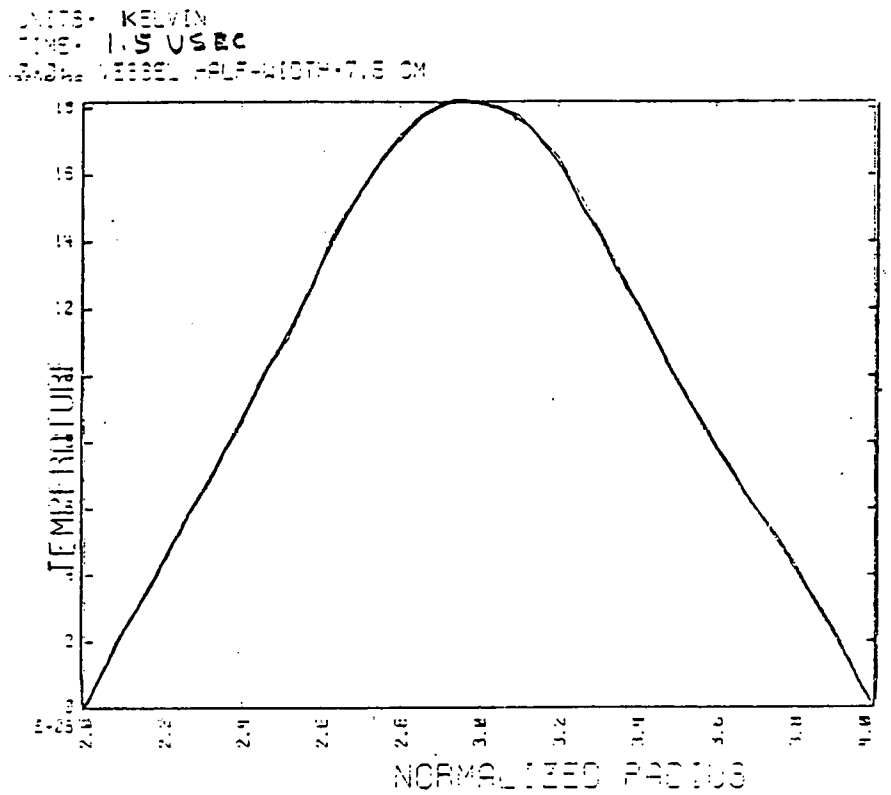

(A)

(B)

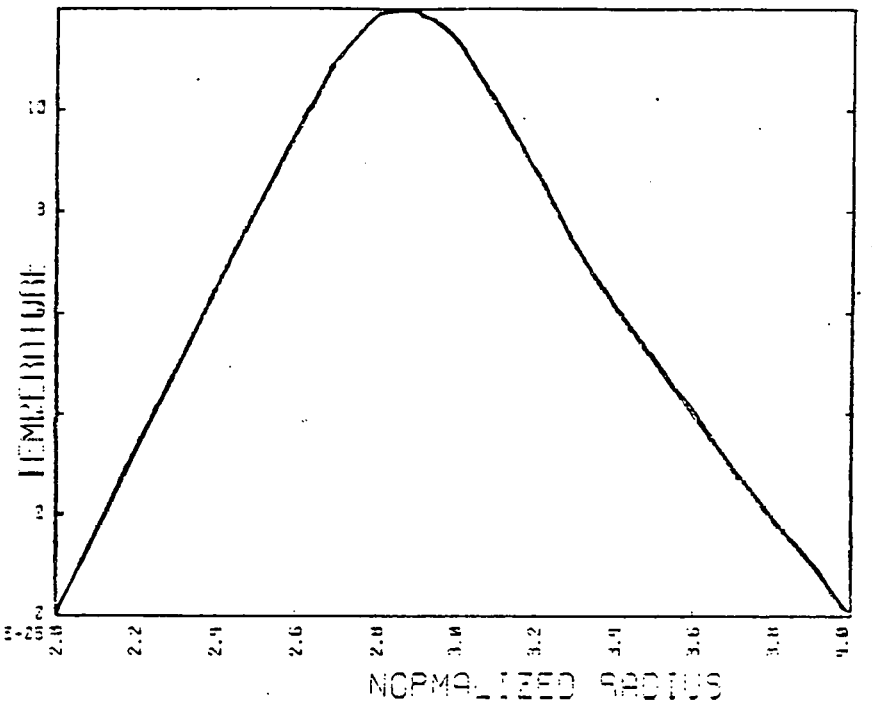

Figure IV.19.C

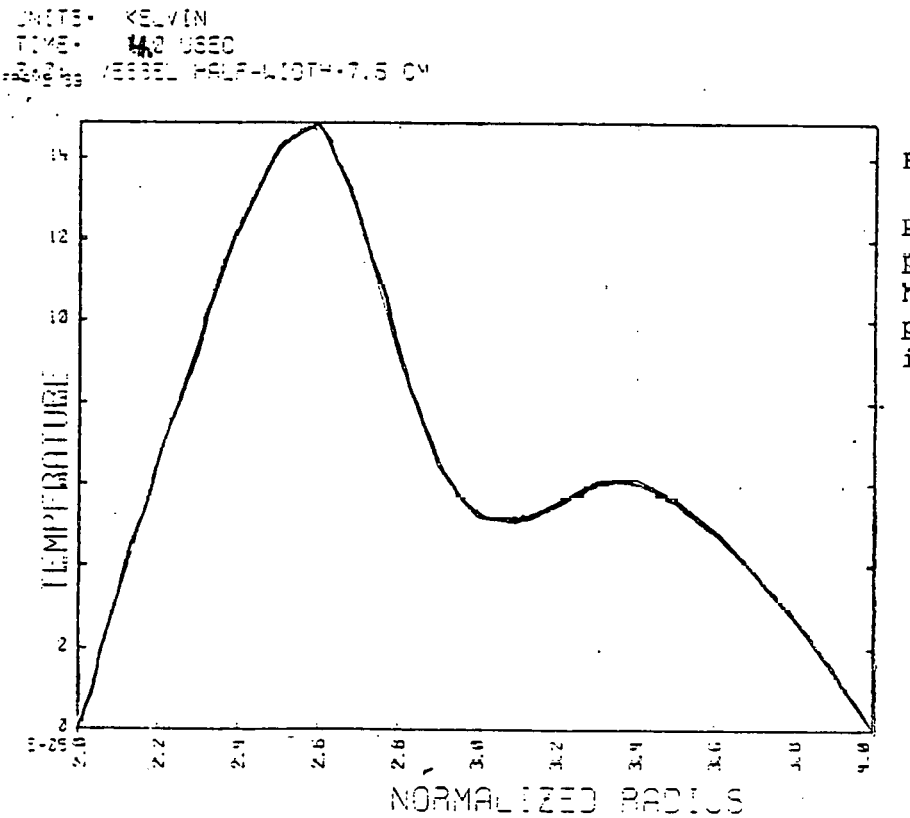

Figure IV.20

Plasma temperature profiles along the horizontal mid-plane for heating case 6.

(A)

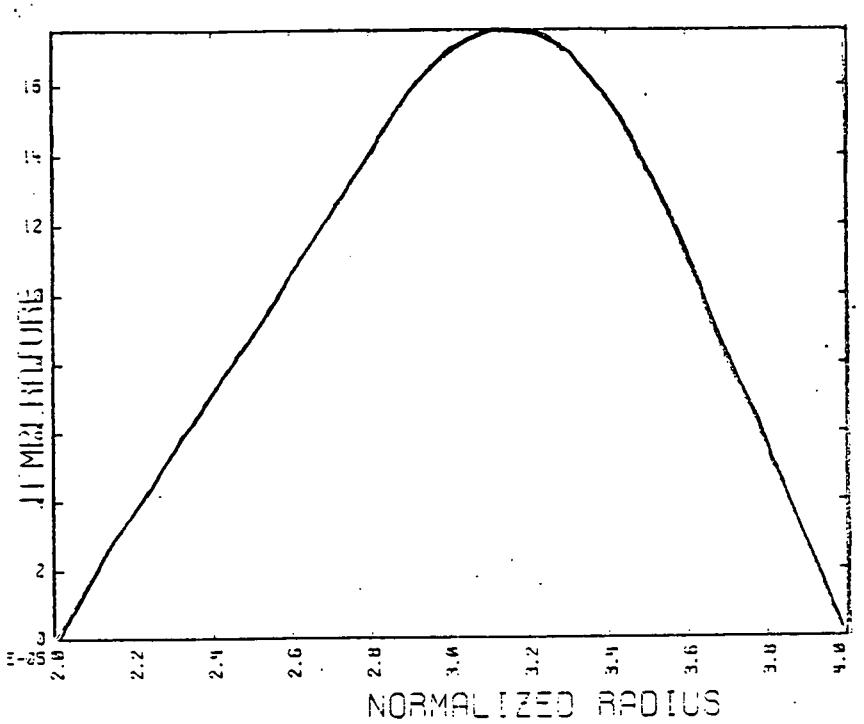

Figure IV.20.B

UNITS: KELVIN
TIME: 3.0 USEC
VESSEL HALF-WIDTH=7.6 CM

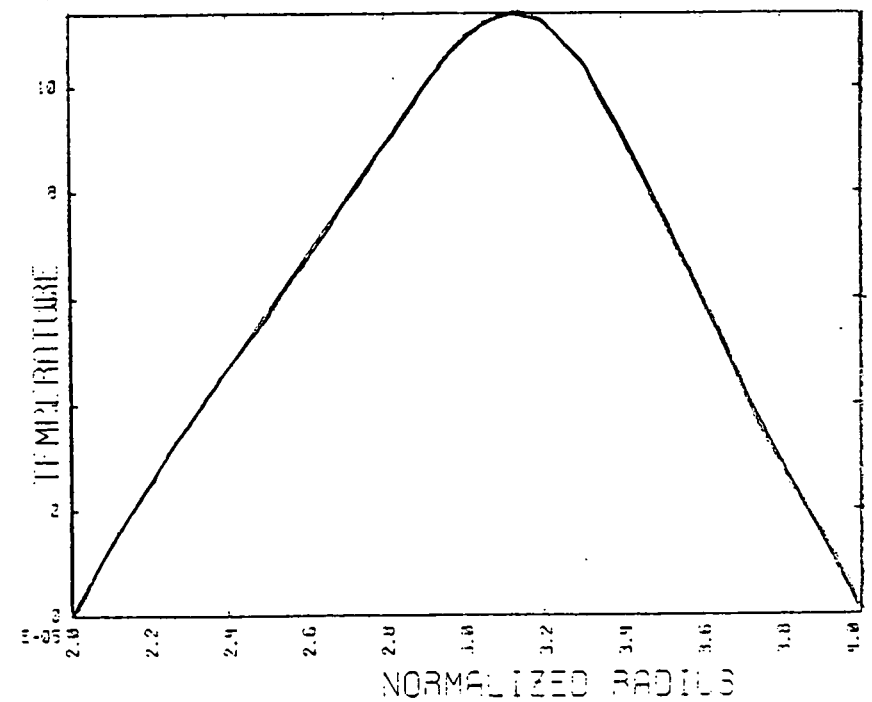

Figure IV.20.C

UNITS: KELVIN
TIME: 4.0 USEC
VESSEL HALF-WIDTH=7.6 CM

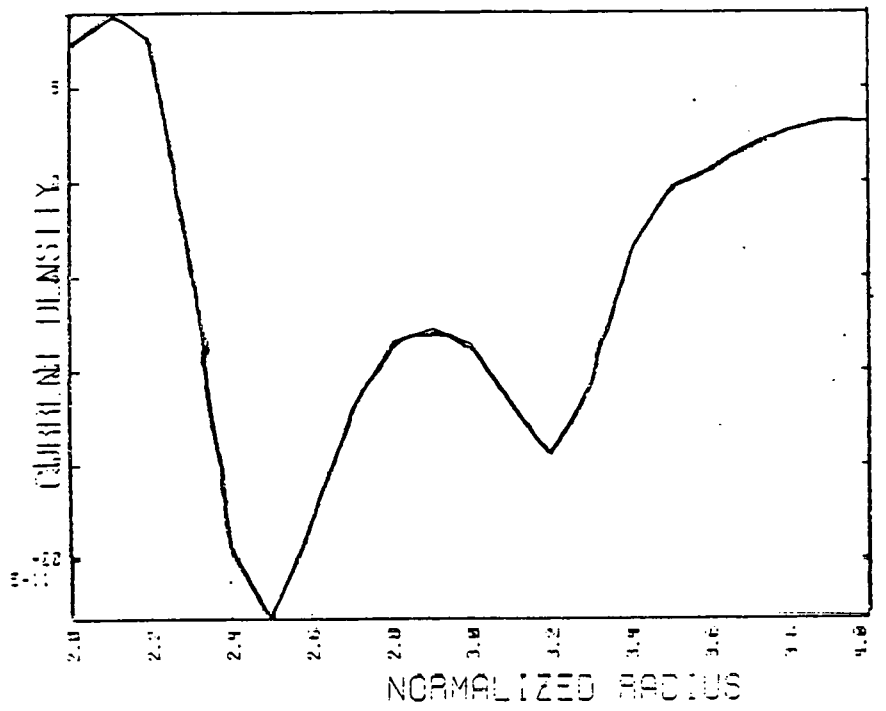

Figure IV.21

Plasma toroidal current profiles along the horizontal midplane for heating case 4.

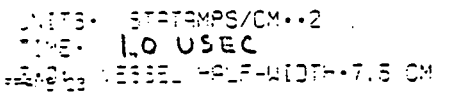

(A)

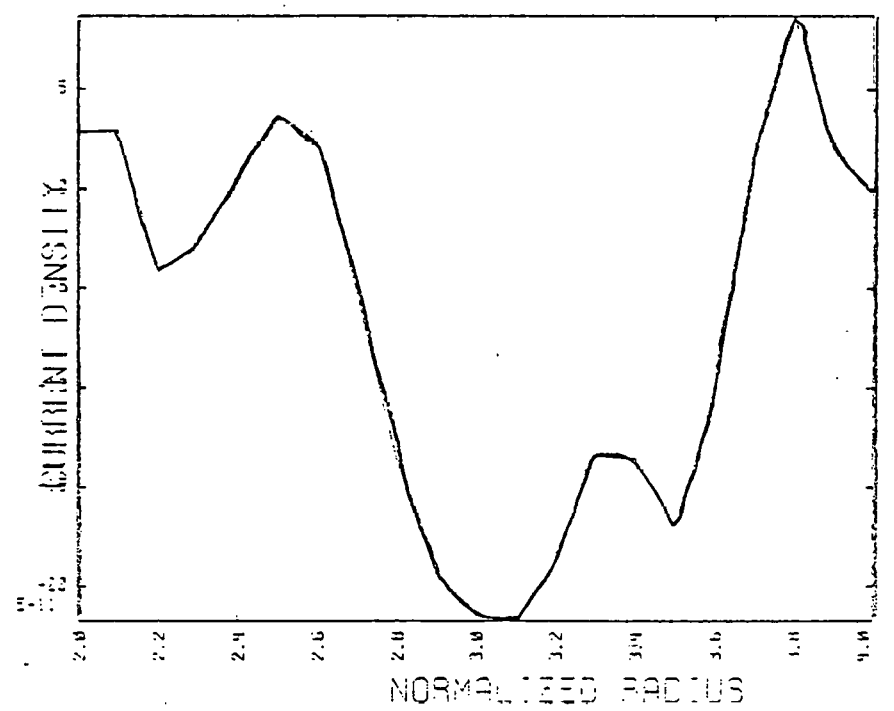

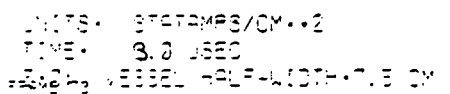

(B)

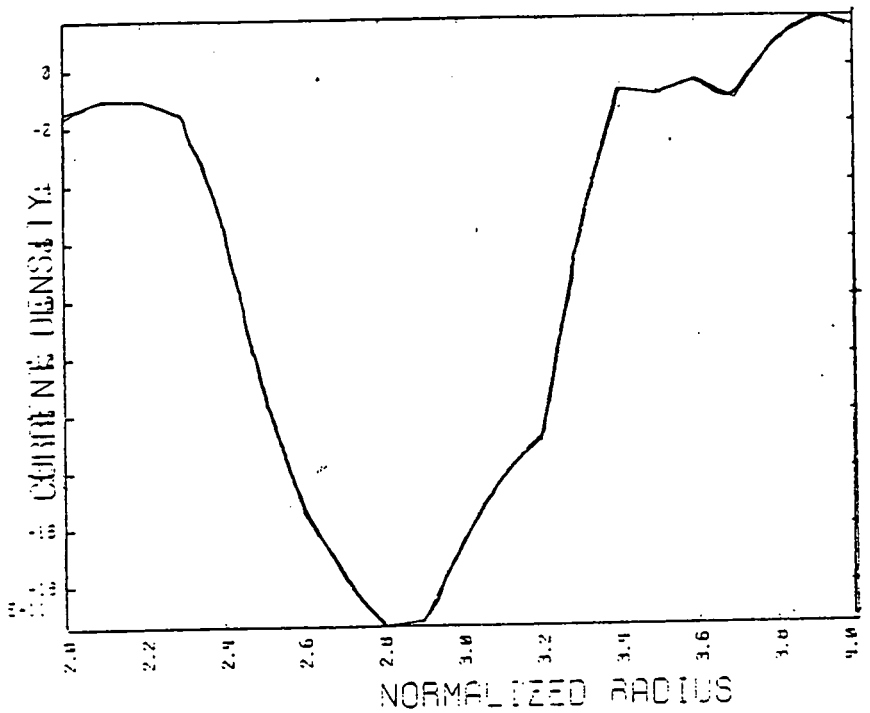

Figure IV.21.C

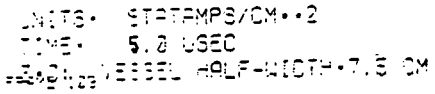

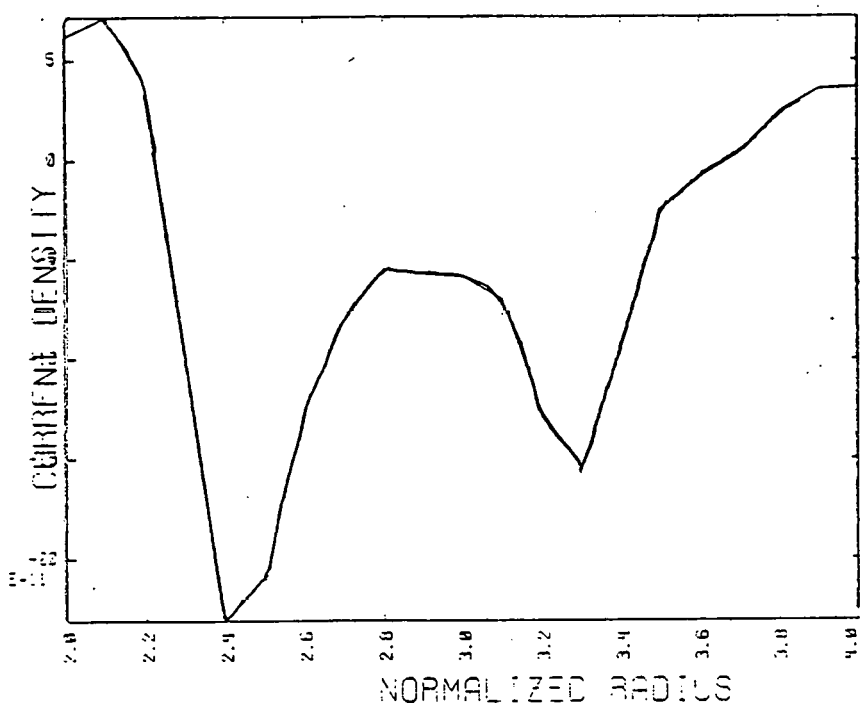

Figure IV.22

Plasma toroidal current profiles along the horizontal midplane for heating case 6.

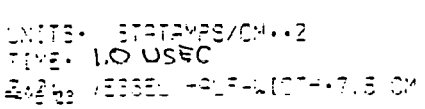

(A)

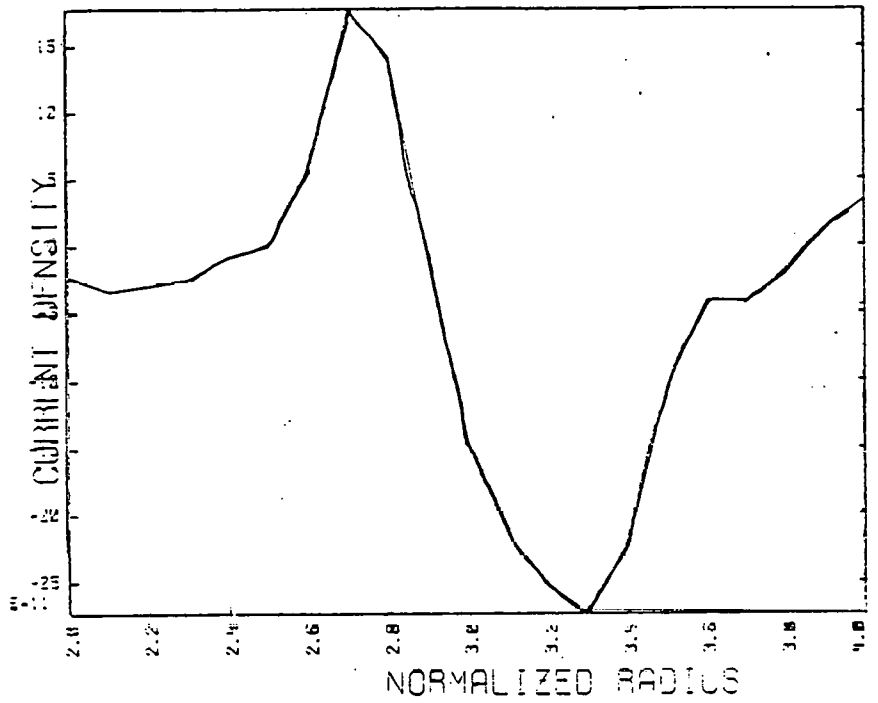

Figure IV.22.B

UNITS: STATAMPS/CM**2
TIME: 3.0 USEC
VESSEL HALF-WIDTH=7.5 CM

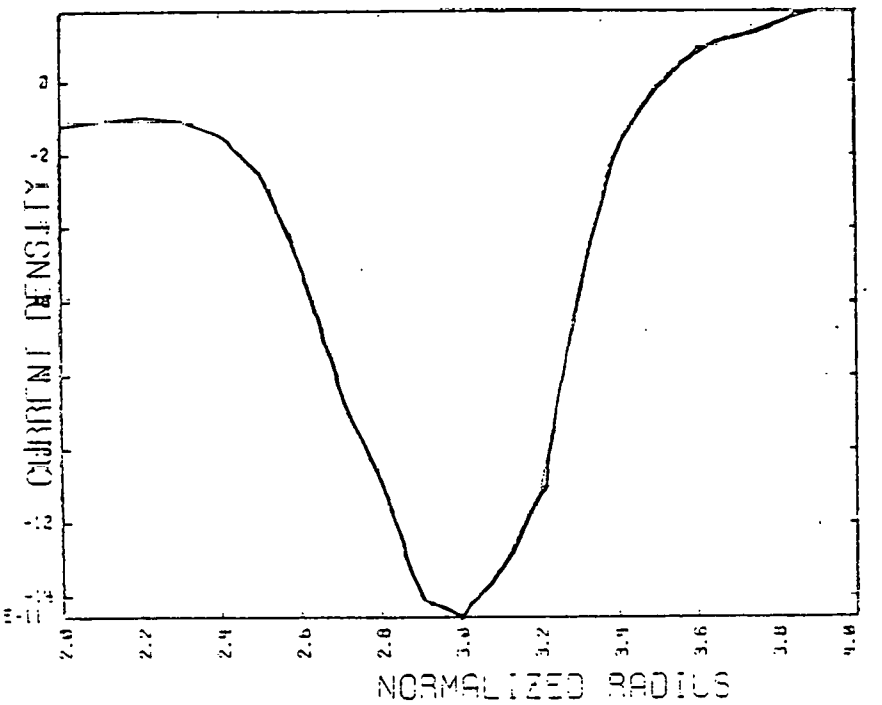

Figure IV.22.C

UNITS: STATAMPS/CM**2
TIME: 5.0 USEC
VESSEL HALF-WIDTH=7.5 CM

the plasma will lose current. This is the "peel off" effect mentioned earlier. Current is lost to the upper regions of the vacuum vessel where the flux leakage is concentrated. For case 6 there is the additional problem of insufficient vertical field needed to keep the plasma off the outer wall during the early part of the heating. Whenever plasma approaches the outer wall, it encounters a greater concentration of open field lines. No current is allowed to flow on these lines since they intersect the non-conducting glass wall. Thus, the current is squeezed out of the plasma. Additional proof of the "peel off" phenomena is presented in Figures IV.23 and IV.24. In Figure IV.24.B, plasma flow patterns have been sketched. While acceptance of this calculation as a true detailed account of the Torus-II plasma velocity spectrum is not possible, it is quite useful in showing once again that the outer layer of the plasma can move along open field lines to the upper regions of the vessel. This has been observed experimentally with streak cameras.[32] This flow pattern is caused by the leakage flux into the vessel at the inner wall and out of the vessel at the outer wall, thus, this is not a transport problem but one of coil geometry. The inner plasma regions experience a counter-clockwise poloidal rotation. Experiments are being conducted to test for this effect.[33]

Continuing with this line of thought, we analyze the poloidal flux contours in Figures IV.25 and IV.26. The contours for plasma subjected to less flux leakage (case 6) are squatter than those of case 4 for $t \leq 2$ μsec, repeating the trend observed in cases 1 - 3.

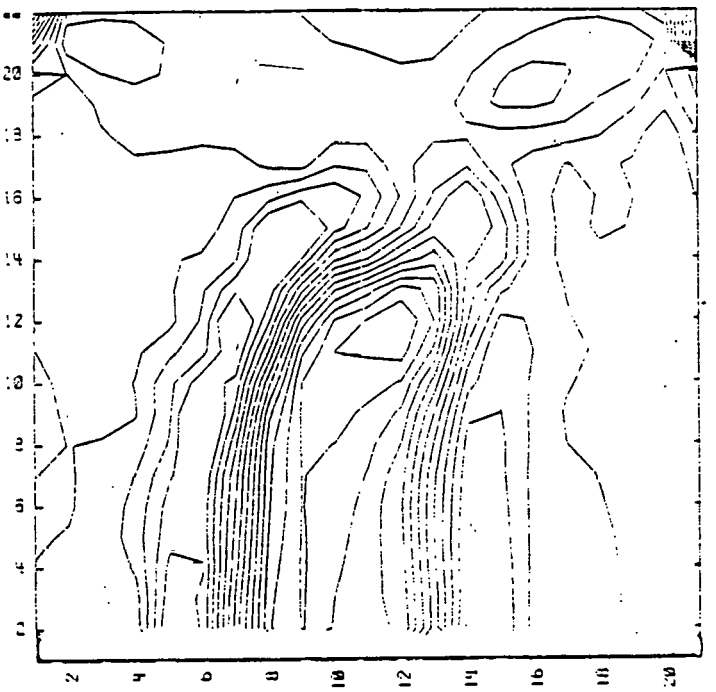

Figure IV.23

Plasma toroidal current density contours in upper half plane for heating case 4.

(A)

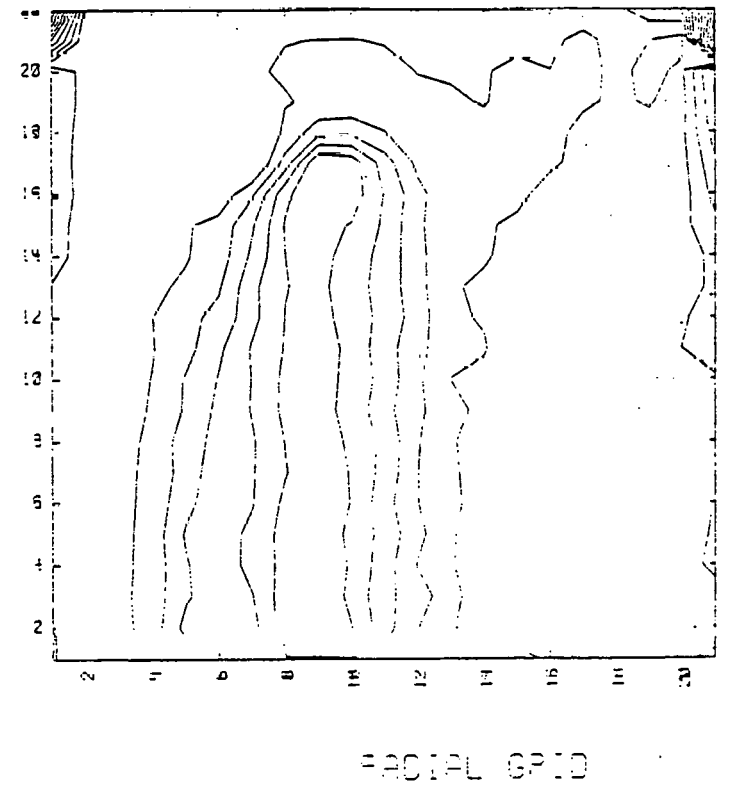

(B)

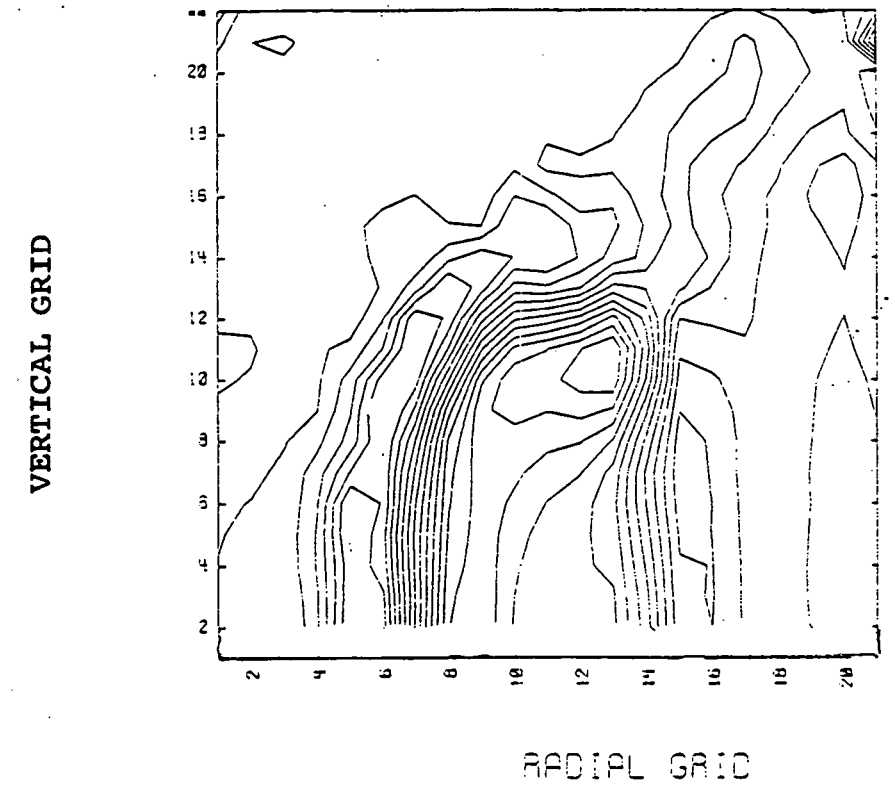

Figure IV.24

Plasma toroidal current density contours in upper half plane for heating case 6.

(A)

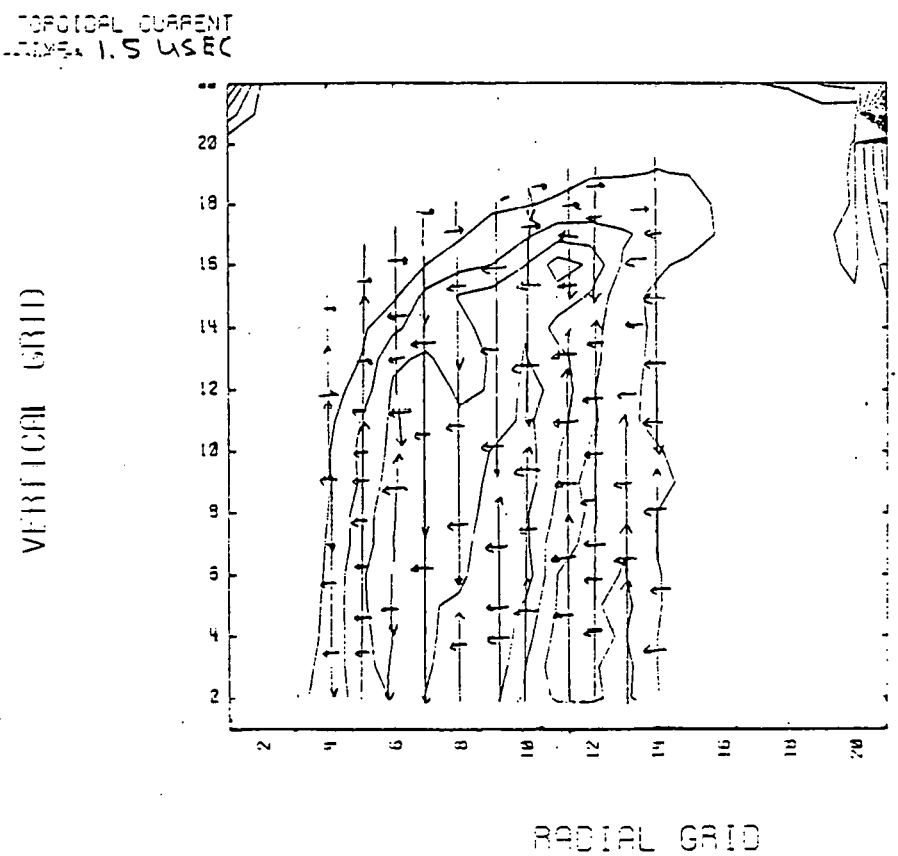

(B)

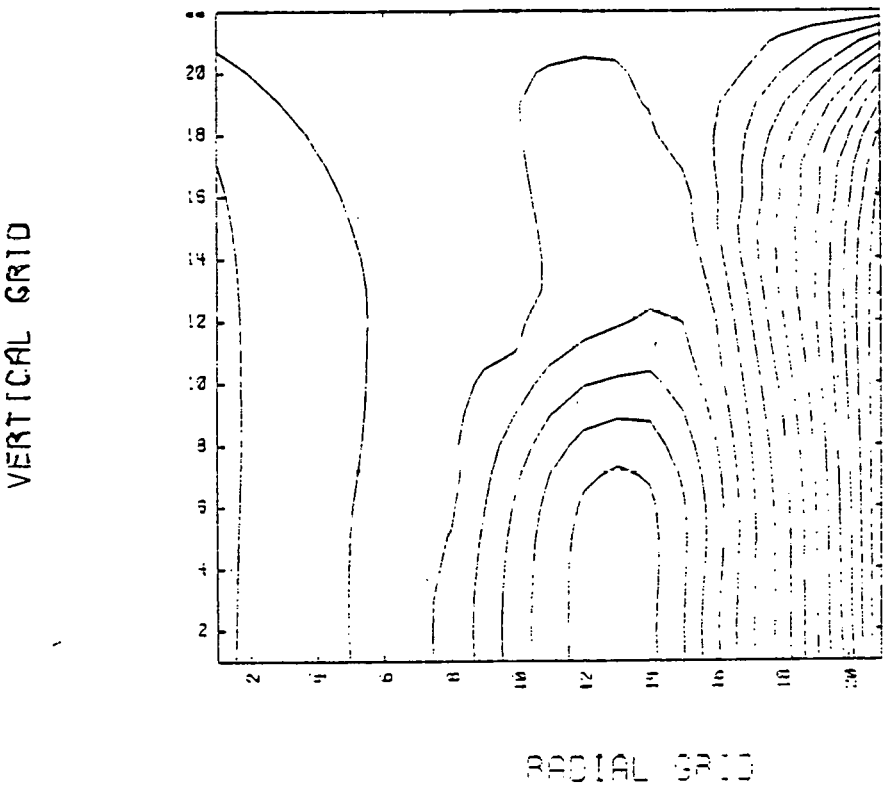

Figure IV.25

Poloidal flux contours in upper half plane for heating case 4.

(A)

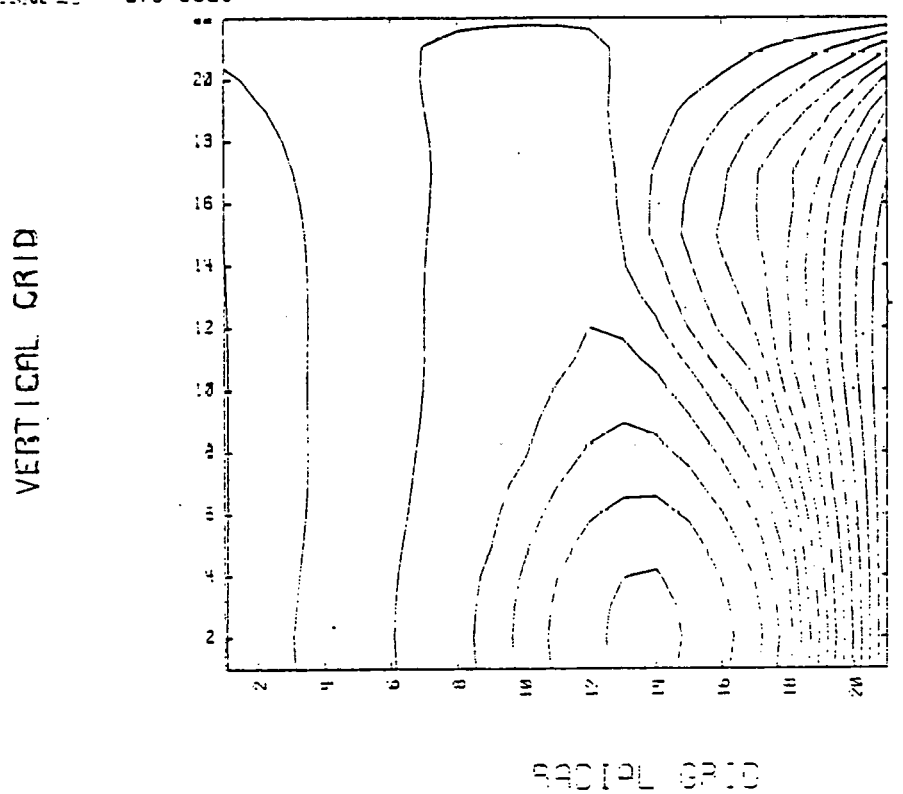

(B)

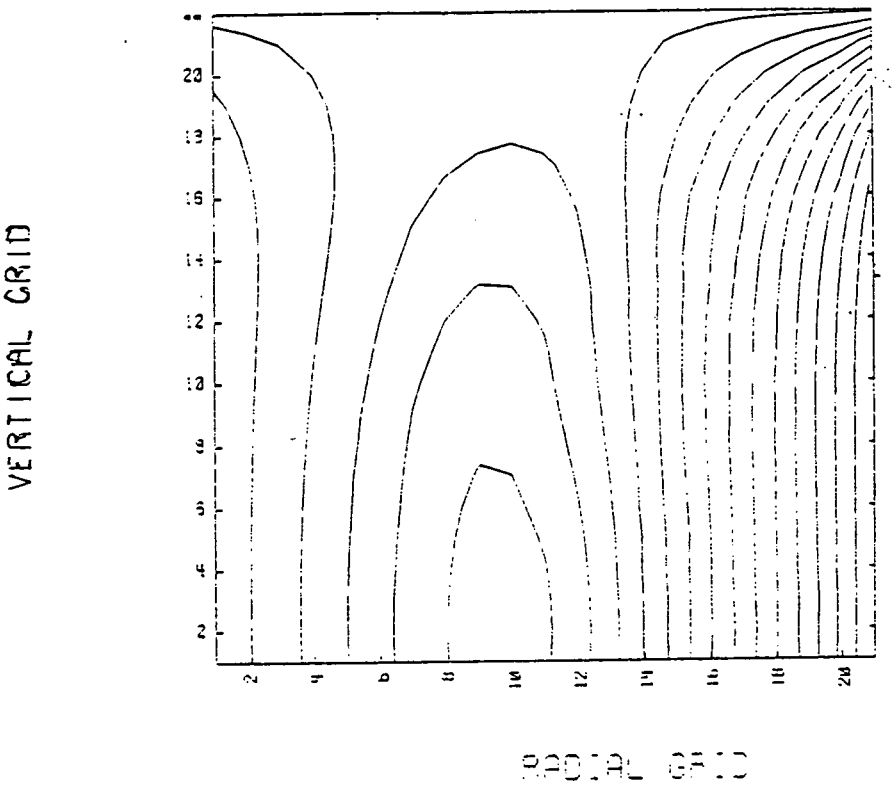

Figure IV.25.C

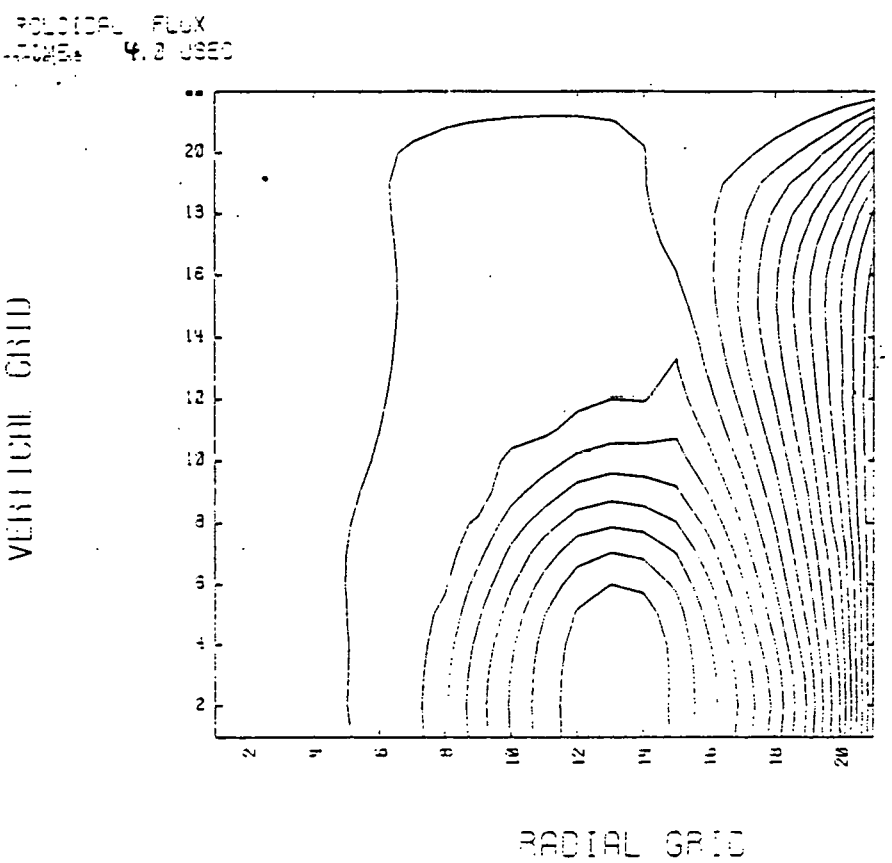

Figure IV.26

Poloidal flux contours in upper half plane for heating case 6.

(A)

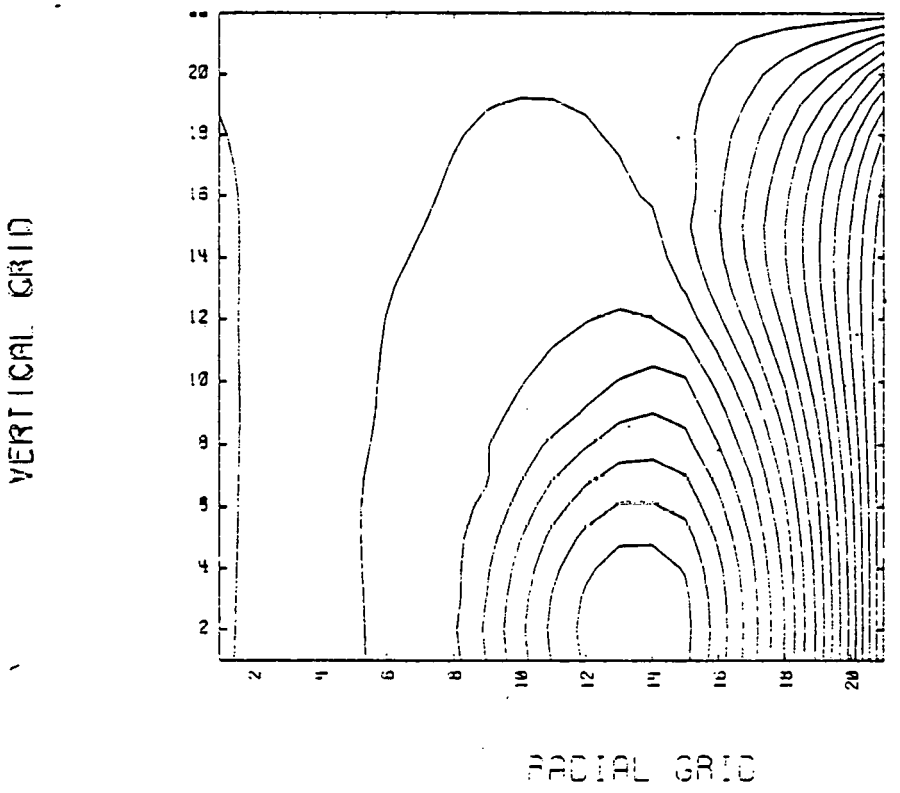

Figure IV.26.B

POLOIDAL FLUX
2.5 USED

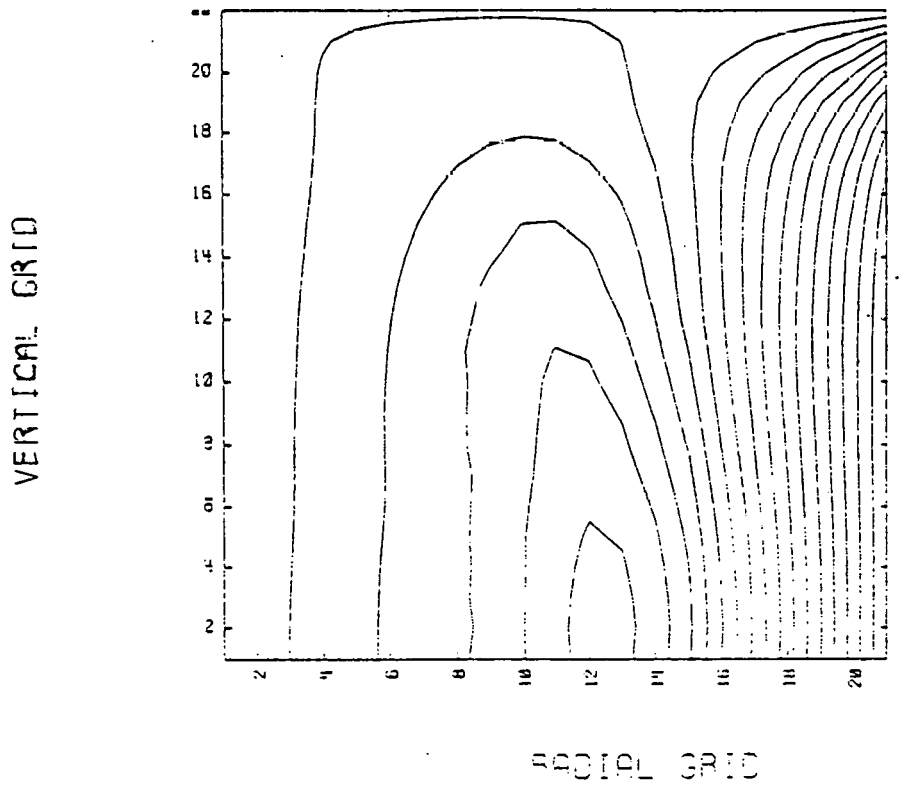

Figure IV.26.C

POLOIDAL FLUX
4.0 USED

However, unlike the earlier results, the flux contours do not remain squat. Case 4 exhibits squatter contours than case 6 for times between 2.5 and 5 μsec. The reason for this is that there is not enough vertical field to confine the hot plasma in case 6. By now it should be evident exactly how confinement is affected by the poloidal flux specification. In most high beta devices, the plasma is confined by diamagnetic poloidal currents crossed with the toroidal magnetic field. This occurs to some extent in Torus-II. However, the geometry of the external toroidal windings are also very important for Torus-II. As plasma is heated it shifts radially outward. For given values of Ψ_{hole} and Ψ_{outer}, if the return leakage along the inside of the device is high ($\geq$20%), there is a large magnetic pressure supplying an additional outward push on the plasma. Another way to look at this phenomenon is that the leakage flux effectively reduces the vertical field applied externally. If there is a large flux leakage out of the vessel towards the outer wall it will push plasma inward. The plasma finds itself squeezed in the middle thereby assuming an elongated shape and squirting out to the top and corners. Again, another way to look at the leakage on the outside of the device is that the vertical field is improperly shaped. It should be directed inwardly at larger heights. The Torus-II coil geometry produces the opposite pattern. Plasma confinement improves with decreasing leakage since the field lines, which exert a smaller pressure, can be more easily compressed. In doing so, the boundary conditions are such that the field lines tend

to bend over the top of the plasma maintaining excellent vertical equilibrium. (See for example Figures IV.6.B and IV.25.B) However, for case 6 the contours do not remain squat for reasons other than the flux leakage. In this simulation the amount of vertical field is simply too small. Therefore, the hot plasma easily compresses all the field without the characteristic "bending over" of magnetic pressure. This is not a new result. Too little external vertical field has long been known to lead to loss of plasma confinement. The weaker vertical field also manifests itself in a smaller computed B_z. Typically, it is 500 G smaller for case 6 than all others. The position of the magnetic axis along r is again dictated by Ψ_{outer}, with larger fluxes pushing the axis inward as expected.

Direct viewing of the plasma density over the upper half plane (Figures IV.27 and IV.28) or along the horizontal midplane (Figures IV.29 and IV.30) substantiates the above discussion of confinement. Case 6 is different from all others. This is the first time plasma hits the outer wall. There is a resulting decrease in plasma density. Earlier we sketched briefly the dynamics of the plasma motion. It is best now to describe it in detail.

In all cases, upon initial heating ($t \lesssim 1$ μsec), the plasma expands along r while contracting slightly along z. As the plasma temperature increases, it begins to move outward radially, expanding in width while doing so. Depending upon the shaping of the prescribed boundary conditions, the plasma is compressed along z to

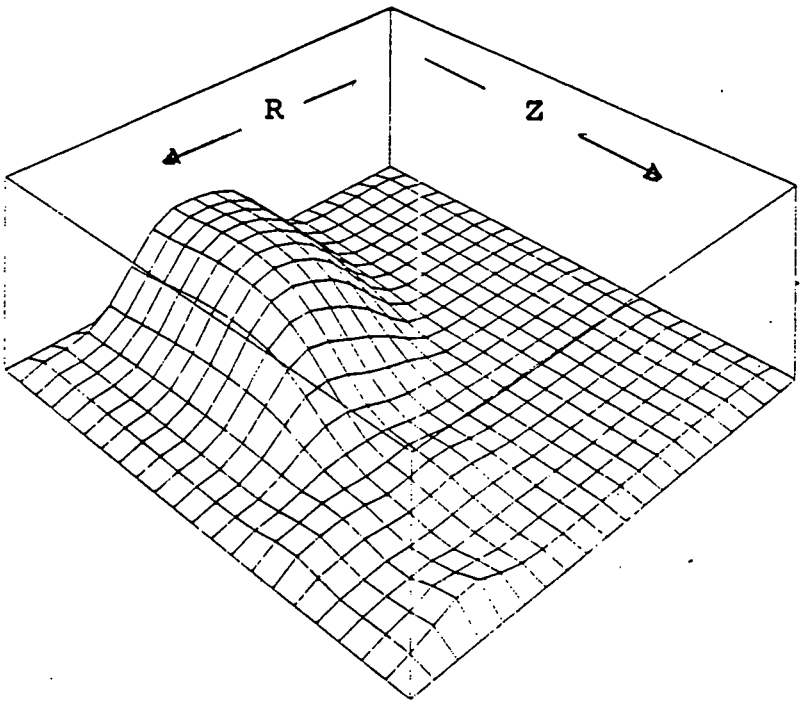

Figure IV.27

Plasma density distribution in upper half plane for heating case 4.

TIME=2.0 usec
DENSITY

(A)

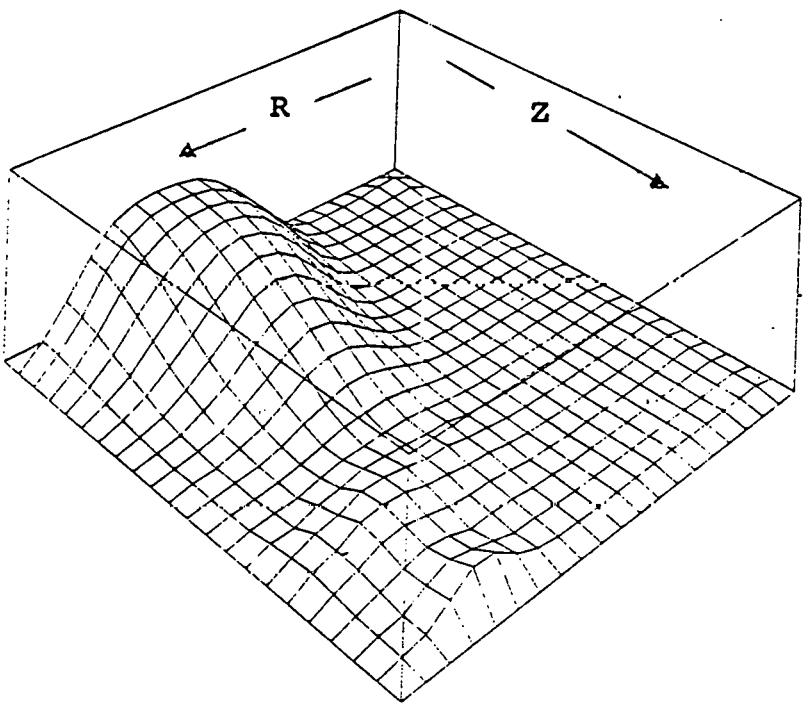

TIME=2.5 usec
DENSITY

(B)

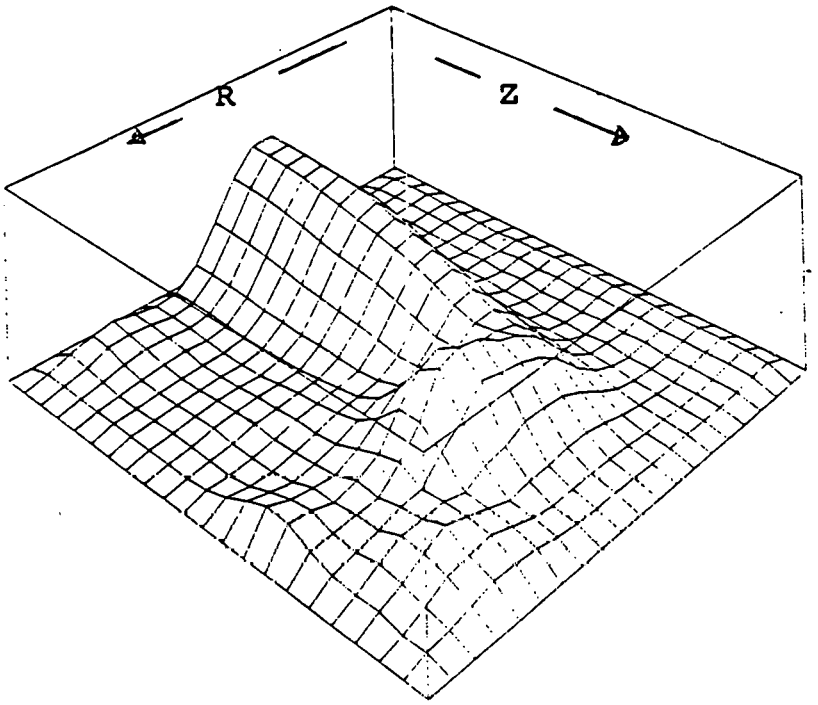

Figure IV.27.C

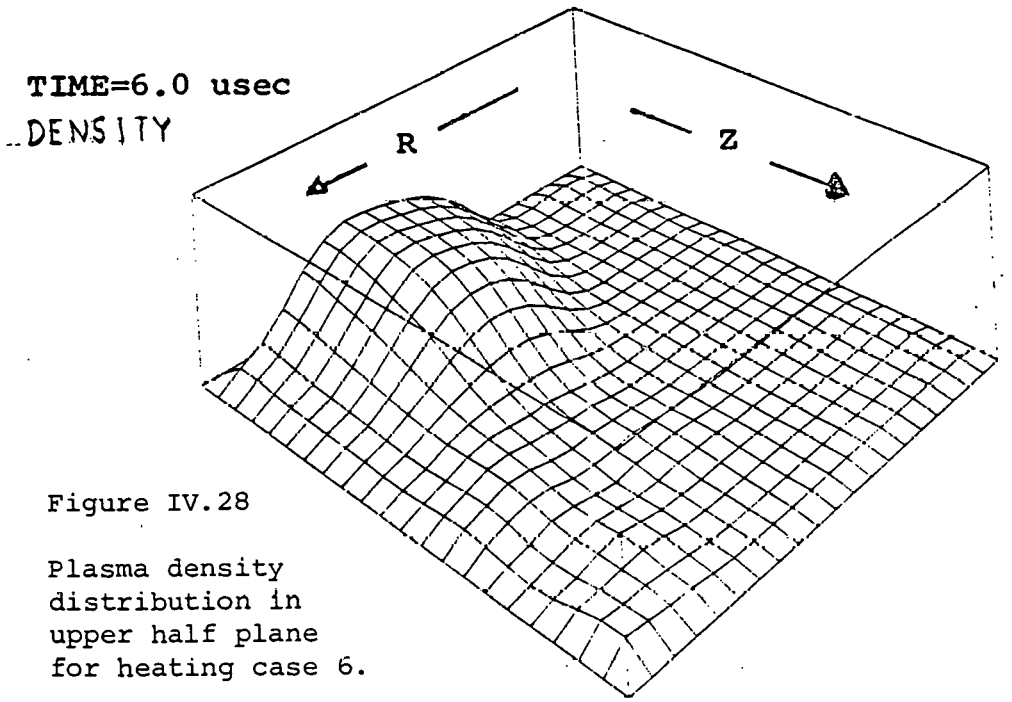

Figure IV.28

Plasma density distribution in upper half plane for heating case 6.

TIME=2.0 usec
DENSITY

(A)

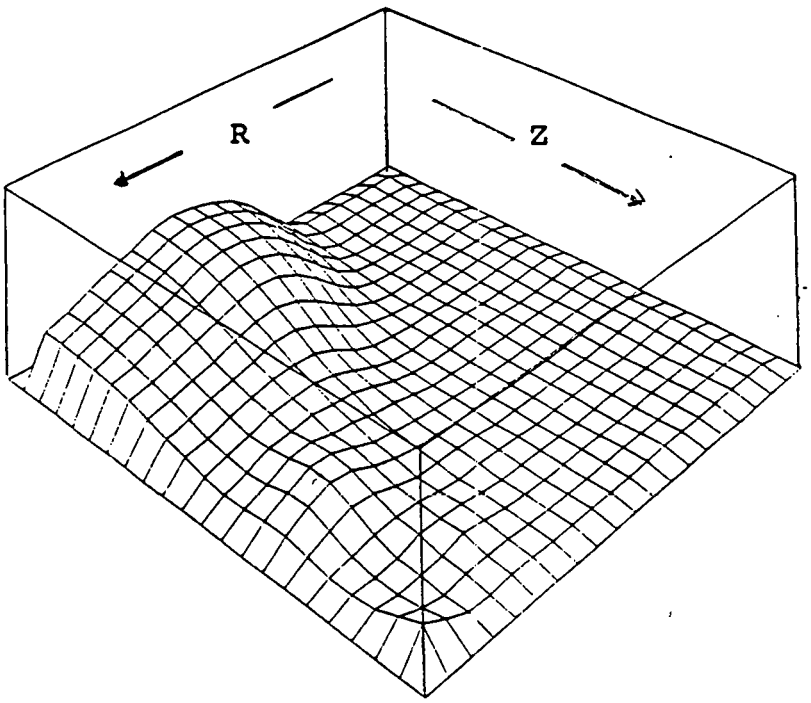

Figure IV.28.B

TIME=2.5 usec
DENSITY

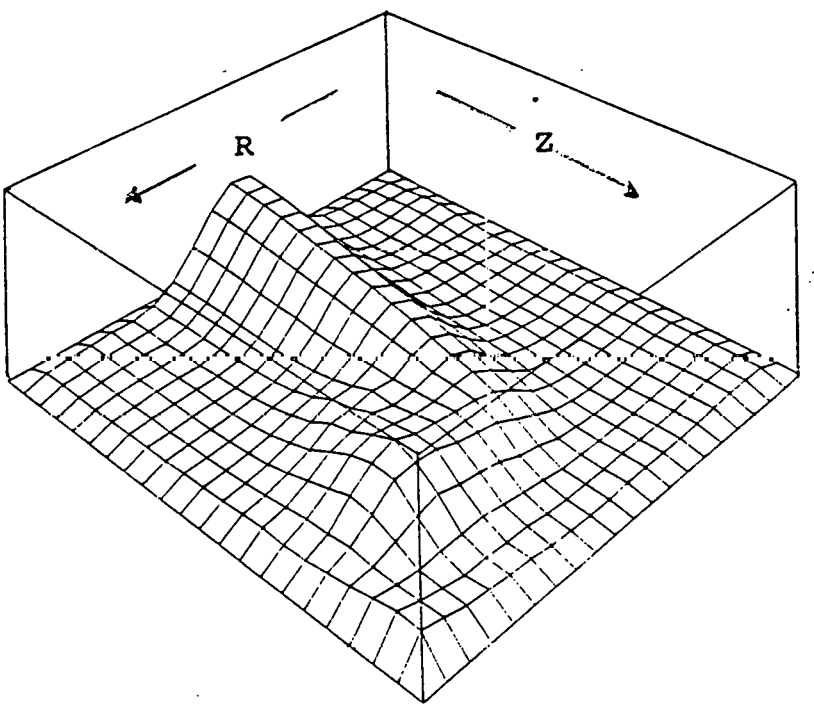

Figure IV.28.C

TIME=6.0 usec
DENSITY

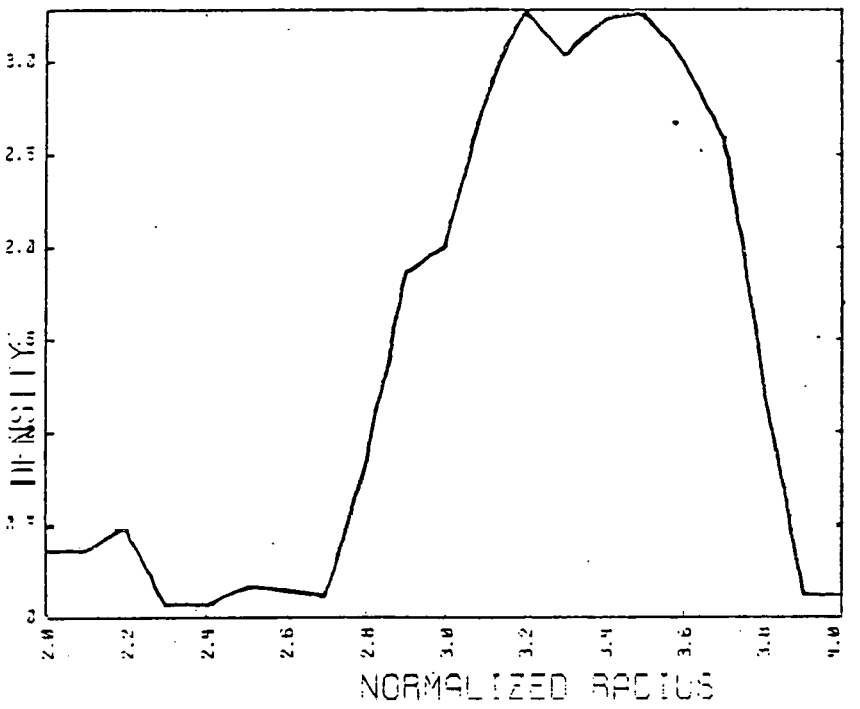

Figure IV.29

Plasma density profiles along the horizontal midplane for heating case 4.

(A)

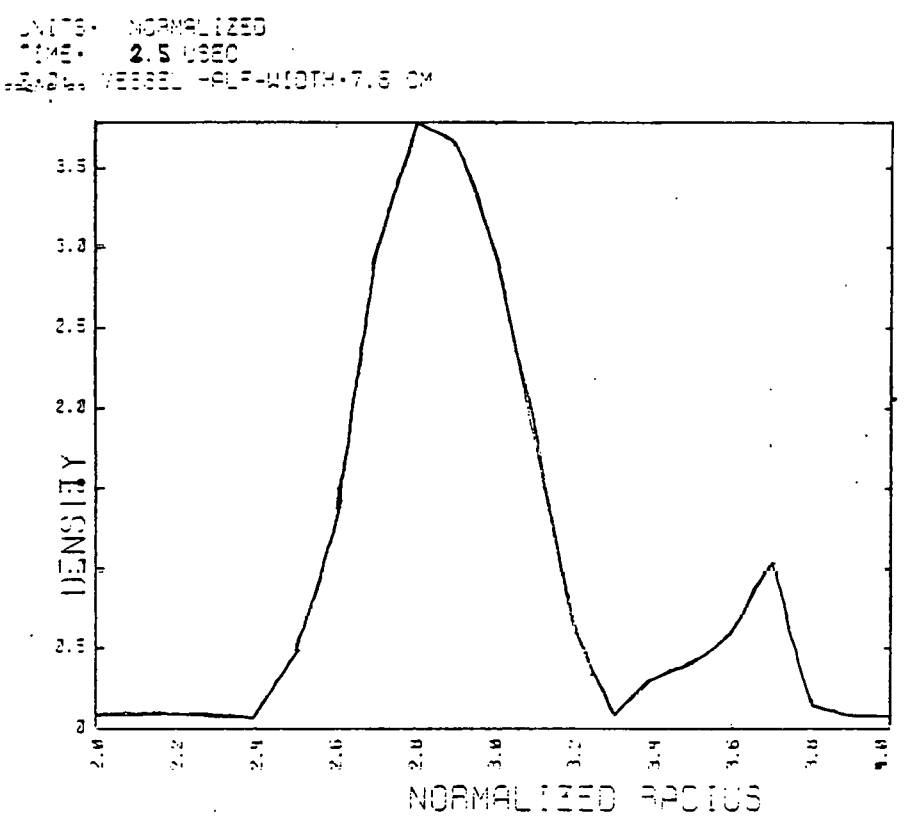

(B)

UNITS: NORMALIZED
TIME: 5.0 USEC
VESSEL HALF-WIDTH=7.5 CM

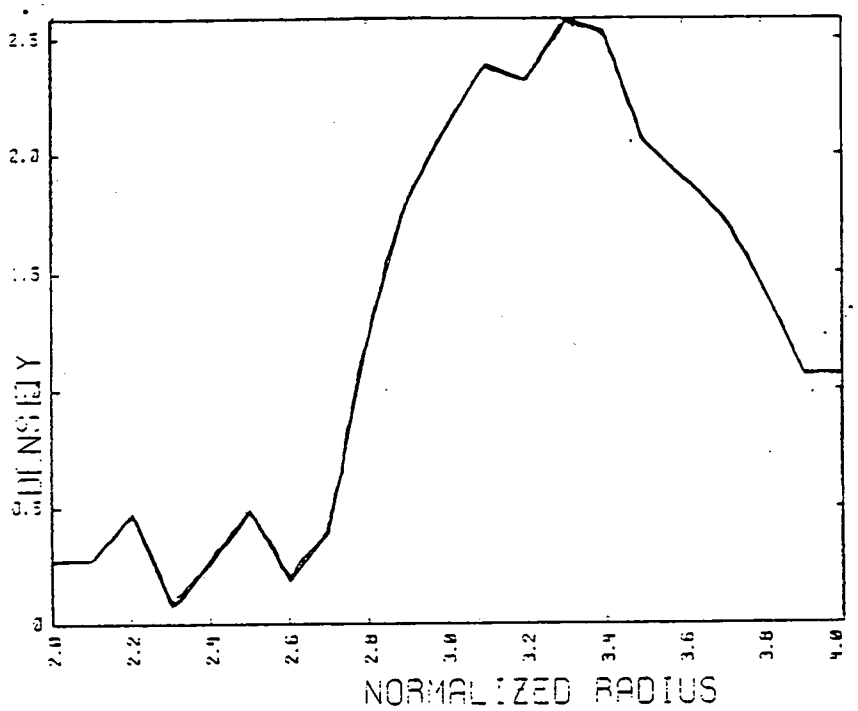

Figure IV.30

Plasma density profiles along the horizontal midplane for heating case 6.

(A)

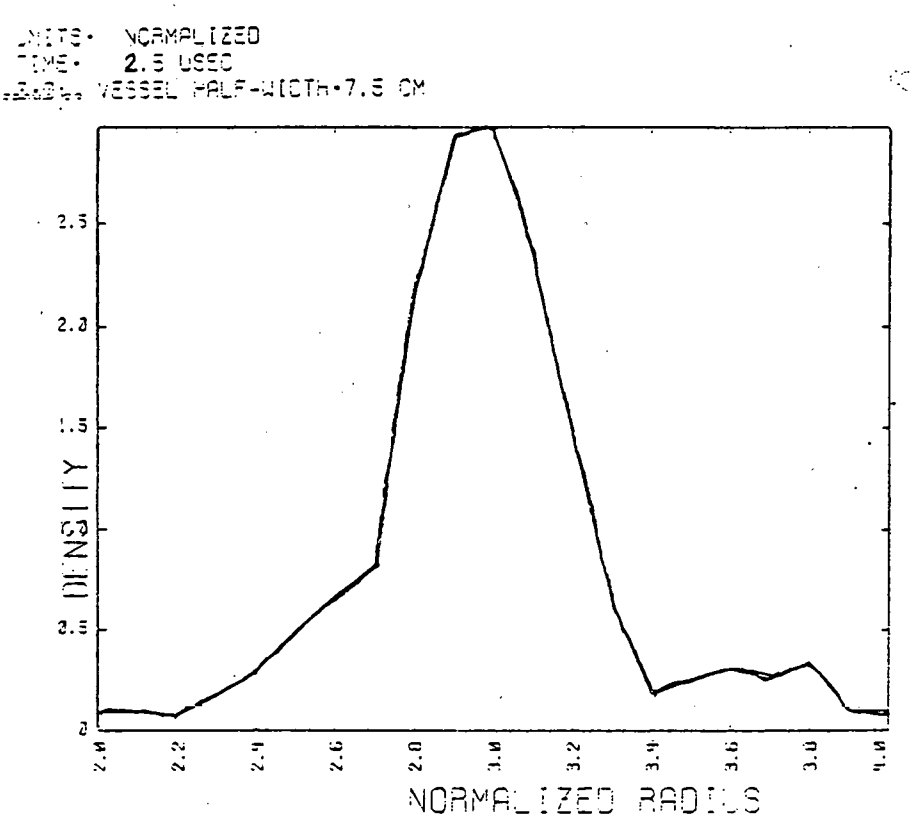

(B)

some extent. When the outer edge of the plasma encounters a large enough vertical field it ceases its radial motion. The trailing edge of the plasma continues moving outward until the plasma pressure is balanced by the magnetic pressure. The contraction of the plasma along z continues. Since the plasma has finite inertia it over-compresses the field on the outside. The plasma is then pushed radially inward, expanding both along r and z. This motion continues until the magnetic pressure near the inner wall is sufficient to retard the plasma motion. If the prescribed vertical field is too large, this balance will not occur and the plasma strikes the inner wall. Such results were observed but are not presented here. The elongation along z is dictated by the relative squeezing of the plasma due to leakage patterns. After radial motion has stopped, the plasma continues to flow in the vertical direction to the outer corners of the vessel. For this reason we believe that the plasma shrinks. Thus, the plasma elongation of ∿5:1 presented here does not exist at later times. It may shrink as low as ∿2.5:1.[34] This behavior has not been simulated due to the computational costs of running the two-dimensional code for such long times.

After 6 μsec we compute all components of $\rho \frac{Dv}{Dt}$, $\underline{J} \times \underline{B}$ and ∇P. The results are interesting. For regions of appreciable plasma density ($\rho \geq 10\% \rho_{peak}$) we find that

$$\rho \left.\frac{D\underline{v}}{Dt}\right|_{r,\phi} \sim 10^{-2} (\nabla P, \underline{J} \times \underline{B})_{r,\phi}$$

$$\nabla P\Big|_{r,\phi} \simeq \underline{J} \times \underline{B}\Big|_{r,\phi}$$

is true half-way up the plasma column. The condition

$$\nabla P\Big|_{z} \simeq \underline{J} \times \underline{B}\Big|_{z}$$

is true in regions close to the horizontal midplane only. No components of ∇P and $\underline{J}\times\underline{B}$ are equal near the top of the plasma column. This is in agreement with the continued flow/loss of plasma into the corners of the vessel. It is important to repeat that this is independent of any loss mechanism other than the coil geometry of the device. Due to this flow, we are unable to compute to the point where pressure is a function of the poloidal flux alone. That is, $P=P(\psi)$. While the plasma is in excellent equilibrium along z=0, the "information" on plasma state is not communicated all along the flux contour. Rather, at the top, equilibrium does not exist and the "flow of information" is disrupted. Thus, along the lower part of the plasma column we find

$$P_L = P_L(\psi) \qquad P_R = P_R(\psi) \qquad P_L(\Psi) \neq P_R(\Psi)$$

where the subscripts L,R refer to left and right of the magnetic axis. Strictly speaking, we are unable to heat to a two-dimensional MHD equilibrium. We do not claim that one does not exist in Torus-II but only that it may take longer to achieve than the study period of

6 μsec.

Figures IV.31 and IV.32 again illustrate the rapid soak-in of the toroidal magnetic field. This is consistent with the results obtained by (8). At 6 μsec we compute peak plasma beta values of 33% and 39% for cases 6 and 4 respectively. Due to the inclusion of the large loss term in the energy equation, plasma temperature drops to 37 eV for case 4 and 31 eV for case 6. The accuracy of such a rapid decay is debatable. As experimental results are obtained from Thompson scattering measurements, the phenomenological loss term can be adjusted to give an appropriate β decay. For completeness we exhibit profiles of B_z and pressure along the horizontal midplane after heating. (Figures IV.33 and IV.34) The poloidal field computed at r=30 cm agrees very well with recent experimental probe data.

A brief discussion of the plasma safety factor, q, is in order. We compute q at 6 μsec by numerically integrating[2]

$$q(\Psi) = \frac{\chi(\Psi)}{2\pi} \oint \frac{dl}{|B_{pol}|} \frac{1}{r^2}$$

Such a calculation is suspect since we do not have a strict equilibrium even at 6 μsec. However, it certainly gives us a rough quantitative estimate of the plasma q-profile. In Figure IV.35 we exhibit such profiles for cases 4, 5 and 6. We can weakly state that within the limits of certainty of the numerics (finite grid spacing-numerical integration), $q \gtrsim 1$ in all cases. For the values of plasma cur-

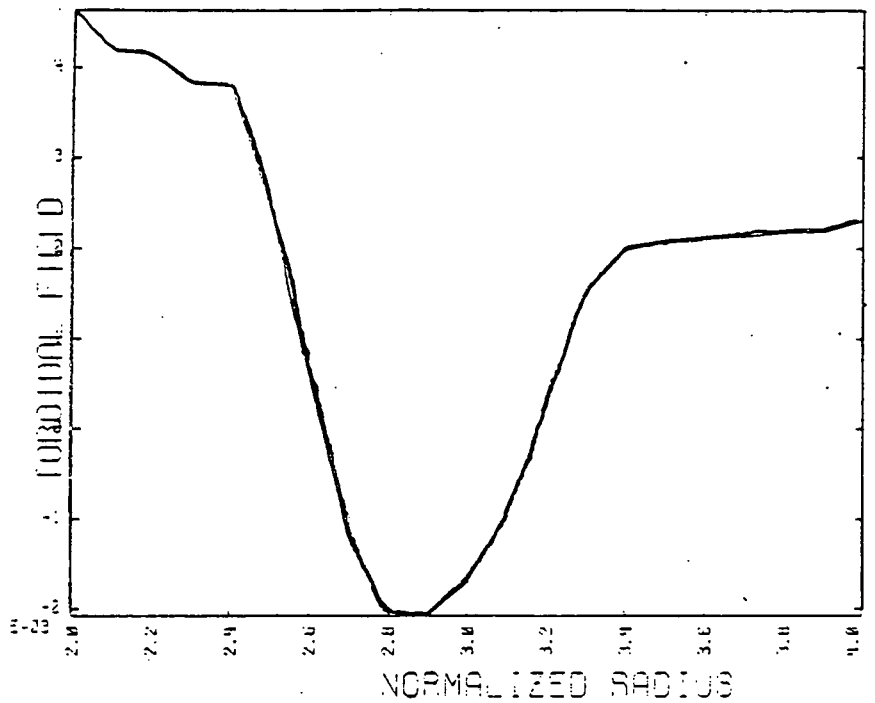

Figure IV.31

Toroidal field profiles along the horizontal midplane for heating case 4.

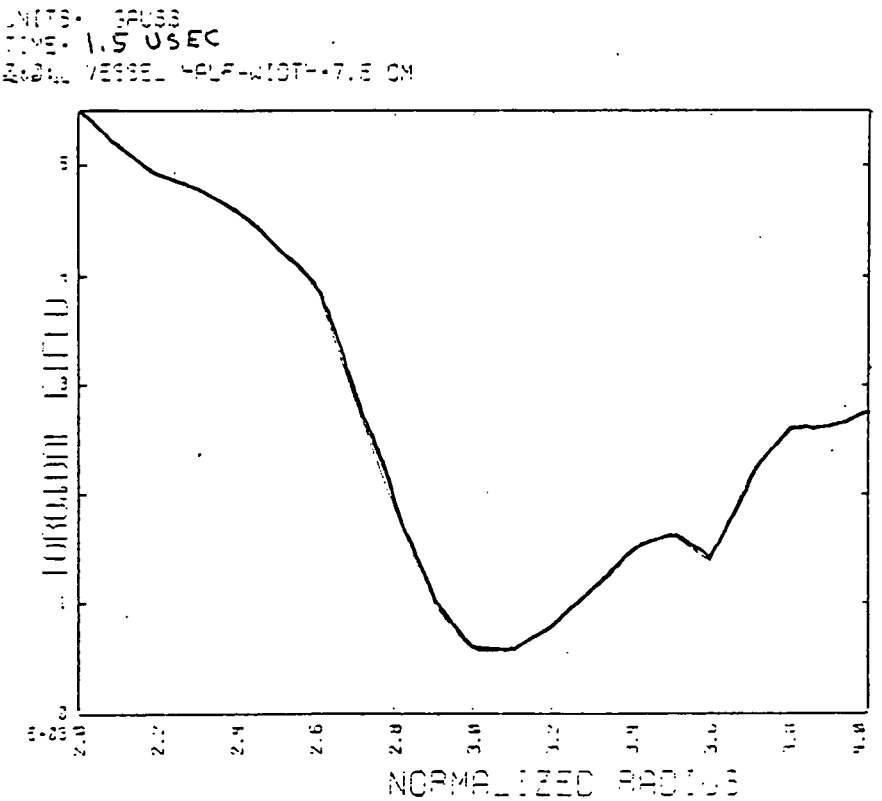

(A)

(B)

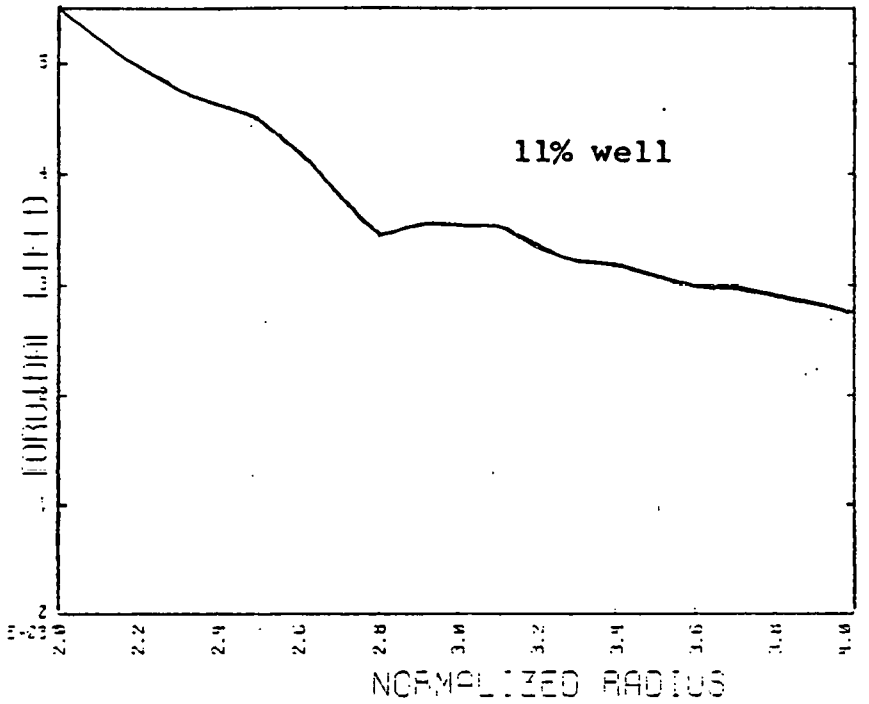

Figure IV.31.C

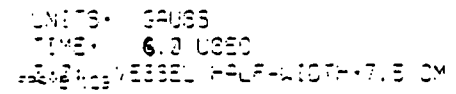

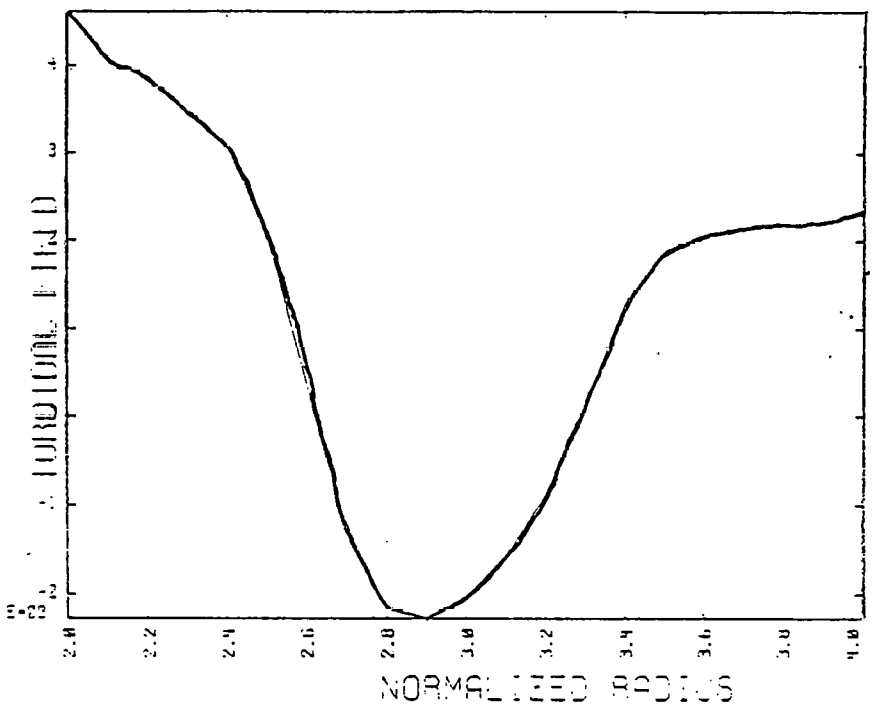

Figure IV.32

Toroidal field profiles along the horizontal midplane for heating case 6.

(A)

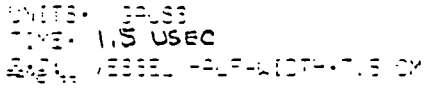

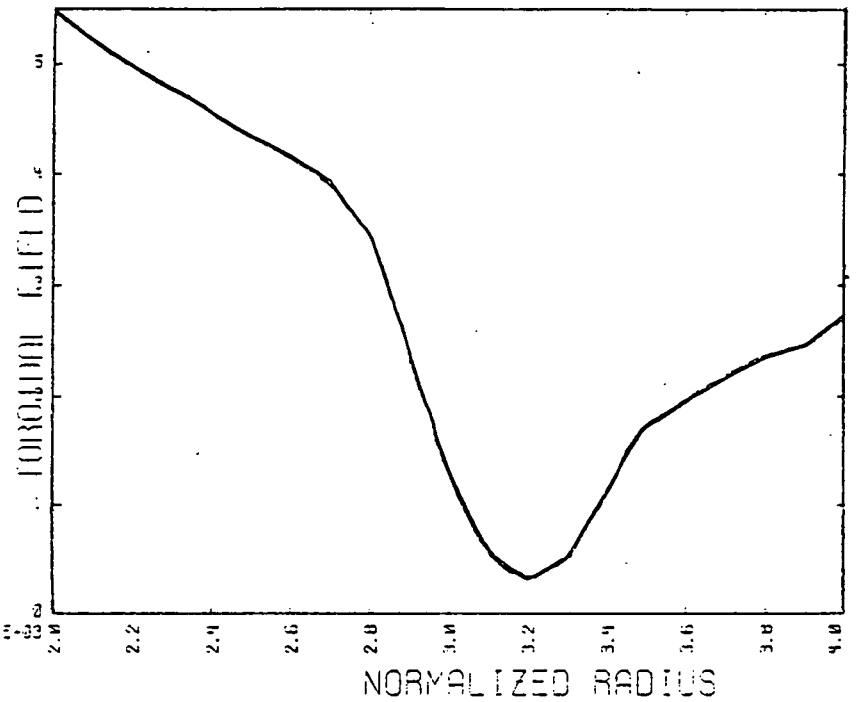

Figure IV.32.B

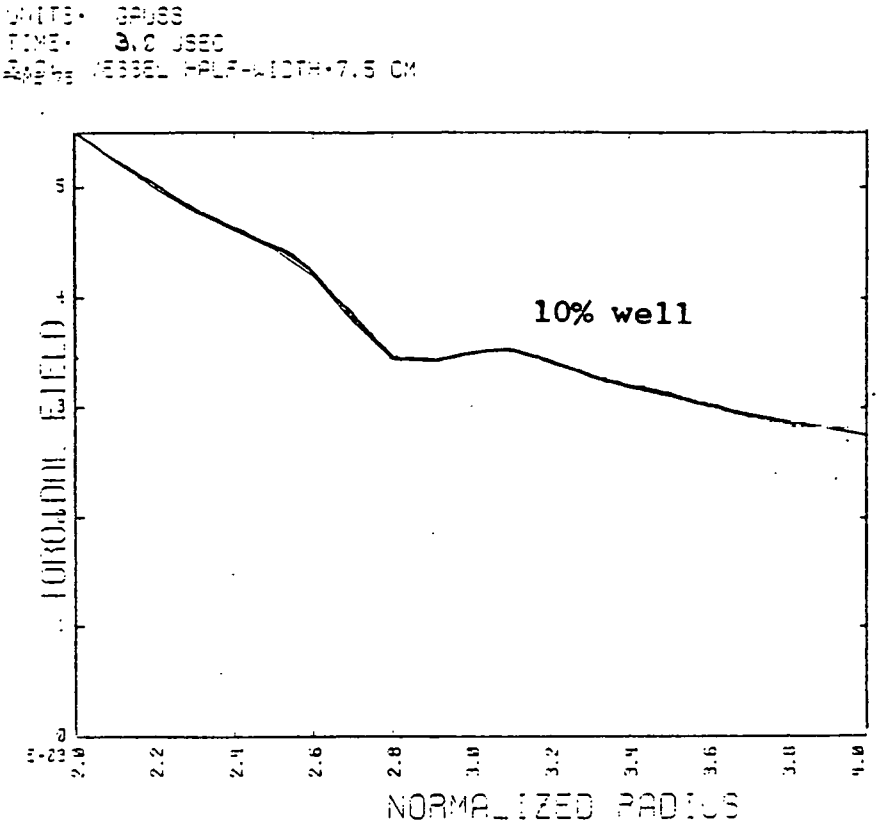

Figure IV.32.C

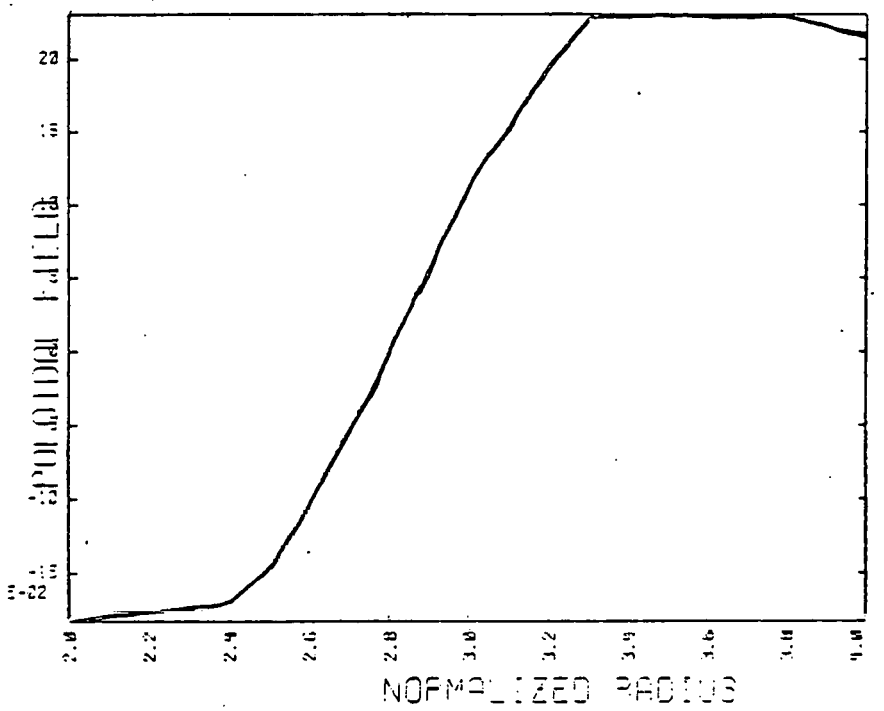

Figure IV.33.A

Poloidal field profile along the horizontal midplane for heating case 4.

UNITS: GAUSS
TIME: 5.0 USEC
VESSEL HALF-WIDTH=7.5 CM

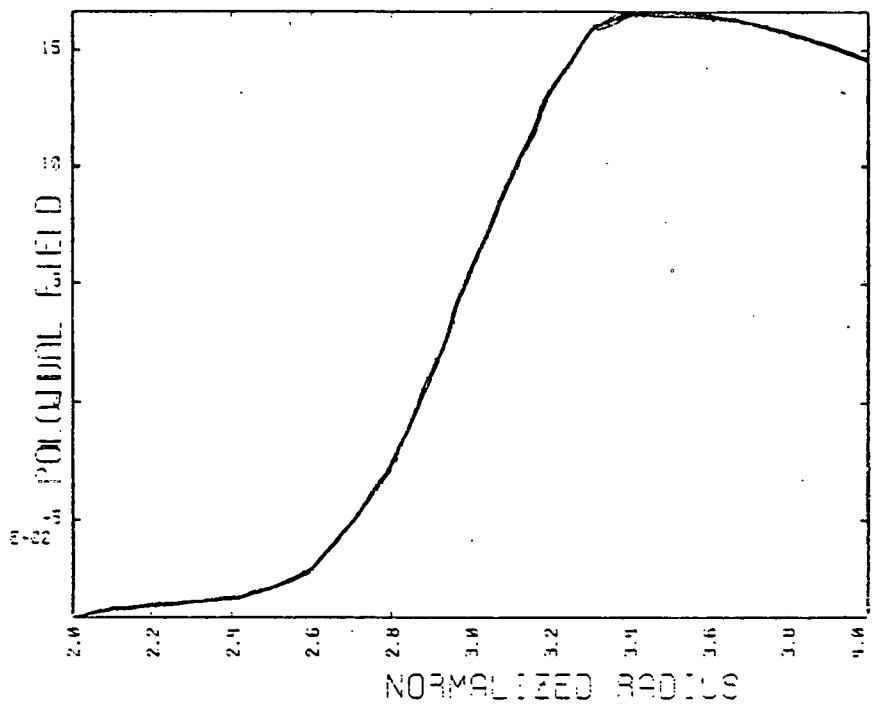

B) Heating case 6

UNITS: GAUSS
TIME: 5.0 USEC
VESSEL HALF-WIDTH=7.5 CM

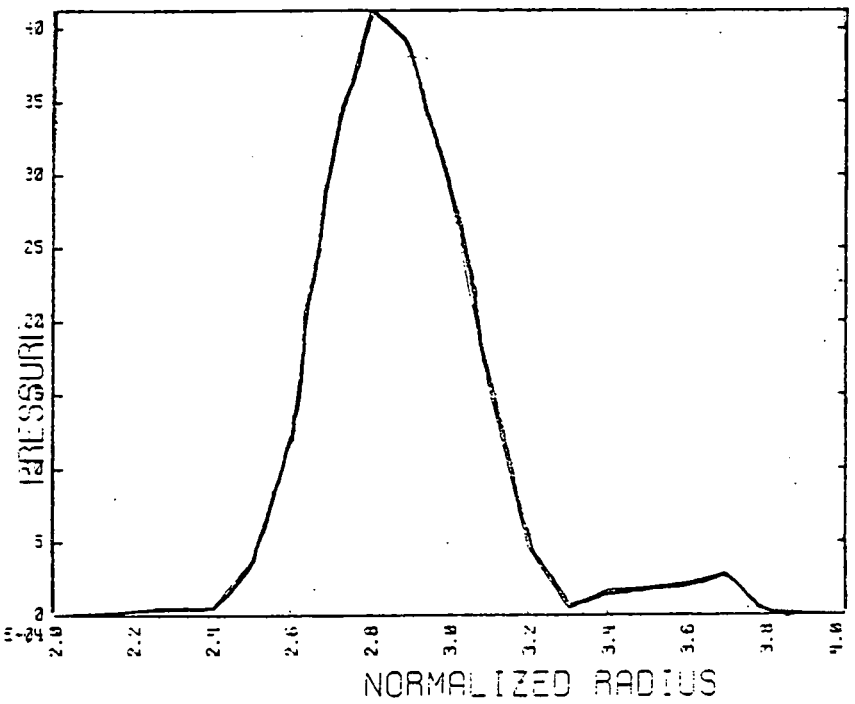

Figure IV.34.A

Plasma pressure profile along the horizontal midplane for heating case 4.

UNITS: DYNES/CM**2
TIME: 5.2 USEC
VESSEL HALF-WIDTH=7.5 CM

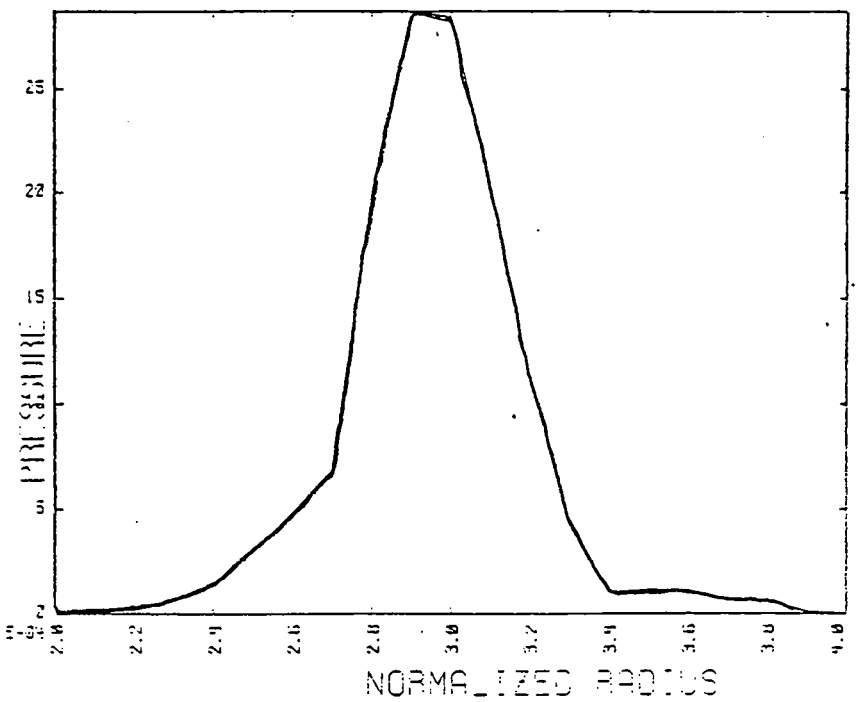

B) Heating case 6

UNITS: DYNES/CM**2
TIME: 5.2 USEC
VESSEL HALF-WIDTH=7.5 CM

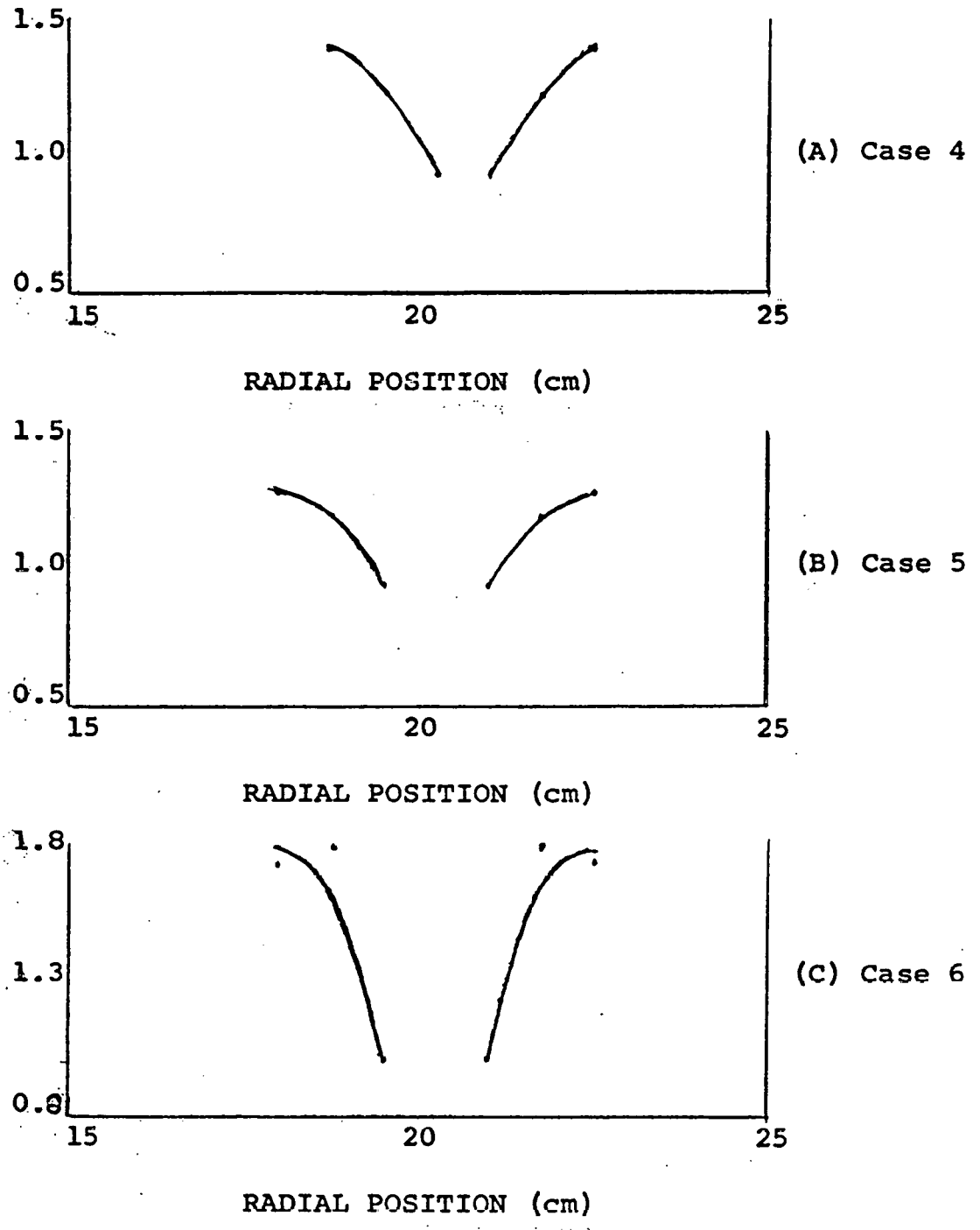

Figure IV.35

Profiles of safety factor for three half-power heating simulations after 6 usec.

rent computed in the half power case (40-70 kA), this result appears surprising. It is the ∿5:1 elongation that saves the large current carrying plasma from going kink unstable ($q < 1$). As the plasma shrinks it is accompanied by a loss of current. While we have not quantified such a phenomena over long times, we expect the loss of plasma current to balance the plasma shrinking such that the safety factor remains greater than one throughout the duration of the experiment.

Implicit in all the above discussion is that the external currents are heating at least a singly ionized (and usually double ionized) helium ion. MHD can not simulate ionization processes. Therefore, to test if Torus-II can indeed "burn through" the ionization of helium and subsequently overcome impurity radiation losses, we must use the zero-dimensional atomic physics code described earlier.

2.C) Zero-Dimensional Heating Study

The results of this phase of our work are particularly sensitive to the amount of time for which we use the anomalous resistivity. The heating phase is characterized by the switching on of the anomalous resistivity. This is done immediately after the 4 μsec z-pinch phase has been simulated. To emphasize the varying results possible we present three typical cases in Table IV.6.

Table IV.6

Inputs for Zero-Dimensional Heating Study

Case number	1	2	3
Z-pinch Peak current (A/cm^2)	200	200	100
Heating Peak current (A/cm^2)	500	500	800
Heating time (μsec)	3	4	4
% Oxygen	2	2	2
% Silicon	1	1	1

In Figures IV.36 and IV.37 we exhibit the computed ion and electron temperatures. The important point to be emphasized from these results is that for typical Torus-II parameters, the heating mechanism can "burn through" the ionization and radiation barriers.

Figure IV.38 shows the time history of fully ionized helium. We clearly see that the ionization of helium occurs during the heating phase. For each case, ionization is complete within 3 μsec after the onset of the turbulent poloidal currents. Minor differences exist. For example, He^{+} exists for a longer time in case 1 than case 2 or case 3. However, since $T_e \gtrsim 40$ eV at 6 μsec for the three simulations, the ionization rate is large enough to give similar values of $He^{++}(t)$.

For the colder temperatures of case 1 we obtain Ox^{+3} and Si^{+4}. The hotter temperature of case 3 yields Ox^{+5} and Si^{+6} at the end

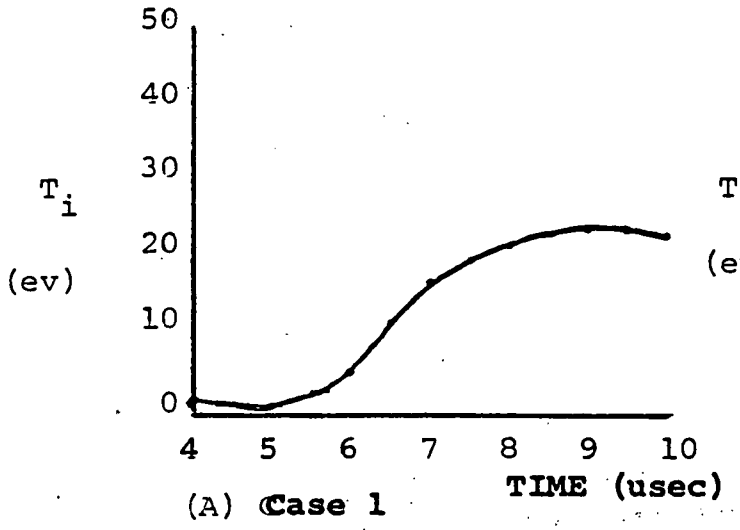

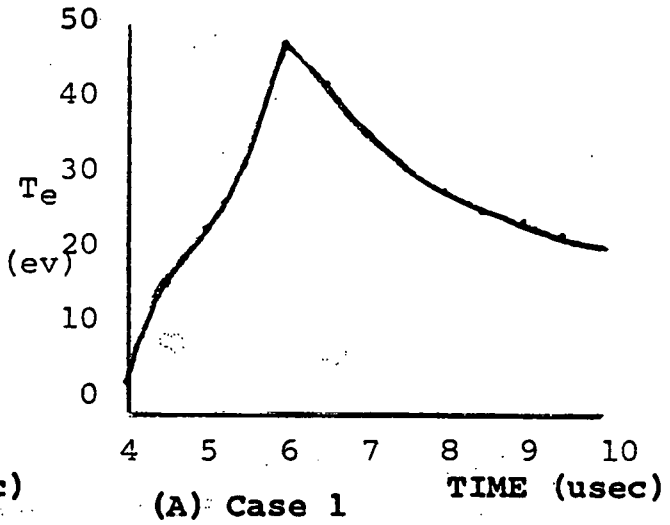

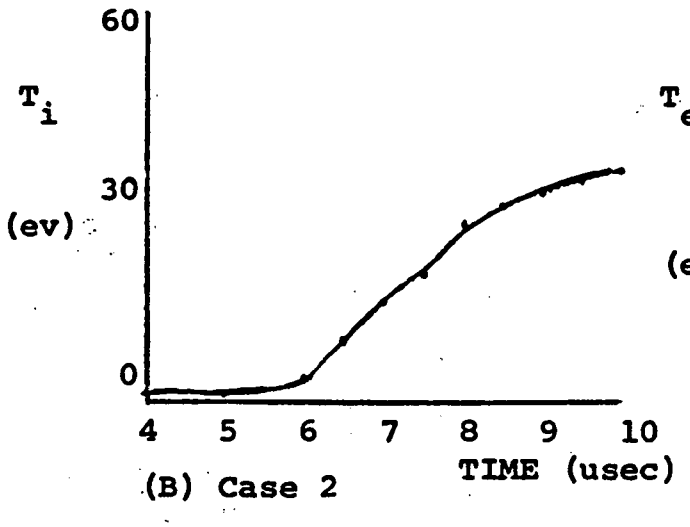

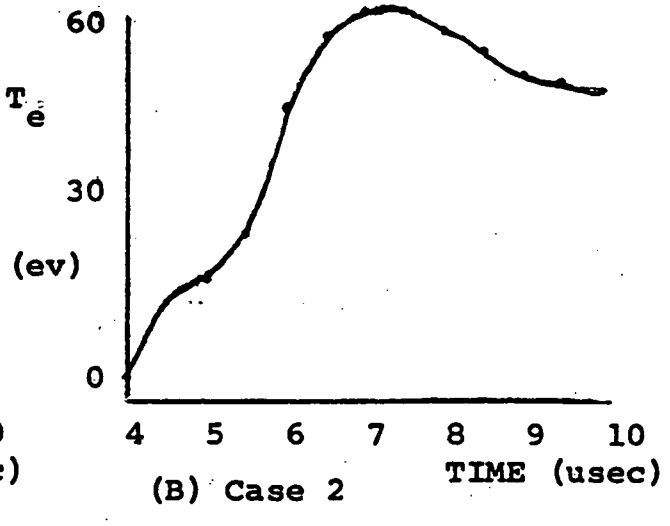

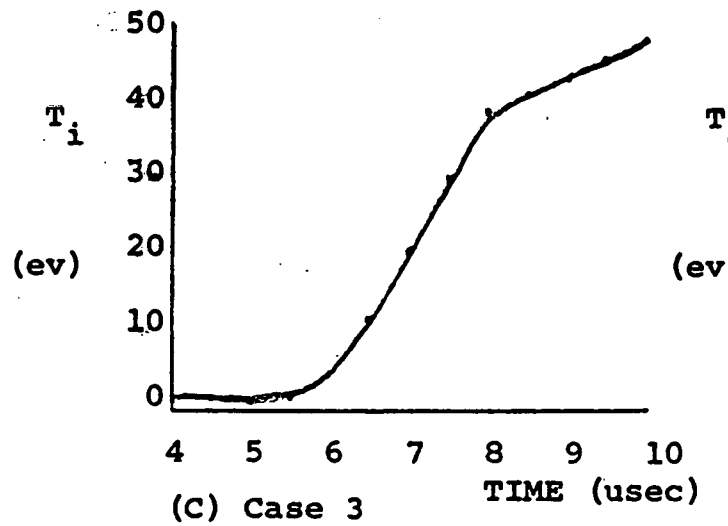

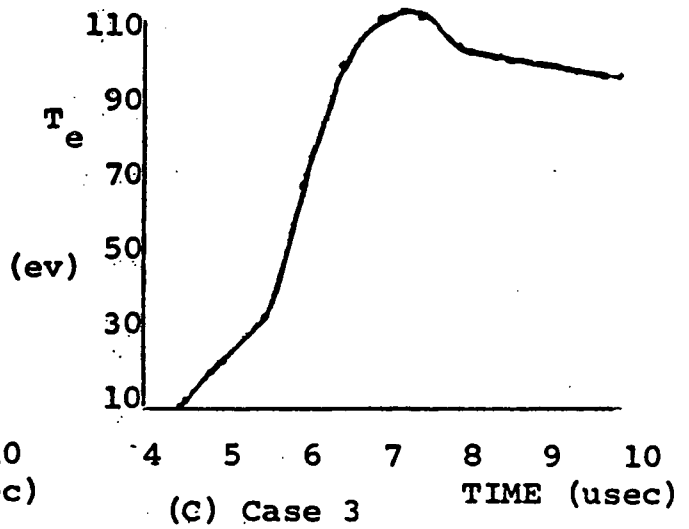

Figure IV.36
Ion temperature from zero-dimensional simulation of Torus-II heating phase.

Figure IV.37
Electron temperature from zero-dimensional simulation of Torus-II heating phase.

of heating. Thus, both plasmas will continue to radiate power away. We observe a 2 μsec delay in ion heating in every simulation despite the anomalous ion-wave heating term. This is coincidental with the rapid ionization of helium, oxygen and silicon. Thus, $d(n_i T_i)/dt$ includes a large dn_i/dt component. When this vanishes at 6 μsec we observe heating of the ions. Here we have another effect of poor plasma preparation.

These results clearly indicate that if Torus-II is to become hot we must have a successful onset and sustained turbulent period. The heating mechanism is enough to produce interesting temperatures despite poor plasma preparation. The dominant loss mechanism during the early part of the heating is due to ionization. As the plasma is heated, transport losses become a more important part of the simulation. When the turbulence is shut off, the principal loss process is impurity line radiation. This leads us to our next topic of discussion, the description of the high beta plasma state.

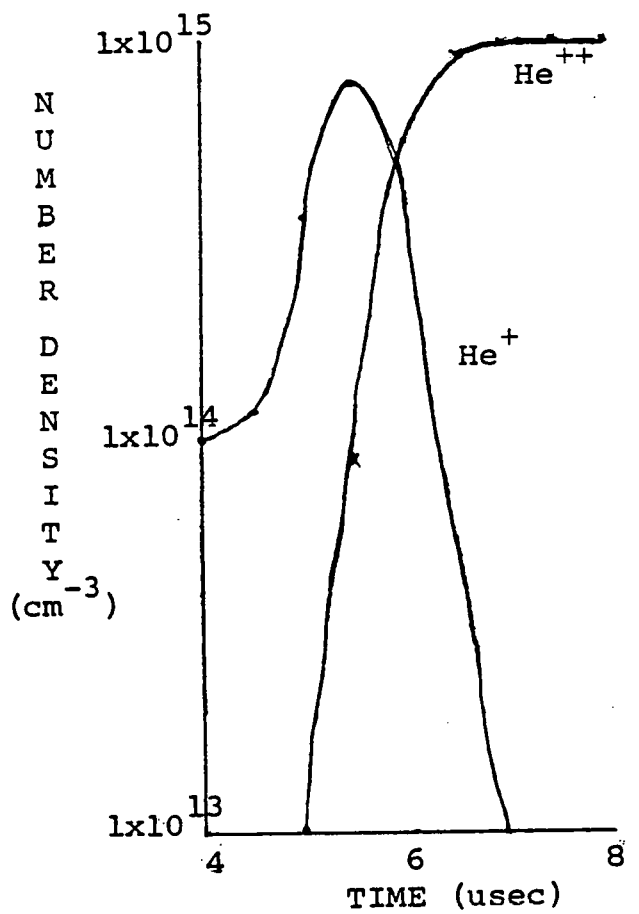

(A) Case 3

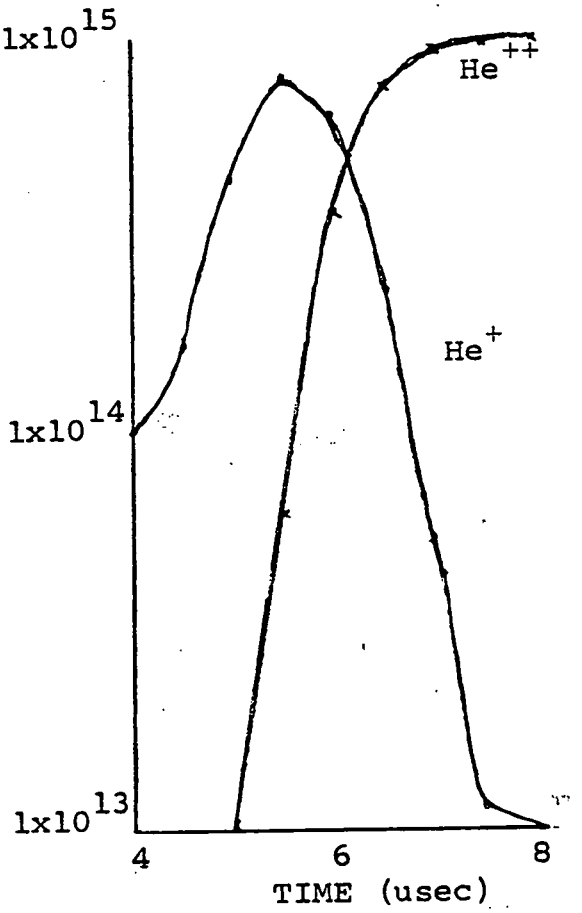

(B) Case 2

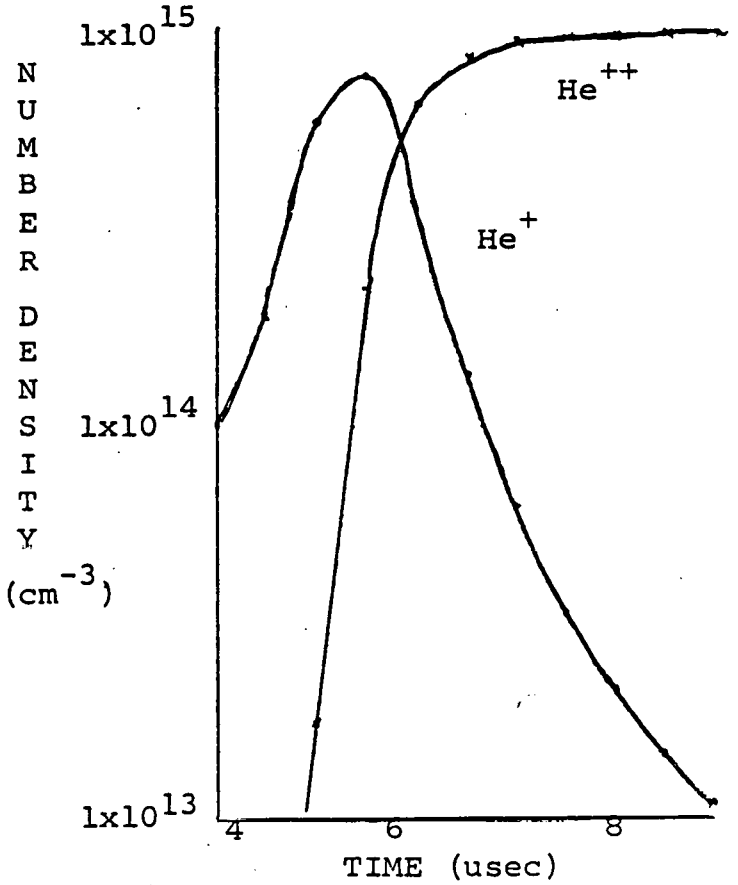

(C) Case 1

Figure IV.38

Helium ion number density as a function of time for zero-dimensional heating simulations.

3) The Torus-II High Beta Tokamak Phase

We now combine the information supplied by the heating simulations with all available experimental data to set up appropriate initial high beta plasma states and follow the decay processes.

A) Quarter Power Study

The heating phase simulation produced high temperature plasmas, $\sim$ 100 eV. Recall however that no radiative losses were included. Experimentally, the peak plasma temperature has been reported[32] as $\sim$30 eV. Also from (32), the plasma is set up further towards the outside (r $\simeq$ 24 cm) than predicted by the heating simulation (r$\simeq$22 cm). Specifying a plasma current of 40 kA and an elongation of 3:1, we vary the oxygen and silicon content. At this temperature, the average ion model predicts a maximum in the radiated power lost due to oxygen. The plasma cools within 10 μsec. Figure IV.39 shows the central plasma temperature as a function of time for different impurity levels. We see that the silicon concentration is not important at these temperatures. The quarter power case is not a promising candidate for high beta research due to this rapid cooling. A time scale analysis was performed for the above initial conditions. Using data generated by the one-dimensional transport code, we found the following.

$$\tau_c \simeq 240 \text{ μsec}$$

$$\tau_h \simeq 190 \text{ μsec}$$

$$\tau_o \simeq 70 \text{ μsec}$$

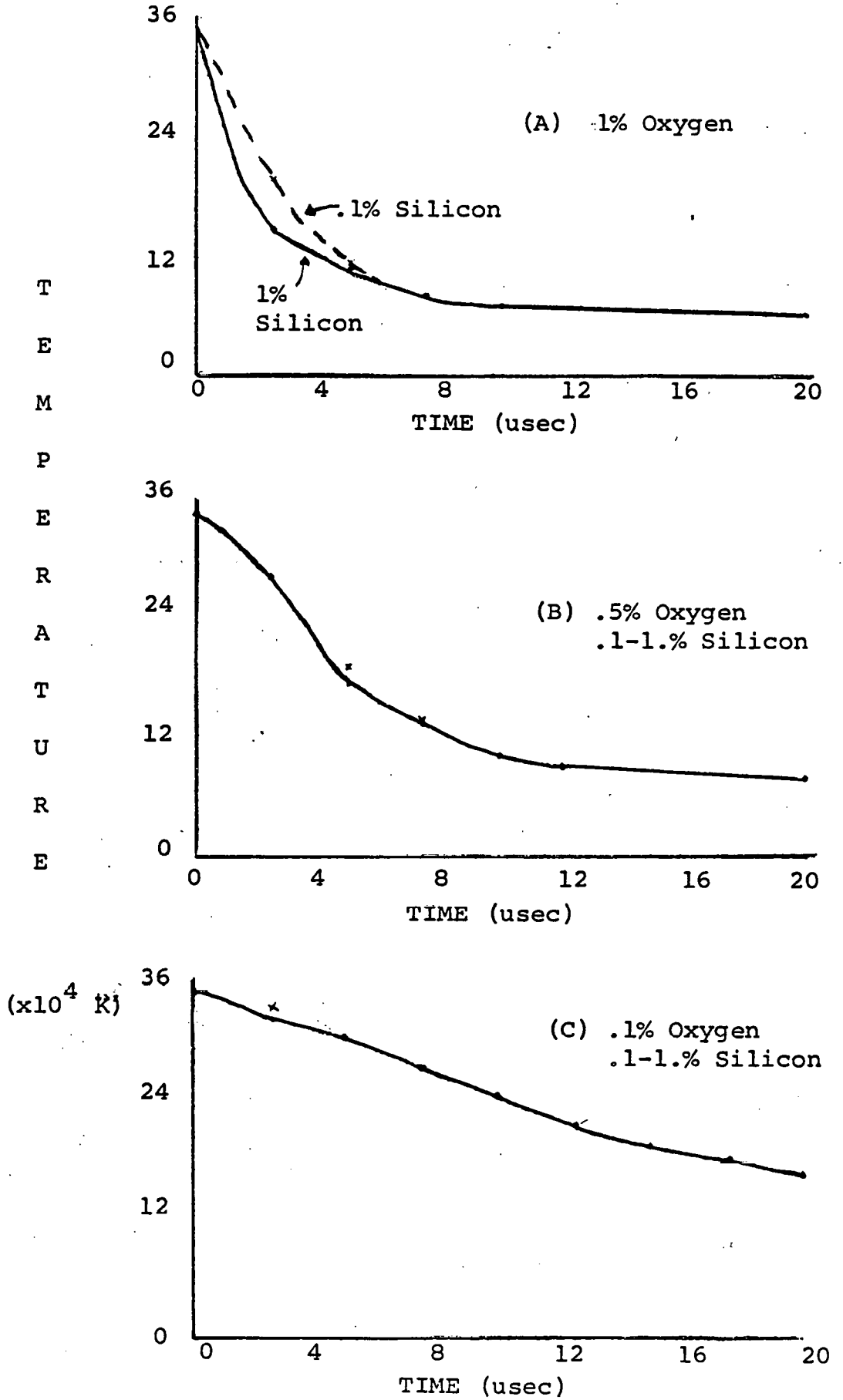

Figure IV.39 Central plasma temperature decay during the high beta tokamak phase. Initial conditions are post-quarter power heating phase.

$$\tau_b \simeq 40\ \mu\text{sec}$$

$$\tau_r \simeq 1\ \mu\text{sec}$$

where τ_c represents a convective (flow) time scale, τ_h is the thermal conduction time scale, τ_o is an ohmic heating time scale due to toroidal plasma currents, τ_b is a magnetic diffusion time scale for a classical resistivity, and τ_r is a radiation time scale for 1% oxygen. The decay rates of the fields measured in Torus-II are in accordance with our computed τ_b. This calculation illustrates the difficulties associated with a high beta plasma resulting from quarter power heating. For these reasons, the effort devoted to the quarter power heating and diffusion simulations was considerably less than that devoted to the half power operating case. We forgo discussion of profiles for the quarter power case and proceed immediately to the half power simulation.

B) Half Power Study

Using our one-dimensional diffusion code, we simulate the high beta state resulting from half power heating. Again we make use of the heating simulation results and experimental observations to prescribe initial conditions. Since the results of plasma heating can never be completely (or totally accurately) known either through simulations or experimental measurements, we also ask the question, what if the plasma state is.....? This is related to the "arbitrary" initial conditions discussion of chapter III. Two-dimensional diffusion design studies of Torus-II were performed by Chu and Byrne.[35]

Presently, H.C. Lui is working on a two-dimensional diffusion code that will eventually be applied to Torus-II.

Extensive probe data is available for the toroidal magnetic field as a function of radial position along the horizontal mid-plane[9] for the quarter power case. Linear extrapolation from this 50 kV case to 70 kV (half power) yields the toroidal field profile used as the initial condition for the high beta simulation. The maximum well depth is 10%. The plasma is 6 cm wide with a peak density of 10^{15} cm^{-3} located at a major radius of 25 cm. The height of the plasma is set to 12 cm. We perform the necessary integrations described earlier. The toroidal plasma current is 25 kA and the poloidal flux, Ψ, in the hole is .01 V-sec. The initial B_z is set to 1.5 kG on the outer wall. Three different initial temperatures are run (65 eV, 130 eV, 175 eV) for combinations of oxygen and silicon concentrations of .5% and 2% yielding 12 simulated cases. We will describe, in detail, the best and worst cases for each of the initial temperature specifications. Based upon earlier discussions it should be obvious that the best prospects for high beta research are for impurity levels of .5% oxygen and .5% silicon. The worst cases are those of 2% oxygen and 2% silicon. We will briefly mention the intermediate cases as we proceed. Table IV.7 summarizes the initial temperature and impurity levels for each case.

Consider first the plasma with an initial temperature of 65 eV. During the very early times ($t \lesssim 10$ μsec) the power radiated by silicon ($\sim$2 MW) dominates the cooling. When the plasma temperature

Table IV.7

Summary of High Beta Tokamak Study

Case Number	Initial T_{peak} ($\times 10^4$ K)	Oxygen	Silicon
1	75	2%	.5%
2	75	2%	2%
3	75	.5%	.5%
4	75	.5%	2%
5	150	2%	.5%
6	150	2%	2%
7	150	.5%	.5%
8	150	.5%	2%
9	200	2%	.5%
10	200	2%	2%
11	200	.5%	.5%
12	200	.5%	2%

reaches ∿40 eV, the oxygen radiated power loss (6.5 MW) destroys the plasma. This is illustrated in Figure IV.40 where we see the plasma rapidly cooling off. The radiated power loss is obtained from a numerical volume integration of the power densities supplied by Post. We conclude the obvious, that oxygen is the primary cause for concern at these temperatures.

Whenever plasma undergoes rapid cooling (typified by cases 1 and 2) the basic assumption of our calculation must be examined.

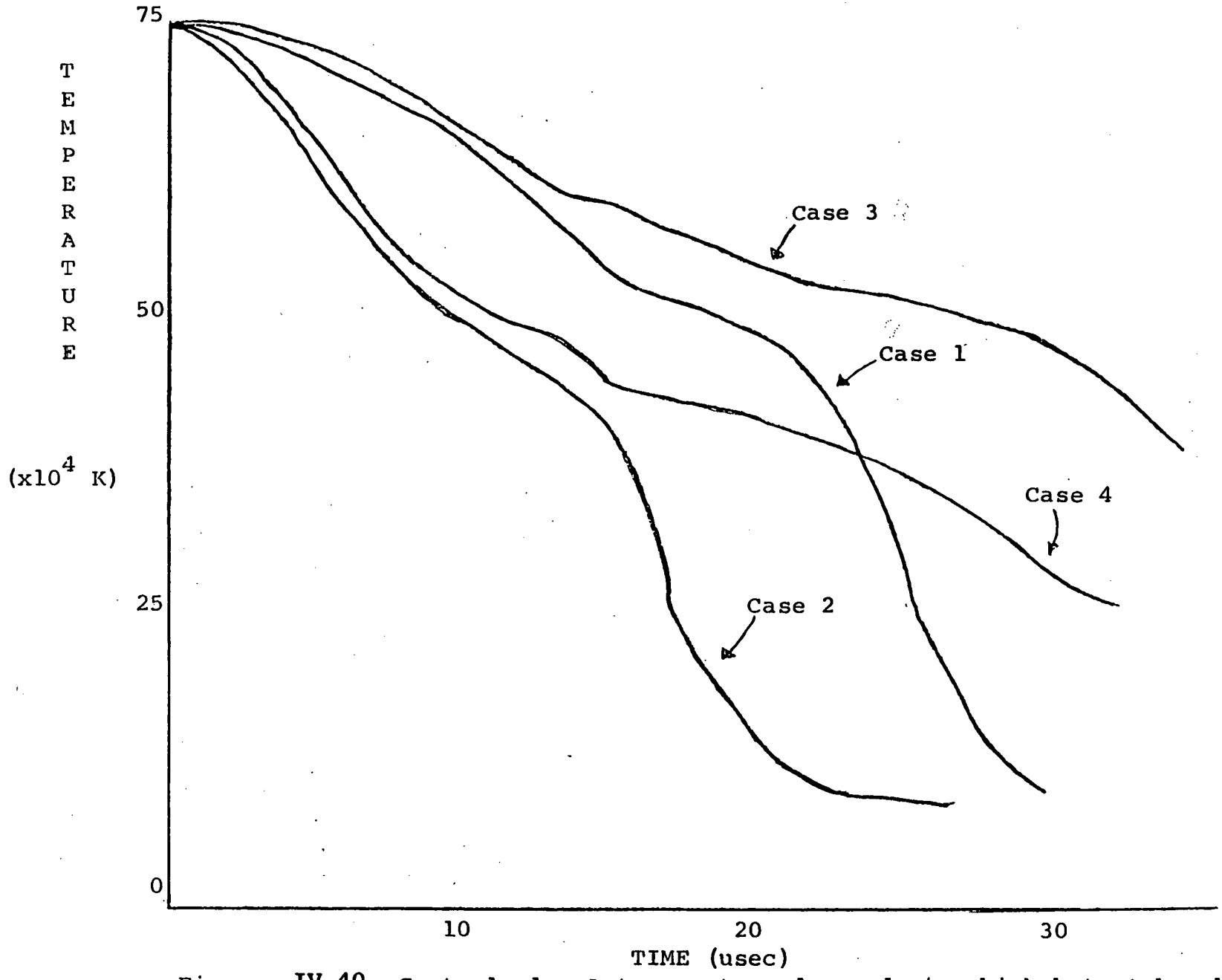

Figure IV.40 Central plasma temperature decay during high beta tokamak phase. Initial temperature (peak) is 65ev.

Recall, the code calls for diffusion through states of successive equilibria so that we can ignore the inertia terms in the momentum equation. Figure IV.41 allows us to follow the plasma density distribution in time for cases 2 and 3. As expected, plasma is lost to the outer wall for the case of large impurity content. The cooling results in an increase in plasma resistivity. This causes a decay in toroidal plasma current and diamagnetic poloidal currents (disappearance of toroidal field well) leading to the subsequent loss of confinement. Figures IV.42 and IV.43 follow these processes.

Calculations show that while both cases start with peak beta values of 23%, case 3 decays to 10% and case 2 drops to 2%. Analysis of code flow data indicates that both cases 2 and 3 have velocities on the order of the plasma diffusion velocity, 10^4-10^5 cm/sec for temperatures of 20-65 eV thereby justifying our ignoring of the inertia terms. This does break down in case 2 by 30 μsec when the plasma velocity reaches 10^6 cm/sec and equilibrium is no longer maintained. The plasma motion about the minor axis is a typical diffusive spread accelerated by the increasing plasma resistivity. The plasma motion along the major radius is more subtle. We claim that the ultimate state is that of zero plasma current. Of course confinement is lost before such a state is ever reached. As the plasma approaches this state, we expect B_z to approach its vacuum profile which is everywhere positive. Therefore, the magnetic axis shifts slowly towards the inner wall resulting in a peaked toroidal

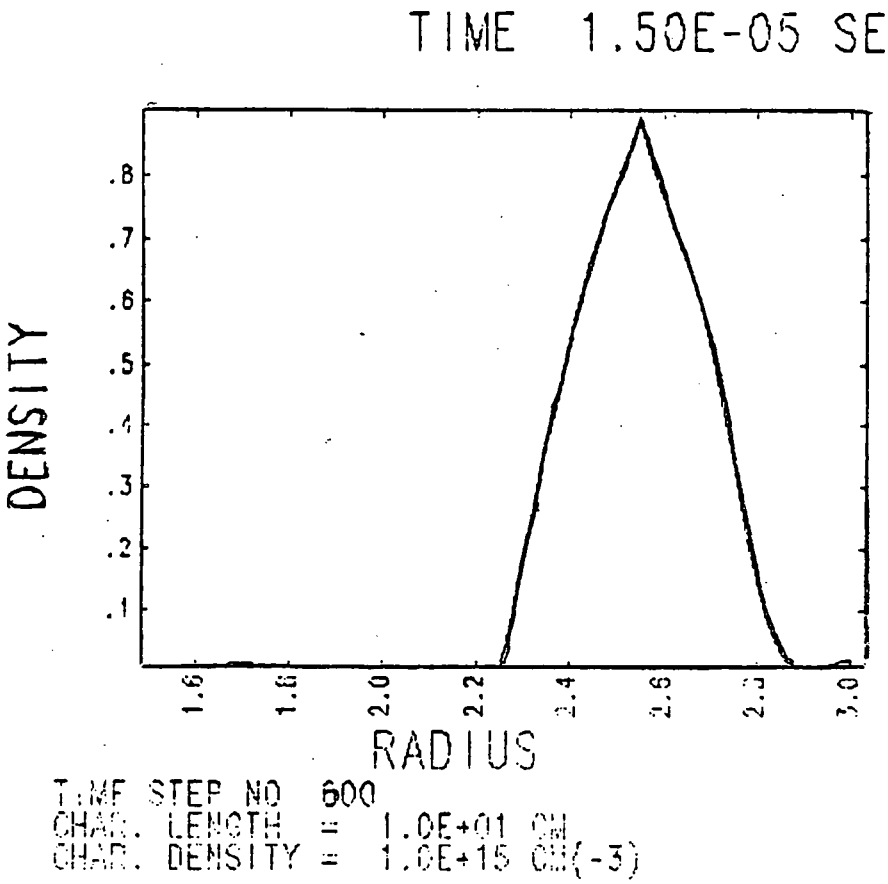

Figure IV.41.A

Density profile for cases 2 and 3 of the high beta tokamak simulation.

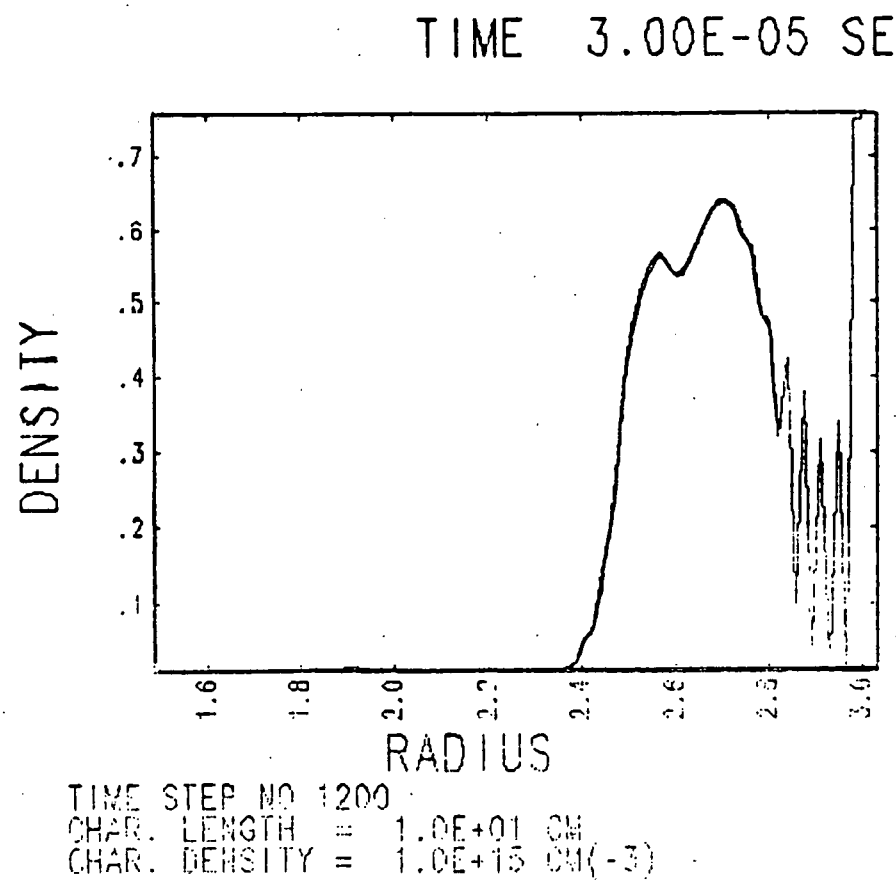

B) Case 2

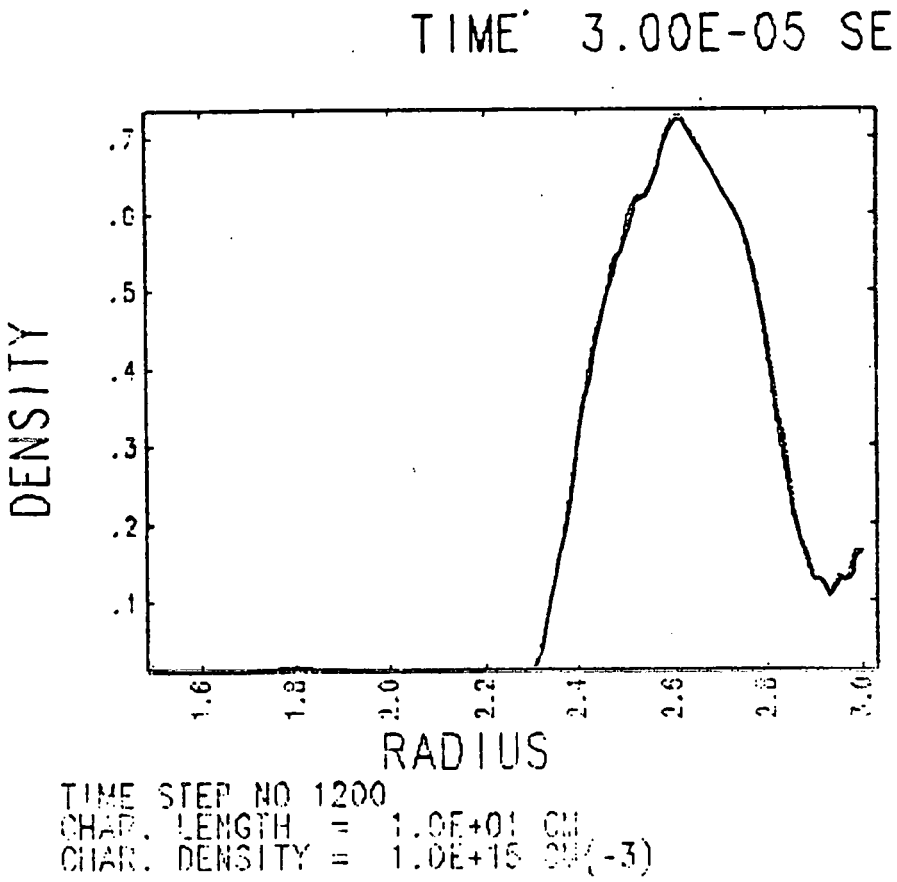

Figure IV.41.C

Case 3

current along the inner half of the plasma. At these late times, the toroidal current is the only heating source in that only it can compensate for radiative losses. The result is that the plasma temperature profile is skewed such that it is hotter on the edge closer to the inner wall. The resulting pressure profiles are shown in Figure IV.44. Note that ∇P is much larger in the positive radial direction. Also, for Torus-II, since B_z is equally strong on either side of the plasma and $B_\phi \sim 1/r$, the total magnetic pressure is less towards the outer wall. These field and pressure characteristics tend to shift the plasma outward towards the wall. This is observed experimentally as well as computationally. There are important implications. The loss of confinement to the wall is caused by loss of

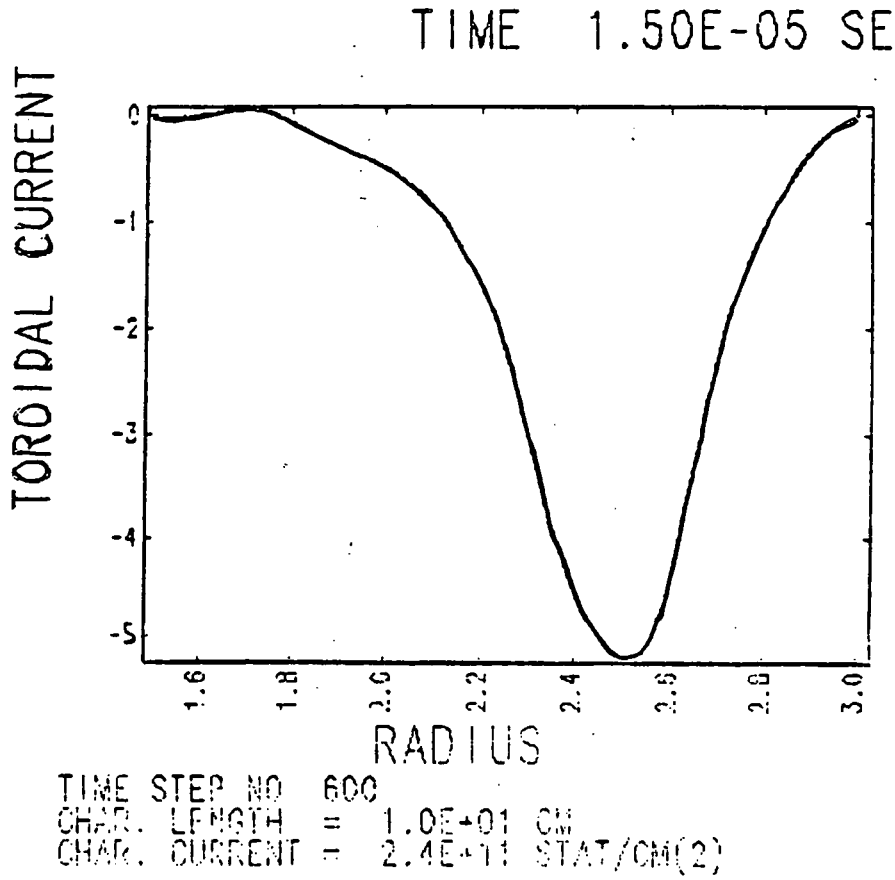

Figure IV.42.A

Toroidal current density for cases 2 and 3 of the high beta tokamak simulation.

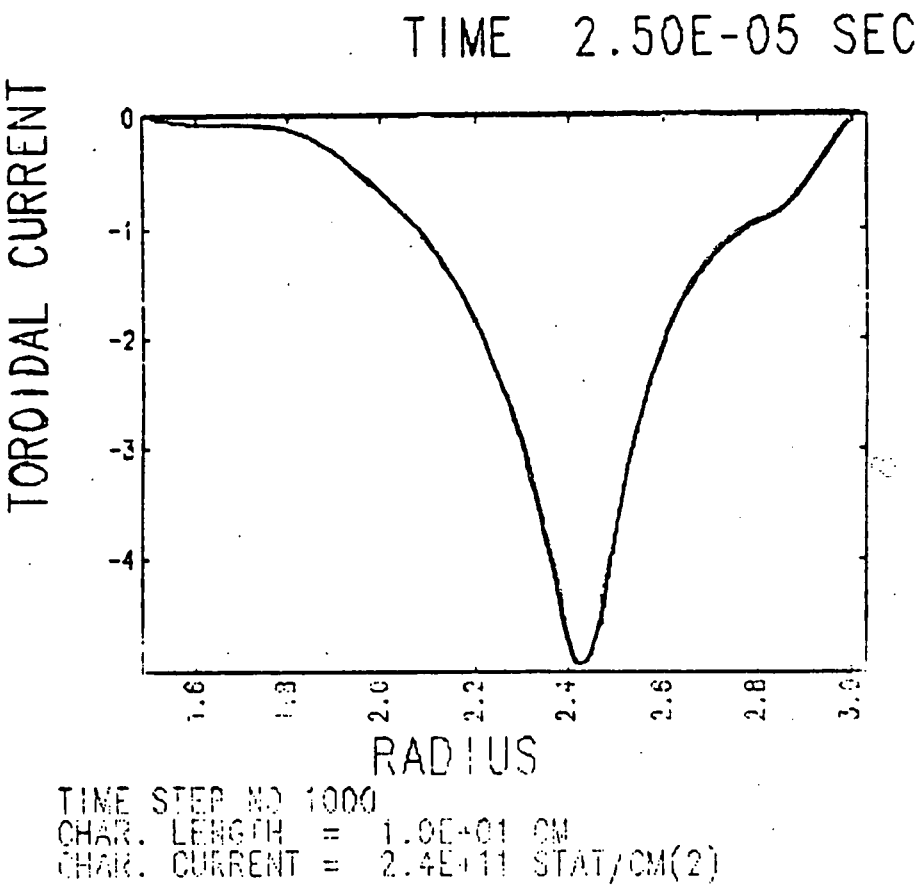

B) Case 2

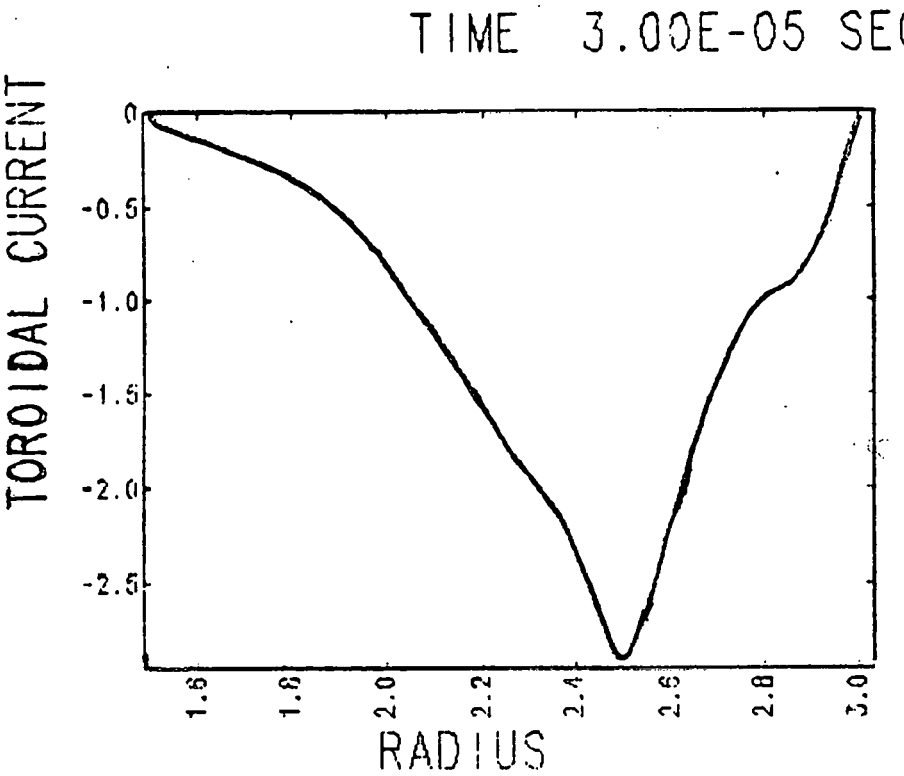

Figure IV.42

C) Case 2

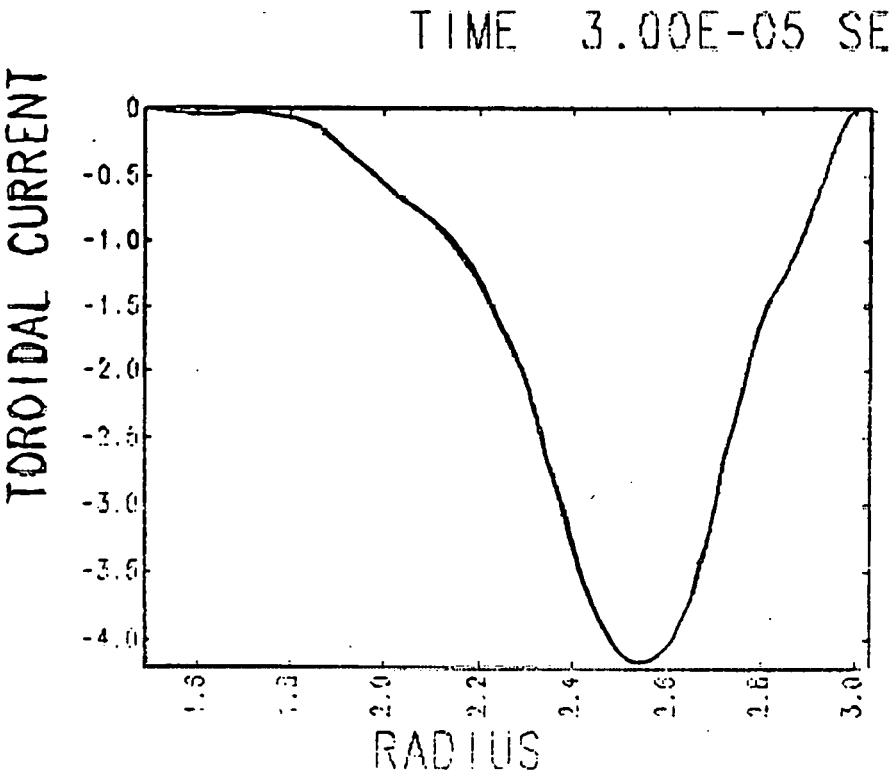

D) Case 3

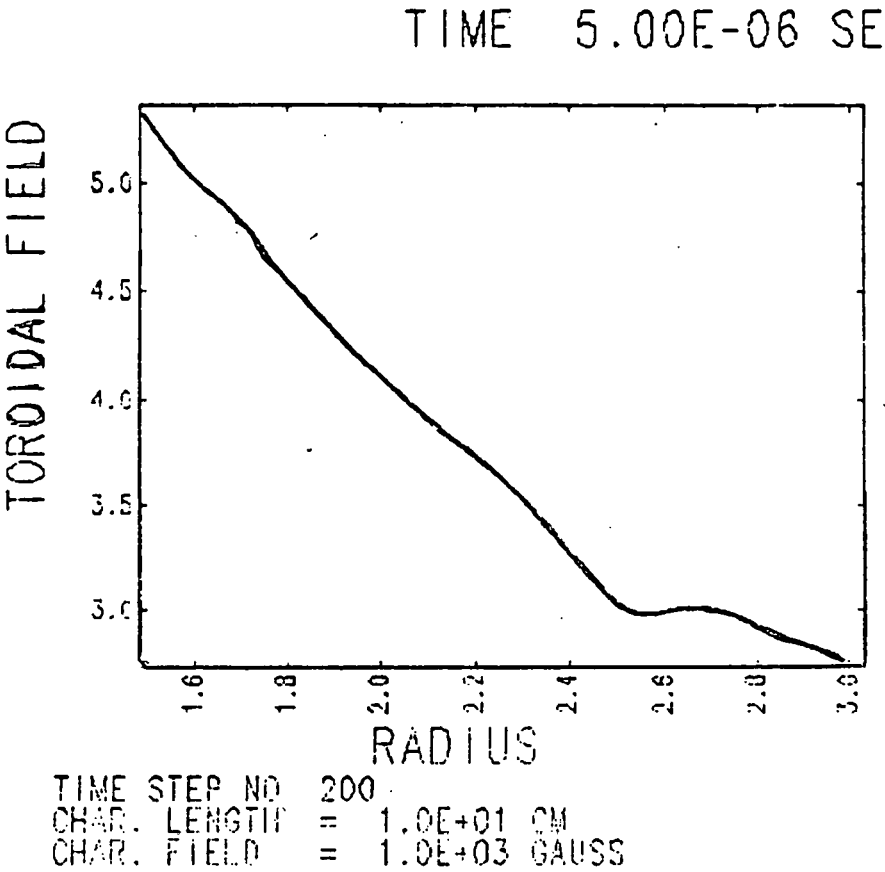

Figure IV.43.A

Toroidal field for cases 2 and 3 of the high beta tokamak simulation.

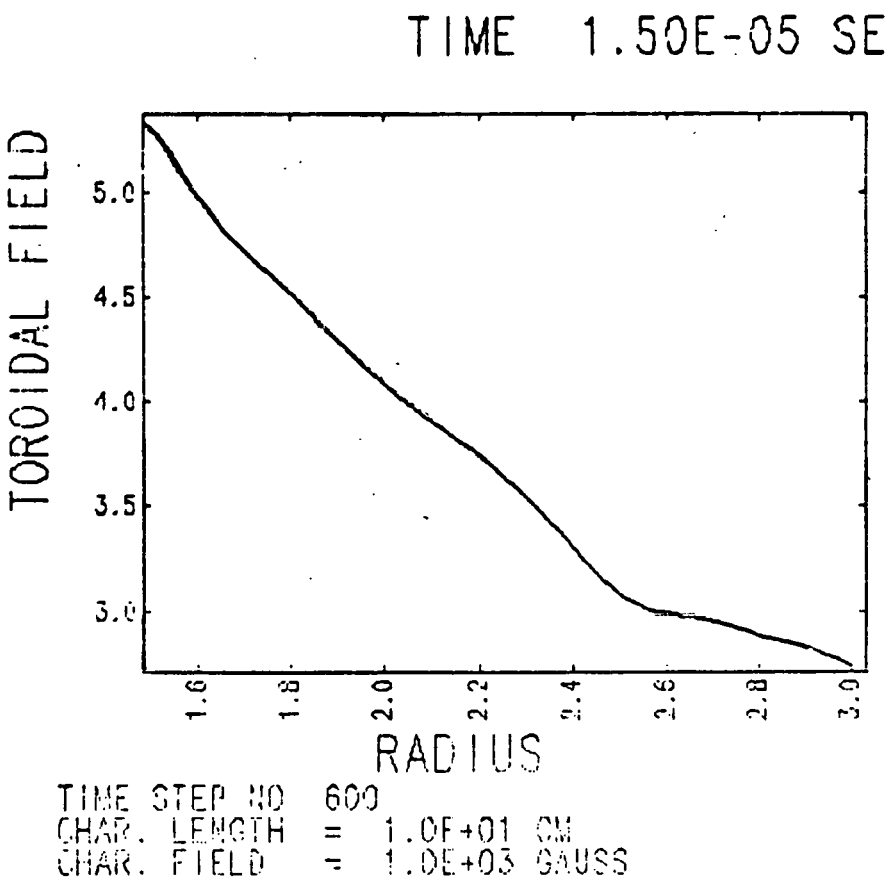

B) Case 2

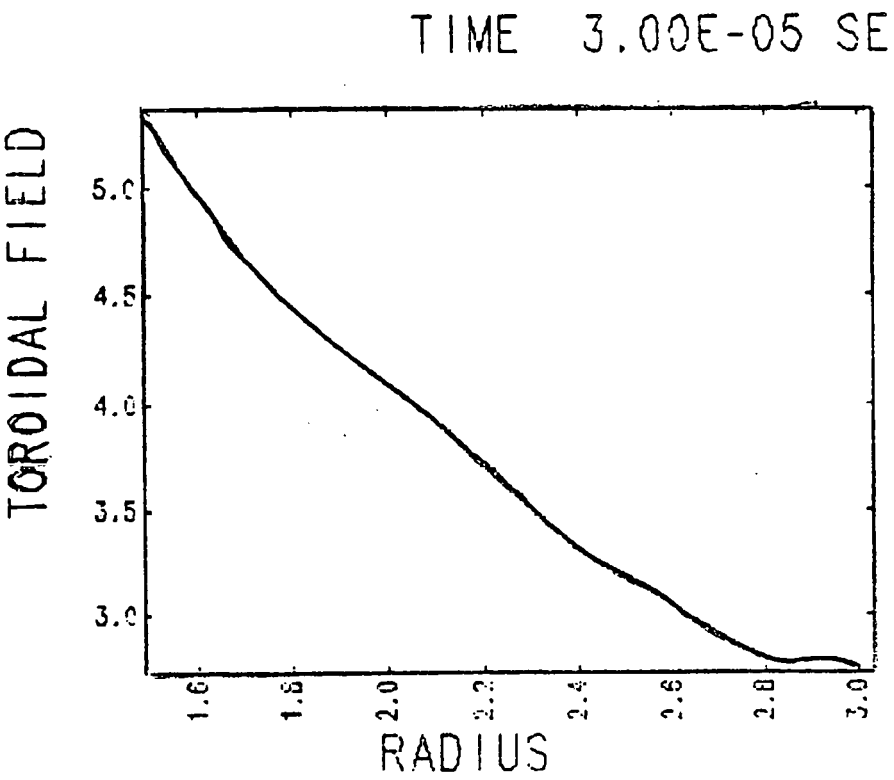

Figure IV.43

C) Case 2

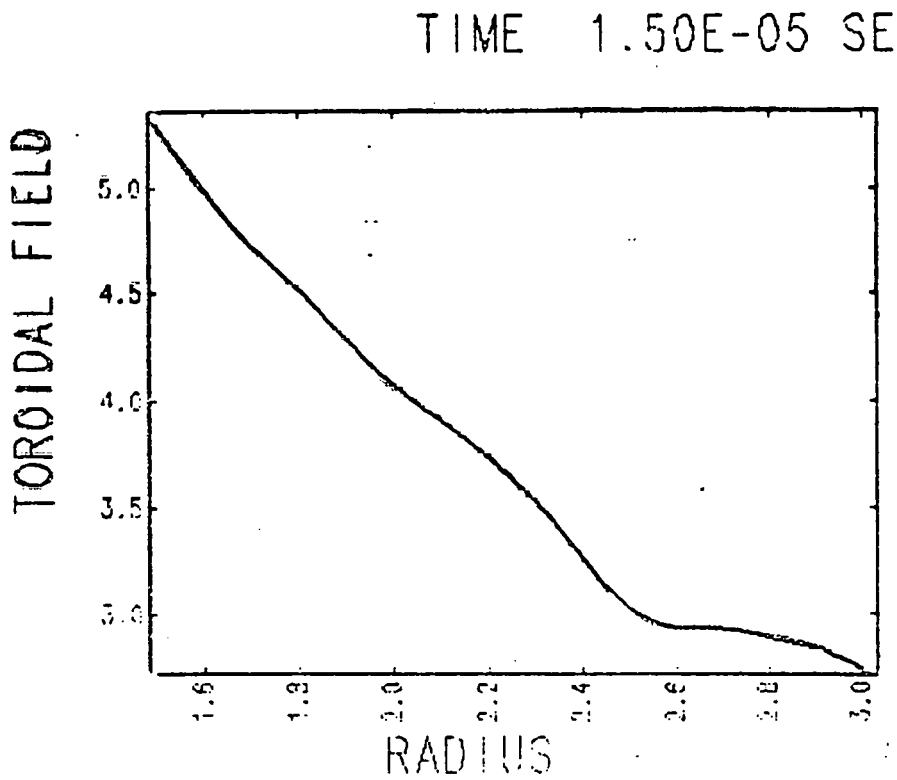

D) Case 3

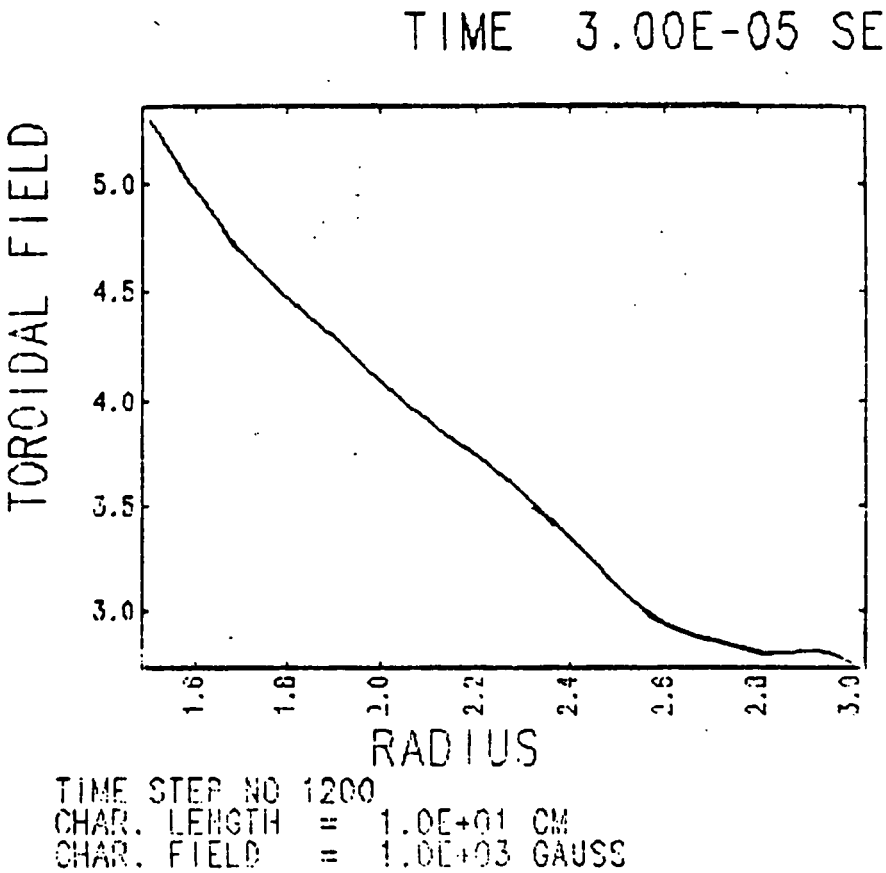

Figure IV.43.E

Case 3

plasma current. In the one-dimensional transport calculation this is due to increasing resistivity resulting from radiation losses. However, any loss of plasma current will yield the same result. Recall that our two-dimensional heating simulations indicated that the coil geometry alone leads to a loss of plasma current. Thus, Torus-II must battle both types of current loss to maintain confinement. It can not. No experiment has lasted 35 μsec beyond the onset of plasma heating. Does heating to high temperatures help?

Consider an initial plasma temperature of 130 eV as in cases 5, 6, 7, and 8. Throughout most of these simulations the dominant

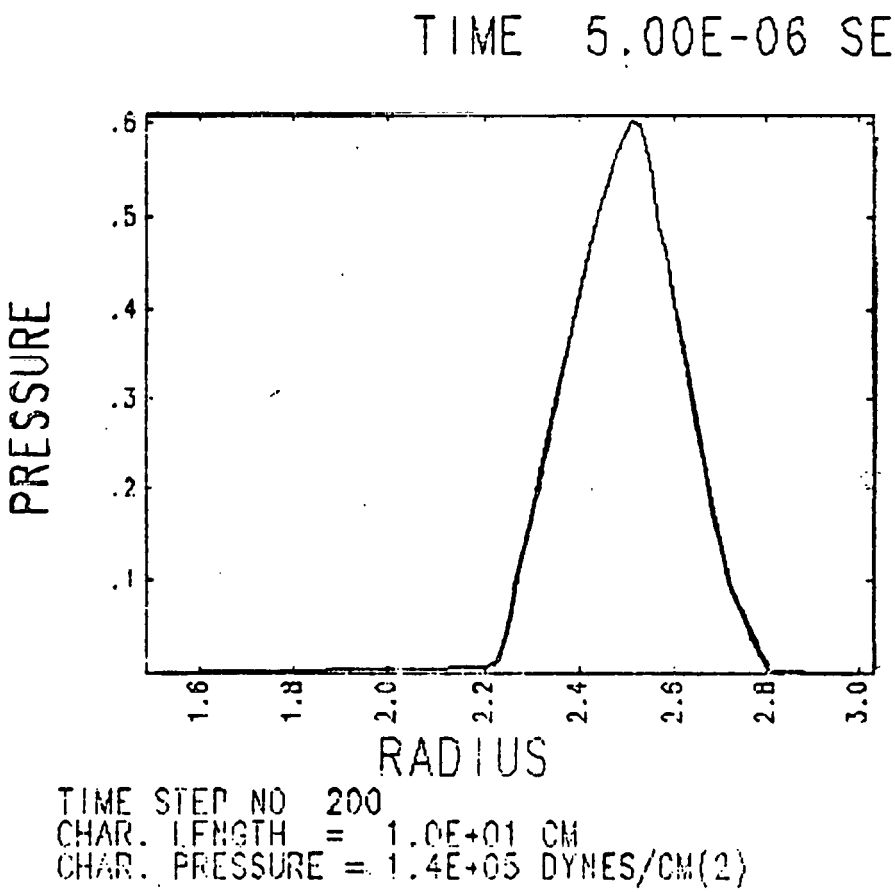

Figure IV.44.A

Plasma pressure for cases 2 and 3 of the high beta tokamak simulation.

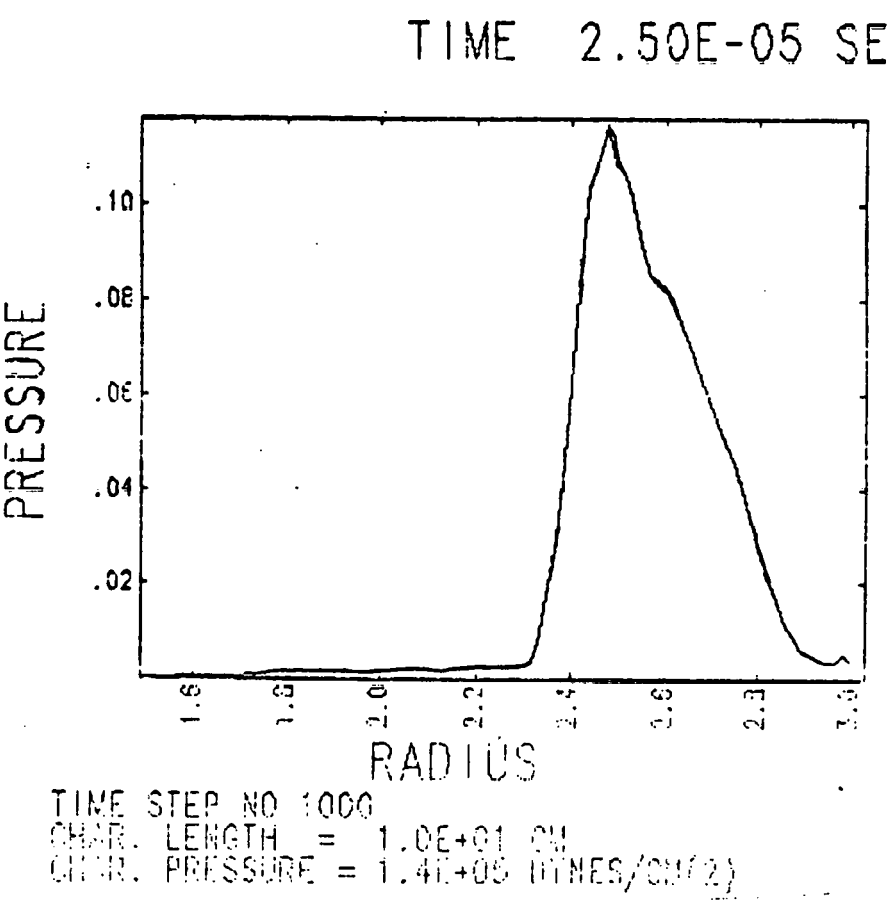

B) Case 2

energy loss mechanism is silicon radiation (5.6 MW). Not until much later times (≃20 μsec) does the oxygen content play a significant role (7 MW) in plasma cooling. The central plasma temperature as a function of time for these cases is given in Figure IV.45. This clearly illustrates the importance of the silicon content. The oxygen content is not a factor until the plasma temperature has cooled to ∿35 eV. Figure IV.46 permits us to follow the plasma density evolution for cases 6 and 7. The two simulations are drastically different. For a 2% silicon level, the plasma pinches thereby becoming skinnier and more dense, contrary to the earlier spreading out observed in cases 1-4. However, case 7 (.5% silicon) remains perfectly confined. The plasma pinching is best explained as follows. As silicon rapidly radiates away energy from the plasma there is a large drop in the thermodynamic pressure. This occurs on a time scale of ∿10 μsec. This is much faster than the diffusion time scale of ∿300 μsec for a 130 eV classical plasma. As energy is lost and temperature decreases, the diffusion time scale is greatly decreased. To maintain equilibrium, as required by the code, the plasma seeks to fight the decrease in pressure. This can be done in two ways. First by increasing density, that is, the pinching effect observed. Secondly, by fighting the energy loss through increased ohmic heating. This is accomplished by pinching of the plasma current density since

$$\frac{\partial T}{\partial t} \sim \eta J^2$$

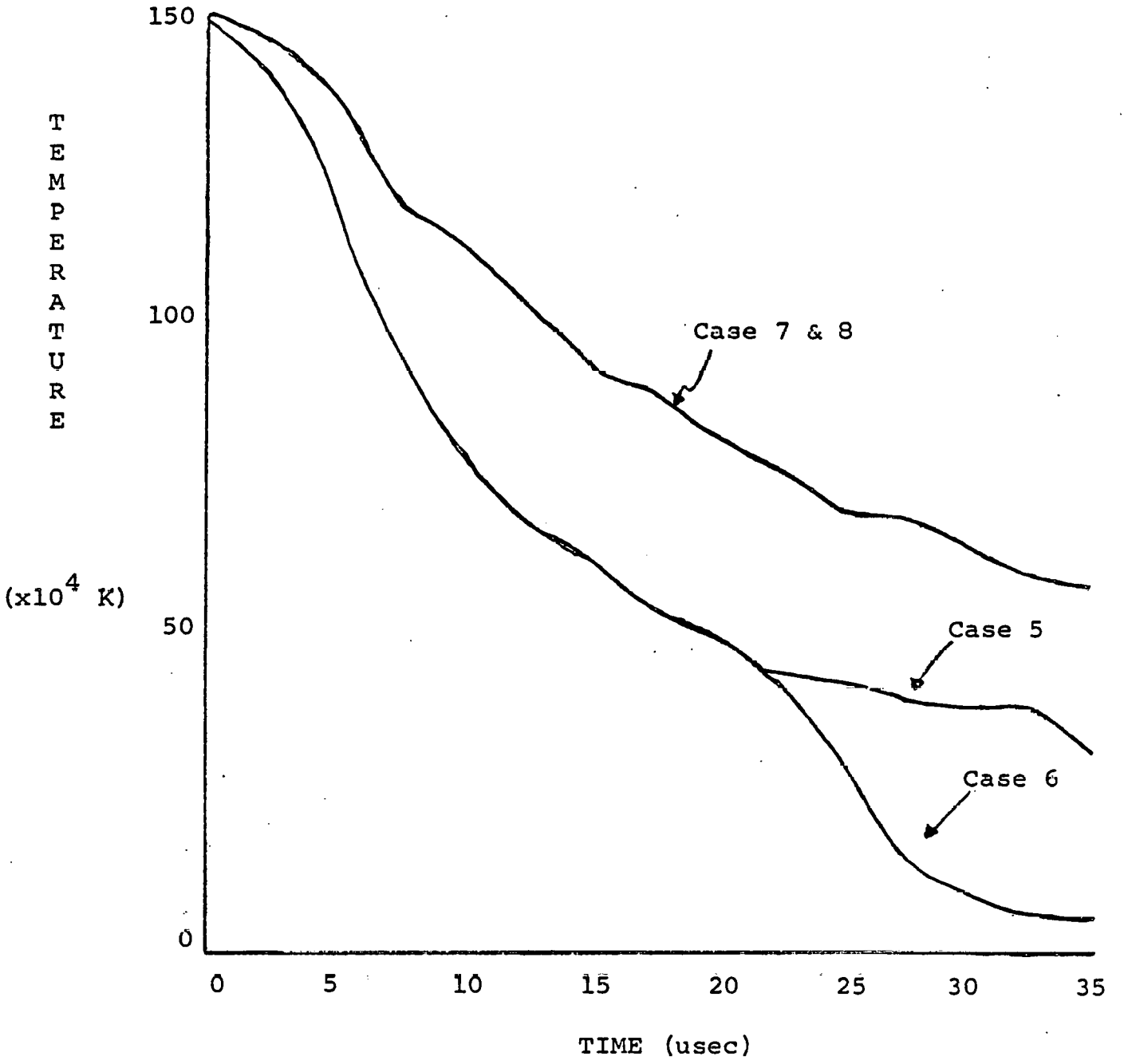

Figure IV.45 Central plasma temperature decay during high beta tokamak phase. Initial temperature (peak) is 130ev.

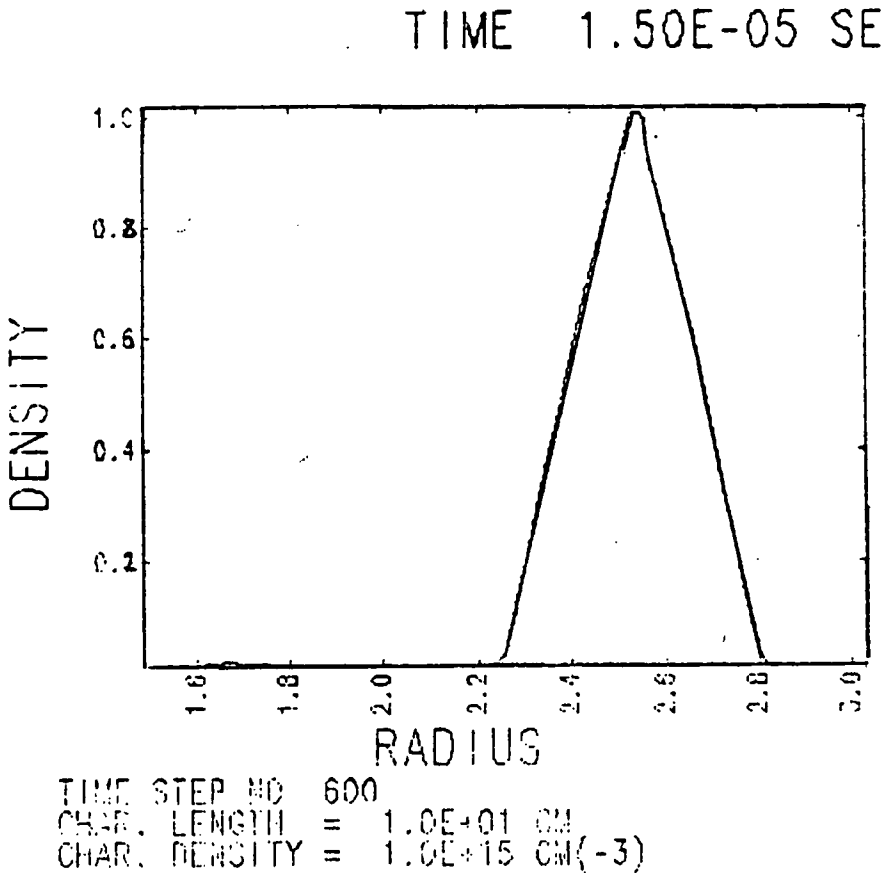

Figure IV.46.A

Plasma density for cases 6 and 7 of the high beta tokamak simulation.

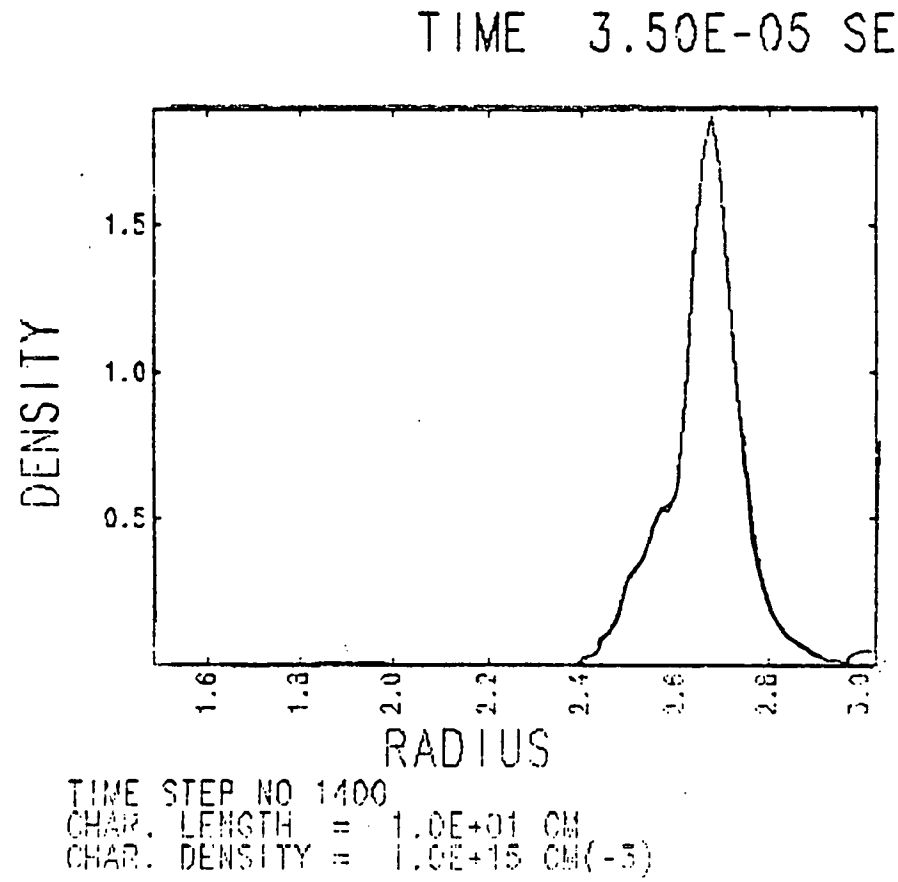

B) Case 6

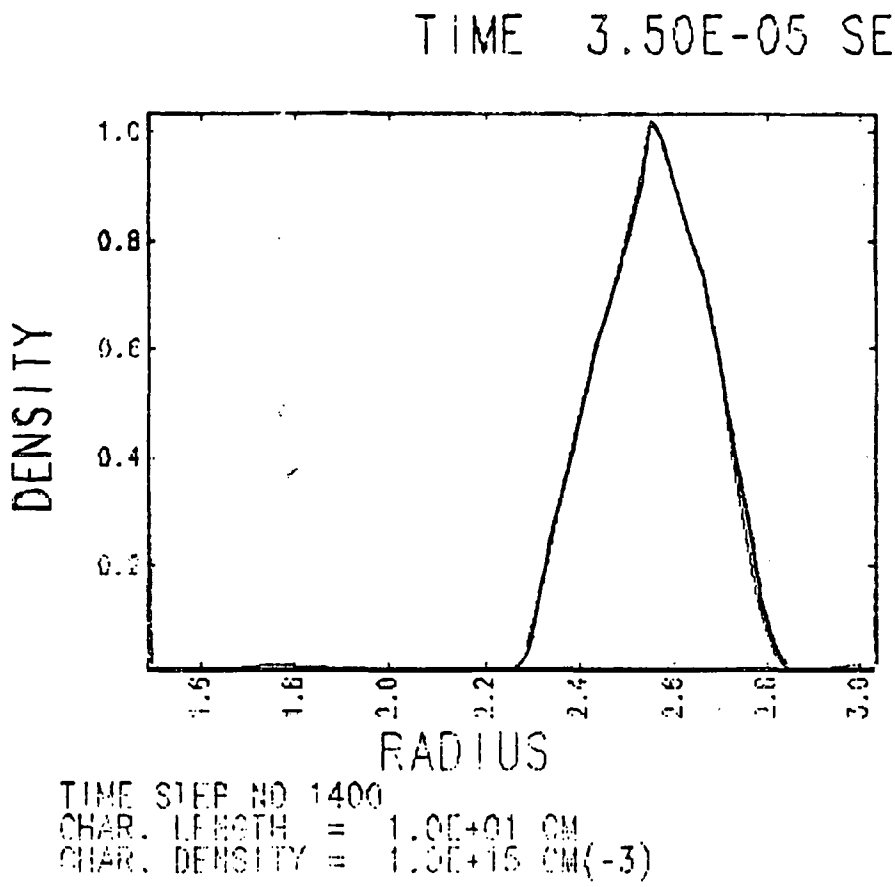

Figure IV.46.C

Case 7

Through the pinching of J_ϕ and ρ the plasma seeks to minimize the rate of pressure loss. The pinching of toroidal current is readily observed in Figure IV.47 for case 6. Note that since case 7 does not experience a rapid loss of energy its current density does not pinch but rather undergoes a gradual resistive decay. Also note that in case 6, the pinching process is eventually overtaken by a sharp resistive decay due to severely deflated temperatures. Thus, there is a large drop in J_ϕ from 30 to 35 μsec.

The plasma has yet another mechanism to maintain equilibrium. It can increase its total pressure not only through the thermodynamic pressure as described above but also by increasing the magnetic pressure. Thus we note the appearance of a paramagnetic bump in

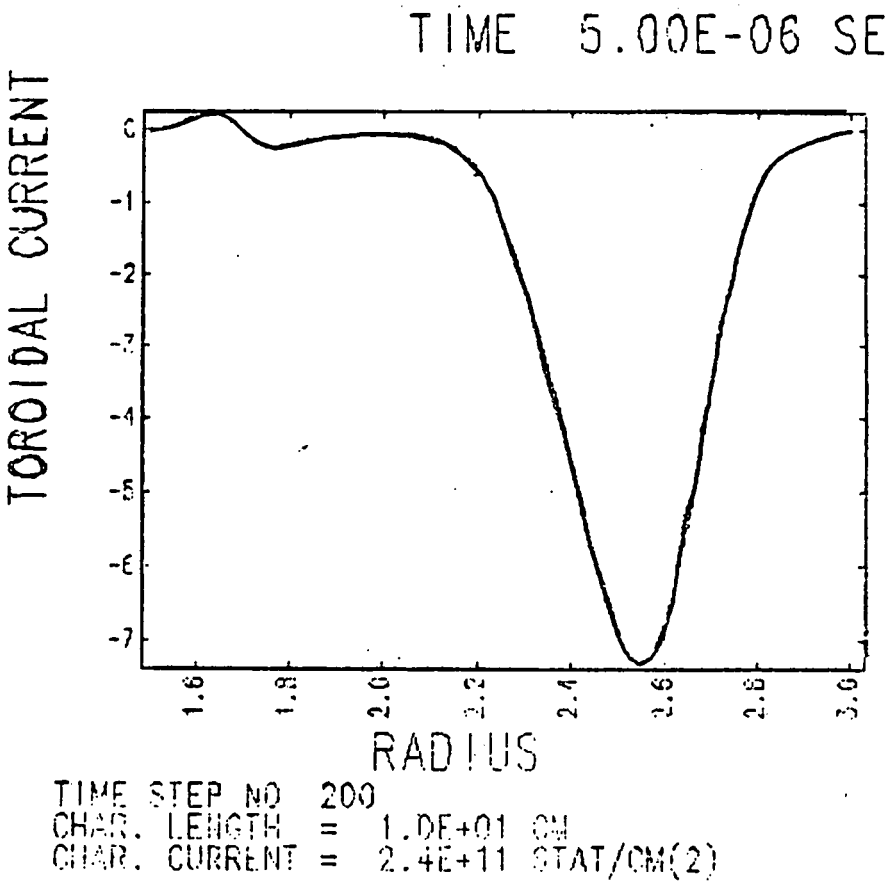

Figure IV.47.A

Toroidal current density for cases 6 and 7 of the high beta tokamak simulation.

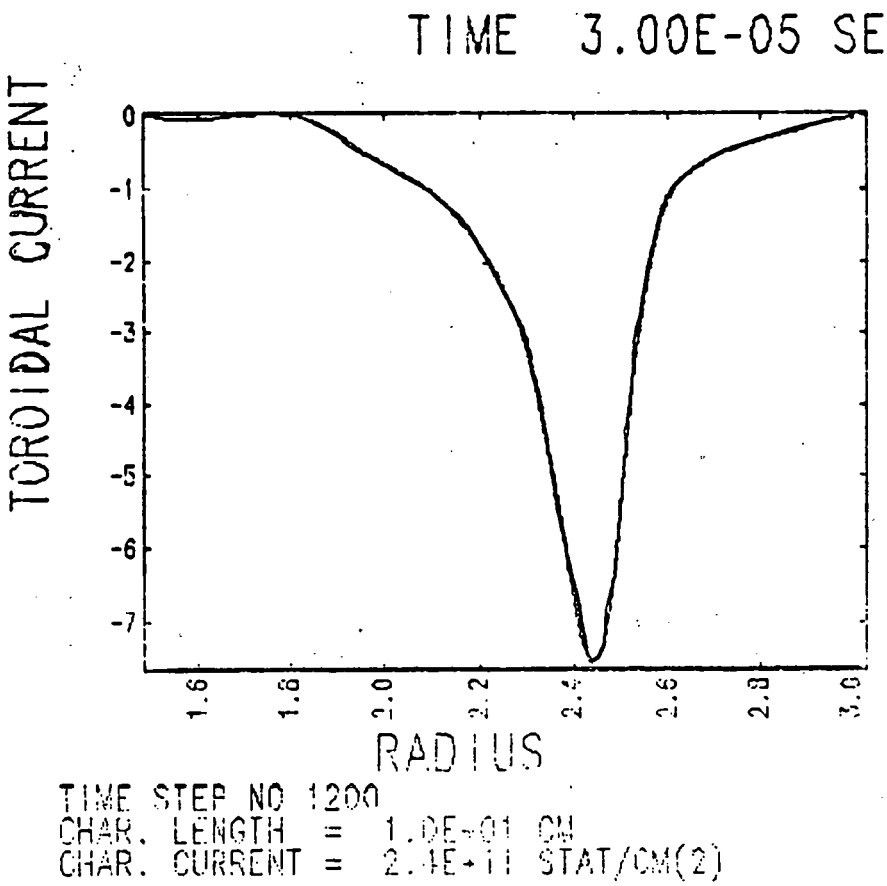

B) Case 6

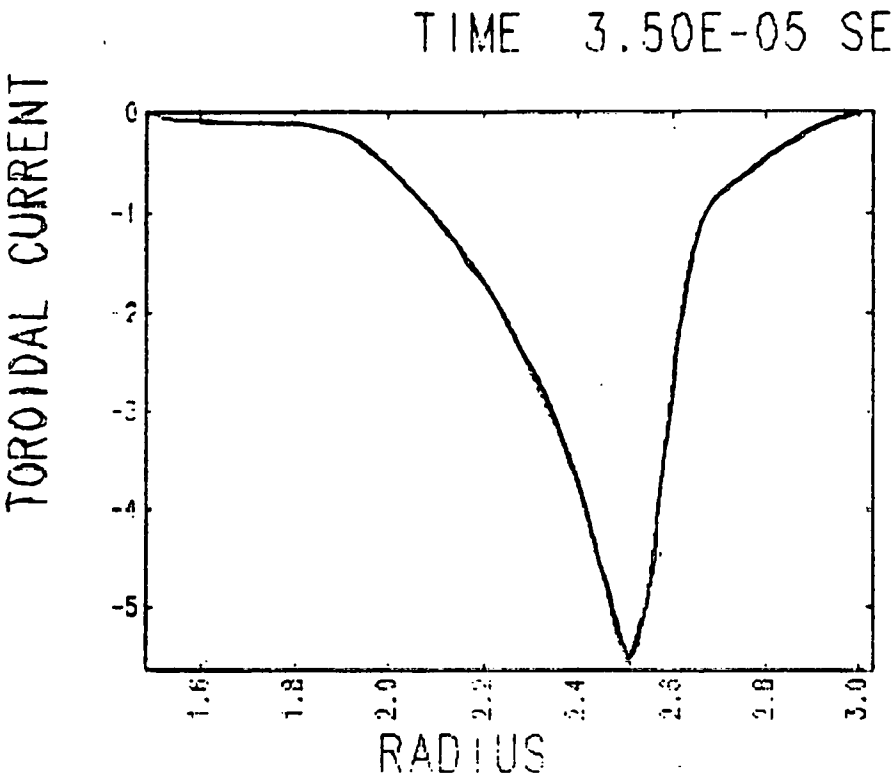

Figure IV.47.C

Case 6

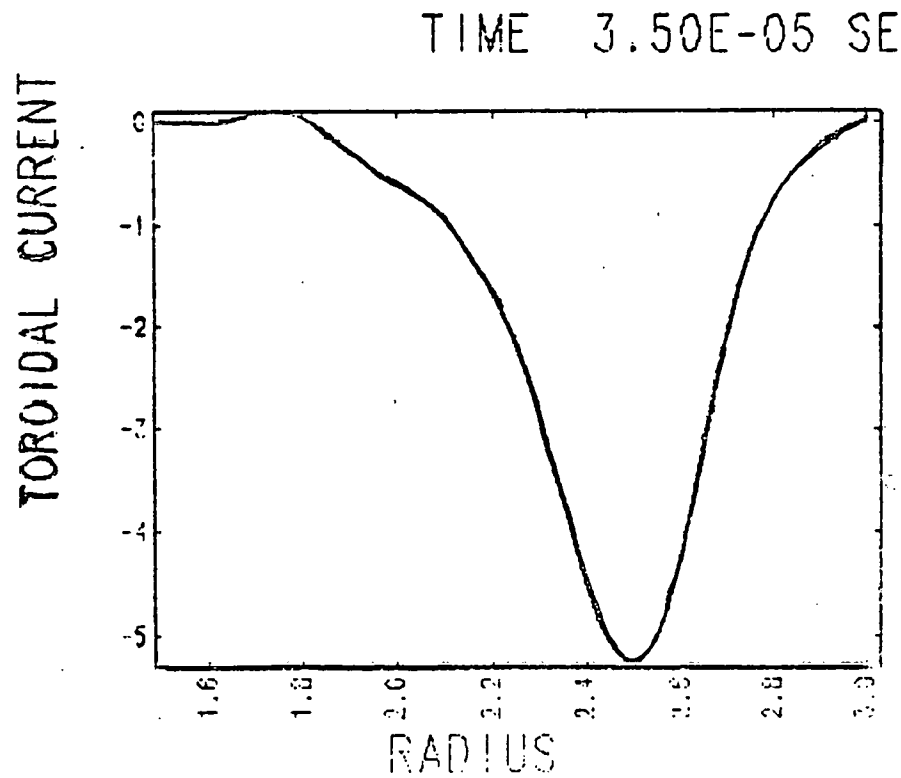

D) Case 7

Figure IV.48 for the case of 2% silicon. This results in paramagnetic currents which aid in confinement much as the diamagnetic currents previously. Once again for the case of .5% silicon we see a more gradual disappearance of the toroidal field well with no onset of paramagnetism evident at these times. While both cases begin with a peak beta of 46%, case 6 decays to a beta of 4% and case 7 to one of 19% after 35 μsec. The evolution of the pressure profile is shown in Figure IV.49 for case 7.

Analysis of the plasma velocity gives the following results. For case 6, the plasma moves at the diffusion speed throughout the temperature decay. Thus, we are moving through successive equilibria, but rather rapidly. Typical velocities are 10^5 cm/sec. Calculations indicate that the poloidal current contributes significantly to confinement. Plasma velocity in case 7 is quite impressive. It never exceeds 10^4 cm/sec, often hovering around 10^3 cm/sec! Confinement is excellent throughout the simulation. Perhaps what is most impressive is that case 7 nearly exactly matches half power experimental results for temperature decay presented in (9). This clearly illustrates the potential of Torus-II as a high beta research device.

The last set of cases we will consider are for an initial plasma temperature of 175 eV. Throughout this set of calculations the dominant energy loss is due to radiation of silicon. The power loss gets as large as 6 MW. For cases where the oxygen content is 2% there is significant cooling at later (≈25 μsec) times. The

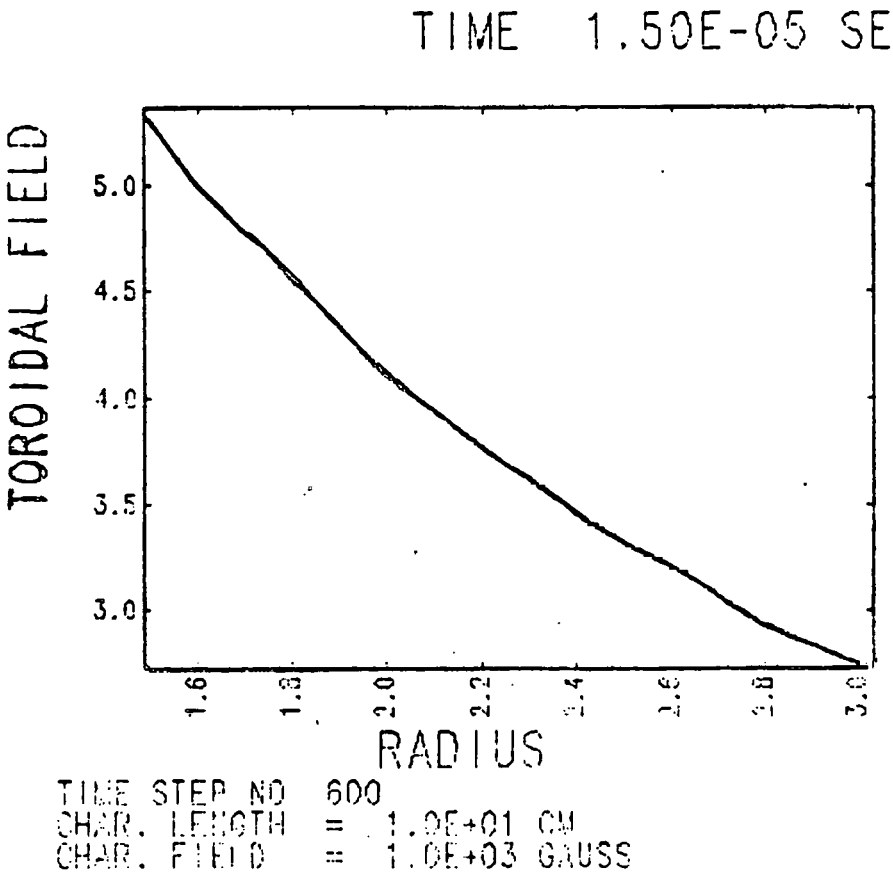

Figure IV.48.A

Toroidal field for case 6 of the high beta tokamak simulation.

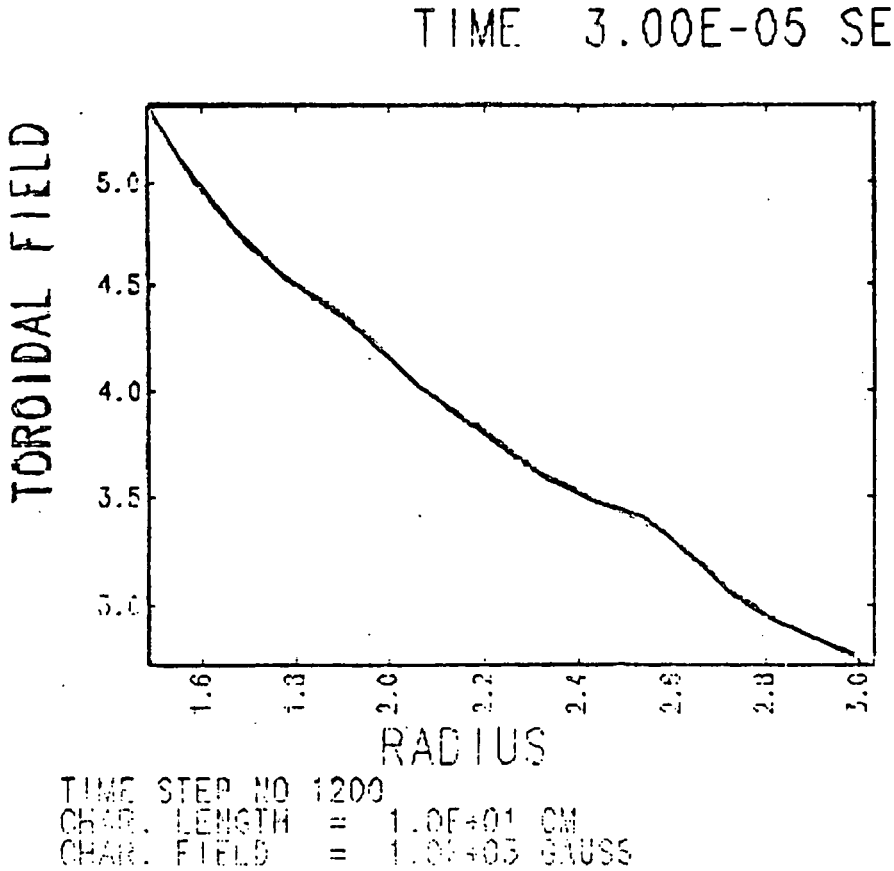

B) Case 6

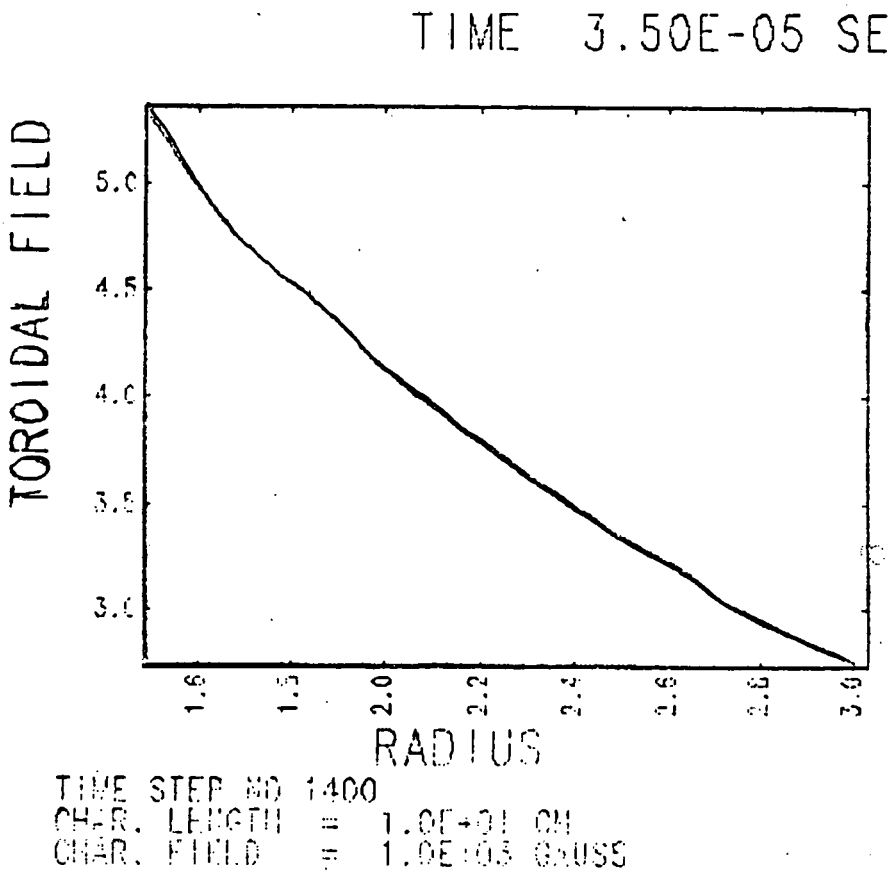

Figure IV.48.C

Case 7

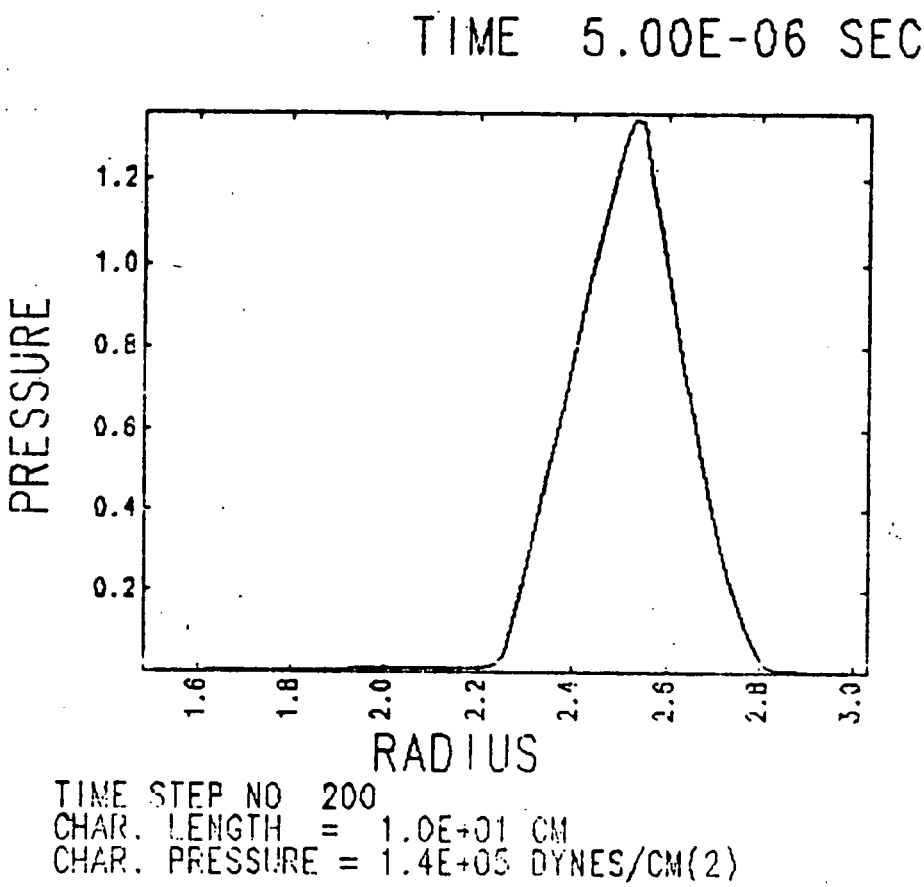

Figure IV.49.A

Plasma pressure for case 7 of the high beta tokamak simulation.

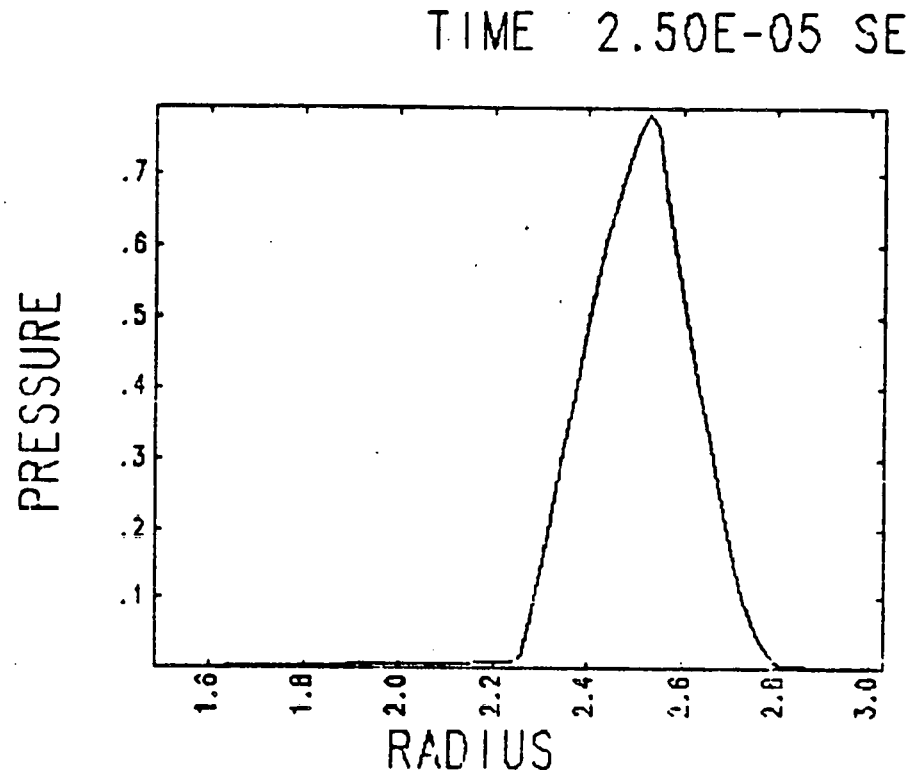

Figure IV.49.B

Case 7

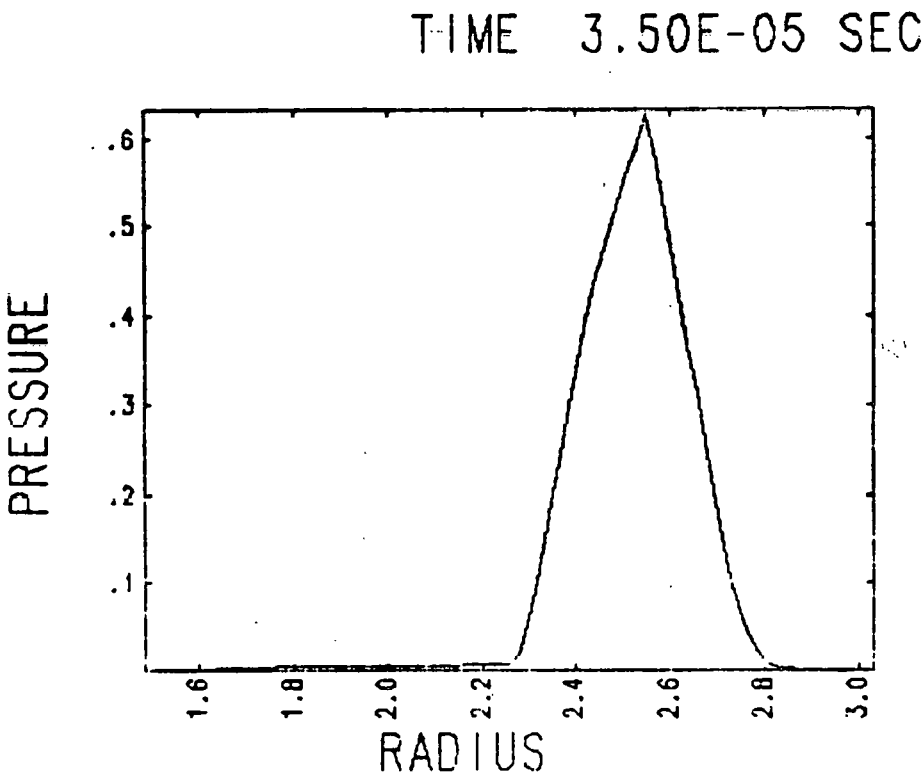

C) Case 7

central plasma temperature as a function of time for cases 9-12 is shown in Figure IV.50. This provides a clear illustration of the dominance of the silicon radiation. Again, we observe a rapid drop in temperature due to radiating oxygen at lower temperatures (ν40 eV). As before, we follow the evolution of the plasma density profile for two cases in Figure IV.51. The results are quite different from eachother. For a high silicon content, we observe a doubling of the peak plasma density along with the formation of an extremely narrow plasma. This is the pinching effect described earlier. Once again it accompanies that case where plasma cooling is most rapid. Case 11 increases its peak plasma density by roughly 20%. For the 130 eV cases we observed a pinching of the toroidal plasma current at 25 μsec followed by a rapid resistive decay (e.g. Case 6). Since our initial temperature is now higher, the plasma current does not begin to pinch until 35 μsec for case 10. For the simulation with a low silicon content we observe a very slow decay in plasma current without pinching. (Figure IV.52)

The toroidal field evolution (Figure IV.53) is characterized by the development of a paramagnetic bump. Unlike earlier simulations the bump now appears in the slow cooling case as well as the fast. It is much more pronounced in case 10 and also appears very early (t ≈10 μsec). Both cases begin with a peak plasma beta of 61%. Case 10 decays to a peak beta of 7.5% and case 11 decays to a peak beta of 27% both within 35 μsec. The evolution of the pressure profile for both cases is shown in Figure IV.54.

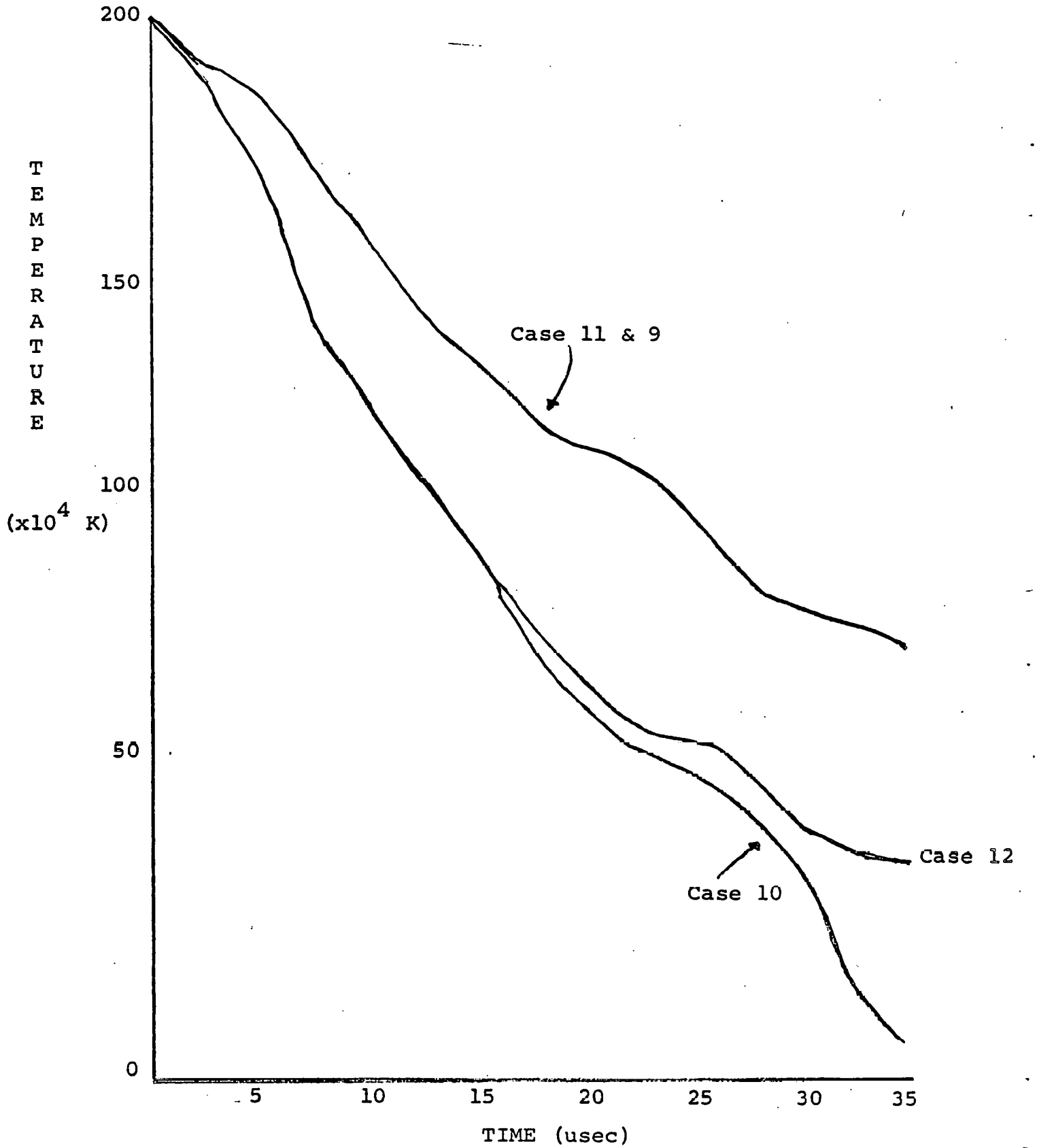

Figure IV.50 Central plasma temperature decay during the high beta tokamak phase. Initial temperature (peak) is 175 eV.

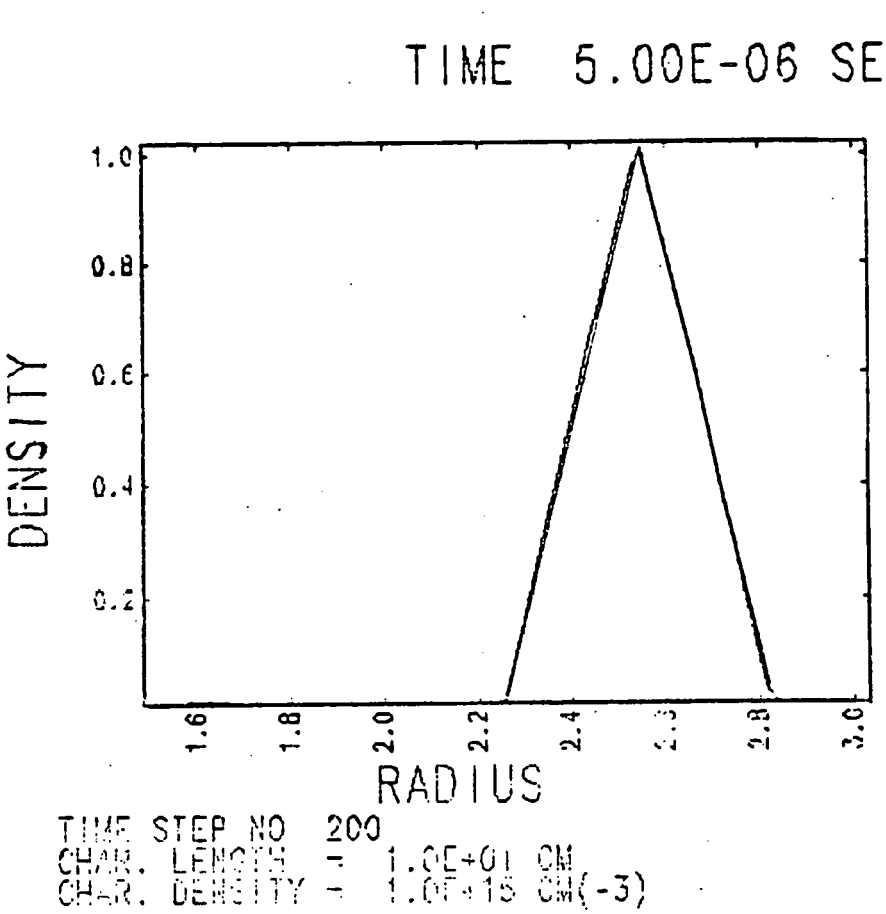

Figure IV.51.A

Plasma density for cases 10 and 11 of the high beta tokamak simulation.

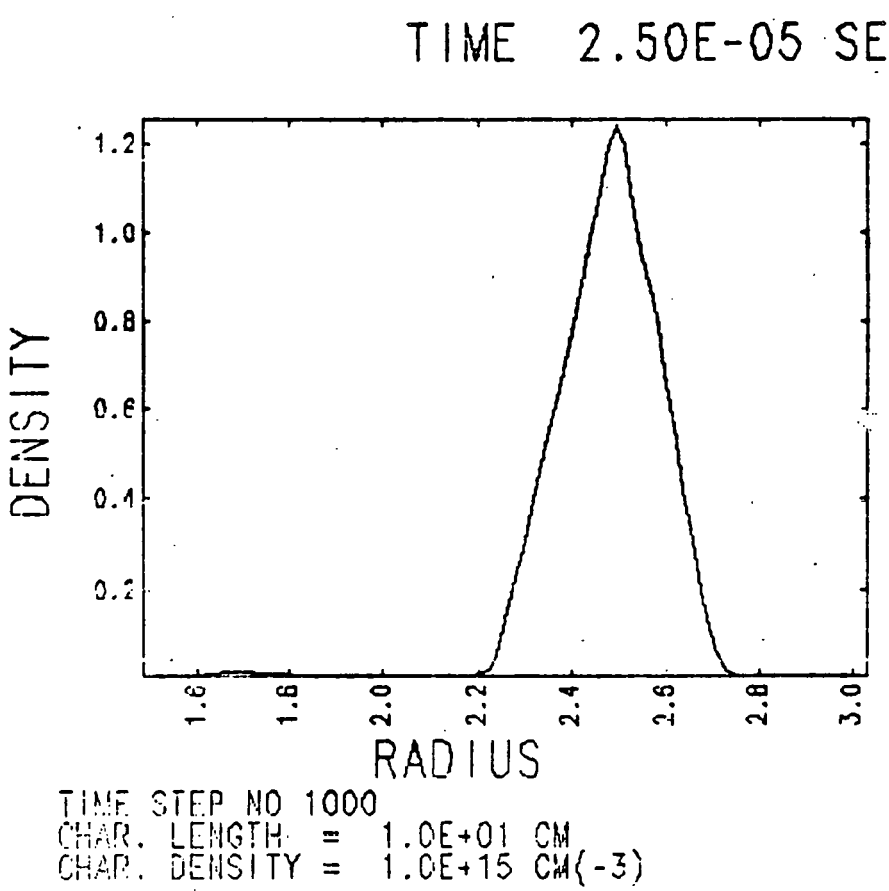

B) Case 10

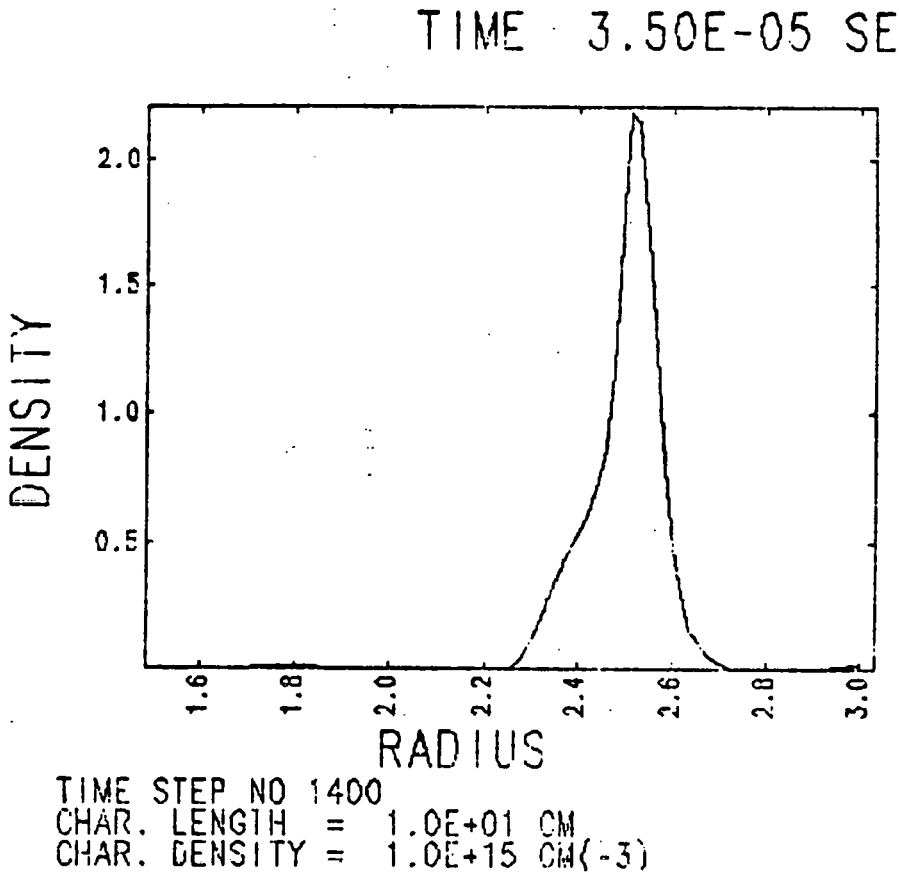

Figure IV.51.C

Case 10

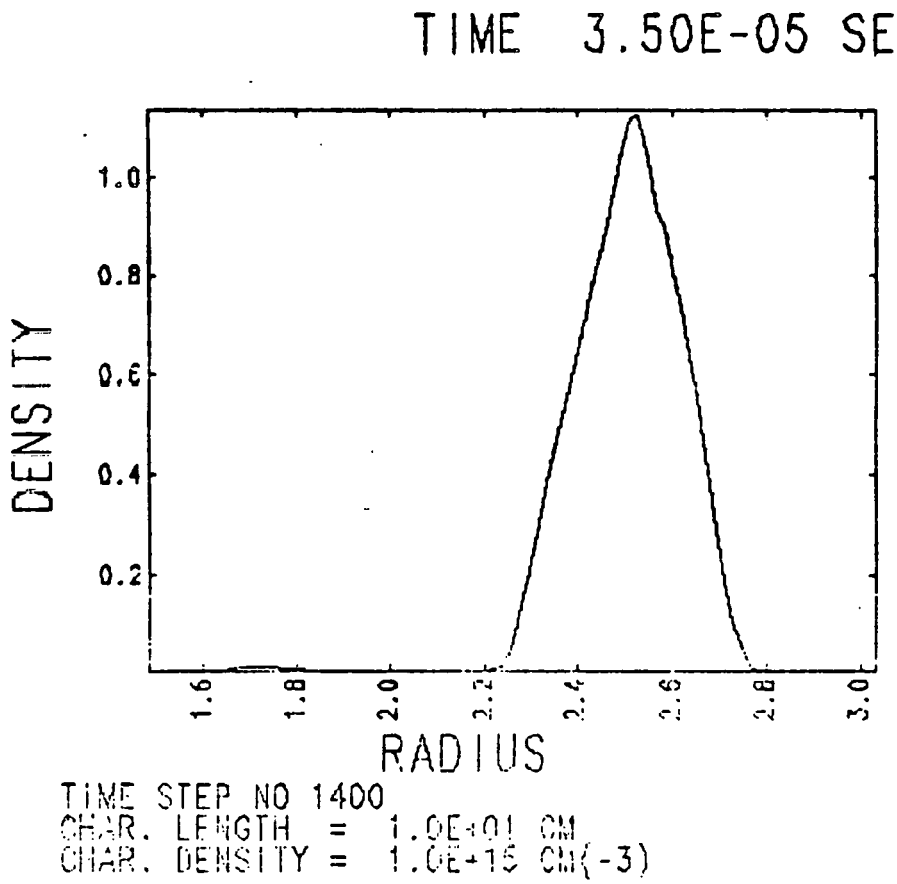

D) Case 11

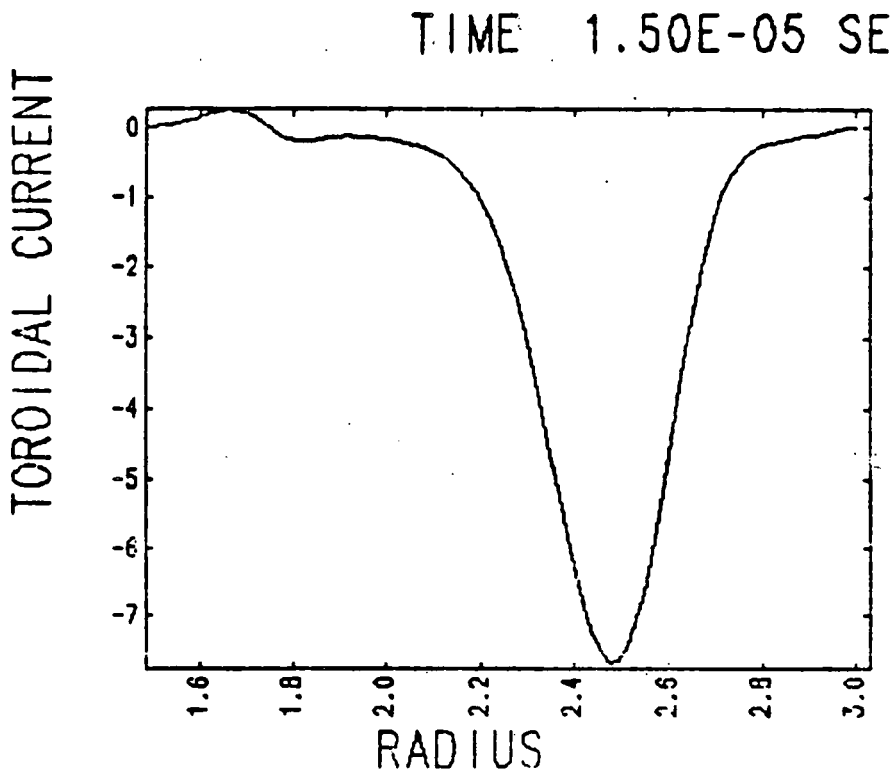

Figure IV.52.A

Toroidal current density for cases 10 and 11 of the high beta tokamak simulation.

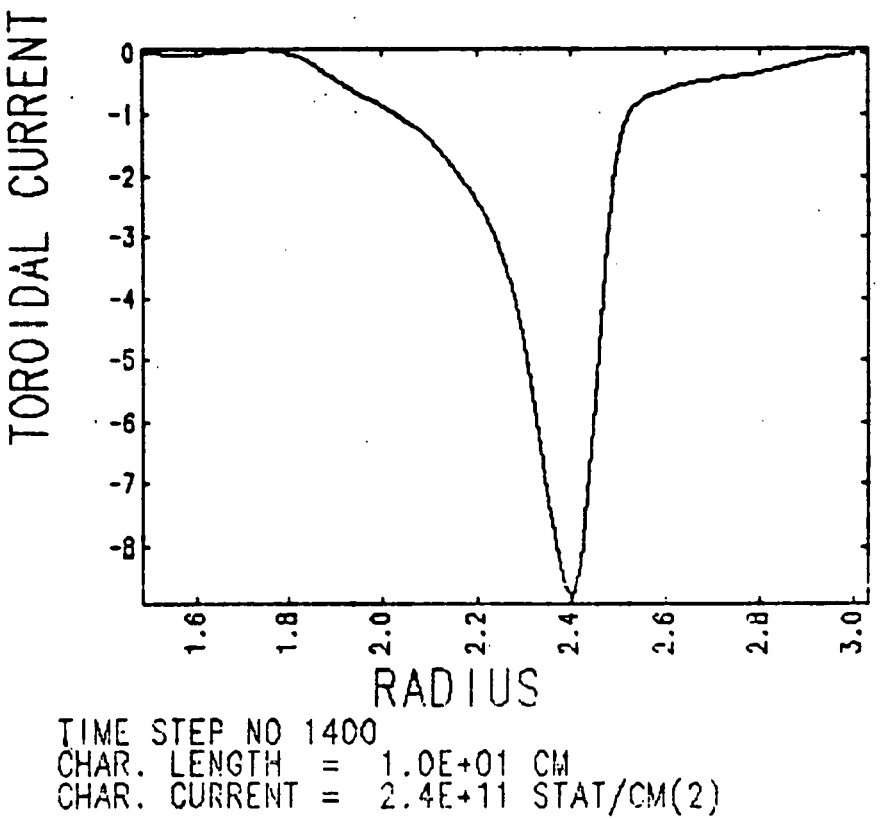

B) Case 10

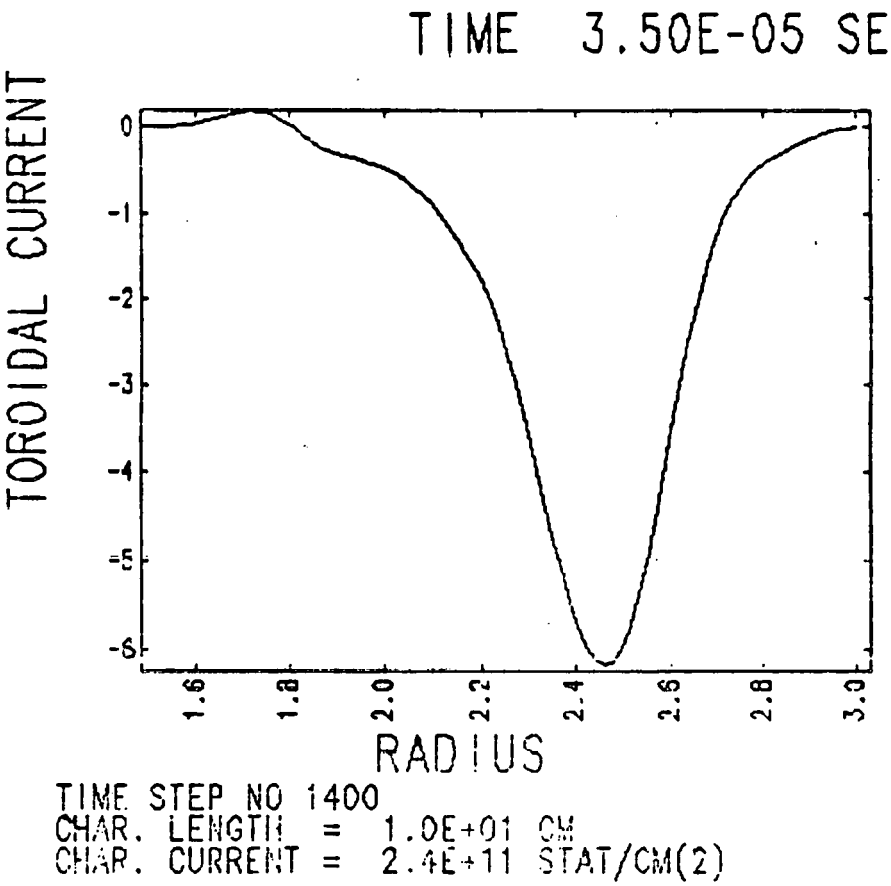

Figure IV.52.C

Case 11

In keeping with our earlier procedure, we now analyze the computed plasma velocity. For case 10 the plasma velocity is 10^4 cm/sec for the initial 30 μsec and climbs to 10^5 cm/sec by 35 μsec. A description of the dynamics of the plasma motion is in order. For $t \lesssim 25$ μsec, the plasma velocity is everywhere in the negative radial direction. However, the velocity increases as we move outward. Thus, plasma is swept inward and the pinching process begins. At later times the direction of plasma flow is modified such that the plasma near the inner wall begins to move outward while the plasma near the outer wall continues to be swept inward resulting in a more rapid pinching. The primary reason for this type of motion is the evolution of the toroidal plasma current. At early times, the well centered

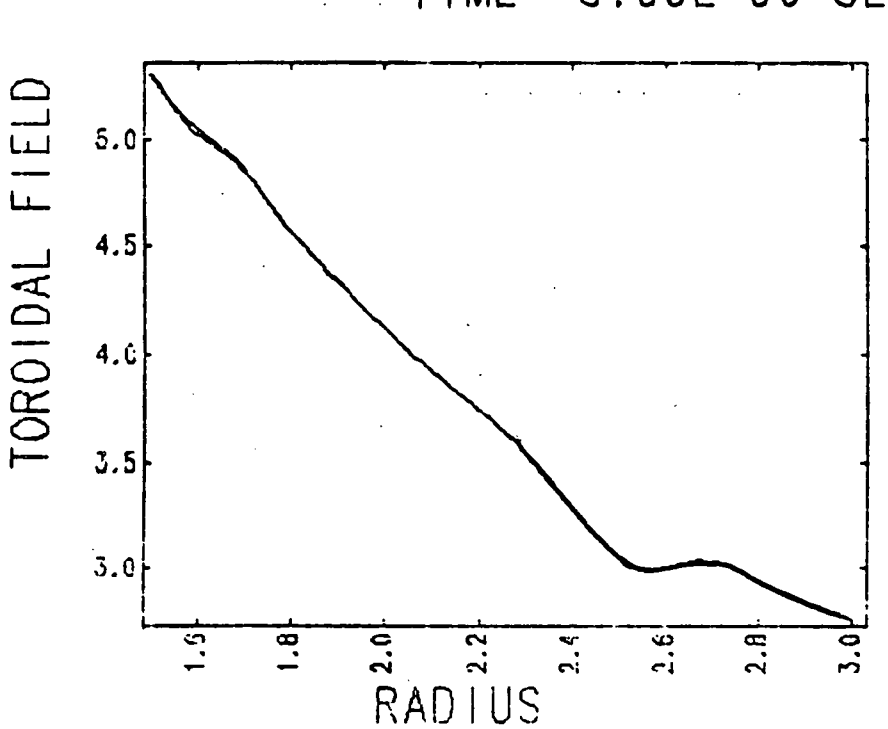

Figure IV.53.A

Toroidal field for cases 10 and 11 of the high beta tokamak simulation.

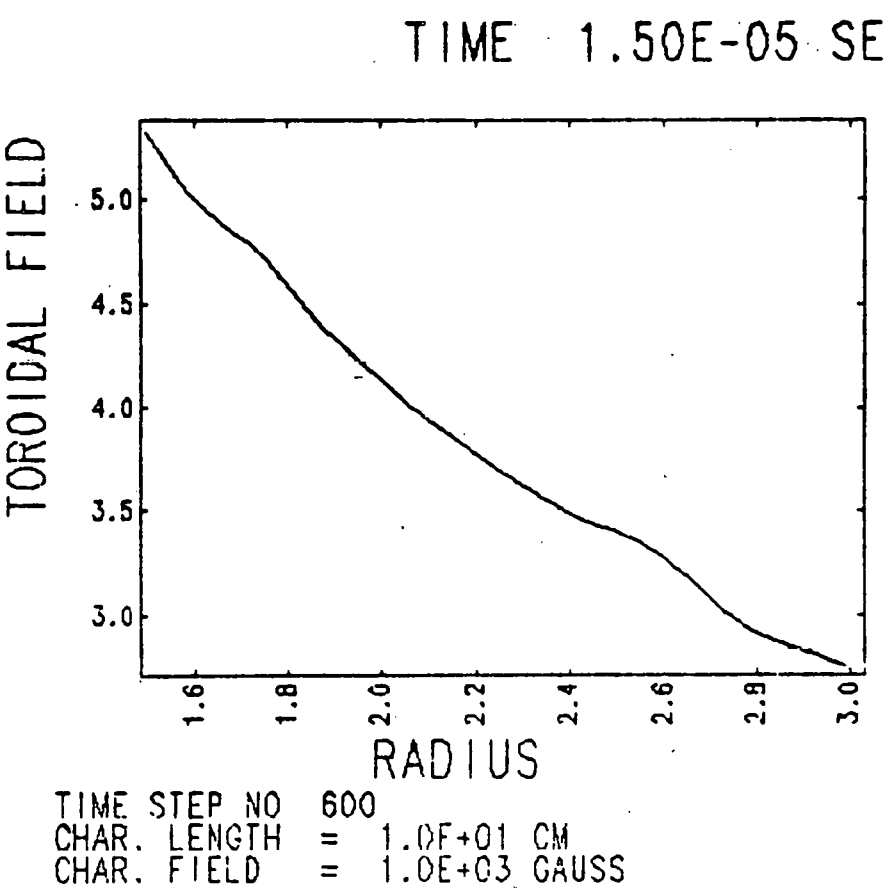

B) Case 10

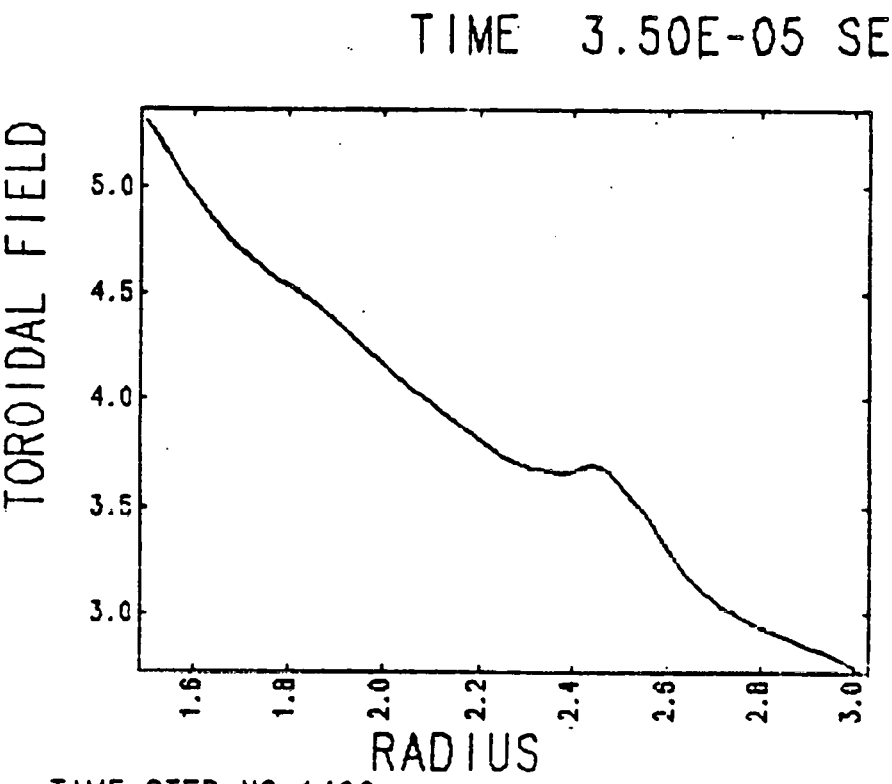

Figure IV.53.C

Case 10

D) Case 11

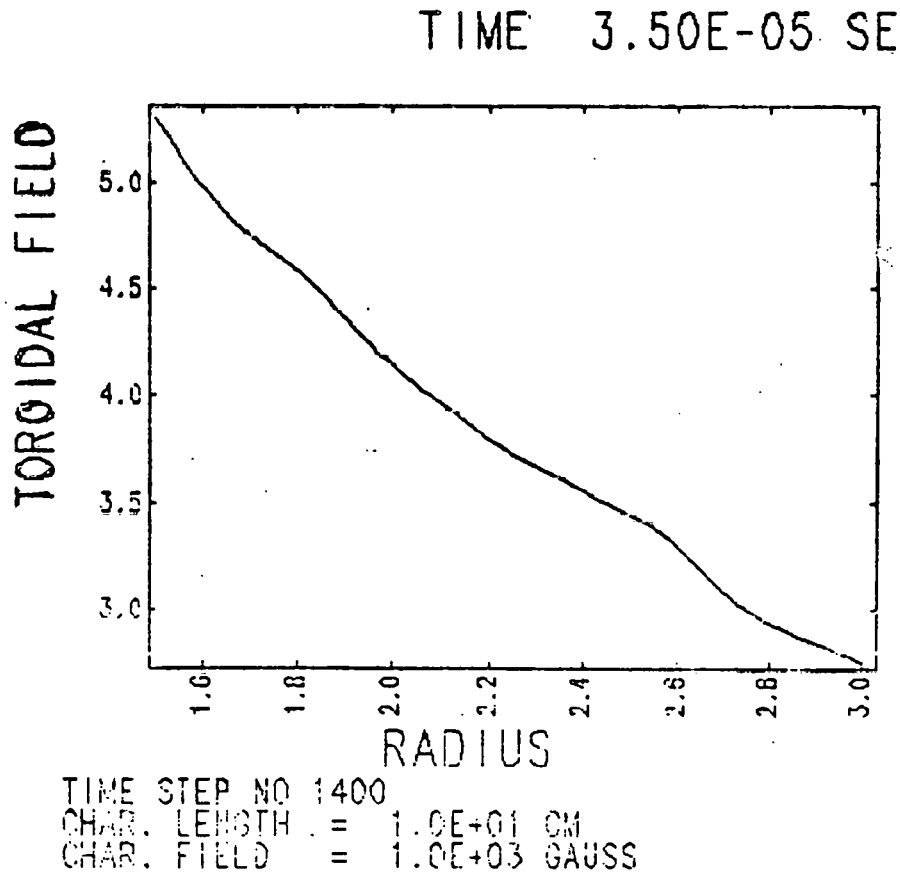

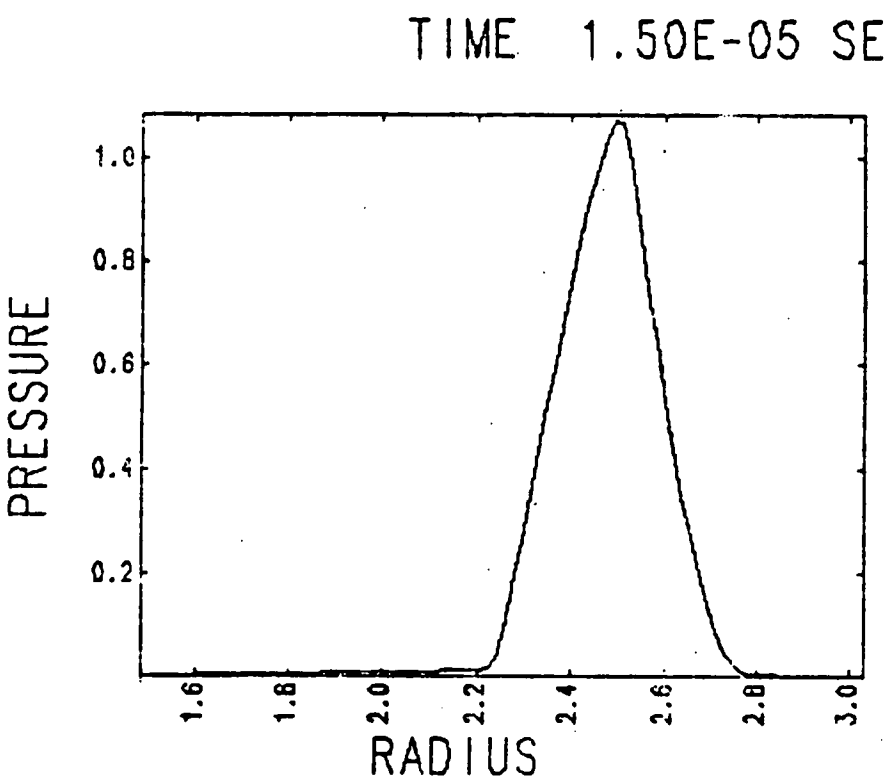

Figure IV.54.A

Plasma pressure for case 10 of the high beta tokamak simulation.

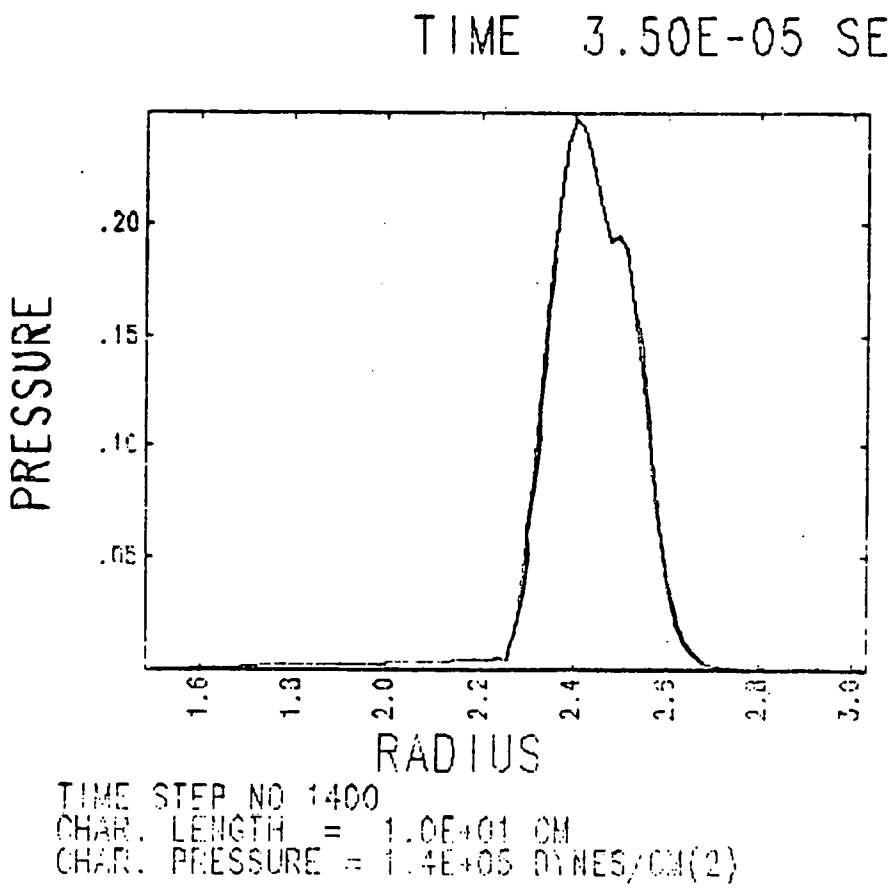

B) Case 10

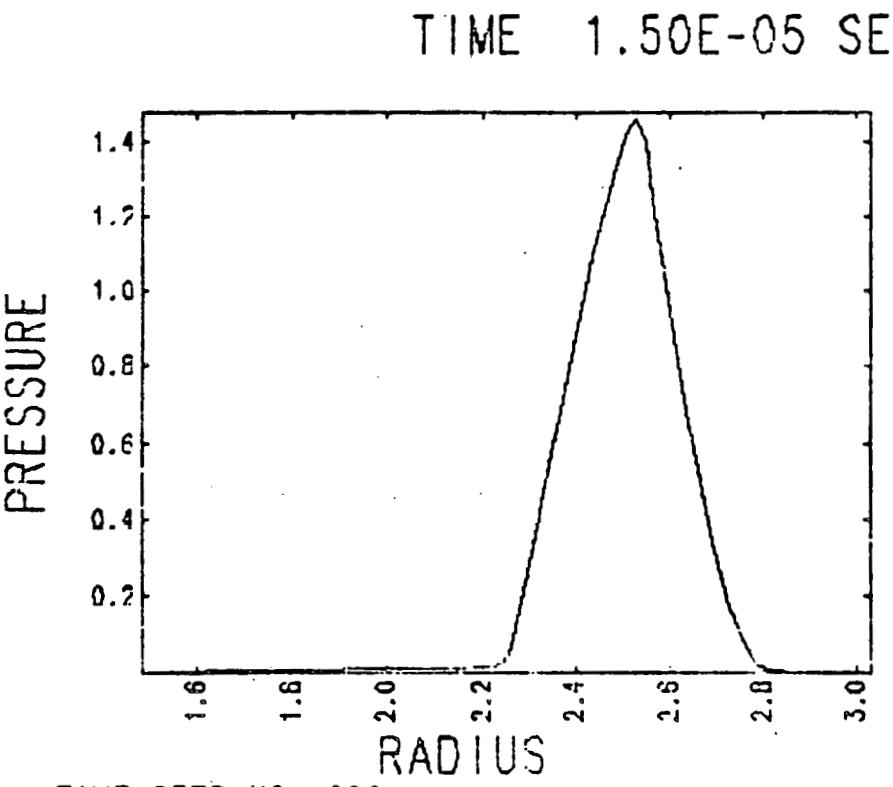

Figure IV.54

C) Case 11

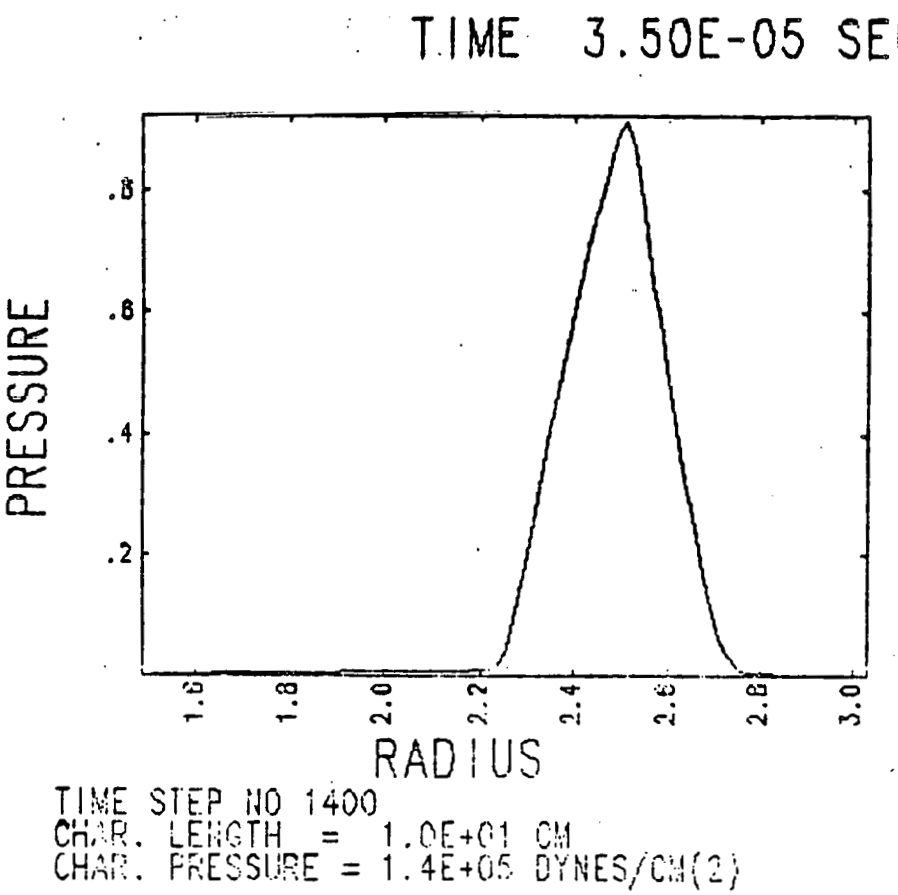

D) Case 11

toroidal current is crossed into a centered B_z generating a force of $J_\phi B_z$ inwards. The diamagnetic currents in the poloidal direction are also centered. However, the toroidal field is not symmetric about the point of maximum plasma density. Thus, the force $J_z B_\phi$ pointing radially outward also decreases as we move radially outward. This results in the observed increasing negative plasma velocity. As the plasma pressure continues to drop, the inward sweeping is no longer sufficient to maintain an equilibrium. The toroidal plasma current then shifts inward, away from the plasma center. The paramagnetic bump becomes quite large and the resulting $\underline{J} \times \underline{B}$ force pushes the inner plasma towards the outer wall in an attempt to slow down the pressure decay. For case 11 the velocity never exceeds 10^4 cm/sec. As in case7, the plasma moves through successive equilibria much more slowly than when the large silicon content forces a rapid cooling. For most of the simulation ($t \lesssim 30$ μsec) the sweeping of plasma inward described above is sufficient to maintain a one-dimensional equilibrium.

4) Conclusions and Future Work

The different operating stages of Torus-II and the resulting plasma states have been studied. Many important questions have been answered, some qualitatively and many quantitatively, through the use of MHD, atomic physics and inductance codes. The singular, most important conclusion we have reached is that Torus-II is quite capable of ohmically heating to a high beta plasma configuration. The heating is indeed a turbulent process resulting from large poloidal currents. An anomalous resistivity must be used for the MHD codes to match experimental field data. The amount of heating is critically sensitive to the duration of the turbulent period. Thus, experimentally, a typical "cold/bad shot" is one in which the turbulence is quickly damped and the plasma never gets hot. We've shown that the present device is able to "burn through" to a hot, high beta plasma. Radiative losses are a problem at later times. If the plasma heats to 30-40 eV (typical of quarter power heating) there is a rapid radiative loss of energy due to oxygen resulting in a second type of "cold/bad shot". Similar problems arise if we heat to the silicon radiation barrier. The important point is that high beta experimental results have been reproduced computationally.

Equally important has been the ability of the simulations to point out some problems associated with the device. Clearly radiative power loss is one such problem. Another is the nature of the coil geometry. We studied the difficulties associated with the "shortness" of the inner and outer windings, the problems caused by

the leakage flux and the effects of the copper plates. Experimental values for the toroidal plasma current are now under careful scrutiny due to code predictions. Coupling between the plasma current and external toroidal windings has been researched, the results of which have led to new programming of these external currents. The coil geometry leads to a decay of the plasma state as badly as impurity radiation. The two are not independent problems since a more effective programming of external currents can keep plasma away from the walls resulting in a cleaner discharge. The high beta tokamak state has been observed as successive high beta (but decaying) plasma equilibria.

Work is in progress to modify the present Torus-II experiment. We will address the problems cited above while holding on to the fundamental operating characteristic of the device. That is, keeping the toroidal field reversal as the heating scheme, how can we set up a more stable plasma state? How do we shape the external windings to avoid the loss of plasma to the top and corners? How can we decrease the impurity levels? Should we switch to a quartz vacuum vessel? Is it desirable to maintain a large toroidal current during the high beta state to offset plasma cooling? How can this be done without going kink unstable? Should we decrease plasma current by decreasing the external current in the inner and/or outer windings? Can we operate at higher heating powers, i.e. larger toroidal fields? These and other questions are now under consideration.

REFERENCES

1. F. F. Chen, Introduction to Plasma Physics (Plenum Press, New York, 1974) p.180.
2. G. Bateman, MHD Instabilities (The MIT Press, Cambridge, Mass., 1978) p. 149.
3. H. R. Strauss, et al., PPPL Report 1535, April 1979.
4. B. Coppi, A. Ferreira, J. W.-K. Mark and J. J. Ramos, Nuclear Fusion 19, 715 (1979).
5. R. A. Gross and C. K. Chu, in Proc. of Finite Beta Tokamak Workshop, Varenna, September 1977.
6. G. A. Navratil, Internal Memorandum, Columbia Plasma Physics Laboratory, June 1980.
7. T. Bhoutros-Ghali, Internal Memorandum, Columbia Plasma Physics Laboratory, November 1976.
8. T. C. Marshall and H. C. Lui, The Physics of Fluids 19, 1417 (1976).
9. G. E. Georgiou, T. C. Marshall and P. G. Weber, Phys. Fluids 23, 2085 (1980).
10. H. C. Lui and C. K. Chu, Phys. Fluids 19, 1947 (1976).
11. A. Y. Aydemir, Ph. D. Thesis, Columbia University (1979).
12. G. Erlebacher, Columbia University, Private Communication.
13. S. J. Sackett, EFFI, Lawrence Livermore Laboratory UCID-17621 (1977).
14. G. Erlebacher, Columbia University, Priv. Comm.

15. S. Ortolani, Los Alamos Scientific Laboratory LA-8261-MS (1980).

16. D. L. Book, NRL Plasma Formulary, Naval Research Laboratory (1980)

17. D. Duchs and H. R. Griem, Phys. Fluids 9, 1099 (1966).

18. R. C. Elton, in Methods of Experimental Physics (Academic Press, New York, 1969), Vol. 9A.

19. C. L. Longmire, Elementary Plasma Physics (John Wiley and Sons, Interscience, New York, 1963), p. 205.

20. S. Glasstone and R. H. Lovberg, Controlled Thermonuclear Reactions (Van Nostrand, Princeton, N.J., 1960) p. 31

21. R. W. P. McWhirter, in Plasma Diagnostic Techniques, R. H. Huddlestone and S. L. Leonard (Eds.) (Academic Press, New York, 1965), p. 243.

22. R. D. Richtmyer and K. W. Morton, Difference Methods for Initial Value Problems (Wiley, Interscience, New York, 1967).

23. D. E. Post, et al., in Atomic Data and Nuclear Tables, Vol. 20, (1977), p. 397-439.

24. G. Erlebacher, Columbia University, Priv. Comm.

25. T. F. Stratton, Plasma Diagnostic Techniques, R. H. Huddlestone and S. L. Leonard (Eds.) (Academic Press, New York, 1965).

26. G. A. Navratil, Columbia University, Priv. Comm.

27. R. L. Merlino, Internal Memorandum, Columbia Plasma Physics Laboratory, April 1981.

28. G. Erlrebacher, Columbia University, Priv. Comm.

29. C. E. Moore, National Standard Reference Data System, National Bureau of Standards (U.S.) 34, September 1970.

30. M. Bagatin, S. Costa, S. Ortolani and A. Stella, University of Padova UPee-80/05, May 1980

31. W. L. Wiese, M. W. Smith and B. M. Miles, Nat. Stand. Ref. Data Ser., Nat. Bur. of Stand. (U.S.) 22, October 1969.

32. G. A. Navratil, Columbia University, Priv. Comm.

33. C. Kostek and T. C. Marshall, Columbia University, Priv. Comm.

34. D. E. Elkin and G. A. Navratil, Columbia University, Priv. Comm.

35. R. N. Byrne and C. K. Chu, Phys. Fluids 20, 2418 (1979).

36. R. Izzo and C. K. Chu, APS Bull. 25, No. 8, paper 5D8, October 1980.

37. R. Izzo and C. K. Chu, Sherwood Theory Meeting, Univ. of Texas at Austin, April 1981.

38. R. Izzo and C. K. Chu, to be presented at October 1981 meeting of the American Physical Society in New York.

APPENDIX

```
C    PROGRAM NAME:  COILS
C    WRITTEN BY: R. IZZO
C    CONTRIBUTOR: G. ERLEBACHER
C    LANGUAGE:    FORTRAN
C    COMPILATION DEVICE:  CDC 7600
C    REFERENCES:FOR GOOD DISCUSSIONS OF INDUCTANCE CALCULATIONS
C               SEE LANDAU AND LIFSHITZ, 'ELECTRODYNAMICS OF CON-
C               TINUOUS MEDIA'; PARIS AND HURD, 'BASIC EM THEORY';
C               HALLEN, 'ELECTROMAGNETIC THEORY'
C               FOR CALCULATIONS OF INDUCTANCES SEE GROVER, 'INDUCTANCE
     CALCULATIONS'; 'NATIONAL BUREAU OF STANDARDS 1912 VOL.8'


C    AN INDUCTANCE CALCULATION OF THE GENERAL FORM PHI=L*I IS
C    USED TO CALCULATE CURRENT DISTRIBUTIONS IN ALL EXTERNAL COILS,
C    IN THE PLASMA, AND IN THE COPPER PLATES ON TOP AND BOTTOM OF
C    TORUS-II.  THE SELF INDUCTANCE IS CALCULATED USING FINITE GEO-
C    METRY CONSIDERATIONS WHILE THE MUTUAL INDUCTANCE IS BASICALLY
C    A FILAMENT APPROXIMATION.  A COMPLETE DESCRIPTION OF VAR-
C    IABLE LABELS, ETC., FOLLOWS.


C    ************BEGIN PROGRAM**********************


      CALL DROPFILE(0)
      CALL CREATE(6,"INOUT",3,-1)
      DOUBLE AA,B,X
      DIMENSION A(12),B1(5),QL(44,44),Q(21),R(44),
     1  D(44,44),Z(44),AA(49,49),B(49),X(49)


C      ************DATA*********

C    U0: MAGNETIC PERMEABILITY IN FREE SPACE
C    N:  NUMBER OF EQUATIONS OR UNKNOWNS
      U0=4.*3.1416E-07
      N=49
      NM1=N-1
      NM2=N-2
      NM3=N-3
      NM4=N-4
      NM5=N-5
      NM6=N-6
C    NS:  HALF THE NUMBER OF COILS
C    COHM: CURRENT IN INNER TORCIDAL WINDINGS (AMPS)
C    CPLA: PLASMA CURRENT (AMPS)
C    CVER: CURRENT IN OUTER TORCIDAL WINDINGS (AMPS)
      NS=22
      COHM=220000.
      CPLA=-35000.
      CVER=95000.
C    A:  MAJOR RADII OF ORIGINAL LARGE COILS
C    B1: MINOR RADII OF NEW SMALL COILS USED TO REPRESENT LARGE ONES.
C    FOR EXAMPLE, IN THIS CODE, 12 COILS ARE USED TO REPRESENT THE
C    INNER TOROIDAL WINDINGS.
```

```
C   Z:  HEIGHT OF COIL AS MEASURED FROM HORIZONTAL MIDPLANE
      DATA A/15.,26.25,30.,15.,17.,19.,21.,23.,25.,27.,29.,31./
      DATA B1/.5,1.5,.5,.75,.25/
      DATA Z/10.875,9.125,7.375,5.625,2.625,.875,5.5,1.5,11.,9.,7.,
     1  5.,3.,17.6,17.6,17.6,17.6,17.6,17.6,17.6,17.6,17.6,17.6,
     2  -10.875,-9.125,-7.375,-5.625,-2.625,-.875,-5.5,-1.5,
     3  -11.,-9.,-7.,-5.,-3.,-16.3,-16.3,-16.3,-16.3,-16.3,
     4  -16.3,-16.3,-16.3,-16.3/


C       **********CALCULATE INDUCTANCES (HENRIES)**********


C   Q:   SELF INDUCTANCE
C   Q(1):  SELF INDUCTANCE OF ANY SMALLER COIL USED TO REPRESENT
C   INNER TOROIDAL WINDING.
C   Q(2):  DITTO FOR PLASMA.
C   Q(3):  DITTO FOR OUTER TOROIDAL WINDINGS.
      DO 1 I=1,3
      Q(I)=0.01*U0*A(I)*(B1(I)*B1(I)/24./A(I)/A(I)-1.75+(1.+B1(I)*B1(I)
     1  /8./A(I)/A(I))*ALOG(8.*A(I)/B1(I)))
1     CONTINUE


C   SELF INDUCTANCES FOR THOSE COILS REPRESENTING COPPER PLATES
      DO 6 I=4,12
      Q(I)=0.01*U0*A(I)*(B1(4)*B1(4)/24./A(I)/A(I)-1.75+(1.+B1(4)*B1(4)
     1  /8./A(I)/A(I))*ALOG(8.*A(I)/B1(4)))
      Q(I+9)=.01*U0*A(I)*(B1(5)*B1(5)/24./A(I)/A(I)-1.75+
     1  (1.+B1(5)*B1(5)/8./A(I)/A(I))*ALOG(8.*A(I)/B1(5)))
6     CONTINUE


C   NOW WE TAKE 'COMMON' INFORMATION AND DISTRIBUTE IT APPROP-
C   RIATELY.  FOR EXAMPLE, ALL OF SMALLER COILS 1-6 AND 23-28 HAVE
C   THE SAME MINOR AND MAJOR RADII AND THEREFORE, SELF INDUCTANCE,
C   SINCE THEY EACH REPRESENT A PART OF THE INNER TOROIDAL WINDING.
C   THE SYSTEM IS SET UP SYMMETRIC TO THE MIDPLANE, THUS, I AND
C   I+NS ARE USED TO REPRESENT THE SAME WINDING.


C   QL:  INDUCTANCE MATRIX.
C   R:  MAJOR RADII OF SMALL COILS.


C   INNER TOROIDAL WINDING
      DO 2 I=1,6
      J=I+NS
      QL(I,I)=Q(1)
      R(I)=A(1)
      QL(J,J)=Q(1)
      R(J)=A(1)
2     CONTINUE


C   PLASMA RING
      DO 3 I=7,8
      J=I+NS
```

```
      QL(I,I)=Q(2)
      R(I)=A(2)
      QL(J,J)=Q(2)
      R(J)=A(2)
3     CONTINUE


C   OUTER TOROIDAL WINDING
      DO 4 I=9,13
      J=I+NS
      QL(I,I)=Q(3)
      R(I)=A(3)
      QL(J,J)=Q(3)
      R(J)=A(3)
4     CONTINUE


C   TOP AND BOTTOM COPPER PLATES
      DO 8 I=14,22
      J=I+NS
      QL(I,I)=Q(I-10)
      QL(J,J)=Q(I-1)
      R(I)=A(I-10)
      R(J)=A(I-10)
8     CONTINUE


**********CALCULATE MUTUAL INDUCTANCES**********
C   DIFFERENT APPROXIMATIONS ARE MADE DEPENDING UPON THE RELATIVE
C   SPACING OF THE TWO COILS BEING CONSIDERED.
      DO 5 J=1,NM6
      K=J+1

      DO 5 I=K,NM5
      D(I,J)=ABS(Z(I)-Z(J))
      XK=((R(I)+R(J))**2+D(I,J)**2)/((R(I)-R(J))**2+D(I,J)**2)
      XK1=2.*SQRT(R(I)*R(J))/SQRT((R(I)+R(J))**2+D(I,J)*D(I,J))
      IF (XK1 .GT. .985) XK2=SQRT(1./XK)
      IF (XK1 .LE. .985) XK2=(1.-XK1)/(1.+XK1)
      V=ALOG(4./XK2)
      F1=V+XK2*XK2/4.*(V-2./1.2)+
     1  XK2**4*9./4./16.*(V-2./1.2-2./3.4)+
     2  XK2**6*9.*25./4./16./36.*(V-2./1.2-2./3.4-2./5.)
      E1=1.+XK2*XK2/2.*(V-1./1.2)+
     1  XK2**4*3./16.*(V-2./1.2-1./3.4)+
     2  XK2**6*9.*5./4./16./6.*(V-2./1.2-2./3.4-1./5.6)
      IF (XK1 .GT. .985) QL(I,J)=0.01*U0*SQRT(R(I)*R(J))*
     1  ((2./XK1-XK1)*F1-2./XK1*E1)
      IF (XK1 .LE. .985) QL(I,J)=0.01*U0*SQRT(R(I)*R(J))*
     1  (F1/(XK1*(1.+XK1)) - (1.+XK1)*E1/XK1)
      QL(J,I)=QL(I,J)
5     CONTINUE


C   THE FOLLOWING WRITE STATEMENT AND DO LOOP IS FOR OUTPUTTING
C   INDUCTANCES.  THESE LINES MAY BE REINSTATED FOR DEBUGGING.
C     WRITE(6,150)


C     DO 7 I=1,NM5
```

```
181 C      WRITE (6,100) (QL(I,J),J=1,I)
182 C   7  CONTINUE
183
184
185 C    WE WRITE THE ENTIRE SYSTEM OF EQUATIONS IN MATRIX FORM.
186 C    COMBINE PHI=L * I AND TOTAL CURRENT=SUM OF SMALL COIL
187 C    CURRENTS TO GENERATE AA*X=B.
188        DO 31 I=NM4,N
189        DO 31 J=1,N
190        AA(I,J)=0.
191        AA(J,I)=0.
192 31     CONTINUE
193
194
195        DO 32 I=1,6
196        AA(NM4,I)=1.
197        AA(NM4,I+NS)=1.
198        AA(I,NM4)=-1.
199        AA(I+NS,NM4)=-1.
200 32     CONTINUE
201
202
203        DO 33 I=7,8
204        AA(NM3,I)=1.
205        AA(NM3,I+NS)=1.
206        AA(I,NM3)=-1.
207        AA(I+NS,NM3)=-1.
208 33     CONTINUE
209
210
211        DO 34 I=9,13
212        AA(NM2,I)=1.
213        AA(NM2,I+NS)=1.
214        AA(I,NM2)=-1.
215        AA(I+NS,NM2)=-1.
216 34     CONTINUE
217
218
219        DO 35 I=14,22
220        AA(NM1,I)=1.
221        AA(N,I+NS)=1.
222        AA(I,NM1)=-1.
223        AA(I+NS,N)=-1.
224 35     CONTINUE
225
226
227        DO 9 I=1,NM5
228 9      B(I)=0.
229
230
231        B(NM4)=COHM/1.E+06
232        B(NM3)=CPLA/1.E+06
233        B(NM2)=CVER/1.E+06
234        B(NM1)=0.
235        B(N)=0.
236
237
238        DO 10 I=1,NM5
239        DO 10 J=1,NM5
240 10     AA(I,J)=QL(I,J)/1.E-06
```

```
241 C    SOLVE THE MATRIX EQUATIONS BY GAUSSIAN ELIMINATION
242        CALL GAUSS(AA,B,X,N)
243 C    OUTPUT THE CURRENT IN EACH SMALL COIL, THE POSITION OF THE COIL,
244 C    THE AVERAGE MAGNETIC FIELD THROUGH THE HOLE OF THE TORUS, THE
245 C     AVERAGE FIELD TO THE LEFT AND RIGHT OF THE PLASMA, AND THE VALUES
246 C    OF POLOIDAL FLUX COMPUTED ALONG THE ORIGINAL WINDINGS.
247        WRITE (6,160)
248
249
250        DO 51 I=1,NM5
251 51     WRITE (6,170) I,R(I),Z(I),X(I)
252
253
254        WRITE (6,180) (X(I),I=NM4,N)
255        BHOLE=X(NM4)*1.E+08/3.1416/A(1)/A(1)
256        BLEFT=(X(NM3)-X(NM4))*1.E+08/3.1416/(A(2)**2-A(1)**2)
257        BRGHT=(X(NM2)-X(NM3))*1.E+08/3.1416/(A(3)**2-A(2)**2)
258        WRITE (6,190) BHOLE,BLEFT,BRGHT
259 100    FORMAT (10E10.3)
260 150    FORMAT ("                              INDUCTION MATRIX")
261 160    FORMAT ("  COIL NO.          RADIUS              Z
262       1              CURRENT (MA)")
263 170    FORMAT (5X,I2,8X,3(E15.7))
264 180    FORMAT (//"    THE FLUX SURFACES ARE (WEBERS):  "//5E15.7//)
265 190    FORMAT (" THE CORRESPONDING AVG. VERTICAL FIELDS ARE (GAUSS):"
266       1  // 3E15.7)
267        CALL CLOSE(6)
268        CALL EXIT(2)
269        STOP
270        END
271 C       **********************SUBROUTINE SECTION*****************
272 C
273 C
274 C
275 C  GAUSSIAN ELIMINATION ROUTINE OBTAINED FROM JOHNSON AND RIESS,
276 C  'NUMERICAL ANALYSIS'.
277        SUBROUTINE GAUSS(AB,BB,X,N)
278        DOUBLE AB,BB,X,TEMP,Q
279        DIMENSION AB(49,49),BB(49),X(49)
280 200    FORMAT (I1)
281        NM1=N-1
282        DO 25 I=1,NM1
283        DO 23 J=I,N
284        IF (AB(J,I) .EQ. 0.) GO TO 23
285        DO 22 K=I,N
286        TEMP=AB(I,K)
287        AB(I,K)=AB(J,K)
288 22     AB(J,K)=TEMP
289        TEMP=BB(I)
290        BB(I)=BB(J)
291        BB(J)=TEMP
292        GO TO 24
293 23     CONTINUE
294        GO TO 28
295 24     IP1=I+1
296        DO 25 K=IP1,N
297        Q=-AB(K,I)/AB(I,I)
298        AB(K,I)=0.
299        BB(K)=Q*BB(I) +BB(K)
300        DO 25 J=IP1,N
```

```
301 25     AB(K,J)=Q*AB(I,J) +AB(K,J)
302        IF (AB(N,N) .EQ. 0.) GO TO 28
303        X(N)=BB(N)/AB(N,N)
304        NP1=N+1
305        DO 27 K=1,NM1
306        Q=0.
307        NMK=N-K
308        DO 26 J=1,K
309 26     Q=Q+AB(NMK,NP1-J)*X(NP1-J)
310 27     X(NMK)=(BB(NMK)-Q)/AB(NMK,NMK)
311        IERR=1
312        WRITE (6,200) IERR
313        RETURN
314 28     IERR=2
315        WRITE (6,200) IERR
316        RETURN
317        END
```

```
C...CODE:  ZERO-DIMENSIONAL ATOMIC PHYSICS COMPUTATION
C...WRITTEN BY:  R. IZZO
C...LANGUAGE:   FORTRAN
C...COMPILATION DEVICE:   CDC 7600
C...REFERENCES:   THE TWO ORTOLANI PAPERS (LOS ALAMOS AND PADOVA
C...              REPORTS) HAVE BEEN INSTRUMENTAL IN THIS WORK.


C...A ZERO-DIMENSIONAL ENERGY BALANCE FOR ELECTRONS AND IONS IS
C...MAINTAINED WHILE FOLLOWING THE IONIZATION OF HELIUM, OXYGEN AND
C...SILICON.  WE TAKE INTO ACCOUNT IONIZATION, THREE-BODY AND RADIA-
C...TIVE RECOMBINATION, LINE RADIATION, BREMSSTRAHLUNG, OHMIC HEATING, WAVE
C...HEATING, ELECTRON-ION ENERGY TRANSFER, TRANSPORT LOSSES AND ANY
C...OTHER PHENOMENOLOGICAL LOSSES DESIRED.


C**********BEGIN PROGRAM**********

C...WE DEFINE ALL VARIABLES AS THEY ARE ENCOUNTERED IN THE CODE.

*SELECT PRINTLOG=LOGZ
*FILE NAME=ZEROD

      DIMENSION RNO1(9),RNO2(9),RNH1(3),RNH2(3),RNS1(15),
     1RNS2(15),OION(9),OREC(9),
     2HION(3),HREC(3),SION(15),SREC(15),EH(3),EO(9),ES(15)
     3,Y(30,2)

      COMMON/T2/RNE1,RNE2,RNI1,RNI2,RNH2,RNO2,RNS2,TE1,
     1NHP1,NOP1,NSP1,EH,EO,ES,TIME,RN,T1,T2,T3,T4,T5,DT
     1,NH,NO,NS

      CALL DROPFILE(0)
      CALL OPEN(10,"DATA",0,0)
      CALL CREATE(6,"OUTZERO",3,-1)

C...ATOMIC NUMBERS FOR HELIUM, OXYGEN AND SILICON.
      NH=2
      NO=8
      NS=14
      NHP1=NH + 1
      NOP1=NO + 1
      NSP1=NS + 1

C...IONIZATION ENERGIES FOR HELIUM, OXYGEN AND SILICON.
      EH(2)=24.587
      EH(3)=54.416

      EO(2)=13.618
      EO(3)=35.116
      EO(4)=54.934
      EO(5)=77.412
      EO(6)=113.896
      EO(7)=138.116
      EO(8)=739.315
      EO(9)=871.387

      ES(2)=8.151
      ES(3)=16.345
```

```
      ES(4)=33.492
      ES(5)=45.141
      ES(6)=166.77
      ES(7)=205.05
      ES(8)=246.52
      ES(9)=303.17
      ES(10)=351.1
      ES(11)=401.43
      ES(12)=476.06
      ES(13)=523.5
      ES(14)=2437.676
      ES(15)=2673.108

C...OXYGEN AND SILICON AS PERCENTAGE OF TOTAL HELIUM.
      PO=.02
      PS=.01
C************INITIALIZE NUMBER DENSITIES AND TEMPERATURES***********

C...INITIAL HELIUM NUMBER DENSITY.
      HEINIT=1.E+15

C...INITIAL FRACTION OF HELIUM SINGLY IONIZED.
      HIO=.1

C...RNH1(J), RNH2(J): NUMBER DENSITY OF HELIUM IN CHARGE STATE (J-1)
C...AT OLD AND NEW TIME RESPECTIVELY.
      RNH2(1)=HEINIT*(1.-HIO)
      RNH2(2)=HEINIT*HIO
      RNH2(3)=0.

C...ALL UNKNOWNS ARE STORED IN MATRIX Y(I,J).  THE FIRST INDEX RUNS
C...FROM 1 TO 30 (TOTAL NUMBER OF UNKNOWNS).  THE SECOND INDEX IS 1 OR 2,
C...FOR OLD OR NEW VALUES.
      Y(2,1)=RNH2(1)
      Y(2,2)=RNH2(1)
      Y(3,1)=RNH2(2)
      Y(3,2)=RNH2(2)
      Y(4,1)=RNH2(3)
      Y(4,2)=RNH2(3)

C...INITIALLY, ALL OXYGEN IS IN NEUTRAL STATE.
      RNO2(1)=HEINIT*PO
      Y(5,1)=RNO2(1)
      Y(5,2)=RNO2(1)
      DO 1 J=2,NOP1
      RNO2(J)=0.
      Y(J+4,2)=RNO2(J)
      Y(J+4,2)=RNO2(J)
 1    CONTINUE

C...INITIALLY, ALL SILICON IS IN NEUTRAL STATE.
      RNS2(1)=HEINIT*PS
      Y(14,1)=RNS2(1)
      Y(14,2)=RNS2(1)
      DO 2 J=2,NSP1
      RNS2(J)=0.
      Y(J+13,1)=RNS2(J)
      Y(J+13,2)=RNS2(J)
 2    CONTINUE

```

```
C...NITMAX: MAXIMUM NUMBER OF ITERATIONS (TIME STEPS)
      NITMAX=70001

C...INITIALIZE ELECTRON AND ION TEMPERATURE.
      TI1=1.5
      TE1=1.5

C...INITIALIZE TOTAL ELECTRON AND ION NUMBER DENSITY.
      RNE2=RNH2(2) + RNO2(2) + RNS2(2)
      RNI2=RNE2

C...INITIALIZE ITERATION COUNTER AND TIME
      NIT=0
      TIME=0.
      Y(1,1)=TIME
      Y(1,2)=TIME
      Y(29,1)=TE1
      Y(30,1)=TI1
      Y(29,2)=TE1
      Y(30,2)=TI1

C...VARIOUS TIMES DURING THE SIMULATION IN MICROSECONDS.  FOR
C...EXAMPLE, START OF HEATING, SWITCH ON OF ANOMALOUS RESISTIVITY,
C...ETC,.
      T1=2.E-6
      T2=4.E-6
      T3=6.5E-6
      T4=6.5E-6
      T5=9.E-6

C...OUTPUT THE INITIAL CONDITIONS.
      WRITE (6,1000) TI1,TE1,HEINIT,HIO,PO,PS,RNE2,DT
 1000 FORMAT("INITIAL CONDITIONS"/"ION TEMPERATURE=  "
     1E11.4," EV"/"ELECTRON TEMPERATURE=  ",E11.4," EV"/
     2"TOTAL INITIAL HELIUM=  ",E11.4," CM(-3)"/"FRACTION OF
     3 HELIUM SINGLY IONIZED=  ",E11.4,/"FRACTION OF OXYGEN
     4 IMPURITIES=  ",E11.4/"FRACTION OF SILICON IMPURITIES=  ",
     5E11.4/"INITIAL ELECTRON DENSITY=  ",E11.4," CM(-3)"/
     6"TIME STEP=  ",E11.4," SEC"/"IMPURITIES ARE INITIALLY NEUTRAL")

C...NBEQ:  NUMBER OF EQUATIONS.
      NBEQ=30
 3    CONTINUE

C...DT: TIME STEP.  HAS DIFFERENT VALUES DEPENDING ON PHASE
C...    BEING SIMULATED.  USUALLY SMALLEST DURING TURBULENT HEATING.
      DT=5.E-10
      IF ((TIME .GT. T2) .AND. (TIME .LT. T5)) DT=10.E-11

C...NITW:  WRITE EVERY NITW ITERATIONS.
      NITW=1000
      IF ((TIME .GT. T2) .AND. (TIME .LT. T5)) NITW=5000

C...SOLVE THE 30 ORDINARY COUPLED DIFFERENTIAL EQUATIONS.
      CALL RGKUT(NBEQ,DT,NIT,Y)

C...STORE THE SOLUTION IN THE MORE FAMILIAR VARIBLES.
      TIME=Y(1,1)

      DO 4 J=1,NHP1
```

```
      RNH1(J)=Y(J+1,1)
 4    CONTINUE

      DO 5 J=1,NOP1
      RNO1(J)=Y(J+4,1)
 5    CONTINUE

      DO 6 J=1,NSP1
      RNS1(J)=Y(J+13,1)
 6    CONTINUE

      TE2=Y(29,1)
      TI2=Y(30,1)

C...RNHE:  NUMBER DENSITY OF ELECTRONS FROM IONIZATION OF HELIUM
      RNHE=RNH1(2) + 2.*RNH1(3)
C...RNOE:  NUMBER DENSITY OF ELECTRONS FROM IONIZATION OF OXYGEN
      RNOE=0.
      DO 16 J=2,NOP1
      Z=J-1
      RNOE=RNOE + Z*RNO1(J)
 16   CONTINUE

C...RNSE:  NUMBER DENSITY OF ELECTRONS FROM IONIZATION OF SILICON
      RNSE=0.
      DO 17 J=2,NSP1
      Z=J-1
      RNSE=RNSE + Z*RNS1(J)
 17   CONTINUE

C...COMPUTE TOTAL ELECTRON NUMBER DENSITY
      RNE1=RNHE + RNOE + RNSE


C...COMPUTE TOTAL NUMBER DENSITY OF HELIUM (RNH), OXYGEN (RNO)
C...AND SILICON (RNS) IONS.
      RNH=0.
      DO 18 J=1,NHP1
      RNH=RNH+RNH1(J)
 18   CONTINUE

      RNO=0.
      DO 19 J=1,NOP1
      RNO=RNO+RNO1(J)
 19   CONTINUE

      RNS=0.
      DO 20 J=1,NSP1
      RNS=RNS + RNS1(J)
 20   CONTINUE

      RN=RNS+RNH+RNO
      RNI1=RNH+RNO+RNS-RNH1(1)-RNO1(1)-RNS1(1)

      IF (MOD(NIT,NITW) .EQ. 1) GO TO 21
      GO TO 3

C...OUTPUT THE NEW DENSITIES AND TEMPERATURES.
 21   WRITE (6,1001)TIME,NIT,RNE1,TE2,TI2,RNH,RNO,RNS,
     1(RNH1(L),L=1,NHP1),(RNO1(L),L=1,NOP1),(RNS1(L),L=1,NSP1)
```

```
 1001 FORMAT(1H1,"TIME=  ",E11.4," SEC   CYCLE=  ",I6/
     1"ELECTRON DENSITY=  ",E11.4," CM(-3)"/"ELECTRON TEMPERATURE=  "
     1,E11.4," EV"/"ION TEMPERATURE=  ",E11.4," EV"/"ALL UNITS
     2 BELOW ARE CM(-3)"/"TOTAL HELIUM=  ",E11.4/"TOTAL OXYGEN=  ",
     3E11.4/"TOTAL SILICON=  ",E11.4/"HELIUM 0=  ",E11.4/"HELIUM 1=  "
     4,E11.4/"HELIUM 2=  ",E11.4/"OXYGEN 0=  ",E11.4/"OXYGEN 1=  ",
     5E11.4/"OXYGEN 2=  ",E11.4/"OXYGEN 3=  ",E11.4/"OXYGEN 4=  ",
     6E11.4/"OXYGEN 5=  ",E11.4/"OXYGEN 6=  ",E11.4/"OXYGEN 7=  ",
     7E11.4/"OXYGEN 8=  ",E11.4/"SILICON 0=  ",E11.4/
     8"SILICON 1=  ",E11.4/"SILICON 2=  ",E11.4/"SILICON 3=  ",E11.4/
     9"SILICON 4=  ",E11.4/"SILICON 5=  ",E11.4/"SILICON 6=  ",E11.4/
     1"SILICON 7=  ",E11.4/"SILICON 8=  ",E11.4/"SILICON 9=  ",E11.4/
     2"SILICON 10= ",E11.4/"SILICON 11= ",E11.4/"SILICON 12= ",E11.4/
     3"SILICON 13= ",E11.4/"SILICON 14= ",E11.4)

      IF (NIT .LT. NITMAX) GO TO 3

      CALL EXIT(2)
      END



C...THIS IS A FOURTH ORDER RUNGE-KUTTA SUBROUTINE SUPPLIED BY
C...G. ERLEBACHER WHICH ACTUALLY SOLVES THE COUPLED SET OF EQUATIONS.


      SUBROUTINE RGKUT(NBEQ,H,NIT,Y)
      DIMENSION Q1(30),Q2(30),Q3(30),Q4(30),Y(30,2)
      HH=H/2.
      DO 11 I=1,NBEQ
      Y(I,2)=Y(I,1)
      Q1(I)=F(Y,I,2)
11    Y(I,1)=Y(I,2)+HH*Q1(I)
      DO 21 I=1,NBEQ
      Q2(I)=F(Y,I,1)
21    Y(I,1)=Y(I,2)+HH*Q2(I)
      DO 31 I=1,NBEQ
      Q3(I)=F(Y,I,1)
31    Y(I,1)=Y(I,2)+H*Q3(I)
      DO 41 I=1,NBEQ
      Q4(I)=F(Y,I,1)
      Y(I,1)=Y(I,2)+H/6.*(Q1(I)+2.*(Q2(I)+Q3(I))+Q4(I))
41    CONTINUE
      NIT=NIT+1
      RETURN
      END


C...FUNCTION CONTAINS THE ALGORITHMS NECESSARY FOR THE ATOMIC
C...PHYSICS CALCULATIONS.

      FUNCTION F(Y,I,J)

      DIMENSION RNO1(9),RNO2(9),RNH1(3),RNH2(3),RNS1(15),RNS2(15),
     1OION(9),OREC(9),HION(3),HREC(3),SION(15),SREC(15),EH(3),
     2EO(9),ES(15),Y(30,2)

      COMMON/T2/RNE1,RNE2,RNI1,RNI2,RNH2,RNO2,RNS2,TE1,
```

```
      1NHP1,NOP1,NSP1,EH,EO,ES,TIME,RN,T1,T2,T3,T4,T5,DT
      2,NH,NO,NS

C...I:  COUNTER FROM RUNGE-KUTTA SUBROUTINE THAT TELLS FUNCTION
C...    WHICH O.D.E. IS BEING SOLVED.  THIS ALLOWS US TO AVOID
C...    NEEDLESS COMPUTATIONS.

C...F=TIME DERIVATIVE OF DIFFERENT VARIABLES DEPENDING UPON 'I'.

       IF (I .GT. 1) GO TO 1

       F=1.
       RETURN

 1     IF(I .GT. 4) GO TO 4

C...COMPUTE THE IONIZATION, RADIATIVE AND THREE-BODY RECOMBINATION
C...COEFFICIENTS FOR HELIUM.
       HION(1)=1.E-5*SQRT(Y(29,J)/EH(2))/EH(2)**1.5/(6.+Y(29,J)/EH(2))
      1*EXP(-EH(2)/Y(29,J))
       HION(2)=1.E-5*SQRT(Y(29,J)/EH(3))/EH(3)**1.5/(6.+Y(29,J)/EH(3))
      1*EXP(-EH(3)/Y(29,J))
       Z=1.
       RADREC=5.2E-14*Z*SQRT(EH(2)/Y(29,J))*(.43+.5*ALOG(EH(2)/Y(29,J))
      1+.469*(Y(29,J)/EH(2))**.333)
       TREC=1.4E-31*((Z+1)/Z)**6*(EH(2)/Y(29,J))**2
      1*EXP(EH(2)/Y(29,J)/(Z+2)/(Z+2))
       HREC(2)=RADREC + RNE2*TREC
       Z=2.
       RADREC=5.2E-14*Z*SQRT(EH(3)/Y(29,J))*(.43+.5*ALOG(EH(3)/Y(29,J))
      1+.469*(Y(29,J)/EH(3))**.333)
       TREC=1.4E-31*((Z+1)/Z)**6*(EH(3)/Y(29,J))**2
      1*EXP(EH(3)/Y(29,J)/(Z+2)/(Z+2))
       HREC(3)=RADREC + RNE2*TREC
       IF (I .EQ. 4) GO TO 3
       IF (I .EQ. 3) GO TO 2

       F=RNE2*(-HION(1)*Y(2,J)+HREC(2)*Y(3,J))
       RETURN

 2     F=RNE2*(HION(1)*Y(2,J)-(HREC(2)+HION(2))*Y(3,J)+HREC(3)*Y(4,J))
       RETURN

 3     F=RNE2*(HION(2)*Y(3,J)-HREC(3)*Y(4,J))
       RETURN

 4     IF (I .GT. 13) GO TO 7
       IF (I .GT. 5)  GO TO 5

C...COMPUTE THE IONIZATION, RADIATIVE AND THREE-BODY RECOMBINATION
C...COEFFICIENTS FOR OXYGEN
       OION(1)=1.E-5*SQRT(Y(29,J)/EO(2))/EO(2)**1.5/(6.+Y(29,J)/EO(2))
      1*EXP(-EO(2)/Y(29,J))
       Z=1.
       RADREC=5.2E-14*Z*SQRT(EO(2)/Y(29,J))*(.43+.5*ALOG(EO(2)/Y(29,J))
      1+.469*(Y(29,J)/EO(2))**.333)
       TREC=1.4E-31*((Z+1)/Z)**6*(EO(2)/TE1)**2
      1*EXP(EO(2)/TE1/(Z+2)/(Z+2))
       OREC(2)=RADREC + RNE2*TREC

```

```
      F=RNE2*(-GION(1)*Y(5,J)+GREC(2)*Y(6,J))
      RETURN

5     IF (I .EQ. 13) GO TO 6
      GION(I-5)=1.E-5*SQRT(Y(29,J)/EG(I-4))/EG(I-4)**1.5/(6.+Y(29,J)
     1/EG(I-4))*EXP(-EG(I-4)/Y(29,J))
      Z=I-5.
      RADREC=5.2E-14*Z*SQRT(EG(I-4)/Y(29,J))*(.43+.5*ALOG(EG(I-4)
     1/Y(29,J))+.469*(Y(29,J)/EG(I-4))**.333)
      TREC=1.4E-31*((Z+1)/Z)**6*(EG(I-4)/Y(29,J))**2
     1*EXP(EG(I-4)/Y(29,J))/(Z+2)/(Z+2))
      GREC(I-4)=RADREC + RNE2*TREC
      GION(I-4)=1.E-5*SQRT(Y(29,J)/EG(I-3))/EG(I-3)**1.5/(6.+Y(29,J)
     1/EG(I-3))*EXP(-EG(I-3)/Y(29,J))
      Z=I-4.
      RADREC=5.2E-14*Z*SQRT(EG(I-3)/Y(29,J))*(.43+.5*ALOG(EG(I-3)
     1/Y(29,J))+.469*(Y(29,J)/EG(I-3))**.333)
      TREC=1.4E-31*((Z+1)/Z)**6*(EG(I-3)/Y(29,J))**2
     1*EXP(EG(I-3)/Y(29,J)/(Z+2)/(Z+2))
      GREC(I-3)=RADREC + RNE2*TREC

      F=RNE2*(GION(I-5)*Y(I-1,J)-(GION(I-4)+GREC(I-4))*Y(I,J)+GREC(I-3)
     1*Y(I+1,J))
      RETURN

6     GION(8)=1.E-5*SQRT(Y(29,J)/EG(9))/EG(9)**1.5/(6.+Y(29,J)/EG(9))
     1*EXP(-EG(9)/Y(29,J))
      Z=8.
      RADREC=5.2E-14*Z*SQRT(EG(9)/Y(29,J))*(.43+.5*ALOG(EG(9)/Y(29,J))
     1+.469*(Y(29,J)/EG(9))**.333)
      TREC=1.4E-31*((Z+1)/Z)**6*(EG(9)/TE1)**2
     1*EXP(EG(9)/TE1/(Z+2)/(Z+2))
      GREC(9)=RADREC + RNE2*TREC

      F=RNE2*(GION(8)*Y(12,J)-GREC(9)*Y(13,J))
      RETURN

7     IF (I .GT. 28) GO TO 10
      IF (I .GT. 14) GO TO 8

C...COMPUTE THE IONIZATION, RADIATIVE AND THREE-BODY RECOMBINATION
C...COEFFICIENTS FOR SILICON
      SION(1)=1.E-5*SQRT(Y(29,J)/ES(2))/ES(2)**1.5/(6.+Y(29,J)/ES(2))
     1*EXP(-ES(2)/Y(29,J))
      Z=1.
      RADREC=5.2E-14*Z*SQRT(ES(2)/Y(29,J))*(.43+.5*ALOG(ES(2)/Y(29,J))
     1+.469*(Y(29,J)/ES(2))**.333)
      TREC=1.4E-31*((Z+1)/Z)**6*(ES(2)/Y(29,J))**2
     1*EXP(ES(2)/Y(29,J)/(Z+2)/(Z+2))
      SREC(2)=RADREC + RNE2*TREC

      F=RNE2*(-SION(1)*Y(14,J)+SREC(2)*Y(15,J))
      RETURN

8     IF (I .EQ. 28) GO TO 9
      SION(I-14)=1.E-5*SQRT(Y(29,J)/ES(I-13))/ES(I-13)**1.5/(6.
     1+Y(29,J)/ES(I-13))*EXP(-ES(I-13)/Y(29,J))
      Z=I-14.
      RADREC=5.2E-14*Z*SQRT(ES(I-13)/Y(29,J))*(.43+.5*ALOG(ES(I-13)
     1/Y(29,J))+.469*(Y(29,J)/ES(I-13))**.333)
```

```
      TREC=1.4E-31*((Z+1)/Z)**6*(ES(I-13)/Y(29,J))**2
     1*EXP(ES(I-13)/Y(29,J)/(Z+2)/(Z+2))
      SREC(I-13)=RADREC + RNE2*TREC
      SION(I-13)=1.E-5*SQRT(Y(29,J)/ES(I-12))/ES(I-12)**1.5/(6.
     1+Y(29,J)/ES(I-12))*EXP(-ES(I-12)/Y(29,J))
      Z=I-13.
      RADREC=5.2E-14*Z*SQRT(ES(I-12)/Y(29,J))*(.43+.5*ALOG(ES(I-12)
     1/Y(29,J))+.469*(Y(29,J)/ES(I-12))**.333)
      TREC=1.4E-31*((Z+1)/Z)**6*(ES(I-12)/Y(29,J))**2
     1*EXP(ES(I-12)/Y(29,J)/(Z+2)/(Z+2))
      SREC(I-12)=RADREC + RNE2*TREC

      F=RNE2*(SION(I-14)*Y(I-1,J)-(SION(I-13)+SREC(I-13))
     1*Y(I,J)+SREC(I-12)*Y(I+1,J))
      RETURN

 9    SION(14)=1.E-5*SQRT(Y(29,J)/ES(15))/ES(15)**1.5/(6.+Y(29,J)
     1/ES(15))*EXP(-ES(15)/Y(29,J))
      Z=14.
      RADREC=5.2E-14*Z*SQRT(ES(15)/Y(29,J))*(.43+.5*ALOG(ES(15)/Y(29,J))
     1+.469*(Y(29,J)/ES(15))**.333)
      TREC=1.4E-31*((Z+1)/Z)**6*(ES(15)/Y(29,J))**2
     1*EXP(ES(15)/Y(29,J)/(Z+2)/(Z+2))
      SREC(15)=RADREC + RNE2*TREC

      F=RNE2*(SION(14)*Y(27,J)-SREC(15)*Y(28,J))
      RETURN

C...COMPUTE THE ELECTRON AND ION NUMBER DENSITY AS BEFORE.
 10   RNHE=Y(3,J) + 2.*Y(4,J)

      RNOE=0.
      DO 16 JJ=6,13
      Z=JJ-5.
      RNOE=RNOE + Z*Y(JJ,J)
 16   CONTINUE

      RNSE=0.
      DO 17 JJ=15,28
      Z=JJ-14.
      RNSE=RNSE + Z*Y(JJ,J)
 17   CONTINUE

      RNE2=RNHE + RNOE + RNSE

      RNH=0.
      DO 18 JJ=2,4
      RNH=RNH+Y(JJ,J)
 18   CONTINUE

      RNO=0.
      DO 19 JJ=5,13
      RNO=RNO+Y(JJ,J)
 19   CONTINUE

      RNS=0.
      DO 20 JJ=14,28
      RNS=RNS + Y(JJ,J)
 20   CONTINUE

```

```
      RN=RNS+RNH+RNO
      RNI2=RNH+RNO+RNS-RNH2(1)-RNO2(1)-RNS2(1)

C...WRITE NEW NUMBER DENSITIES IN FAMILIAR FORM

      DO 11 JJ=1,NHP1
      RNH2(JJ)=Y(JJ+1,J)
 11   CONTINUE
      DO 12 JJ=1,NOP1
      RNO2(JJ)=Y(JJ+4,J)
 12   CONTINUE
      DO 13 JJ=1,NSP1
      RNS2(JJ)=Y(JJ+13,J)
 13   CONTINUE

C...SOME NUMBERS THAT APPEAR REPEATEDLY.
      Z2H=0.
      DO 14 JJ=2,NHP1
      Z=JJ-1
      Z2H=Z2H+Z*Z*RNH2(JJ)
 14   CONTINUE
      Z2O=0.
      DO 15 JJ=2,NOP1
      Z=JJ-1
      Z2O=Z2O+Z*Z*RNO2(JJ)
 15   CONTINUE
      Z2S=0.
      DO 21 JJ=2,NSP1
      Z=JJ-1
      Z2S=Z2S+Z*Z*RNS2(JJ)
 21   CONTINUE
      Z2M=(Z2H/4. +Z2O/16. +Z2S/28.)*6.02E23
      IF (Y(29,J) .LT. 36.2) A=1.
      IF (Y(29,J) .GE. 36.2) A=36.2/Y(29,J)

C...XLAM:  COULOMB LOGARITHM
      XLAM=1.55E10*A*SQRT(Y(29,J)**3/RNE2)

C...PEQEI:  ELECTRON-ION ENERGY EXCHANGE
      PEQEI=-RNE2*7.95E-33*ALOG(XLAM)*Z2M*(Y(30,J)-Y(29,J))/Y(29,J)**1.5
      IF (I .GT. 29) GO TO 22

      DO 23 JJ=1,NH
      HION(JJ)=1.E-5*SQRT(Y(29,J)/EH(JJ+1))/EH(JJ+1)**1.5/(6.+Y(29,J)
     1/EH(JJ+1))*EXP(-EH(JJ+1)/Y(29,J))
 23   CONTINUE
      DO 24 JJ=1,NO
      OION(JJ)=1.E-5*SQRT(Y(29,J)/EO(JJ+1))/EO(JJ+1)**1.5/(6.+Y(29,J)
     1/EO(JJ+1))*EXP(-EO(JJ+1)/Y(29,J))
 24   CONTINUE
      DO 25 JJ=1,NS
      SION(JJ)=1.E-5*SQRT(Y(29,J)/ES(JJ+1))/ES(JJ+1)**1.5/(6.+Y(29,J)
     1/ES(JJ+1))*EXP(-ES(JJ+1)/Y(29,J))
 25   CONTINUE

C...PIONH:  POWER LOST TO IONIZATION OF HELIUM
C...PIONO:  POWER LOST TO IONIZATION OF OXYGEN
C...PIONS:  POWER LOST TO IONIZATION OF SILICON
      PIONH=0.
      DO 26 JJ=1,NH
```

```
      PIONH=PIONH+EH(JJ+1)*RNH2(JJ)*HION(JJ)
26    CONTINUE
      PIONH=RNE2*PIONH
      PIONO=0.
      DO 27 JJ=1,NO
      PIONO=PIONO+EO(JJ+1)*RNO2(JJ)*OION(JJ)
27    CONTINUE
      PIONO=RNE2*PIONO
      PIONS=0.
      DO 28 JJ=1,NS
      PIONS=PIONS+ES(JJ+1)*RNS2(JJ)*SION(JJ)
28    CONTINUE
      PIONS=RNE2*PIONS

C...PADDE:  PHENOMENOLOGICAL ELECTRON POWER LOSS
      PADDE=1.5*RNE2*Y(29,J)/1.E-3

C...PCDIFF:  POWER LOST DUE TO CLASSICAL TRANSPORT
      PCDIFF=1.5*RNE2*Y(29,J)/1.E-3

C...PTDIFF:  POWER LOST DUE TO TURBULENT TRANSPORT
      PTDIFF=0.
      IF ((TIME .GT. T2) .AND. (TIME .LE. T5)) PTDIFF=1.5*RNE2*Y(29,J)
     1/1.E-5

C...PBREM:  BREMSSTRAHLUNG RADIATION
      PBREM=1.06E-13*RNE2*(Z2H+Z2O+Z2S)*SQRT(Y(29,J))

      DO 29 L=2,NHP1
      Z=L-1
      RADREC=5.2E-14*Z*SQRT(EH(L)/Y(29,J))*(.43+.5*ALOG(EH(L)/Y(29,J))
     1+.469*(Y(29,J)/EH(L))**.333)
      TREC=1.4E-31*((Z+1)/Z)**6*(EH(L)/Y(29,J))**2
     1*EXP(EH(L)/Y(29,J)/(Z+2)/(Z+2))
      HREC(L)=RADREC + RNE2*TREC
29    CONTINUE
      DO 30 L=2,NOP1
      Z=L-1
      RADREC=5.2E-14*Z*SQRT(EO(L)/Y(29,J))*(.43+.5*ALOG(EO(L)/Y(29,J))
     1+.469*(Y(29,J)/EO(L))**.333)
      TREC=1.4E-31*((Z+1)/Z)**6*(EO(L)/Y(29,J))**2
     1*EXP(EO(L)/Y(29,J)/(Z+2)/(Z+2))
      OREC(L)=RADREC + RNE2*TREC
30    CONTINUE
      DO 31 L=2,NSP1
      Z=L-1
      RADREC=5.2E-14*Z*SQRT(ES(L)/Y(29,J))*(.43+.5*ALOG(ES(L)/Y(29,J))
     1+.469*(Y(29,J)/ES(L))**.333)
      TREC=1.4E-31*((Z+1)/Z)**6*(ES(L)/Y(29,J))**2
     1*EXP(ES(L)/Y(29,J)/(Z+2)/(Z+2))
      SREC(L)=RADREC + RNE2*TREC
31    CONTINUE

C...PRECH:  POWER LOST DUE TO RECOMBINATION OF HELIUM
C...PRECO:  POWER LOST DUE TO RECOMBINATION OF OXYGEN
C...PRECS:  POWER LOST DUE TO RECOMBINATION OF SILICON
      PRECH=0.
      DO 32 JJ=2,NHP1
      PRECH=PRECH+HREC(JJ)*RNH2(JJ)
32    CONTINUE
```

```
      PRECH=RNE2*PRECH*1.5*Y(29,J)
      PRECO=0.
      DO 33 JJ=2,NOP1
      PRECO=PRECO+OREC(JJ)*RNO2(JJ)
33    CONTINUE
      PRECO=RNE2*PRECO*1.5*Y(29,J)
      PRECS=0.
      DO 34 JJ=2,NSP1
      PRECS=PRECS+SREC(JJ)*RNS2(JJ)
34    CONTINUE
      PRECS=RNE2*PRECS*1.5*Y(29,J)

C...COMPUTE PLASMA Z-EFFECTIVE
      ZEFFH=0.
      DO 35 JJ=2,NHP1
      Z=JJ-1
      ZEFFH=ZEFFH+Z*RNH2(JJ)
35    CONTINUE
      ZEFFO=0.
      DO 36 JJ=2,NOP1
      Z=JJ-1
      ZEFFO=ZEFFO+Z*RNO2(JJ)
36    CONTINUE
      ZEFFS=0.
      DO 37 JJ=2,NSP1
      Z=JJ-1
      ZEFFS=ZEFFS+Z*RNS2(JJ)
37    CONTINUE
      ZEFF=(ZEFFH +ZEFFO+ZEFFS)/RN

C...COMPUTE PLASMA RESISTIVITY, CURRENT AND OHMIC POWER
      CMIN=2.E6
      CMAX=.9E7
      IF ((Y(1,J) .GT. T2) .AND. (Y(1,J) .LT. T5)) GO TO 38
      RESIST=ZEFF*ALOG(XLAM)/2920./Y(29,J)**1.5
      IF ((Y(1,J) .GT. T5) .OR. (Y(1,J) .GT. T1)) CURRENT=CMIN
      IF (Y(1,J) .LT. T1) CURRENT=CMIN*Y(1,J)/T1
      GO TO 39
38    CURRENT=5.5E7
      IF (Y(1,J) .LT. T3) CURRENT=CMIN + CMAX*(Y(1,J)-T2)/(T3-T2)
      IF (Y(1,J) .GT. T4) CURRENT=CMIN+CMAX-CMAX*(Y(1,J)-T4)/(T5-T4)
      RESIST=CURRENT/1.E3/(CMAX+CMIN)
39    POHM=6.25E12*RESIST*CURRENT*CURRENT

C...COMPUTE POWER LOST DUE TO LINE RADIATION OF HELIUM (HPLR),
C...OXYGEN (OPLR) AND SILICON (SPLR).  NOTE THAT THE TRANSITION
C...ENERGIES AND OSCILLATOR STRENGTHS ARE INCORPORATED INTO THE
C...EQUATIONS.
      HPLR=RNH2(1)*.2762*EXP(-21.213/Y(29,J)) +
     1RNH2(2)*.4162*EXP(-40.785/Y(29,J))
      OPLR=RNO2(1)*.105*EXP(-10.7/Y(29,J)) +
     1RNO2(2)*.551*EXP(-15.91/Y(29,J)) +
     2RNO2(3)*.628*EXP(-16.03/Y(29,J)) +
     3RNO2(4)*.657*EXP(-14.65/Y(29,J)) +
     4RNO2(5)*.53*EXP(-12.58/Y(29,J)) +
     5RNO2(6)*.196*EXP(-11.99/Y(29,J)) +
     6RNO2(7)*.813*EXP(-561./Y(29,J)) +
     7RNO2(8)*.4162*EXP(-653./Y(29,J))
      SPLR=RNS2(1)*.6246*EXP(-4.93/Y(29,J)) +
     1RNS2(2)*3.62*EXP(-9.9/Y(29,J))+RNS2(3)*3.96*EXP(-9.6/Y(29,J))+
```

```
661       2RNS2(4)*1.61*EXP(-8.9/Y(29,J))+RNS2(5)*.21*EXP(-105./Y(29,J))+
662       3RNS2(6)*.33*EXP(-49.9/Y(29,J))+RNS2(7)*.74*EXP(-44.9/Y(29,J))+
663       4RNS2(8)*.443*EXP(-39./Y(29,J))+RNS2(9)*.34*EXP(-36./Y(29,J))+
664       5RNS2(10)*.54*EXP(-48./Y(29,J))+RNS2(11)*.4*EXP(-33.7/Y(29,J))+
665       6RNS2(12)*2.*EXP(-281./Y(29,J))
666
667        PLR=3.16E-6*RNE2/SQRT(Y(29,J))*(HPLR+OPLR+SPLR)
668
669        F=2./3./RNE2*(POHM-PEQEI-PBREM-PIONH-PIONS-PIONO
670       1-PRECH-PRECO-PRECS-PCDIFF-PTDIFF-PADDE-PLR) -
671       2Y(29,J)/RNE2*(RNE2-RNE1)/DT
672        RETURN
673
674 C...PADDI:  PHENOMENOLOGICAL ION POWER LOSS TERM
675  22    PADDI=1.5*RNI2*Y(30,J)/1.E-3
676
677 C...PWAVE:  ION WAVE HEATING TERM
678        PWAVE=0.
679        IF ((TIME .GT. T2) .AND. (TIME .LT. T5))
680       1PWAVE=1.65E-3*ZEFF*Y(29,J)*SQRT(RNI2)
681
682        F=2./3./RNI2*(PEQEI-PADDI)-Y(30,J)/RNI2*(RNI2-RNI1)/DT+PWAVE
683        RETURN
684        END
685 *CHATR I=ZEROD,LIB=(T',F'),X=CONTROZ,D=SYMBOL,GO
```

```
C      PROGRAM NAME: ONE-DIMENSIONAL MHD CODE (W/ INERTIA)
C      WRITTEN BY: H.C. LUI
C      MODIFIED BY: R. IZZO
C      LANGUAGE: FORTRAN
C      COMPILATION DEVICE: CDC 7600




C.....THE FULL SET OF RESISTIVE MHD EQUATIONS FOR A SINGLE FLUID ARE
C.....SOLVED NUMERICALLY WITH ONLY A RADIAL SPATIAL DEPENDENCE.  THIS
C.....CODE IS VERY USEFUL IN CARRYING OUT NUMERICAL EXPERIMENTS
C.....TO TEST FOR PROPER MODELING OF TRANSPORT PARAMETERS, ETC,..
C.....VARIABLES ARE DEFINED AS THEY ARE ENCOUNTERED IN THE CODE.



C*********************MAIN PROGRAM*********************


      DIMENSION W(3,51,2),SG(51,2),CN(51,2),R(51),AA(150,9)
     1,BB(3,3),P(6,51),F(3,51,2),PSI(51,2),XI(51,2)
     2,BZ(51,2),BC(51,2),CZ(51,2),CC(51,2),GA(51),GB(51),GC(51)
     3,GD(51),E(51),RO(51),BXJ(51),GRADP(51),CCZ(51)

      COMMON SG,R,AA,CN,BB,COE,DOE,BZ,BC,CZ,CC,GA,GB,GC,GD

C.....FK:  RATIO OF SPECIFIC HEATS
C.....C:   SPEED OF LIGHT IN VACUUM
C.....FR:  HELIUM GAS CONSTANT
C.....CV:  SPECIFIC HEAT AT CONSTANT VOLUME
C.....MS:  STOP AFTER THIS MANY TIME STEPS
C.....MW:  WRITE AFTER THIS MANY TIME STEPS
C.....K:   TIME INDEX

      DATA FK,C/1.666666,2.998E+10/
      FR=0.6231E+08
      CV=FR/(FK-1.)
      K=1
      MS=4
      MW=250

      CALL DROPFILE(0)
      CALL OPEN(5,"INPUT",0,0)
      CALL CREATE(6,"OUTPUT",3,-1)
      CALL KEEP80(1,2)
      CALL DD80ID(6HTORUS2,1)

C.....SET UP THE RADIAL GRID
```

```
C.....DX:  SPACE INCREMENT

      JB=2
      JE=50
      JS=JB-1
      JD=JE+1
      JP=JE-JS
      DX=2./JE
      DO 3 J=JS,JD
      SJ=J
      R(J)=(SJ-1.)*DX +15./7.5
      WRITE (6,101) J,R(J)
    3 CONTINUE
  101 FORMAT (1H ,"J=",I3,"RADIUS=",E14.7)

C.....RBIG:  MAJOR RADIUS IN CM
C.....RSM:   COMPUTATIONAL VESSEL HALF-WIDTH
C.....SMALL: ANY NUMBER SMALLER THAN THIS WILL BE SET TO ZERO
C.....BTOR:  CHARACTERISTIC MAGNETIC FIELD
C.....EMASS: MASS OF ELECTRON
C.....CHARGE:CHARGE OF ION
C.....DN:    INITIAL FILL DENSITY
C.....BMIN:  INITIAL (BIAS) TOROIDAL FIELD OUTSIDE PLASMA
C.....BVI, BVO:  INITIAL VERTICAL COMPONENTS OF MAGNETIC FIELD TO THE
C                INSIDE AND OUTSIDE OF PLASMA REGION
C.....CCT:   INITIAL TOROIDAL CURRENT DENSITY
C.....BMIN1: BIAS TOROIDAL FIELD INSIDE PLASMA
C.....BVT:   EXTERNAL VERTICAL FIELD IN HOLE OF TORUS
C.....UN:    CHARACTERISTIC ALFVEN VELOCITY
      RBIG=22.5
      SMALL=0.10E-16
      RSM=7.5
      Q=RSM/RBIG
      BTOR=4000.
      EMASS=9.1E-28
      CHARGE=2.*4.8E-10
      DN=0.24E-08
      BMIN=-1333./BTOR
      BVI=-1750./BTOR
      BVO=+1750./BTOR
      CCT=(BVO-BVI)/(R(39)-R(13))
      BMIN1=-2500./BTOR
      BVT=600./BTOR
      UN=BTOR/SQRT(4.*3.14159*DN)

C.....DT:     NORMALIZED TIME STEP
C.....TPO,1,2,3,PETIME:  IMPORTANT TIMES DURING START-UP
C.....FLUXH,Z: NORMALIZED POLOIDAL FLUX FUNCTION THROUGH HOLE AFTER
C               HEATING AND Z-PINCH
C.....SGO:    CHARACTERISTIC ANOMALOUS CONDUCTIVITY
C.....XJM:    MAXIMUM TORUS-II CURRENT DENSITY (NORMALIZED)
C.....CNO:    CHARACTERISTIC THERMAL CONDUCTIVITY
C.....CMIN:   CUTOFF CURRENT TO AVOID INFINITE CONDUCTIVITY REGIONS
```

```
C.....M:       ITERATION COUNTER
      DT=0.10E-08*UN/RSM
      TP0=4.0E-06*UN/RSM
      TP1=4.7E-06*UN/RSM
      TP3=6.0E-06*UN/RSM
      TP2=18.0E-06*UN/RSM
      PETIME=1.70E-06*UN/RSM
      FLUXH=5.0E+05/BTOR/RSM/RSM
      FLUXZ=2.0E+05/BTOR/RSM/RSM
      SGO=8.0E+12
      XJM=1.5E+13*4.*3.1416*RSM/BTOR/C
      CNO=0.28E+07
      CMIN=XJM/166.
      M=0

C.....SOME OUTPUT
      WRITE (6,102)
  102 FORMAT("   THESE ARE NORMALIZED RESULTS. TO DIMENSIONALIZE
     1DO THE FOLLOWING:")
      WRITE (6,103)
  103 FORMAT (1H ,"DENSITY=W(1)*DN VELOCITY=W(2)*UN/W(1) TEMP=W(3)*UN*
     1UN/CV  JTOR=CC*BTOR*C/A/4/PI JPOL=CZ*BTOR*C/A/4/PI")
      WRITE (6,98)
   98 FORMAT (1H ," TORB=BC*BTOR  POLB=BZ*BTOR")

C.....FLEAK: FRACTION OF RETURN LEAKAGE INTO VESSEL
      FLEAK=0.

C.....INITIAL CONDITIONS (ALL VARIABLES ARE NORMALIZED)
C.....W(1,J,K):  DENSITY AT GRID POINT J AND TIME K
C.....XI:        POLOIDAL CURRENT FUNCTION
C.....SG:        ELECTRICAL CONDUCTIVITY
C.....CN:        THERMAL CONDUCTIVITY
C.....BC:        TOROIDAAL MAGNETIC FIELD
C.....BZ:        Z-COMPONENT OF MAGNETIC FIELD
C.....PSI:       POLOIDAL FLUX FUNCTION
C.....CC:        TOROIDAL CURRENT DENSITY
C.....CZ:        Z-COMPONENT OF CURRENT DENSITY
C.....W(2,J,K):  RADIAL VELOCITY
C.....W(3,J,K):  TEMPERATURE
      DO 5 K=1,2

      DO 210 J=JS,13
      W(1,J,K)=.05
      XI(J,K)=BMIN/Q
      SG(J,K)=166.
      CN(J,K)=1.
      BC(J,K)=XI(J,K)/R(J)
      BZ(J,K)=BVI
      PSI(J,K)=(FLUXZ+BZ(J,K)*(R(J)*R(J)-R(JS)*R(JS))/2.)*(1.-FLEAK)
      CC(J,K)=0.
      CZ(J,K)=0.
      W(3,J,K)=10000./UN/UN*CV
```

```
      W(2,J,K)=0.
  210 CONTINUE

      DO 211 J=14,39
      XI(J,K)=BMIN1/Q
      CN(J,K)=1.
      BC(J,K)=XI(J,K)/R(J)
      BZ(J,K)=BZ(13,K)+CCT*(R(J)-R(13))
      PSI(J,K)=(PSI(13,K)+(R(J)*R(J)-R(13)*R(13))/2.*BZ(13,K)+
     1CCT*(R(J)**3/3.+R(13)**3/6.-R(J)**2*R(13)/2.))*(1.-FLEAK)
      CZ(J,K)=0.
      W(2,J,K)=0.
      CC(J,K)=-CCT
      SG(J,K)=166.
      IF (J .LE. 26) W(1,J,K)=W(1,13,K)+5.9*(R(J)-R(13))
      IF (J .GT. 26) W(1,J,K)=W(1,26,K)-5.9*(R(J)-R(26))
      IF (J .LE. 26) W(3,J,K)=W(3,13,K)+1.E+04*CV/UN/UN*(R(J)-R(13))
      IF (J .GT. 26) W(3,J,K)=W(3,26,K)-1.E+04*CV/UN/UN*(R(J)-R(26))
  211 CONTINUE

      DO 212 J=40,JD
      W(1,J,K)=.05
      XI(J,K)=BMIN/Q
      SG(J,K)=166.
      CN(J,K)=1.
      BC(J,K)=XI(J,K)/R(J)
      BZ(J,K)=+BV0
      PSI(J,K)=(PSI(39,K)+(R(J)*R(J)-R(39)*R(39))*BZ(J,K)/2.)*(1.-FLEAK)
      CC(J,K)=0.
      CZ(J,K)=0.
      W(3,J,K)=10000./UN/UN*CV
      W(2,J,K)=0.
  212 CONTINUE

    5 CONTINUE

C.....TIME:  REAL TIME
C.....HU:    MINIMUM PLASMA DENSITY
C.....C0E:   OFTEN USED NUMERICAL FACTOR
C.....D0E:           DITTO
C.....TX:            DITTO
      TIME=0.
      HU=0.01
      C0E=C*C*DT/(4.*3.14159*UN*RSM*SG0)
      D0E=CN0*DT/(DN*CV*UN*RSM)
      TX=DT/DX
      K=1
      FLUXJD=PSI(JD,K)

    6 M=M+1
      TIME=TIME+DT

C.....SPECIFICATION OF BOUNDARY VALUES FOR THE POLOIDAL FLUX AND CURRENT
```

```
C.....FUNCTION
      IF (TIME .GT. PETIME) GO TO 43
      XI(JS,K+1)=(BMIN+TIME/PETIME)/Q
      XI(JD,K+1)=(BMIN+TIME/PETIME)/Q
   43 IF (TIME .GT. TP1) GO TO 42
      PSI(JS,K+1)=FLUXZ+(FLUXH+BVT*R(JS)**2/2.-FLUXZ)*TIME/TP1
      PSI(JD,K+1)=FLUXJD+(FLUXH+BVT*R(JD)**2/2.-FLUXJD)*TIME/TP1
      PSIJS=PSI(JS,K+1)
      PSIJD=PSI(JD,K+1)
      GO TO 44
   42 PSI(JS,K+1)=PSIJS-(TIME-TP1)/TP2*FLUXH/5.
      PSI(JD,K+1)=PSIJD-(TIME-TP1)/TP2*FLUXH/5.

C.....SOLVE FOR NEW VALUES OF DENSITY, VELOCITY, TEMPERATURE AND MAGNETIC
C.....FIELD.
   44 CALL IMPL(K,TX,DT,DX,CV,FK,JB,JE,JP,UN,SGO,CNO,W,F,PSI,XI,M)

  118 FORMAT (1H ,2(I10))

C.....CHECK FOR NEGATIVE TEMPERATURE AND SMALL VELOCITY.
C.....SET-UP THE ELECTRICAL CONDUCTIVITY.  IS IT ANOMOLOUS, CLASSICAL
C.....SWITCHING BETWEEN THE TWO, ETC,.?
      DO 12 J=JB,JE
      IF (W(3,J,K+1) .LT. 0.) WRITE (6,118) J,M
      IF (W(3,J,K+1) .LT. 0.) GO TO 34
      IF (ABS(W(2,J,K+1)) .LT. SMALL) W(2,J,K+1)=0.
      IF (ABS(PSI(J,K+1)) .LT. SMALL) PSI(J,K+1)=0.
      IF (TIME .GT. TP0) GO TO 60
      CT=SQRT(CZ(J,K+1)*CZ(J,K+1)+CC(J,K+1)*CC(J,K+1))
      IF (CT .LE. CMIN) SG(J,K)=166.
      IF (CT .GT. CMIN) SG(J,K)=XJM/CT
      GO TO 12
   60 SG(J,K)=1.3E+13*(UN*UN/CV*W(3,J,K+1)/11600.)**1.5/SGO
      IF (TIME .GT. TP3) GO TO 12
      SGR=((TIME-TP0)/(TP3-TP0))**3
      CT=SQRT(CZ(J,K+1)*CZ(J,K+1)+CC(J,K+1)*CC(J,K+1))
      IF (CT .LE. CMIN) SGA=166.
      IF (CT .GT. CMIN) SGA=XJM/CT
      SG(J,K)=SGR*SG(J,K)+(1.-SGR)*SGA
   12 CONTINUE

C.....EXTRAPOLATE DENSITY AT THE BOUNDARY
      W(1,JS,K+1)=W(1,JB,K+1)
      W(1,JD,K+1)=W(1,JE,K+1)

C.....SET 'NEW' VALUES TO 'OLD' VALUES.
      DO 14 J=JS,JD
      DO 15 L=1,3
   15 W(L,J,K)=W(L,J,K+1)
      PSI(J,K)=PSI(J,K+1)
      XI(J,K)=XI(J,K+1)
   14 CONTINUE

```

```
C.....LOW DENSITY TREATMENT
      JBB=JB+1
      JEE=JE-1
      DO 2 J=JBB,JEE
      IF (J .EQ. JBB) GO TO 208
      IF (J .EQ. JEE) GO TO 208
      RO(J)=(W(1,J,K)+W(1,J+1,K)+W(1,J-1,K)+W(1,J-2,K)+
     2W(1,J+2,K)+W(1,J+3,K)+W(1,J-3,K))/7.
      GO TO 209
  208 RO(J)=(W(1,J,K)+W(1,J+1,K)+W(1,J+2,K)+W(1,J-1,K)+W(1,J-2,K))/5.
  209 IF (RO(J) .LE. 0.2) SG(J,K)=1.
    2 CONTINUE
      RO(JB)=(W(1,JS,K)+W(1,JB,K)+W(1,JB+1,K)+W(1,JB+2,K))/4.
      RO(JE)=(W(1,JE-2,K)+W(1,JE-1,K)+W(1,JE,K)+W(1,JD,K))/4.
      IF (RO(JB) .LE. 0.2) SG(JB,K)=1.
      IF (RO(JE) .LE. 0.2) SG(JE,K)=1.

      DO 13 J=JB,JE
      IF (ABS(W(2,J,K)) .LT. SMALL) W(2,J,K)=0.
      IF (ABS(PSI(J,K)) .LT. SMALL) PSI(J,K)=0.
      IF (W(1,J,K) .LT. HU) W(1,J,K)=HU
   13 CONTINUE

      SG(JS,K)=SG(JB,K)
      SG(JD,K)=SG(JE,K)
      W(1,JS,K)=W(1,JB,K)
      W(1,JD,K)=W(1,JE,K)

      IF (MOD(M,MW) .EQ. 1) GO TO 28
      GO TO 29
   28 CONTINUE
      SIME=TIME*RSM/UN
      WRITE (6,104) M,SIME,DT,FR,CV,COE,UN
  104 FORMAT (1HO,"CYCLE=",I4,"TIME=",E14.7,"DT=",E14.7,"FR=",4E15.7)
      WRITE (6,105)
  105 FORMAT (1HO,2X,"I",4X,"TOROIDAL B",4X,"POLOIDAL BZ",4X,
     1"TEMPERATURE",4X,"DENSITY",5X,"VELOCITY",6X,"POLOIDAL CZ",8X,
     2"PSI",9X,"TOROID CC")

C.....MORE LOW DENSITY TREATMENT. SMOOTHEN THE FIELD QUANTITIES.
      DO 204 J=JB,JE
      IF (RO(J) .GT. 0.2) GO TO 204
      PSI(J,K)=(PSI(J-1,K)+PSI(J,K)+PSI(J+1,K))/3.
      XI(J,K)=(XI(J-1,K)+XI(J,K)+XI(J+1,K))/3.
  204 CONTINUE

      DO 32 J=JB,JE
      BC(J,K)=XI(J,K)/R(J)
      CZ(J,K)=(XI(J+1,K)-XI(J-1,K))/(R(J)*2.*DX)
      BZ(J,K)=(PSI(J+1,K)-PSI(J-1,K))/(2.*DX*R(J))
   32 CONTINUE

      BC(JS,K)=XI(JS,K)/R(JS)
```

```
      BC(JD,K)=XI(JD,K)/R(JD)
      BZ(JS,K)=(PSI(JS+1,K)-PSI(JS,K))/(R(JS)*DX)
      BZ(JD,K)=(PSI(JD,K)-PSI(JD-1,K))/(R(JD)*DX)

      DO 203 J=JB,JE
      IF (RO(J) .GT. 0.2) GO TO 203
      BZ(J,K)=(BZ(J-1,K)+BZ(J,K)+BZ(J+1,K))/3.
  203 CONTINUE

      DO 27 J=JB,JE
      CC(J,K)=-(BZ(J+1,K)-BZ(J-1,K))/(2.*DX)
   27 CONTINUE

      DO 31 J=JS,JD
      BC(J,K)=BC(J,K)
      BZ(J,K)=BZ(J,K)
      F(1,J,K+1)=W(1,J,K)
      F(3,J,K+1)=W(3,J,K)
      F(2,J,K+1)=W(2,J,K)/W(1,J,K)
      WRITE (6,106) J,BC(J,K),BZ(J,K),F(3,J,K+1),
     1F(1,J,K+1),F(2,J,K+1),CZ(J,K),PSI(J,K),CC(J,K)
   31 CONTINUE
  106 FORMAT (1H ,I3,8E15.7)

C.....SET UP DATA FOR PLOTTING.
      DO 11 J=JS,JD
      P(2,J)=F(1,J,K+1)*DN
      P(1,J)=F(3,J,K+1)*UN*UN/CV
      P(6,J)=P(1,J)*P(2,J)*FR
      P(5,J)=BC(J,K)*BTOR
      P(4,J)=BZ(J,K)*BTOR
      P(3,J)=CC(J,K)*C*BTOR/(4.*3.1413*RSM)
      CCZ(J)=CZ(J,K)*C*BTOR/(4.*3.1416*RSM)
   11 CONTINUE
      CALL PLOT1(P,R,JD,M)

   29 CONTINUE
      IF (M .GT. MS) GO TO 34
      GO TO 6
   34 CONTINUE

C.....CHECK ON GRAD P AND J X B
      DR=2.*RSM /JE
      DO 10 J=JB,JE
      BXJ(J)=ABS((P(6,J)*P(5,J)-CCZ(J)*P(4,J))/C)
      GRADP(J)=ABS((P(3,J+1)-P(3,J-1))/(2.*DR))
      E(J)=(GRADP(J)-BXJ(J))/(GRADP(J)+BXJ(J))
      WRITE (6,107) R(J),E(J),BXJ(J),GRADP(J),SG(J,K)
   10 CONTINUE
  107 FORMAT (1H ,"RADIUS=",E13.6,"   EQUILIBRIUM =", E13.6,
     1"   GRAD   P =",E13.6,"   J X B =",2(E13.6))
      CALL PLOTE
      CALL EXIT(2)
```

```
      END
C.....THIS SUBROUTINE SOLVES FOR THE NEW VALUES OF DENSITY, VELOCITY,
C.....TEMPERATURE, POLOIDAL FLUX FUNCTION AND POLOIDAL CURRENT FUNCTION.
C.....THE EQUATIONS ARE WRITTEN IN THE FORM AX(J-1) + BX(J) +CX(J+1) = D
C.....WHERE EVERYTHING ON THE LEFT SIDE (X) IS AT THE NEW TIME AND THE
C.....RIGHT SIDE (D) IS AT THE OLD TIME.  IF WE SET FAC AND FFAC EQUAL TO
C.....TO ONE, THE SCHEMES ARE FULLY IMPLICIT.  A SETTING OF ZERO IS FULLY
C.....EXPLICIT.  CAUTION: THE CODE HAS NEVER SUCCESSFULLY OPERATED AT A
C.....SETTING OF LESS THAN .9

      SUBROUTINE IMPL(K,TX,DT,DX,CV,FK,JB,JE,JP,UN,SGO,CNO,W,F,PSI,
     1XI,M)
      DIMENSION W(3,51,2),SG(51,2),CN(51,2),R(51),AA(150,09)
     1,BB(3,3),F(3,51,2),PSI(51,2),XI(51,2),TYY(51),TXY(51)
     2,BZ(51,2),BC(51,2),CZ(51,2),CC(51,2),GA(51),GB(51),GC(51),GD(51)
      COMMON SG,R,AA,CN,BB,COE,DOE,BZ,BC,CZ,CC,GA,GB,GC,GD

      FAC=1.
      FFAC=FAC
      JD=JE+1
      JS=JB-1

C.....SET UP NUMERICAL DISSIPATION (LAPIDUS TYPE)
      DO 1 J=JS,JD
      TYY(J)=0.4
      TXY(J)=0.0
    1 CONTINUE

C.....SET UP PSI EQUATION IN FORMAT DESCRIBED ABOVE AND IN DISSERTATION.
      DO 19 J=JB,JE
      GC(J)=FFAC*COE*R(J)/(SG(J,K)*DX*DX*(R(J-1)+R(J))/2.)
     1+FFAC*DT*W(2,J,K)/W(1,J,K)/(2.*DX)
      GA(J)=FFAC*COE*R(J)/(SG(J,K)*DX*DX*(R(J+1)+R(J))/2.)
     1-FFAC*DT*W(2,J,K)/W(1,J,K)/(2.*DX)
      GB(J)=1.+FFAC*COE*R(J)/(SG(J,K)*DX*DX)
     1*(2./(R(J+1)+R(J))+2./(R(J-1)+R(J)))
      GD(J)=PSI(J,K)*(1.-(COE*R(J)*(1.-FFAC)/DX/DX/SG(J,K))*
     1(2./(R(J+1)+R(J))+2./(R(J)+R(J-1))))
     2+PSI(J-1,K)*(1.-FFAC)*(W(2,J,K)*DT/2./DX/W(1,J,K)+
     3COE*R(J)/DX/DX/SG(J,K)/(.5*(R(J)+R(J-1))))+
     4PSI(J+1,K)*(1.-FFAC)*(-W(2,J,K)*DT/2./DX/W(1,J,K)+
     5COE*R(J)/DX/DX/SG(J,K)/(.5*(R(J+1)+R(J))))
     6+0.5/4.*TX*TXY(J)*(ABS(W(2,J+1,K)/W(1,J+1,K)-W(2,J,K)
     7/W(1,J,K))*(PSI(J+1,K)-PSI(J,K))-ABS(W(2,J,K)/W(1,J,K)
     8-W(2,J-1,K)/W(1,J-1,K))*(PSI(J,K)-PSI(J-1,K)))
   19 CONTINUE

```

```
C.....SOLVE TRI-DIAGONAL MATRIX.
      CALL CROUT(M,K,JB,JE,JP,JD,GA,GB,GC,GD,PSI)

C.....SET UP EQUATION FOR POLOIDAL CURRENT FUNCTION.
      DO 22 J=JB,JE
      GC(J)=FFAC*COE*R(J)/(DX*DX*(SG(J-1,K)+
     1SG(J,K))/2.*(R(J-1)+R(J))/2.)+FFAC*DT*R(J)
     1*W(2,J-1,K)/W(1,J-1,K)/(2.*DX*R(J-1))
      GA(J)=FFAC*COE*R(J)/(DX*DX*(SG(J+1,K)+
     1SG(J,K))/2.*(R(J+1)+R(J))/2.)-FFAC*DT*R(J)
     2*W(2,J+1,K)/W(1,J+1,K)/(2.*DX*R(J+1))
      GB(J)=1.+FFAC*COE*R(J)/DX/DX*(1./((SG(J+1,K)
     1+SG(J,K))/2.*(R(J+1)+R(J))/2.)+
     21./((SG(J-1,K)+SG(J,K))/2.*(R(J-1)+R(J))/2.))
      GD(J)=XI(J,K)*(1. + COE*R(J)*(1.-FFAC)/DX/DX*(-4./((SG(J+1,K)
     1+SG(J,K))*(R(J+1)+R(J)))-4./((SG(J,K)+SG(J-1,K))*(R(J)+R(J-1))))
     2+XI(J-1,K)*((1.-FFAC)*(R(J)*DT*W(2,J-1,K)/2./DX/R(J-1)+
     3COE*R(J)/DX/DX/(.25*(SG(J,K)+SG(J-1,K))*(R(J)+R(J-1)))))
     4-XI(J+1,K)*(1.-FFAC)*(W(2,J+1,K)*R(J)*TX/2./R(J+1)/W(1,J+1,K)
     5-COE*R(J)/DX/DX/(.25*(SG(J+1,K)+SG(J,K))*(R(J)+R(J+1))))
     6+0.5/4.*TX*TXY(J)*(ABS(W(2,J+1,K)/W(1,J+1,K)-W(2,J,K)
     7/W(1,J,K))*(XI(J+1,K)-XI(J,K))-ABS(W(2,J,K)/W(1,J,K)
     8-W(2,J-1,K)/W(1,J-1,K))*(XI(J,K)-XI(J-1,K)))
   22 CONTINUE

      CALL CROUT(M,K,JB,JE,JP,JD,GA,GB,GC,GD,XI)
   17 CONTINUE

C.....CALCULATE NEW FIELDS AND CURRENTS FROM NEWLY OBTAINED VALUES OF
C.....PSI AND XI.
      DO 32 J=JB,JE
      BC(J,K+1)=XI(J,K+1)/R(J)
      CZ(J,K+1)=+(XI(J+1,K+1)-XI(J-1,K+1))/(R(J)*2.*DX)
      BZ(J,K+1)=+(PSI(J+1,K+1)-PSI(J-1,K+1))/(2.*DX*R(J))
   32 CONTINUE
      BC(JS,K+1)=XI(JS,K+1)/R(JS)
      BC(JD,K+1)=XI(JD,K+1)/R(JD)
      BZ(JS,K+1)=(PSI(JS+1,K+1)-PSI(JS,K+1))/(R(JS)*DX)
      BZ(JD,K+1)=(PSI(JD,K+1)-PSI(JD-1,K+1))/(R(JD)*DX)
      DO 27 J=JB,JE
      CC(J,K+1)=-(BZ(J+1,K+1)-BZ(J-1,K+1))/(2.*DX)
   27 CONTINUE


C.....SET UP MATRIX TO SOLVE FOR NEW W-VECTOR.  NOTE THAT THIS MATRIX
C.....WILL ALSO BE TRI-DIAGONAL, HOWEVER, EACH ELEMENT IS A 3 X 3 MATRIX.
      DO 107 J=1,JP
      IF (J .EQ. 1) GO TO 415
      AA(3*J-2,1)=0.
      AA(3*J-2,2)=-0.5*FAC*TX*R(J)/R(J+1)
      AA(3*J-2,3)=0.
      AA(3*J-1,1)=+0.5*TX*R(J)/R(J+1)*(
     1(W(2,J,K)/W(1,J,K))**2)-0.5*(FK-1.)*FAC*TX*W(3,J,K)
```

```
      AA(3*J-1,2)=-TX*R(J)/R(J+1)*(W(2,J,K)/W(1,J,K))
      AA(3*J-1,3)=-0.5*(FK-1.)*FAC*TX*W(1,J,K)
      AA(3*J,1)=0.5*(FK-1.)*TX*R(J)/R(J+1)*W(2,J,K)*
     1W(3,J+1,K)/W(1,J,K)**2
      AA(3*J,2)=-(FK-1.)*TX*R(J)/R(J+1)*W(3,J+1,K)/W(1,J,K)
      AA(3*J,3)=-0.5*FAC*TX*W(2,J+1,K)/W(1,J+1,K)
     1-FAC*DOE/(R(J+1)*DX*DX)*0.25*(CN(J+1)+CN(J,K))*(R(J+1)+R(J))/
     2W(1,J+1,K)
  415 CONTINUE
      IF (J .EQ. JP) GO TO 416
      AA(3*J-2,7)=0.
      AA(3*J-2,8)=+0.5*FAC*TX*R(J+2)/R(J+1)
      AA(3*J-2,9)=0.
      AA(3*J-1,7)=-0.5*TX*R(J+2)/R(J+1)*(
     1(W(2,J+2,K)/W(1,J+2,K))**2)
     2+0.5*(FK-1.)*FAC*TX*W(3,J+2,K)
      AA(3*J-1,8)=+TX*R(J+2)/R(J+1)*(
     1W(2,J+2,K)/W(1,J+2,K))
      AA(3*J-1,9)=+0.5*(FK-1.)*FAC*TX*W(1,J+2,K)
      AA(3*J,7)=-0.5*(FK-1.)*TX*R(J+2)/R(J+1)*W(2,J+2,K)*
     1W(3,J+1,K)/W(1,J+2,K)**2
      AA(3*J,8)=(FK-1.)*TX*R(J+2)/R(J+1)*
     1W(3,J+1,K)/W(1,J+2,K)
      AA(3*J,9)=0.5*FAC*TX*W(2,J+1,K)/W(1,J+1,K)
     1-FAC*DOE/(R(J+1)*DX*DX)*0.25*(CN(J+1,K)+CN(J+2,K))*(R(J+1)+R(J+2))
     2/W(1,J+1,K)
  416 CONTINUE
      AA(3*J-2,4)=1.
      AA(3*J-2,5)=0.
      AA(3*J-2,6)=0.
      AA(3*J-1,4)=0.
      AA(3*J-1,5)=1.
      AA(3*J-1,6)=0.
      AA(3*J,4)=0.
      AA(3*J,5)=0.
      AA(3*J,6)=1.+FAC*DOE/(R(J+1)*DX*DX)*0.25*((CN(J+1,K)+CN(J+2,K))*
     1(R(J+1)+R(J+2))+(CN(J+1,K)+CN(J,K))*(R(J+1)+R(J)))/W(1,J+1,K)
  107 CONTINUE
      DO 108 J=JB,JE
      F(1,J,K)=W(1,J,K)-(1.-FAC)*(R(J+1)*W(2,J+1,K)-R(J-1)*W(2,J-1,K))
     1+0.5/4.*TX*TYY(J)*(ABS(W(2,J+1,K)/W(1,J+1,K)-W(2,J,K)
     2/W(1,J,K))*(W(1,J+1,K)-W(1,J,K))-ABS(W(2,J,K)/W(1,J,K)
     3-W(2,J-1,K)/W(1,J-1,K))*(W(1,J,K)-W(1,J-1,K)))
      F(2,J,K)=W(2,J,K)+FAC*DT*(CC(J,K+1)*BZ(J,K+1)-CZ(J,K+1)*BC(J,K+1))
     1+0.5*(2.*FAC-1.)*TX*(FK-1.)*(W(1,J+1,K)*W(3,J+1,K)
     2-W(1,J-1,K)*W(3,J-1,K))+0.5/4.*TX*TYY(J)*(ABS(W(2,J+1,K)/W(1,J+1
     2,K)-W(2,J,K)/W(1,J,K))*(W(2,J+1,K)-W(2,J,K))-ABS(W(2,J,K)/W(1,J,K)
     3-W(2,J-1,K)/W(1,J-1,K))*(W(2,J,K)-W(2,J-1,K)))
     4+(1.-FAC)*DT*(CC(J,K)*BZ(J,K)-CZ(J,K)*BC(J,K))
      F(3,J,K)=W(3,J,K)+COE/SG(J,K)/W(1,J,K)*(1.-FAC)*
     1(CC(J,K)**2+CZ(J,K)**2)-(1.-FAC)*W(2,J,K)/W(1,J,K)*
     2(W(3,J+1,K)-W(3,J-1,K))*TX/2. +DOE*(1.-FAC)/W(1,J,K)/R(J)
     3/DX/DX*(.25*(R(J)+R(J+1))*(CN(J,K)+CN(J+1,K))*(W(3,J+1,K)
```

```
      4-W(3,J,K))-(.25*(R(J)+R(J-1))*(CN(J,K)+CN(J-1,K))*
      5(W(3,J,K)-W(3,J-1,K))))+0.5/4.*TX*TYY(J)*(ABS(W(2,J+1,K)/W(1,J+1
      2,K)-W(2,J,K)/W(1,J,K))*(W(3,J+1,K)-W(3,J,K))-ABS(W(2,J,K)/W(1,J,K)
      3-W(2,J-1,K)/W(1,J-1,K))*(W(3,J,K)-W(3,J-1,K)))
      4+FAC*COE*(CZ(J,K+1)**2+CC(J,K+1)**2)/SG(J,K)/W(1,J,K)
  108 CONTINUE
       JPP=3*JP
       AA(3-1,4)=AA(3-1,4)-0.5*FAC*TX*(FK-1.)*W(3,JS,K)
       F(2,JB,K)=F(2,JB,K)+0.5*(FK-1.)*W(1,JS,K)*FAC*TX*W(3,JS,K+1)
       F(3,JB,K)=F(3,JB,K)+FAC*DOE*0.25*((CN(JS,K)+CN(JB,K))*(R(JS)+
      1R(JB))*W(3,JS,K+1))/(W(1,JB,K)*R(JB)*DX*DX)
      2+.5*FAC*TX*W(3,JS,K+1)*W(2,JB,K)/W(1,JB,K)
       AA(JPP-1,4)=AA(JPP-1,4)+0.5*FAC*TX*(FK-1.)*W(3,JD,K)
       F(2,JE,K)=F(2,JE,K)-0.5*(FK-1.)*W(1,JD,K)*FAC*TX*W(3,JD,K+1)
       F(3,JE,K)=F(3,JE,K)+FAC*DOE*0.25*((CN(JD,K)+CN(JE,K))*(R(JD)+
      1R(JE))*W(3,JD,K+1))/(W(1,JE,K)*R(JE)*DX*DX)
      2-.5*FAC*TX*W(3,JD,K+1)*W(2,JE,K)/W(1,JE,K)

C.....SOLVE THE MATRIX EQUATIONS FOR THE W-VECTOR.
       CALL CRO(K,TX,DT,DX,FK,JB,JE,JP,UN,SGO,CNO,W,F)
       RETURN
       END




C.....THIS SUBROUTINE ALLOWS US TO SOLVE FOR THE W-VECTOR, I.E, DENSITY,
C.....RADIAL VELOCITY AND TEMPERATURE.


       SUBROUTINE CRO(K,TX,DT,DX,FK,JB,JE,JP,UN,SGO,CNO,W,F)
       DIMENSION W(3,51,2),SG(51,2),CN(51,2),R(51),AA(150,09),BB(3,3)
      1,F(3,51,2),BZ(51,2),BC(51,2),CZ(51,2),CC(51,2),GA(51),GB(51)
      2,GC(51),GD(51)
       COMMON SG,R,AA,CN,BB,COE,DOE,BZ,BC,CZ,CC,GA,GB,GC,GD
       JPP=3*JP
       TMALL=0.10E-29
       DO 101 L=5,09
  101 AA(1,L)=AA(1,L)/AA(1,4)
       F(1,2,K)=F(1,2,K)/AA(1,4)
       DO 102 J=2,3
  102 AA(J,5)=AA(J,5)-AA(J,4)*AA(1,5)
       DO 112 J=4,06
  112 AA(J,2)=AA(J,2)-AA(J,1)*AA(1,5)
       DO 122 L=6,09
  122 AA(2,L)=(AA(2,L)-AA(2,4)*AA(1,L))/AA(2,5)
       F(2,2,K)=(F(2,2,K)-AA(2,4)*F(1,2,K))/AA(2,5)
       DO 103 J=3,3
  103 AA(J,6)=AA(J,6)-AA(J,4)*AA(1,6)-AA(J,5)*AA(2,6)
       DO 113 J=4,06
  113 AA(J,3)=AA(J,3)-AA(J,1)*AA(1,6)-AA(J,2)*AA(2,6)
       DO 123 L=7,09
```

```
584   123 AA(3,L)=(AA(3,L)-AA(3,4)*AA(1,L)-AA(3,5)*AA(2,L))/AA(3,6)
585       F(3,2,K)=(F(3,2,K)-AA(3,4)*F(1,2,K)-AA(3,5)*F(2,2,K))/AA(3,6)
586       DO 117 J=4,JPP,3
587       DO 188 L=1,3
588       DO 189 LL=1,3
589       BB(L,LL)=0.
590       DO 121 LLL=1,3
591       IF (ABS(AA(J+L-1,LLL)) .LT. TMALL) AA(J+L-1,LLL)=0.
592       IF (ABS(AA(J+LLL-4,06+LL)) .LT. TMALL) AA(J+LLL-4,06+LL)=0.
593   121 BB(L,LL)=BB(L,LL)+AA(J+L-1,LLL)*AA(J+LLL-4,06+LL)
594   189 CONTINUE
595   188 CONTINUE
596       DO 22 L=1,3
597    22 AA(J-1+L,4)=AA(J-1+L,4)-BB(L,1)
598       DO 23 L=1,2
599    23 AA(J,4+L)=(AA(J,4+L)-BB(1,L+1))/AA(J,4)
600       IF (J .EQ. (JPP-2)) GO TO 924
601       DO 24 L=1,3
602    24 AA(J,06+L)=AA(J,06+L)/AA(J,4)
603   924 CONTINUE
604       DO 25 L=1,2
605    25 AA(J+L,5)=AA(J+L,5)-BB(L+1,2)-AA(J+L,4)*AA(J,5)
606       DO 26 L=1,1
607    26 AA(J+1,5+L)=(AA(J+1,5+L)-BB(2,2+L)-AA(J+1,4)*AA(J,5+L))/AA(J+1,5)
608       IF (J .EQ. (JPP-2)) GO TO 127
609       DO 128 L=1,3
610       AA(J+L+2,2)=AA(J+L+2,2)-AA(J+L+2,1)*AA(J,5)
611       AA(J+1,06+L)=(AA(J+1,06+L)-AA(J+1,4)*AA(J,06+L))/AA(J+1,5)
612   128 CONTINUE
613   127 CONTINUE
614       AA(J+2,06)=AA(J+2,06)-BB(3,3)-AA(J+2,4)*AA(J,06)-AA(J+2,5)*
615      1AA(J+1,06)
616         IF (J .EQ. (JPP-2)) GO TO 133
617       DO 134 L=1,3
618       DO 135 LL=1,2
619       AA(J+L+2,3)=AA(J+L+2,3)-AA(J+L+2,LL)*AA(J+LL-1,06)
620       AA(J+2,06+L)=AA(J+2,06+L)-AA(J+2,3+LL)*AA(J+LL-1,06+L)
621   135 CONTINUE
622       AA(J+2,06+L)=AA(J+2,06+L)/AA(J+2,06)
623   134 CONTINUE
624   133 CONTINUE
625       DO 136 L=1,3
626       DO 137 LL=1,3
627   137 F(L,(J+5)/3,K)=F(L,(J+5)/3,K)-AA(J+L-1,LL)*F(LL,(J+5)/3-1,K)
628       LE=L-1
629       IF (L .EQ. 1) GO TO 148
630       DO 147 LL=1,LE
631       F(L,(J+5)/3,K)=F(L,(J+5)/3,K)-AA(J+L-1,3+LL)*F(LL,(J+5)/3,K)
632   147 CONTINUE
633   148 CONTINUE
634       F(L,(J+5)/3,K)=F(L,(J+5)/3,K)/AA(J+L-1,4+L-1)
635   136 CONTINUE
636   117 CONTINUE
```

```
      W(3,JE,K+1)=F(3,JE,K)
      W(2,JE,K+1)=F(2,JE,K)-AA(JPP-1,06)*W(3,JE,K+1)
      W(1,JE,K+1)=F(1,JE,K)-AA(JPP-2,06)*W(3,JE,K+1)
     1-AA(JPP-2,5)*W(2,JE,K+1)
      DO 138 L=4,JPP,3
      JJ=JPP+4-J-3
      DO 139 L=1,3
      BB(1,L)=0.
      DO 941 LL=1,3
  941 BB(1,L)=BB(1,L)+AA(JJ+1-L,06+LL)*W(LL,(JJ+3)/3+1,K+1)
  139 CONTINUE
      W(3,(JJ+3)/3,K+1)=F(3,(JJ+3)/3,K)-BB(1,1)
      W(2,(JJ+3)/3,K+1)=F(2,(JJ+3)/3,K)-BB(1,2)
     1-AA(JJ-1,06)*W(3,(JJ+3)/3,K+1)
      W(1,(JJ+3)/3,K+1)=F(1,(JJ+3)/3,K)-BB(1,3)
     1-AA(JJ-2,06)*W(3,(JJ+3)/3,K+1)-AA(JJ-2,5)*W(2,(JJ+3)/3,K+1)
  138 CONTINUE
      RETURN
      END




C.....CROUT REDUCTION OF A TRI-DIAGONAL MATRIX.  USED TO OBTAIN THE NEW
C.....VALUES OF PSI AND XI.


      SUBROUTINE CROUT (N,K,JB,JE,JP,JD,A,B,C,D,V)
      DIMENSION AA(51,3),E(51),X(51),A(51),B(51),C(51),D(51),V(51,2)
      SMALL=0.10E-32
      JS=1
      DO 22 J=JS,JP
      E(J)=D(J+1)
      AA(J,2)=B(J+1)
      IF (J .EQ. JP) GO TO 24
      AA(J,3)=-A(J+1)
      GO TO 25
   24 E(JP)=D(JP+1)+A(JP+1)*V(JP+2,K+1)
   25 CONTINUE
      IF (J .EQ. JS) GO TO 26
      AA(J,1)=-C(J+1)
      GO TO 27
   26 CONTINUE
      E(JS)=D(JS+1)+C(JS+1)*V(JS,K+1)
   27 CONTINUE
   22 CONTINUE
      AA(JS,3)=AA(JS,3)/AA(JS,2)
      E(JS)=E(JS)/AA(JS,2)
      DO 30 J=JB,JP
      IF (ABS(AA(J,1)) .LE. SMALL) AA(J,1)=0.
      IF (ABS(AA(J-1,3)) .LE. SMALL) AA(J-1,3)=0.
      AA(J,2)=AA(J,2)-AA(J,1)*AA(J-1,3)
```

```
      IF (ABS(E(J-1)) .LE. SMALL) E(J-1)=0.
      E(J)=(E(J)-AA(J,1)*E(J-1))/AA(J,2)
      IF (J .EQ. JP) GO TO 30
      AA(J,3)=AA(J,3)/AA(J,2)
   30 CONTINUE
      X(JP)=E(JP)
      JQ=JP-1
      DO 33 J=JS,JQ
      KK=JQ+JS-J
      IF (ABS(AA(KK,3)) .LE. SMALL) AA(KK,3)=0.
      X(KK)=E(KK)-AA(KK,3)*X(KK+1)
   33 CONTINUE
      DO 28 J=JS,JP
      V(J+1,K+1)=X(J)
      IF (ABS(V(J+1,K+1)) .LT. SMALL) V(J+1,K+1)=0.
   28 CONTINUE
      RETURN
      END



C.....PLOTTING SUBROUTINE


      SUBROUTINE PLOT1(P,SR,JD,M)
      DIMENSION P(6,51),SR(51),PP(51),P1(12),P2(12),P4(12)
      DATA P1/"TEMPERAT","URE","DENSITY"," ","CURRENT ",
     1"DENSITY","POLOIDAL"," FIELD","TOROIDAL"," FIELD","PRESSURE",
     2" "/,P2/"KELVIN"," ","NORMALIZ","ED","STATAMPS","/CM**2",
     3"GAUSS"," ","GAUSS"," ","DYNES/CM","**2"/
      DATA P4/"0.5 USEC","1.0 USEC","1.5 USEC","2.0 USEC","2.5 USEC",
     1"3.0 USEC","3.5 USEC","4.0 USEC","4.5 USEC","5.0 USEC","5.5 USEC",
     2"6.0 USEC"/
 1001 FORMAT(2A8)
      DO 1 I=1,6
      AMAX=0.
      AMIN=0.
      DO 2 J=1,JD
      PP(J)=P(I,J)
      AMAX=AMAX1(PP(J),AMAX)
      AMIN=AMIN1(PP(J),AMIN)
    2 CONTINUE
      CALL MAPS(2.,4.,AMIN,AMAX,.1,1.,.3,1.)
      CALL TRACE(SR,PP,JD)
      CALL SETCH(20.,5.,0,0,3,0)
      CALL CRTBCD("NORMALIZED RADIUS")
      CALL SETCH(2.,20.,0,0,3,1)
      WOT 100,1001,P1(2*I-1),P1(2*I)
      CALL SETCH(2.,1.,0,0,2,0)
      CALL CRTBCD("Z=0;  VESSEL HALF-WIDTH=7.5 CM")
      CALL SETCH(2.,3.,0,0,2,0)
      CALL CRTBCD("UNITS=")
      CALL SETCH(10.,3.,0,0,2,0)
```

```
      WOT 100,1001,P2(2*I-1),P2(2*I)
      CALL SETCH(2.,2.,0,0,2,0)
      CALL CRTBCD("TIME=")
      CALL SETCH(10.,2.,0,0,2,0)
      IF (M .LT. 250) CALL CRTBCD("INITIAL CONDITIONS")
      IF (M .LT. 250) GO TO 3
      WOT 100,1001,P4(M/250)
3     CALL FRAME
1     CONTINUE
      RETURN
      END
```

```
C...PROGRAM NAME:  TWO-DIMENSIONAL MHD CODE (W/ INERTIA)
C...WRITTEN BY:    H.C. LUI
C...MODIFIED BY:   R. IZZO
C...LANGUAGE:      FORTRAN
C...COMPILATION DEVICE:  CDC 7600


C...RESISTIVE MHD EQUATIONS FOR A SINGLE FLUID ARE SOLVED NUMERICALLY
C...IN TWO DIMENSIONS.  ENERGY LOSS DUE TO RADIATION IS INCLUDED.
C...REALISTIC MODELING OF BOUNDARIES IS POSSIBLE IN TWO DIMENSIONS.
C...THE CODE IS USEFUL IN SIMULATING THE PLASMA HEATING PHASE.
C...VARIABLES ARE DEFINED AS THEY ARE ENCOUNTERED.

C************************MAIN PROGRAM*************************


      DIMENSION PSI(21,22,2),B1(21,22,2),B2(21,22,2),XI(21,22,2),
     1C1(21,22,2),C2(21,22,2),C3(21,22,2),T(21,22,2),BIAS(21),
     2W(4,21,22,3),F(4,21,22,3),EI(21,22,2),B3(21,22,2),SR(21),
     4GA(21,22),GB(21,22),GC(21,22),GD(21,22),CN(21,22,2),RO(21,22),
     5AA(100,12),BB(4,4),SZ(22),FF(2,22),P(6,21),CRS(2,21,22),
     6PSI1(21),GRADPR(21,22),GRADPZ(21,22),BXJR(21,22),
     7BXJO(21,22),BXJZ(21,22),PSI2(22),PSI3(22),IX(60),JY(60)

      LCM (T2)
      COMMON/T2/ PSI,B1,B2,B3,XI,C1,C2,C3,T,W,F,SR,PERO,PERS,T01,T02
     1,GA,GB,GC,GD,CN,EI,AA,BB,T03,T04,TS1,TS2,TS3

      CALL DROPFILE(0)
      CALL OPEN(5,"INPUT",0,0)
      CALL CREATE(6,"OUTPUT",3,-1)
      CALL GFSIZE(3,75000)
      CALL KEEP80(1,3)
      CALL FR80ID(8HTORUS-II,1)

C...MS:     STOP AFTER THIS MANY TIME STEPS
C...MW:     WRITE AND PLOT AFTER THIS MANY TIME STEPS
C...FR:     GAS CONSTANT FOR HELIUM (SINGLY OR DOUBLY IONIZED)
C...FK:     RATIO OF SPECIFIC HEATS
C...SMALL:  ROUND-OFF TO ZERO IF A NUMBER IS SMALLER THAN THIS
C...TMALL:            DITTO
C...CV:     SPECIFIC HEAT AT CONSTANT VOLUME
C...C:      SPEED OF LIGHT IN VACUUM
      MS=2501
      MW=250
      FR2=0.6231E+08
      FR1=2./3.*0.6231E+08
      FR=FR2
      FK=1.666666
      SMALL=0.10E-16
      TMALL=SMALL**2
```

```
      CV=FR2/(FK-1.)
      C=2.9980E+10

C...SET TIME (K), RADIAL GRID (I) AND VERTICAL GRID (J) PARAMETERS.
      K=1
      IB=2
      IE=20
      JB=2
      JE=21
      IS=IB-1
      ID=IE+1
      JS=JB-1
      JD=JE+1
      JP=JE-JS
      IP=IE-IS

C...BTOR:    CHARACTERISTC FIELD
C...BMIN:    BIAS TOROIDAL FIELD OUTSIDE PLASMA
C...BMIN1:   BIAS TOROIDAL FIELD WITHIN PLASMA
C...BVI,BVO:Z-COMPONENT OF MAGNETIC FIELD ON INNER AND OUTER WALL
C...RB:      MAJOR RADIUS OF DEVICE
C...RSMA:    COMPUTATIONAL VESSEL HALF-WIDTH
C...HU:      PLASMA CUTOFF DENSITY
C...RORAD:   LOW DENSITY RADIATION TREATMENT
C...DN:      INITIAL FILL DENSITY
C...UN:      CHARACTERISTIC ALFVEN VELOCITY
      BTOR=5000.
      BMIN=-1333./BTOR
      BMIN1=-2500./BTOR
      BVI=-1500./BTOR
      BVO=1500./BTOR

C...COMPUTE NEW F-VECTOR. (J X B TERMS)
      RB=22.5
      RSMA=7.5
      Q=RSMA/RB
      HU=.075
      RORAD=.5
      DN=0.239E-08
      UN=BTOR/SQRT(4.*3.1416*DN)

C...SOME RADIATION PARAMETERS
C...TO,TS:    IMPORTANT TEMPERATURES WHEN MAKING POLYNOMIAL FIT TO
C...          OXYGEN AND SILICON RADIATED POWER LOSS CURVES
C...PERO,PERS: PERCENTAGE OF OXYGEN AND SILICON
      TO1=5.*11600.*CV/UN/UN
      TO2=20.*11600.*CV/UN/UN
      TO3=200.*11600.*CV/UN/UN
      TO4=2000.*11600.*CV/UN/UN
      TS1=20.*11600.*CV/UN/UN
      TS2=200.*11600.*CV/UN/UN
      TS3=2000.*11600.*CV/UN/UN
      PERO=.01
```

```
C...SOME IMPORTANT TIMES DURING HEATING PHASE
C...  DT,DDT:  TIMES STEPS
      TP0=4.00E-06 *UN/RSMA
      TP1=4.70E-06*UN/RSMA
      TP2=1.70E-06 *UN/RSMA
      TP3=18.0E-06*UN/RSMA
      TP4=6.00E-06 *UN/RSMA
      DT=0.20E-08 *UN/RSMA
      DDT=0.1E-10 *UN/RSMA

C...SOME PARAMETERS TO BE USED IN SPECIFICATION OF POLOIDAL FLUX AT
C...THE BOUNDARY.
C...FLUXH,FLUXZ:     POLOIDAL FLUX FUNBCTION AT HORIZONTAL MIDPLANE
C...                 AND INNER WALL AFTER HEATING AND Z-PINCH.
C...FLUXHT,FLUXZT:   POLOIDAL FLUX FUNCTION AT TOP OF VESSEL AND INNER
C...                 WALL AFTER HEATING AND Z-PINCH.
C...BVT:    EXTERNAL VERTICAL FIELD THROUGH HOLE IN TORUS
C...BSLOPE: LINEAR RAMP IN EXTERNAL VERTICAL FIELD THROUGH VESSEL
      FLUXH=1.5E+05/BTOR/RSMA/RSMA
      FLUXZ=.5*FLUXH
      FLUXZT=FLUXZ*.90
      FLUXHT=FLUXH*.90
      BVT=150./BTOR
      BSLOPE=300./BTOR

C...SGO:    BUNEMAN CONDUCTIVITY
C...XJM:    MAXIMUM CURRENT DENSITY
C...CMIN:   MINIMUM CURRENT DENSITY
      M=0
      SGO=8.E+12
      XJM=1.5E+13*4.*3.1416*RSMA/BTOR/C
      CMIN=XJM/166.

C...SET UP GRID.
C...DX:    NORMALIZED RADIAL INCREMENT
C...DY:    NORMALIZED Z-INCREMENT (NORMALIZATION IN BOTH DIRECTIONS
C...       IS 7.5 CM).
      DY=0.1
      DX=0.1
      DO 3 I=IS,ID
      SI=I
      SR(I)=(SI-1.)*DX+15./7.5
      WRITE (6,101) I,SR(I)
    3 CONTINUE
  101 FORMAT(1H ,"I=",I4,"RADIUS=",E14.7)
      DO 991 J=1,JD
      SJ=J
      SZ(J)=(SJ-2.)*DY
  991 CONTINUE

C...SET UP INITIAL CONDITIONS
```

```
C...CCT:    INITIAL TOROIDAL CURRENT DENSITY (PEAK)
C...NVAR:   POLYNOMIAL DEPENDENCE ALONG Z
      CCT=(BVO-BVI)/(SR(16)-SR(5))
      NVAR=8

      DO 5 K=1,2
      DO  5  J=JS,JD
      ZVAR1=(ABS(SZ(J))/SZ(JD))**NVAR
      ZVAR=1.-ZVAR1
      ZVAR2=(ABS(SZ(J))/SZ(11))**NVAR
      ZVAR3=1.-ZVAR2

C...CN:      THERMAL CONDUCTIVITY
C...EI:      TEMPERATURE
C...W(1):    DENSITY
C...W(2):    RADIAL MOMENTUM
C...W(3):    TOROIDAL MOMENTUM
C...W(4):    VERTICAL MOMENTUM
C...XI:      POLOIDAL CURRENT FUNCTION
C...T:       ELECTRICAL CONDUCTIVITY
C...B1:      RADIAL MAGNETIC FIELD
C...B2:      Z-COMPONENT OF MAGNETIC FIELD
C...B3:      TOROIDAL FIELD
C...PSI:     POLOIDAL FLUX FUNCTION
C...C1:      RADIAL CURRENT DENSITY
C...C2:      Z-COMPONENT OF CURRENT DENSITY
C...C3:      TOROIDAL CURRENT DENSITY
      DO  10  I=IS,5
      CN(I,J,K)=.3E+07/(DN*RSMA*UN*CV)
      EI(I,J,K)=10000.*CV/UN/UN
      W(1,I,J,K+1)=0.1
      W(1,I,J,K)=0.1
      XI(I,J,K)=BMIN/Q
      T(I,J,K)=166.
      B1(I,J,K)=0.
      B2(I,J,K)=BVI*ZVAR
      B3(I,J,K)=XI(I,J,K)/SR(I)
      PSI(I,J,K)=ZVAR*(FLUXZ+BVI*(SR(I)**2-SR(IS)**2)/2.)+FLUXZT*ZVAR1
      C1(I,J,K)=0.
      C2(I,J,K)=0.
      C3(I,J,K)=0.
      W(2,I,J,K+1)=0.
      W(3,I,J,K+1)=0.
      W(4,I,J,K+1)=0.
      W(2,I,J,K)=0.
      W(3,I,J,K)=0.
      W(4,I,J,K)=0.
 10   CONTINUE
      DO  11  I=6,16
      CN(I,J,K)=.3E+07/(DN*RSMA*UN*CV)
      EI(I,J,K)=10000.*CV/UN/UN
      IF (J .GT. 11) GO TO 666
      IF (I .LE. 11) W(1,I,J,K+1)=0.1 + 3.8*(SR(I)-SR(5))*ZVAR3
```

```
      IF (I .GT. 11) W(1,I,J,K+1)=W(1,11,J,K+1)-3.8*(SR(I)-SR(11))*ZVAR3
      IF (I .LE. 11) W(1,I,J,K)=0.1 + 3.8*(SR(I)-SR(5))*ZVAR3
      IF (I .GT. 11) W(1,I,J,K)=W(1,11,J,K)-3.8*(SR(I)-SR(11))*ZVAR3
      GO TO 667
666   W(1,I,J,K)=.1
      W(1,I,J,K+1)=.1
667   XI(I,J,K)=(BMIN*ZVAR1 +BMIN1*ZVAR)/Q
      B1(I,J,K)=0.
      B2(I,J,K)=(BVI+CCT*(SR(I)-SR(5)))*ZVAR
      B3(I,J,K)=XI(I,J,K)/SR(I)
      PSI(I,J,K)=PSI(5,J,K)+ZVAR*(BVI*(SR(I)**2-SR(5)**2)/2.
     1+CCT*(SR(I)**3/3.+SR(5)**3/6.-SR(I)**2*SR(5)/2.))
      C1(I,J,K)=0.
      C2(I,J,K)=0.
      C3(I,J,K)=-CCT*ZVAR
      CT=ABS(C3(I,J,K))
      IF (CT .GE. CMIN) T(I,J,K)=XJM/CT
      IF (CT .LT. CMIN) T(I,J,K)=166.
      W(2,I,J,K+1)=0.
      W(3,I,J,K+1)=0.
      W(4,I,J,K+1)=0.
      W(2,I,J,K)=0.
      W(3,I,J,K)=0.
      W(4,I,J,K)=0.
 11   CONTINUE
      DO  12  I=17,ID
      CN(I,J,K)=.3E+07/(DN*RSMA*UN*CV)
      EI(I,J,K)=10000.*CV/UN/UN
      W(1,I,J,K+1)=0.1
      W(1,I,J,K)=0.1
      XI(I,J,K)=BMIN/Q
      T(I,J,K)=166.
      B1(I,J,K)=0.
      B2(I,J,K)=BVO*ZVAR
      B3(I,J,K)=XI(I,J,K)/SR(I)
      PSI(I,J,K)=PSI(16,J,K)+ZVAR*BVO*(SR(I)**2-SR(16)**2)/2.
      C1(I,J,K)=0.
      C2(I,J,K)=0.
      C3(I,J,K)=0.
      W(2,I,J,K+1)=0.
      W(3,I,J,K+1)=0.
      W(4,I,J,K+1)=0.
      W(2,I,J,K)=0.
      W(3,I,J,K)=0.
      W(4,I,J,K)=0.
 12   CONTINUE
  5   CONTINUE
      DO 16 I=IS,ID
      BIAS(I)=XI(I,JD,1)
 16   CONTINUE
      DO 222 J=JS,JD
      FF(1,J)=PSI(IS,J,1)
      FF(2,J)=PSI(ID,J,1)
```

```
222  CONTINUE
     TIME=0.

C...SOME FREQUENTLY USED TERMS.
     BATA=DT/(2.*DX)
     BATB=DT/(2.*DY)
     COE= C*C*DT/(4.*3.1416*RSMA*UN*SGO)

C...BEGIN THE CALCLATION.
   6 M=M+1
     TIME=TIME+DT
     K=1

C...SET UP BOUNDARY VALUES FOR THE POLOIDAL FLUX AND CURRENT
C...FUNCTIONS.
     IF (TIME .GE. TP2) GO TO 7
     DO 8 I=IS,ID
     XI(I,JD,K+1)=BIAS(I) + (1.*TIME/TP2)/Q
   8 CONTINUE
     DO 9 J=JS,JD
     XI(ID,J,K+1)=XI(ID,JD,K+1)
     XI(IS,J,K+1)=XI(IS,JD,K+1)
   9 CONTINUE
   7 CONTINUE
     IF (TIME .GE. TP1) GO TO 17
     DO 14 I=IS,ID
     PSI(I,JD,K+1)=(FLUXHT-FLUXZT)*TIME/TP1 + FLUXZT
     PSI1(I)=PSI(I,JD,K+1)
  14 CONTINUE
     DO 15 J=JS,JD
     ZVAR1=(ABS(SZ(J))/SZ(JD))**NVAR
     ZVAR=1. - ZVAR1
     PSI(IS,J,K+1)=FF(1,J)+(FLUXH*ZVAR+FLUXHT*ZVAR1-FF(1,J))*TIME/TP1
     PSI(ID,J,K+1)=FF(2,J)+(ZVAR*(FLUXH+BVT*(SR(ID)**2-SR(IS)**2)
    1+BSLOPE*(SR(ID)**3/3.+SR(IS)**3/6.-SR(IS)*SR(ID)**2/2.))
    2+FLUXHT*ZVAR1-FF(2,J))*TIME/TP1
     PSI2(J)=PSI(IS,J,K+1)
     PSI3(J)=PSI(ID,J,K+1)
  15 CONTINUE
     GO TO 19
  17 CONTINUE
     DO 18 I=IS,ID
     PSI(I,JD,K+1)=PSI1(I)
  18 CONTINUE
     DO 350 J=JS,JD
     PSI(IS,J,K+1)=PSI2(J)
     PSI(ID,J,K+1)=PSI3(J)
 350 CONTINUE
  19 CONTINUE
  13 CONTINUE

C...PRESCRIBE DENSITY AND VELOCITY AT BOUNDARY.
     DO 28 J=JS,JD
```

```
      DO 29 L=1,4
      W(L,ID,J,K)= W(L,IE,J,K)
      W(L,IS,J,K)= W(L,IB,J,K)
   29 CONTINUE
      W(2,ID,J,K)=0.
      W(2,IS,J,K)=0.
   28 CONTINUE
      DO 53 I=IS,ID
      DO 54 L=1,4
      W(L,I,JD,K)= W(L,I,JE,K)
      W(L,I,JS,K)= W(L,I,JB+1,K)
   54 CONTINUE
      W(3,I,JD,K)=0.
      W(3,I,JS,K)=-W(3,I,JB+1,K)
      W(4,I,JS,K)=-W(4,I,JB+1,K)
   53 CONTINUE

      K=1
      K2=1
      K3=1
      K4=1
      K5=1

C...OBTAIN PREDICTOR VALUES FOR W-VECTOR USING AN EXPLICIT LAX-
C...FRIEDRICHS SCHEME.
      DO 433 J=JB,JE
      DO 434 I=IB,IE
      F(1,I,J,K)=0.
      W(1,I,J,K+1)=0.25*(W(1,I+1,J,K)+W(1,I-1,J,K)+W(1,I,J+1,K)+
     1W(1,I,J-1,K))-0.50*DT/DX/SR(I)*(SR(I+1)*W(2,I+1,J,K)-
     2SR(I-1)*W(2,I-1,J,K))-0.50*DT/DY*(W(3,I,J+1,K)-W(3,I,J-1,K))
     3+2.*F(1,I,J,K)
      F(2,I,J,K)=(W(4,I,J,K)**2/(W(1,I,J,K)*SR(I))+(FK-1.)*W(1,I,J,K)*
     1EI(I,J,K)/SR(I)+(C3(I,J,K)*B2(I,J,K)-C2(I,J,K)*B3(I,J,K)))*DT/2.
      W(2,I,J,K+1)=0.25*(W(2,I+1,J,K)+W(2,I-1,J,K)+W(2,I,J+1,K)+
     1W(2,I,J-1,K))-0.50*DT/DX/SR(I)*(SR(I+1)*(W(2,I+1,J,K)**2
     2/W(1,I+1,J,K)+(FK-1.)*W(1,I+1,J,K)*EI(I+1,J,K))-
     3SR(I-1)*(W(2,I-1,J,K)**2/W(1,I-1,J,K) +(FK-1.)*W(1,I-1,J,K)
     4*EI(I-1,J,K)))-0.50*DT/DY*(W(2,I,J+1,K)*W(3,I,J+1,K)
     5/W(1,I,J+1,K)-W(2,I,J-1,K)*W(3,I,J-1,K)/W(1,I,J-1,K))
     6+2.*F(2,I,J,K)
      F(3,I,J,K)=((C1(I,J,K)*B3(I,J,K)-C3(I,J,K)*B1(I,J,K)))*DT/2.
      W(3,I,J,K+1)=0.25*(W(3,I+1,J,K)+W(3,I-1,J,K)+W(3,I,J+1,K)+
     1W(3,I,J-1,K))-0.50*DT/DX/SR(I)*(SR(I+1)*W(2,I+1,J,K)*
     2W(3,I+1,J,K)/W(1,I+1,J,K)-SR(I-1)*W(2,I-1,J,K)*W(3,I-1,J,K)
     3/W(1,I-1,J,K))-0.50*DT/DY*((W(3,I,J+1,K)**2/W(1,I,J+1,K)+
     4(FK-1.)*W(1,I,J+1,K)*EI(I,J+1,K))-(W(3,I,J-1,K)**2/
     5W(1,I,J-1,K)+(FK-1.)*W(1,I,J-1,K)*EI(I,J-1,K)))
     6+2.*F(3,I,J,K)
      F(4,I,J,K)=((C2(I,J,K)*B1(I,J,K)-C1(I,J,K)*B2(I,J,K))
     1-W(2,I,J,K)*W(4,I,J,K)/(W(1,I,J,K)*SR(I)))*DT/2.
      W(4,I,J,K+1)=0.25*(W(4,I+1,J,K)+W(4,I-1,J,K)+W(4,I,J+1,K)+
     1W(4,I,J-1,K))-0.50*DT/DX/SR(I)*(SR(I+1)*W(2,I+1,J,K)
```

```
      2*W(4,I+1,J,K)/W(1,I+1,J,K)-SR(I-1)*W(2,I-1,J,K)*W(4,I-1,J,K)
      3/W(1,I-1,J,K))-0.50*DT/DY*(W(3,I,J+1,K)*W(4,I,J+1,K)
     4/W(1,I,J+1,K)-W(3,I,J-1,K)*W(4,I,J-1,K)/W(1,I,J-1,K))
     5+2.*F(4,I,J,K)
      DO 435 L=1,4
      IF (ABS(W(L,I,J,K+1)) .LT. SMALL) W(L,I,J,K+1)=0.
  435 CONTINUE
  434 CONTINUE
  433 CONTINUE
      DO 208 J=JS,JD
      DO 209 L=1,4
      W(L,ID,J,K+1)= W(L,IE,J,K+1)
      W(L,IS,J,K+1)= W(L,IB,J,K+1)
  209 CONTINUE
      W(2,ID,J,K+1)=0.
      W(2,IS,J,K+1)=0.
  208 CONTINUE
      DO 300 I=IS,ID
      DO 301 L=1,4
      W(L,I,JD,K+1)= W(L,I,JE,K+1)
      W(L,I,JS,K+1)= W(L,I,JB+1,K+1)
  301 CONTINUE
      W(3,I,JD,K+1)=0.
      W(3,I,JS,K+1)=-W(3,I,JB+1,K+1)
      W(4,I,JS,K+1)=-W(4,I,JB+1,K+1)
  300 CONTINUE

C...USING THE PREDICTOR VALUES OBTAINED ABOVE IN THE NON-LINEAR
C...TERMS, WE SOLVE THE FIELD AND ENERGY EQUATIONS USING AN ADI SCHEME.
      CALL       ADI(K,M,DT,DX,DY,CV,FK,COE,DOE,UN,BATA,BATB,SGO,
     1IS,IB,IE,ID,JS,JB,JE,JD,C,IP,JP,DN,RSMA,HU,RORAD)

C...FOR THE NEW TEMPERATURES AND FIELDS, WE NOW:
C...TEST FOR NEGATIVE TEMPERATURES.
C...TEST FOR LOW DENSITY REGION.
C...SPECIFY THE ELECTRICAL CONDUCTIVITY TO BE USED DEPENDING UPON
C...POSITION AND TIME, I.E, LOW DENSITY VS. HIGH DENSITY REGION
C...AND TURBULENT PHASE VS. CLASSICAL PHASE.
  118 FORMAT (1HO,3I12)
      DO 86 J=JB,JE
      DO 86 I=IB,IE
      IF (EI( I,J,K+1) .LT. 0.) WRITE (6,118) I,J,M
      IF (EI(I,J,K+1) .LT. 0.) GO TO 94
      RO(I,J)=0.2*(W(1,I,J,K+1)+W(1,I+1,J,K+1)+W(1,I-1,J,K+1)+
     1W(1,I,J+1,K+1)+W(1,I,J-1,K+1))
      IF (TIME .GT. TPO) GO TO 60
      CT=SQRT(C1(I,J,K+1)**2+C2(I,J,K+1)**2+C3(I,J,K+1)**2)
      IF (CT .GE. CMIN) T(I,J,K-1)=XJM/CT
      IF (CT .LT. CMIN) T(I,J,K-1)=166.
      GO TO 61
   60 T(I,J,K+1)=1.05E+6*(UN*UN/CV*EI(I,J,K+1))**1.5/SGO
      IF (TIME .GT. TP4) GO TO 61
      SGR=((TIME - TPO)/(TP4 - TPO))**10
```

```
425        CT=SQRT(C1(I,J,K+1)**2+C2(I,J,K+1)**2+C3(I,J,K+1)**2)
426        IF (CT .GE. CMIN) SGA=XJM/CT
427        IF (CT .LT. CMIN) SGA=166.
428        T(I,J,K+1)=SGR*T(I,J,K+1) + (1.-SGR)*SGA
429  61    IF (RO(I,J) .LT. 0.25) T(I,J,K-1)=1.
430        IF (J .GT. 17) T(I,J,K+1)=1.
431        IF ((I .LE. 6) .OR. (I .GE. 17)) T(I,J,K+1)=1.
432     86 CONTINUE
433        DO 87 I=IB,IE
434        T(I,JS,K+1)=T(I,JB+1,K+1)
435        T(I,JD,K+1)=T(I,JE,K+1)
436     87 CONTINUE
437        DO 84 J=JS,JD
438        T(IS,J,K+1)=T(IB,J,K+1)
439        T(ID,J,K+1)=T(IE,J,K+1)
440  84    CONTINUE
441        K2=2
442
443 C...USING THE NEWLY OBTAINED FIELD QUANTITIES, COMPUTE THE NEW F-
444 C...VECTOR (J X B TERMS).
445 C...IF M IS EVEN, WE WILL SOLVE THE CONTINUITY AND MOMENTUM
446 C...EQUATIONS IMPLICIT IN R.  IF M IS ODD,
447 C...WE WILL SOLVE THESE SAME EQUATIONS IMPLICIT IN Z.
448        DO 33 J=JB,JE
449        DO 34 I=IB,IE
450        F(1,I,J,K2)=0.
451        F(2,I,J,K2)=(W(4,I,J,K2)**2/W(1,I,J,K2)/SR(I)+(FK-1.)*W(1,I,J,K2)
452       1*EI(I,J,K2)/SR(I)+(C3(I,J,K2)*B2(I,J,K2)-C2(I,J,K2)*B3(I,J,K2)))*
453       2DT/2.
454        F(3,I,J,K2)=((C1(I,J,K2)*B3(I,J,K2)-C3(I,J,K2)*B1(I,J,K2)))*DT/2.
455        F(4,I,J,K2)=((C2(I,J,K2)*B1(I,J,K2)-C1(I,J,K2)*B2(I,J,K2))
456       1-W(2,I,J,K2)*W(4,I,J,K2)/(W(1,I,J,K2)*SR(I)))*DT/2.
457     34 CONTINUE
458     33 CONTINUE
459        IF (MOD(M,2) .EQ. 1) GO TO 55
460        GO TO 52
461   55   CALL        YIMCRO(K,M,DT,DX,DY,CV,FK,COE,DOE,UN,BATA,BATB,SGO,
462       1IS,IB,IE,ID,JS,JB,JE,JD,C,IP,JP,TMALL)
463        GO TO 253
464  52    CALL        XIMCRO(K,M,DT,DX,DY,CV,FK,COE,DOE,UN,BATA,BATB,SGO,
465       1IS,IB,IE,ID,JS,JB,JE,JD,C,IP,JP,TMALL)
466   253  CONTINUE
467
468 C...OUTPUT THE RESULTS.
469        IF (MOD(M,MW) .EQ. 1) GO TO 89
470        GO TO 91
471    89  CONTINUE
472        SIME=TIME*RSMA/UN
473        WRITE (6,104) M,SIME,DT,UN,COE
474   104  FORMAT(1H1,"CYCLE=",I4,"TIME=",E14.7,"DT=",E14.7,
475       1"UN=",E14.7,E16.7)
476        WRITE (6,105)
477   105  FORMAT (1HO,2X,"I",2X,"J",2X,"POLOID FLUX", 4X,"TOROID FLUX",4X,
```

```
478       1"RADIAL MAGNET",3X,"Z-- MAGNET",4X,"TOROID MAGNET",2X,
479       2"RADIAL CURRENT",2X,"Z-- CURRENT",3X,"TOROID CURRENT")
480        DO 92 I=IS,ID
481        DO 92 J=JS,JD
482        XI (I,J,K)=XI (I,J,K+1)*BTOR *RSMA
483        PSI(I,J,K)=PSI(I,J,K+1)*BTOR*RSMA**2
484        B1 (I,J,K)=B1 (I,J,K+1)*BTOR
485        B2 (I,J,K)=B2 (I,J,K+1)*BTOR
486        B3 (I,J,K)=B3 (I,J,K+1)*BTOR
487        C1 (I,J,K)=C1 (I,J,K+1)*C*BTOR/(4.*3.1416*RSMA)
488        C2 (I,J,K)=C2 (I,J,K+1)*C*BTOR/(4.*3.1416*RSMA)
489        C3 (I,J,K)=C3 (I,J,K+1)*C*BTOR/(4.*3.1416*RSMA)
490        WRITE (6,106) I,J,PSI(I,J,K  ),XI(I,J,K  ),B1(I,J,K  ),
491       1B2(I,J,K  ),B3(I,J,K  ),C1(I,J,K  ),C2(I,J,K  ),C3(I,J,K  )
492     92 CONTINUE
493    106 FORMAT (1H ,2I3,8E15.7)
494        WRITE (6,107)
495    107 FORMAT (1HO,2X,"I",2X,"J",2X,"DENSITY",9X,"RADIAL VELOCITY",1X,
496       1"Z-- VELOCITY",3X,"TOROID VELOCITY",1X,"INTERNAL ENERGY",1X,
497       2"CONDUCTIVITY",4X,"TEMPERATURE")
498        DO 1 J=JS,JD
499        W(1,ID,J,K+2)=W(1,IE,J,K+2)
500        W(1,IS,J,K+2)=W(1,IB,J,K+2)
501    1   CONTINUE
502        DO 2 I=IS,ID
503        W(1,I,JD,K+2)=W(1,I,JE,K+2)
504        W(1,I,JS,K+2)=W(1,I,JB+1,K+2)
505    2   CONTINUE
506        DO 93 I=IB,IE
507        DO 93 J=JB,JE
508        F(2,I,J,K+1)=W(2,I,J,K+2)/W(1,I,J,K+2)*UN
509        F(3,I,J,K+1)=W(3,I,J,K+2)/W(1,I,J,K+2)*UN
510        F(4,I,J,K+1)=W(4,I,J,K+2)/W(1,I,J,K+2)*UN
511        F(1,I,J,K+1)=EI(I,J,K+1)/CV*UN*UN
512        T  (I,J,K)=T  (I,J,K+1)*SGO
513        WRITE (6,108) I,J,W(1,I,J,K+2),F(2,I,J,K+1),F(3,I,J,K+1),
514       1F(4,I,J,K+1),EI( I,J,K+1),T(I,J,K  ),F(1,I,J,K+1)
515     93 CONTINUE
516    108 FORMAT (1H ,2I3,8E16.7)
517        DO 40 J=JB,JE
518        DO 40 I=IB,IE
519        IF (RO(I,J) .GT. 0.25) GO TO 40
520        PSI(I,J,K)=.2*(PSI(I,J,K)+PSI(I+1,J,K)+PSI(I-1,J,K)
521       1+PSI(I,J+1,K)+PSI(I,J-1,K))
522        XI(I,J,K)=.2*(XI(I,J,K)+XI(I+1,J,K)+XI(I-1,J,K)+XI(I,J+1,K)
523       1+XI(I,J-1,K))
524    40  CONTINUE
525
526 C...SET UP VALUES FOR PLOTTING.
527        DO 70 I=IS,ID
528        P(1,I)=F(1,I,JB,K+1)
529        P(2,I)=W(1,I,JB,K+2)
530        P(5,I)=XI(I,JB,K)/SR(I)/RSMA
```

```
      P(6,I)=P(1,I)*P(2,I)*FR*DN
 70   CONTINUE
      DO 77 I=IB,IE
 77   P(4,I)=(PSI(I+1,JB,K)-PSI(I-1,JB,K))/SR(I)/2./DX/RSMA**2
      P(4,IS)=(PSI(IB,JB,K)-PSI(IS,JB,K))/SR(IS)/DX/RSMA**2
      P(4,ID)=(PSI(ID,JB,K)-PSI(IE,JB,K))/SR(ID)/DX/RSMA**2
      DO 78 I=IB,IE
      P(3,I)=((B1(I,JB+1,K)-B1(I,JS,K))/2./DY/RSMA -
     1(P(4,I+1)-P(4,I-1))/2./DX/RSMA)*C/4./3.1416
 78   CONTINUE
      P(3,IS)=((B1(IS,JB+1,K)-B1(IS,JS,K))/2./DY -
     1(P(4,IB)-P(4,IS))/DX)*C/4./3.1416/RSMA
      P(3,ID)=((B1(ID,JB+1,K)-B1(ID,JS,K))/2./DY -
     1(P(4,ID)-P(4,IE))/DX)*C/4./3.1416/RSMA
      DO 71 I=1,ID
      DO 71 J=1,JD
      CRS(1,I,J)=PSI(I,J,K)
      CRS(2,I,J)=C3(I,J,K)
 71   CONTINUE
      CALL PLOT1(P,CRS,SR,ID,JD,M,RO)

   91 CONTINUE
      IF (M .GT. MS) GO TO 94

C...TAKE ALL NEW VALUES AND STORE THEM AS OLD VALUES.
      DO 96 I=IS,ID
      DO 96 J=JS,JD
      T  (I,J,K)=T  (I,J,K+1)
      EI(I,J,K) = EI(I,J,K+1)
      PSI(I,J,K)=PSI(I,J,K+1)
      B3(I,J,K)= B3(I,J,K+1)
      B1 (I,J,K)=B1 (I,J,K+1)
      B2 (I,J,K)=B2 (I,J,K+1)
      XI (I,J,K)=XI (I,J,K+1)
      C1 (I,J,K)=C1 (I,J,K+1)
      C2 (I,J,K)=C2 (I,J,K+1)
      C3 (I,J,K)=C3 (I,J,K+1)
      DO 97 L=1,4
      W(L,I,J,K)= W(L,I,J,K+2)
      IF (ABS(W(L,I,J,K)) .LT. SMALL) W(L,I,J,K)=0.
   97 CONTINUE
      IF (W(1,I,J,K) .LT. HU) W(1,I,J,K)=HU
   96 CONTINUE

      GO TO 6
   94 CONTINUE

C...COMPUTE J X B VS. GRAD P IN ALL DIRECTIONS.
      WRITE (6,111)
      DO 600 I=IB,IE
      DO 600 J=JB,JE
      GRADPR(I,J)=FR*DN*UN*UN/CV*(EI(I+1,J,K+1)*W(1,I+1,J,K+2) -
     1EI(I-1,J,K+1)*W(1,I-1,J,K+2))/2./DX/RSMA
```

```
      600  CONTINUE
      110  FORMAT (1H,213,5E16.7)
      111  FORMAT (1HO,2X,"I",2X,"J",2X,"GRAD P (RADIAL)",1X,
     1"J X B (RADIAL)",2X,"J X B(TOROIDAL)",1X,"GRAD P (Z)",6X,
     2"J X B (Z)")

C...COMPUTE THE FINAL TOROIDAL PLASMA CURRENT.
      CPLASMA=0.
      DO 601 J=JB,JE
      DO 601 I=IB,IE
      IF (RO(I,J) .LT. .25) GO TO 601
      CPLASMA=CPLASMA + C3(I,J,K+1)*C*BTOR/4./3.1416/RSMA*DX*DY*
     1RSMA**2
  601 CONTINUE
      CPLASMA=CPLASMA*2.*.333E-9
      WRITE (6,602) CPLASMA
  602 FORMAT ("THE TOROIDAL PLASMA CURRENT IS (AMPS)  ",E14.7)
      WRITE (6,109) DT,M,I,J
  109 FORMAT(1H ," TORUS II IMPLOSION",4X,"DT=",E14.7," CYCLE= "
     1,I5,1X,2I3)

C...COMPUTE THE VALUES FOR SAFETY FACTOR AS A FUNCTION OF POLOIDAL
C...FLUX.  PRINT OUT Q(R) ALONG THE HORIZONTAL MIDPLANE.
      IEND=IE/2
      I1=0
      DO 700 I=IB,IEND
      IF ((W(I,I-1,JB,K+2) .LE. 0.4) .AND.
     1    (W(I,I,JB,K+2) .GE. 0.4)) I1=I
  700 CONTINUE
      IF (I1 .EQ. 0) GO TO 701
      I1P4=I1+4
      DO 709 I2=I1,I1P4
      MM=1
      IX(MM)=I2
      JY(MM)=JB
      FLUXIJ=PSI(I2,JB,K+1)
      D1=1.0E+20
      I2M1=I2-1
      I2P1=I2+1
      JBP1=JB+1
      QPSI=0.
      DO 702 L=I2M1,I2P1
      DO 702 N=JB,JBP1
```

```
      IF ((N .EQ. JY(MM)) .AND. (L .EQ. IX(MM))) GO TO 702
      D=ABS(FLUXIJ-PSI(L,N,K+1))
      IF (D .GT. D1) GO TO 702
      LL=L
      NN=N
      D1=D
  702 CONTINUE
  704 MM=MM+1
      IX(MM)=LL
      JY(MM)=NN
      DL=SQRT((DX*(IX(MM)-IX(MM-1)))**2+(DY*(JY(MM)-JY(MM-1)))**2)
      R2=((SR(IX(MM))+SR(IX(MM-1)))/2.)**2
      B11=(B1(IX(MM),JY(MM),K+1)+B1(IX(MM-1),JY(MM-1),K+1))/2.
      B22=(B2(IX(MM),JY(MM),K+1)+B2(IX(MM-1),JY(MM-1),K+1))/2.
      BPOL=SQRT(B11**2 + B22**2)
      XII=ABS(XI(IX(MM),JY(MM),K+1)+XI(IX(MM-1),JY(MM-1),K+1))/2.
      QPSI=QPSI+XII*DL/BPOL/R2/3.1416
      WRITE (6,711) IX(MM),JY(MM),QPSI
      IF (JY(MM) .EQ. JB) GO TO 705
      LM1=IX(MM)
      LP1=IX(MM)+1
      JM1=JY(MM)-1
      JP1=JY(MM)+1
      D1=1.0E+20
      DO 703 L=LM1,LP1
      DO 703 N=JM1,JP1
      DO 715 M3=1,MM
      IF ((L .EQ. IX(M3)) .AND. (N .EQ. JY(M3))) GO TO 703
  715 CONTINUE
      D=ABS(FLUXIJ - PSI(L,N,K+1))
      IF (D .GT. D1) GO TO 703
      LL=L
      NN=N
      D1=D
  703 CONTINUE
      GO TO 704
  705 WRITE (6,706) MM,SR(I2),SR(IX(MM)),QPSI
  706 FORMAT (1H,I4,4X,3(E12.5,4X))
  709 CONTINUE
      GO TO 707
  701 WRITE (6,708)
  708 FORMAT (1H,"COULD NOT FIND HIGH DENSITY REGION")
  711 FORMAT(1H,2I4,E12.5)

  707 CALL PLOTE
      CALL EXIT(2)
      END



C...THIS SUBROUTINE SOLVES THE FIELD AND ENERGY EQUATIONS USING
```

```
690 C...AN ADI SCHEME AS OUTLINED IN DISSERTATION.
691 C...IF M IS EVEN, THE EQUATIONS ARE WRITTEN IMPLICIT IN R.
692 C...IF M IS ODD, THE EQUATIONS ARE WRITTEN IMPLICIT IN Z.
693
694
695
696
697       SUBROUTINE ADI(K,M,DT,DX,DY,CV,FK,COE,DOE,UN,BATA,BATB,SGO,
698      1IS,IB,IE,ID,JS,JB,JE,JD,C,IP,JP,DN,RSMA,HU,RORAD)
699
700       DIMENSION PSI(21,22,2),B1(21,22,2),B2(21,22,2),XI(21,22,2),
701      1C1(21,22,2),C2(21,22,2),C3(21,22,2),T(21,22,2),
702      2W(4,21,22,3),F(4,21,22,3),EI(21,22,2),B3(21,22,2),SR(21),
703      4GA(21,22),GB(21,22),GC(21,22),GD(21,22),CN(21,22,2),
704      5AA(100,12),BB(4,4),PR(21,22),PAS(6,21,22),PAO(6,21,22)
705       LCM (T2)
706       COMMON/T2/ PSI,B1,B2,B3,XI,C1,C2,C3,T,W,F,SR,PERO,PERS,TO1,TO2
707      1,GA,GB,GC,GD,CN,EI,AA,BB,TO3,TO4,TS1,TS2,TS3
708
709       K=1
710       IF (MOD(M,2) .EQ. 1) GO TO 11
711       GO TO 12
712
713 C...PSI EQUATION IMPLICIT IN Z.
714    11 CONTINUE
715       DO 14 J=JB,JE
716       DO 13 I=IB,IE
717       GC(I,J)=COE/(T(I,J,K+1)*DY*DY)
718      1+DT*W(3,I,J,K+1)/W(1,I,J,K+1)/(2.*DY)
719       GA(I,J)=COE/(T(I,J,K+1)*DY*DY)
720      1-DT*W(3,I,J,K+1)/W(1,I,J,K+1)/(2.*DY)
721       GB(I,J)=1.+2.*COE/(T(I,J,K+1)*DY*DY)
722       GD(I,J)=PSI(I,J,K)+COE*SR(I)/(T(I,J,K)*DX*DX)
723      1*((PSI(I+1,J,K)-PSI(I,J,K))/((SR(I+1)+SR(I))/2.)
724      2-(PSI(I,J,K)-PSI(I-1,J,K))/((SR(I-1)+SR(I))/2.))
725      4-DT*W(2,I,J,K)/W(1,I,J,K)*(PSI(I+1,J,K)-PSI(I-1,J,K))/(2.*DX)
726    13 CONTINUE
727    14 CONTINUE
728
729 C...REDUCE THE RESULTING TRI-DIAGONAL MATRIX USING A CROUT METHOD.
730       CALL        CROUT(M,K,IB,IE,JB,JE,IP,JP,GA,GB,GC,GD,PSI,JD,ID)
731       GO TO 17
732
733 C...PSI EQUATION IMPLICIT IN R.
734    12 CONTINUE
735       DO 19 J=JB,JE
736       DO 18 I=IB,IE
737       GC(I,J)=COE*SR(I)
738      1/(T(I,J,K+1)*DX*DX*(SR(I-1)+SR(I))/2.)
739      2+DT*W(2,I,J,K+1)/W(1,I,J,K+1)/(2.*DX)
740       GA(I,J)=COE*SR(I)
741      1/(T(I,J,K+1)*DX*DX*(SR(I+1)+SR(I))/2.)
742      2-DT*W(2,I,J,K+1)/W(1,I,J,K+1)/(2.*DX)
```

```
743         GB(I,J)=1.+COE/(T(I,J,K+1)*DX*DX)
744        1*SR(I)*(2./(SR(I+1)+SR(I))+2./(SR(I-1)+SR(I)))
745         GD(I,J)=PSI(I,J,K)+COE/(T(I,J,K)*DY*DY)
746        1*((PSI(I,J+1,K)-PSI(I,J,K))
747        2-(PSI(I,J,K)-PSI(I,J-1,K))
748        3)-DT*W(3,I,J,K)/W(1,I,J,K)/(2.*DY)*(PSI(I,J+1,K)-
749        4PSI(I,J-1,K))
750     18 CONTINUE
751     19 CONTINUE
752
753 C...REDUCE THE RESULTING TRI-DIAGONAL MATRIX USING A CROUT METHOD.
754         CALL        CROUT(M,K,IB,IE,JB,JE,IP,JP,GA,GB,GC,GD,PSI,JD,ID)
755
756 C...COMPUTE THE NEW RADIAL AND Z-COMPONENTS OF MAGNETIC FIELD.
757     17 CONTINUE
758        DO 25 I=IS,ID
759        PSI(I,JB-1,K+1)=PSI(I,JB+1,K+1)
760     25 CONTINUE
761        DO 32 J=JB,JE
762        DO 31 I=IB,IE
763        B1(I,J,K+1)=-(PSI(I,J+1,K+1)-PSI(I,J-1,K+1))/(2.*SR(I)*DY)
764        B2(I,J,K+1)= (PSI(I+1,J,K+1)-PSI(I-1,J,K+1))/(2.*SR(I)*DX)
765     31 CONTINUE
766     32 CONTINUE
767        DO 3 J=JS,JD
768        B2(ID,J,K+1)=(PSI(ID,J,K+1)-PSI(IE,J,K+1))/SR(ID)/DX
769        B2(IS,J,K+1)=(PSI(IB,J,K+1)-PSI(IS,J,K+1))/SR(IS)/DX
770   3    CONTINUE
771        DO 4 I=IS,ID
772        B1(I,JS,K+1)=-(PSI(I,JB,K+1)-PSI(I,JS,K+1))/SR(I)/DY
773        B1(I,JD,K+1)=-(PSI(I,JD,K+1)-PSI(I,JE,K+1))/SR(I)/DY
774   4    CONTINUE
775        DO 5 I=IB,IE
776        B1(I,JS,K+1)=-(PSI(I,JS+1,K+1)-PSI(I,JS,K+1))/(SR(I)*DY)
777        B1(I,JD,K+1)=-(PSI(I,JD,K+1)-PSI(I,JD-1,K+1))/(SR(I)*DY)
778   5    CONTINUE
779        DO 6 J=JB,JE
780        B2(IS,J,K+1)=(PSI(IB,J,K+1)-PSI(IS,J,K+1))/SR(IS)/DX
781        B2(ID,J,K+1)=(PSI(ID,J,K+1)-PSI(IE,J,K+1))/SR(ID)/DX
782   6    CONTINUE
783
784 C...COMPUTE THE NEW TOROIDAL CURRENT DENSITY.
785        DO 8 J=JB,JE
786        DO 7 I=IB,IE
787        C3(I,J,K+1)=(B1(I,J+1,K+1)-B1(I,J-1,K+1))/2./DY -
788       1(B2(I+1,J,K+1)-B2(I-1,J,K+1))/2./DX
789   7    CONTINUE
790        C3(IS,J,K+1)=(B1(IS,J+1,K+1)-B1(IS,J-1,K+1))/2./DY -
791       1(B2(IB,J,K+1)-B2(IS,J,K+1))/DX
792        C3(ID,J,K+1)=(B1(ID,J+1,K+1)-B1(ID,J-1,K+1))/2./DY
793       1-(B2(ID,J,K+1)-B2(IE,J,K+1))/DX
794   8    CONTINUE
795        DO 9 I=IB,IE
```

```
796         C3(I,JS,K+1)=(B1(I,JB,K+1)-B1(I,JS,K+1))/DY -
797        1(B2(I+1,JS,K+1)-B2(I-1,JS,K+1))/2./DX
798         C3(I,JD,K+1)=(B1(I,JD,K+1)-B1(I,JE,K+1))/DY -
799        1(B2(I+1,JD,K+1)-B2(I-1,JD,K+1))/2./DX
800    9    CONTINUE
801         C3(IS,JS,K+1)=(B1(IS,JB,K+1)-B1(IS,JS,K+1))/DY -
802        1(B2(IB,JS,K+1)-B2(IS,JS,K+1))/DX
803         C3(ID,JS,K+1)=(B1(ID,JB,K+1)-B1(ID,JS,K+1))/DY -
804        1(B2(ID,JS,K+1)-B2(IE,JS,K+1))/DX
805         C3(IS,JD,K+1)=(B1(IS,JD,K+1)-B1(IS,JE,K+1))/DY -
806        1(B2(IB,JD,K+1)-B2(IS,JD,K+1))/DX
807         C3(ID,JD,K+1)=(B1(IS,JD,K+1)-B1(IS,JE,K+1))/DY -
808        1(B2(ID,JD,K+1)-B2(IE,JD,K+1))/DX
809
810         IF (MOD(M,2) .EQ. 1) GO TO 311
811         GO TO 312
812
813 C...XI EQUATION IMPLICIT IN Z.
814     311 CONTINUE
815         DO 16 J=JB,JE
816         DO 15 I=IB,IE
817         HON=0.5
818         IF (W(1,I,J,K) .GE. 0.5) HON=0.
819         IF (W(1,I,J,K) .LT. 0.3) HON=2.5
820         GC(I,J)=COE/(DY*DY*(T(I,J-1,K+1)+T(I,J,K-1))/2.)
821        1+DT*W(3,I,J-1,K+1)/W(1,I,J-1,K+1)/(2.*DY)
822         GA(I,J)=COE/(DY*DY*(T(I,J+1,K+1)+T(I,J,K+1))/2.)
823        1-DT*W(3,I,J+1,K+1)/W(1,I,J+1,K+1)/(2.*DY)
824         GB(I,J)=1.+COE/(DY*DY)
825        1*(2./(T(I,J+1,K+1)+T(I,J,K+1))
826        2+2./(T(I,J-1,K+1)+T(I,J,K+1)))
827         GD(I,J)=XI(I,J,K)+COE*SR(I)/(DX*DX)*(
828        1(XI(I+1,J,K)-XI(I,J,K))/((T(I+1,J,K)+T(I,J,K))/2.
829        2*(SR(I+1)+SR(I))/2.) -(XI(I,J,K)-XI(I-1,J,K))
830        3/((T(I-1,J,K)+T(I,J,K))/2.*(SR(I-1)+SR(I))/2.))
831        4 -DT*SR(I)*((W(2,I+1,J,K)/W(1,I+1,J,K)*
832        5XI(I+1,J,K)/SR(I+1)-W(2,I-1,J,K)/
833        6W(1,I-1,J,K)*XI(I-1,J,K)/SR(I-1))/(2.*DX))+ DT*SR(I)*(
834        7 (B1(I+1,J,K)*W(4,I+1,J,K)/W(1,I+1,J,K)
835        8 -B1(I-1,J,K)*W(4,I-1,J,K)/W(1,I-1,J,K))/(2.*DX)
836        9+(B2(I,J+1,K+1)*W(4,I,J+1,K+1)/W(1,I,J+1,K+1)
837        1 -B2(I,J-1,K+1)*W(4,I,J-1,K+1)/W(1,I,J-1,K+1))/(2.*DY))
838         GD(I,J)=GD(I,J)
839        6+0.5/4.*HON*DT/DX*(ABS(W(2,I+1,J,K)/W(1,I+1,J,K)-W(2,I,J,K)
840        7/W(1,I,J,K))*(XI(I+1,J,K)-XI(I,J,K))-ABS(W(2,I,J,K)/W(1,I,J,K)
841        8-W(2,I-1,J,K)/W(1,I-1,J,K))*(XI(I,J,K)-XI(I-1,J,K)))
842        6+0.5/4.*HON*DT/DY*(ABS(W(3,I,J+1,K)/W(1,I,J+1,K)-W(3,I,J,K)
843        7/W(1,I,J,K))*(XI(I,J+1,K)-XI(I,J,K))-ABS(W(3,I,J,K)/W(1,I,J,K)
844        8-W(3,I,J-1,K)/W(1,I,J-1,K))*(XI(I,J,K)-XI(I,J-1,K)))
845     15 CONTINUE
846     16 CONTINUE
847
848 C...REDUCE THE RESULTING TRI-DIAGONAL MATRIX USING A CROUT METHOD.
```

```
      CALL        CROUT(M,K,IB,IE,JB,JE,IP,JP,GA,GB,GC,GD, XI,JD,ID)
      GO TO 317

C...XI EQUATION IMPLICIT IN R.
  312 CONTINUE
      DO 22 J=JB,JE
      DO 21 I=IB,IE
      HON=0.5
      IF (W(1,I,J,K) .GE. 0.5) HON=0.
      IF (W(1,I,J,K) .LT. 0.3) HON=2.5
      GC(I,J)=COE*SR(I)/(DX*DX*(T(I-1,J,K+1)+
     1T(I,J,K+1))/2.*(SR(I-1)+SR(I))/2.) +DT*SR(I)*
     2W(2,I-1,J,K+1)/W(1,I-1,J,K+1)/(2.*SR(I-1)*DX)
      GA(I,J)=COE*SR(I)/(DX*DX*(T(I+1,J,K+1)+
     1T(I,J,K+1))/2.*(SR(I+1)+SR(I))/2.) -DT*SR(I)*
     2W(2,I+1,J,K+1)/W(1,I+1,J,K+1)/(2.*SR(I+1)*DX)
      GB(I,J)=1.+COE*SR(I)/(DX*DX)*(2./(T(I+1,J,K+1)
     1+T(I,J,K+1))*2./(SR(I+1)+SR(I))+
     22./(T(I-1,J,K+1)+T(I,J,K+1))*2./(SR(I-1)+SR(I)))
      GD(I,J)=XI(I,J,K)+COE/(DY*DY)*((XI(I,J+1,K)-XI(I,J,K))/
     1((T(I,J+1,K)+T(I,J,K))/2.)
     2-(XI(I,J,K)-XI(I,J-1,K))/((T(I,J-1,K)+T(I,J,K))/2.)
     3) -DT/(2.*DY)*(W(3,I,J+1,K)
     4/W(1,I,J+1,K)*XI(I,J+1,K)-
     5W(3,I,J-1,K)/W(1,I,J-1,K)*XI(I,J-1,K))
     7+DT*SR(I)*((B1(I+1,J,K+1)*W(4,I+1,J,K+1)/W(1,I+1,J,K+1)
     8 -B1(I-1,J,K+1)*W(4,I-1,J,K+1)/W(1,I-1,J,K+1))/(2.*DX)
     9+(B2(I,J+1,K)*W(4,I,J+1,K)/W(1,I,J+1,K)
     1 -B2(I,J-1,K)*W(4,I,J-1,K)/W(1,I,J-1,K))/(2.*DY))
      GD(I,J)=GD(I,J)
     6+0.5/4.*HON*DT/DX*(ABS(W(2,I+1,J,K)/W(1,I+1,J,K)-W(2,I,J,K)
     7/W(1,I,J,K))*(XI(I+1,J,K)-XI(I,J,K))-ABS(W(2,I,J,K)/W(1,I,J,K)
     8-W(2,I-1,J,K)/W(1,I-1,J,K))*(XI(I,J,K)-XI(I-1,J,K)))
     6+0.5/4.*HON*DT/DY*(ABS(W(3,I,J+1,K)/W(1,I,J+1,K)-W(3,I,J,K)
     7/W(1,I,J,K))*(XI(I,J+1,K)-XI(I,J,K))-ABS(W(3,I,J,K)/W(1,I,J,K)
     8-W(3,I,J-1,K)/W(1,I,J-1,K))*(XI(I,J,K)-XI(I,J-1,K)))
   21 CONTINUE
   22 CONTINUE

C...REDUCE THE RESULTING TRI-DIAGONAL MATRIX USING A CROUT METHOD.
      CALL        CROUT(M,K,IB,IE,JB,JE,IP,JP,GA,GB,GC,GD, XI,JD,ID)
  317 CONTINUE

C...COMPUTE THE NEW TOROIDAL FIELD, AND RADIAL AND Z-COMPONENTS OF
C...CURRENT DENSITY.
      DO 325 I=IS,ID
       XI(I,JB-1,K+1)= XI(I,JB+1,K+1)
  325 CONTINUE
      DO 331 J=JB,JE
      DO 331 I=IB,IE
      B3(I,J,K+1)=XI(I,J,K+1)/SR(I)
      C1(I,J,K+1)=-(XI(I,J+1,K+1)-XI(I,J-1,K+1))/(SR(I)*
     12.*DY)
```

```
      C2(I,J,K+1)= (XI(I+1,J,K+1)-XI(I-1,J,K+1))/(SR(I)*
     12.*DX)
  331 CONTINUE
      DO 133 I=IS,ID
      B3(I,JD,K+1)=XI(I,JD,K+1)/SR(I)
      B3(I,JS,K+1)=XI(I,JS,K+1)/SR(I)
  133 CONTINUE
      DO 134 J=JS,JD
      B3(ID,J,K+1)=XI(ID,J,K+1)/SR(ID)
      B3(IS,J,K+1)=XI(IS,J,K+1)/SR(IS)
  134 CONTINUE
      DO 40 I=IS,ID
      C1(I,JD,K+1)=-(XI(I,JD,K+1)-XI(I,JE,K+1))/SR(I)/DY
      C1(I,JS,K+1)=-(XI(I,JB,K+1)-XI(I,JS,K+1))/SR(I)/DY
40    CONTINUE
      DO 41 J=JS,JD
      C2(IS,J,K+1)=(XI(IB,J,K+1)-XI(IS,J,K+1))/SR(IS)/DX
      C2(ID,J,K+1)=(XI(ID,J,K+1)-XI(IE,J,K+1))/SR(ID)/DX
41    CONTINUE
      DO 42 I=IB,IE
      C2(I,JD,K+1)=(XI(I+1,JD,K+1)-XI(I-1,JD,K+1))/2./SR(I)/DX
      C2(I,JS,K+1)=(XI(I+1,JS,K+1)-XI(I-1,JS,K+1))/2./SR(I)/DX
42    CONTINUE
      DO 43 J=JB,JE
      C1(IS,J,K+1)=-(XI(IS,J+1,K+1)-XI(IS,J-1,K+1))/SR(IS)/2./DY
      C1(ID,J,K+1)=-(XI(ID,J+1,K+1)-XI(ID,J-1,K+1))/SR(ID)/2./DY
43    CONTINUE

C...COMPUTE THE POWER LOSS DUE TO OXYGEN AND SILICON RADIATION.
C...WARNING: THE ACCURACY OR VALIDITY OF "CORONAL EQUILIBRIUM"
C...DURING THE HEATING PHASE IS SUSPECT.
C...HERE WE EMPLOY THE "FOST" AVERAGE ION MODEL.
      DO R J=JB,JE
      DO R I=IB,IE
      IF ((EI(I,J,K) .GE. T01)  AND. (EI(I,J,K) .LE. T02)) GO TO R1
      IF ((EI(I,J,K) .GT. T02)  AND. (EI(I,J,K) .LE. T03)) GO TO R2
      IF ((EI(I,J,K) .GT. T03)  AND. (EI(I,J,K) .LE. T04)) GO TO R3
      IF (EI(I,J,K) .LT. T01) GO TO R4
      IF (EI(I,J,K) .GT. T04) CALL EXIT(1)
R1    PAO(1,I,J)=652.374
      PAO(2,I,J)=1835.499
      PAO(3,I,J)=1984.266
      PAO(4,I,J)=1059.846
      PAO(5,I,J)=280.0476
      PAO(6,I,J)=29.33792
      GO TO R
R2    PAO(1,I,J)=-55.15118
      PAO(2,I,J)=-154.3956
      PAO(3,I,J)=-248.992
      PAO(4,I,J)=-180.8154
      PAO(5,I,J)=-57.64175
      PAO(6,I,J)=-6.149181
      GO TO R
```

```
      R3    PAO(1,I,J)=-20.68816
            PAO(2,I,J)=-.7482238
            PAO(3,I,J)=.7390959
            PAO(4,I,J)=-.672159
            PAO(5,I,J)=1.338345
            PAO(6,I,J)=3.734628
            GO TO R
      R4    PAO(1,I,J)=1.
            PAO(2,I,J)=1.
            PAO(3,I,J)=1.
            PAO(4,I,J)=1.
            PAO(5,I,J)=1.
            PAO(6,I,J)=1.
      R     CONTINUE
            DO RA J=JB,JE
            DO RA I=IB,IE
            IF ((EI(I,J,K) .GE. TS1) .AND. (EI(I,J,K) .LE. TS2)) GO TO RA1
            IF ((EI(I,J,K) .GT. TS2) .AND. (EI(I,J,K) .LE. TS3)) GO TO RA2
            GO TO RA3
      RA1   PAS(1,I,J)=-52.75519
            PAS(2,I,J)=-134.613
            PAS(3,I,J)=-208.2753
            PAS(4,I,J)=-159.1874
            PAS(5,I,J)=-59.89162
            PAS(6,I,J)=-8.684849
            GO TO RA
      RA2   PAS(1,I,J)=-19.54323
            PAS(2,I,J)=.0499481
            PAS(3,I,J)=-5.726766
            PAS(4,I,J)=-2.710884
            PAS(5,I,J)=30.75145
            PAS(6,I,J)=26.89966
            GO TO RA
      RA3   PAS(1,I,J)=1.
            PAS(2,I,J)=1.
            PAS(3,I,J)=1.
            PAS(4,I,J)=1.
            PAS(5,I,J)=1.
            PAS(6,I,J)=1.
      RA    CONTINUE
            DO RAD J=JB,JE
            DO RAD I=IB,IE
            XLZO=PAO(1,I,J)
            XLZS=PAS(1,I,J)
            XLOG=ALOG10(EI(I,J,K)*UN*UN/CV/11600./1000.)
            DO RADI KK=1,5
            XLOGK=(ABS(XLOG))**KK
            IF ((XLOG .LT. 0.) .AND. (MOD(KK,2) .EQ. 1)) XLOGK=-XLOGK
            XLZO=XLZO + PAO(KK+1,I,J)*XLOGK
            XLZS=XLZS + PAS(KK+1,I,J)*XLOGK
      RADI  CONTINUE
            XXLZO=10.**XLZO
            XXLZS=10.**XLZS
```

```
      IF (EI(I,J,K) .LT. TO1) XXLZO=0.
      IF (EI(I,J,K) .LT. TS1) XXLZS=0.
      RO=(W(1,I+1,J,K)+W(1,I-1,J,K)+W(1,I,J,K)+
     1W(1,I,J-1,K)+W(1,I,J+1,K))/5.
      IF (RO .LT. HU) RO=HU
      IF (RO .LE. RORAD) GO TO RAD1
      PRO=PERO*XXLZO
      PRS=PERS*XXLZS
      GO TO RAD2
RAD1  PRO=(.5-(.5-PERO)*((RO-HU)/(RORAD-HU)))*XXLZO
      PRS=(.5-(.5-PERS)*((RO-HU)/(RORAD-HU)))*XXLZS
RAD2  PR(I,J)=(PRO+PRS)*4.5E46*W(1,I,J,K)*DN*RSMA/UN*DT/UN/UN
RAD   CONTINUE

C...FOR A ZERO-DIMENSIONAL LOSS CONSTANT, TAU,
C...FORMULATION; WE SIMPLY PUT A TERM DT/TAU IN THE EXPRESSION
C...FOR "GB" BELOW.  TAU IS A NORMALIZED LOSS TIME.
      IF (MOD(M,2) .EQ. 1) GO TO 211
      GO TO 212

C...ENERGY EQUATION IMPLICIT IN Z.
  211 CONTINUE
      DO 214 J=JB,JE
      DO 213 I=IB,IE
      HON=0.5
      IF (W(1,I,J,K) .GE. 0.5) HON=0.
      GC(I,J)=DT*(CN(I,J,K+1)+
     1CN(I,J-1,K+1))/(2.*W(1,I,J,K+1)*
     2DY*DY) +DT*W(3,I,J,K+1)/
     3W(1,I,J,K+1)/(2.*DY)
      GA(I,J)=DT*(CN(I,J,K+1)+
     1CN(I,J+1,K+1))/(2.*W(1,I,J,K+1)*
     2DY*DY) -DT*W(3,I,J,K+1)/
     3W(1,I,J,K+1)/(2.*DY)
      GB(I,J)=1.+DT/(W(1,I,J,K+1)*DY*DY)*(
     1 (CN(I,J,K+1)+CN(I,J+1,K+1))/2.
     2+(CN(I,J,K+1)+CN(I,J-1,K+1))/2.)
     4+DT*(FK-1.)/2.*((SR(I+1)*W(2,I+1,J,K+1)/W(1,I+1,J,K+1)
     5-SR(I-1)*W(2,I-1,J,K+1)/W(1,I-1,J,K+1))/(2.*SR(I)*DX)
     7+(W(3,I,J+1,K+1)/W(1,I,J+1,K+1)-
     8W(3,I,J-1,K+1)/W(1,I,J-1,K+1))/(2.*DY))
      GD(I,J)=EI(I,J,K)+DT/(W(1,I,J,K)*SR(I)*DX*DX)*(0.5*(SR(I+1)+SR(I))
     2* 0.5*(CN(I,J,K)+CN(I+1,J,K))*(EI(I+1,J,K)-EI(I,J,K))-0.5*(SR(I-1)
     4+SR(I))* 0.5*(CN(I,J,K)+CN(I-1,J,K))*(EI(I,J,K)-EI(I-1,J,K)))
     5-DT*W(2,I,J,K)/W(1,I,J,K)
     6*(EI(I+1,J,K)-EI(I-1,J,K))/(2.*DX)-0.5*DT*(FK-1.)*EI(I,J,K)*
     4((SR(I+1)*W(2,I+1,J,K)/W(1,I+1,J,K)
     5 -SR(I-1)*W(2,I-1,J,K)/W(1,I-1,J,K)
     6)/(2.*SR(I)*DX)
     7+(W(3,I,J+1,K)/W(1,I,J+1,K)-
     8W(3,I,J-1,K)/W(1,I,J-1,K))/(
     92.*DY))
     8+COE*(C1(I,J,K+1)**2+C2(I,J,K+1)**2+C3(I,J,K+1)**2)/
```

```
     9(T(I,J,K  )*W(1,I,J,K+1))
      GD(I,J)=GD(I,J) - PR(I,J)
     6+0.5/4.*HON*DT/DX*(ABS(W(2,I+1,J,K)/W(1,I+1,J,K)-W(2,I,J,K)
     7/W(1,I,J,K))*(EI(I+1,J,K)-EI(I,J,K))-ABS(W(2,I,J,K)/W(1,I,J,K)
     8-W(2,I-1,J,K)/W(1,I-1,J,K))*(EI(I,J,K)-EI(I-1,J,K)))
     6+0.5/4.*HON*DT/DY*(ABS(W(3,I,J+1,K)/W(1,I,J+1,K)-W(3,I,J,K)
     7/W(1,I,J,K))*(EI(I,J+1,K)-EI(I,J,K))-ABS(W(3,I,J,K)/W(1,I,J,K)
     8-W(3,I,J-1,K)/W(1,I,J-1,K))*(EI(I,J,K)-EI(I,J-1,K)))
  213 CONTINUE
  214 CONTINUE

C...REDUCE THE RESULTING TRI-DIAGONAL MATRIX USING A CROUT METHOD.
      CALL       CROUT(M,K,IB,IE,JB,JE,IP,JP,GA,GB,GC,GD, EI,JD,ID)
      GO TO 217

C...ENERGY EQUATION IMPLICIT IN R.
  212 CONTINUE
      DO 235 J=JB,JE
      DO 234 I=IB,IE
      HON=0.5
      IF (W(1,I,J,K) .GE. 0.5) HON=0.
      GC(I,J)=DT*0.5*(CN(I,J,K+1)+CN(I-1,J,K+1))*0.5*(SR(I-1)+SR(I))/
     2(W(1,I,J,K+1)*SR(I)*DX*DX) +DT*W(2,I,J,K+1)/
     3W(1,I,J,K+1)/(2.*DX)
      GA(I,J)=DT*0.5*(CN(I,J,K+1)+CN(I+1,J,K+1))*0.5*(SR(I+1)+SR(I))/
     2(W(1,I,J,K+1)*SR(I)*DX*DX) -DT*W(2,I,J,K+1)/
     3W(1,I,J,K+1)/(2.*DX)
      GB(I,J)=1.+DT/(W(1,I,J,K+1)*SR(I)*DX*DX)*(
     10.5*(CN(I,J,K+1)+CN(I+1,J,K+1))*0.5*(SR(I)+SR(I+1))+
     30.5*(CN(I,J,K+1)+CN(I-1,J,K+1))*0.5*(SR(I)+SR(I-1)))
     4+DT*(FK-1.)/2.*((SR(I+1)*W(2,I+1,J,K+1)/
     5W(1,I+1,J,K+1)-SR(I-1)*W(2,I-1,J,
     6K+1)/W(1,I-1,J,K+1))/(2.*SR(I)*DX) +
     7(W(3,I,J+1,K+1)/W(1,I,J+1,K+1)-
     8W(3,I,J-1,K+1)/W(1,I,J-1,K+1))/
     9(2.*DY))
      GD(I,J)=EI(I,J,K)    +DT/(W(1,I,J,K)*DY*DY)*(
     10.5*(CN(I,J,K)+CN(I,J+1,K))*(EI(I,J+1,K)-
     2EI(I,J,K))-0.5*(CN(I,J,K)+
     3CN(I,J-1,K))*(EI(I,J,K)-EI(I,J-1,K)))
     4-DT*W(3,I,J,K)/W(1,I,J,K)*(EI(I,J+1,K)-
     5EI(I,J-1,K))/(2.*DY)-DT*(FK-1.)*EI(I,J,K)*0.5*
     4((SR(I+1)*W(2,I+1,J,K)/W(1,I+1,J,K)
     5 -SR(I-1)*W(2,I-1,J,K)/W(1,I-1,J,K)
     6)/(2.*SR(I)*DX) +(
     7W(3,I,J+1,K)/W(1,I,J+1,K)-
     8W(3,I,J-1,K)/W(1,I,J-1,K))/(
     92.*DY))
     8+COE*(C1(I,J,K+1)**2+C2(I,J,K+1)**2+C3(I,J,K+1)**2)/
     9(T(I,J,K  )*W(1,I,J,K+1))
      GD(I,J)=GD(I,J) - PR(I,J)
     6+0.5/4.*HON*DT/DX*(ABS(W(2,I+1,J,K)/W(1,I+1,J,K)-W(2,I,J,K)
     7/W(1,I,J,K))*(EI(I+1,J,K)-EI(I,J,K))-ABS(W(2,I,J,K)/W(1,I,J,K)
```

```
      8-W(2,I-1,J,K)/W(1,I-1,J,K))*(EI(I,J,K)-EI(I-1,J,K)))
      6+0.5/4.*HON*DT/DY*(ABS(W(3,I,J+1,K)/W(1,I,J+1,K)-W(3,I,J,K)
      7/W(1,I,J,K))*(EI(I,J+1,K)-EI(I,J,K))-ABS(W(3,I,J,K)/W(1,I,J,K)
      8-W(3,I,J-1,K)/W(1,I,J-1,K))*(EI(I,J,K)-EI(I,J-1,K)))
  234 CONTINUE
  235 CONTINUE

C...REDUCE THE RESULTING TRI-DIAGONAL MATRIX USING A CROUT METHOD.
      CALL       CROUT(M,K,IB,IE,JB,JE,IP,JP,GA,GB,GC,GD, EI,JD,ID)
  217 CONTINUE
      DO 225 I=IS,ID
      EI(I,JB-1,K+1)= EI(I,JB+1,K+1)
  225 CONTINUE

      RETURN
      END




C...THIS SUBROUTINE SOLVES THE CONTINUITY AND MOMENTUM EQUATIONS
C...IMPLICIT IN Z.



      SUBROUTINE YIMCRO(K,M,DT,DX,DY,CV,FK,COE,DOE,UN,BATA,BATB,SGO,
     1IS,IB,IE,ID,JS,JB,JE,JD,C,IP,JP,TMALL)

      DIMENSION PSI(21,22,2),B1(21,22,2),B2(21,22,2),XI(21,22,2),
     1C1(21,22,2),C2(21,22,2),C3(21,22,2),T(21,22,2),
     2W(4,21,22,3),F(4,21,22,3),EI(21,22,2),B3(21,22,2),SR(21),
     4GA(21,22),GB(21,22),GC(21,22),GD(21,22),CN(21,22,2),
     5AA(100,12),BB(4,4)
      LCM (T2)
      COMMON/T2/ PSI,B1,B2,B3,XI,C1,C2,C3,T,W,F,SR
     1,GA,GB,GC,GD,CN,EI,AA,BB

C...USING NEW VALUES OF FIELDS, CURRENTS AND TEMPERATURE WE AGAIN
C...SOLVE THE MOMENTUM AND CONTINUITY EQUATION FULLY EXPLICITLY TO
C...OBTAIN PREDICTOR VALUES FOR W-VECTOR.  THESE VALUES ARE THEN USED
C...IN THE NON-LINEAR TERMS WHEN SOLVING THE ADI SCHEME.
      K1=1
      K2=3
      K3=1
      K=1
      DO 38 J=JB,JE
      DO 39 I=IB,IE
      F(1,I,J,K2)=W(1,I,J,K1)
     1-BATA/SR(I)*(SR(I+1)*W(2,I+1,J,K3)-
     2SR(I-1)*W(2,I-1,J,K3))+F(1,I,J,K)+F(1,I,J,K+1)
     6+0.5/4.*0.5*DT/DX*(ABS(W(2,I+1,J,K)/W(1,I+1,J,K)-W(2,I,J,K)
```

```
      7/W(1,I,J,K))*(W(1,I+1,J,K)-W(1,I,J,K))-ABS(W(2,I,J,K)/W(1,I,J,K)
      8-W(2,I-1,J,K)/W(1,I-1,J,K))*(W(1,I,J,K)-W(1,I-1,J,K)))
      6+0.5/4.*0.5*DT/DY*(ABS(W(3,I,J+1,K)/W(1,I,J+1,K)-W(3,I,J,K)
      7/W(1,I,J,K))*(W(1,I,J+1,K)-W(1,I,J,K))-ABS(W(3,I,J,K)/W(1,I,J,K)
      8-W(3,I,J-1,K)/W(1,I,J-1,K))*(W(1,I,J,K)-W(1,I,J-1,K)))
       F(2,I,J,K2)=W(2,I,J,K1)
      1-BATA/SR(I)*(SR(I+1)*(W(2,I+1,J,K3)**2
      2/W(1,I+1,J,K3)+(FK-1.)*W(1,I+1,J,K3)*EI(I+1,J,K3))-SR(I-1)*
      3(W(2,I-1,J,K3)**2/W(1,I-1,J,K3) +(FK-1.)*W(1,I-1,J,K3)
      4*EI(I-1,J,K3)))+F(2,I,J,K)+F(2,I,J,K+1)
      6+0.5/4.*0.5*DT/DX*(ABS(W(2,I+1,J,K)/W(1,I+1,J,K)-W(2,I,J,K)
      7/W(1,I,J,K))*(W(2,I+1,J,K)-W(2,I,J,K))-ABS(W(2,I,J,K)/W(1,I,J,K)
      8-W(2,I-1,J,K)/W(1,I-1,J,K))*(W(2,I,J,K)-W(2,I-1,J,K)))
      6+0.5/4.*0.5*DT/DY*(ABS(W(3,I,J+1,K)/W(1,I,J+1,K)-W(3,I,J,K)
      7/W(1,I,J,K))*(W(2,I,J+1,K)-W(2,I,J,K))-ABS(W(3,I,J,K)/W(1,I,J,K)
      8-W(3,I,J-1,K)/W(1,I,J-1,K))*(W(2,I,J,K)-W(2,I,J-1,K)))
       F(3,I,J,K2)=W(3,I,J,K1)
      1-BATA/SR(I)*(SR(I+1)*W(2,I+1,J,K3)*
      2W(3,I+1,J,K3)/W(1,I+1,J,K3)-SR(I-1)*W(2,I-1,J,K3)*W(3,I-1,J,K3)
      3/W(1,I-1,J,K3))+F(3,I,J,K)+F(3,I,J,K+1)
      6+0.5/4.*0.5*DT/DX*(ABS(W(2,I+1,J,K)/W(1,I+1,J,K)-W(2,I,J,K)
      7/W(1,I,J,K))*(W(3,I+1,J,K)-W(3,I,J,K))-ABS(W(2,I,J,K)/W(1,I,J,K)
      8-W(2,I-1,J,K)/W(1,I-1,J,K))*(W(3,I,J,K)-W(3,I-1,J,K)))
      6+0.5/4.*0.5*DT/DY*(ABS(W(3,I,J+1,K)/W(1,I,J+1,K)-W(3,I,J,K)
      7/W(1,I,J,K))*(W(3,I,J+1,K)-W(3,I,J,K))-ABS(W(3,I,J,K)/W(1,I,J,K)
      8-W(3,I,J-1,K)/W(1,I,J-1,K))*(W(3,I,J,K)-W(3,I,J-1,K)))
       F(4,I,J,K2)=W(4,I,J,K1)
      1-BATA/SR(I)*(SR(I+1)*W(2,I+1,J,K3)
      2*W(4,I+1,J,K3)/W(1,I+1,J,K3)-SR(I-1)*W(2,I-1,J,K3)*W(4,I-1,J,K3)
      1/W(1,I-1,J,K3))+F(4,I,J,K)+F(4,I,J,K+1)
      6+0.5/4.*0.5*DT/DX*(ABS(W(2,I+1,J,K)/W(1,I+1,J,K)-W(2,I,J,K)
      7/W(1,I,J,K))*(W(4,I+1,J,K)-W(4,I,J,K))-ABS(W(2,I,J,K)/W(1,I,J,K)
      8-W(2,I-1,J,K)/W(1,I-1,J,K))*(W(4,I,J,K)-W(4,I-1,J,K)))
      6+0.5/4.*0.5*DT/DY*(ABS(W(3,I,J+1,K)/W(1,I,J+1,K)-W(3,I,J,K)
      7/W(1,I,J,K))*(W(4,I,J+1,K)-W(4,I,J,K))-ABS(W(3,I,J,K)/W(1,I,J,K)
      8-W(3,I,J-1,K)/W(1,I,J-1,K))*(W(4,I,J,K)-W(4,I,J-1,K)))
   39  CONTINUE
   38  CONTINUE

C...SET UP THE MATRIX FORM OF THE CONTINUITY AND MOMENTUM EQUATIONS.
C...REDUCE THE MATRIX USING A CROUT METHOD THEREBY OBTAINING THE NEW
C...DENSITY AND VELOCITY.
       DO 113 I=IB,IE
       F(3,I,JE,K2)=F(3,I,JE,K2)-(FK-1.)*W(1,I,JD,K+1)*EI(I,JD,K+1)*BATB
       DO 114 J=JS,JP
       IF (J .EQ. JS) GO TO 115
       AA(4*J-3,1)=0.
       AA(4*J-3,2)=0.
       AA(4*J-3,3)=-BATB
       AA(4*J-3,4)=0.
       AA(4*J-2,1)= BATB*(W(2,I,J,K+1)*W(3,I,J,K+1)/W(1,I,J,K+1)
      1**2)
       AA(4*J-2,2)=-BATB*(W(3,I,J,K+1)/W(1,I,J,K+1))
```

```
      AA(4*J-2,3)=-BATB*(W(2,I,J,K+1)/W(1,I,J,K+1))
      AA(4*J-2,4)=0.
      AA(4*J-1,1)=-BATB*((FK-1.)*EI(I,J,K+1)-(W(3,I,J,K+1)
     1/W(1,I,J,K+1))**2)
      AA(4*J-1,2)=0.
      AA(4*J-1,3)=-BATB*(2.*W(3,I,J,K+1)/W(1,I,J,K+1))
      AA(4*J-1,4)=0.
      AA(4*J  ,1)= BATB*(W(3,I,J,K+1)*W(4,I,J,K+1)/W(1,I,J,K+1)
     1**2)
      AA(4*J  ,2)=0.
      AA(4*J  ,3)=-BATB*(W(4,I,J,K+1)/W(1,I,J,K+1))
      AA(4*J  ,4)=-BATB*(W(3,I,J,K+1)/W(1,I,J,K+1))
  115 CONTINUE
      IF (J .EQ. JP) GO TO 116
      AA(4*J-3,9)=0.
      AA(4*J-3,10)=0.
      AA(4*J-3,11)=+BATB
      AA(4*J-3,12)=0.
      AA(4*J-2,9)=-BATB*(W(2,I,J+2,K+1)*W(3,I,J+2,K+1)/W(1,I,J+2,K+1)
     1**2)
      AA(4*J-2,10)=+BATB*(W(3,I,J+2,K+1)/W(1,I,J+2,K+1))
      AA(4*J-2,11)=+BATB*(W(2,I,J+2,K+1)/W(1,I,J+2,K+1))
      AA(4*J-2,12)=0.
      AA(4*J-1, 9)=+BATB*((FK-1 )*EI(I,J+2,K+1)-(W(3,I,J+2,K+1)
     1/W(1,I,J+2,K+1))**2)
      AA(4*J-1,10)=0.
      AA(4*J-1,11)=+BATB*(2.*W(3,I,J+2,K+1)/W(1,I,J+2,K+1))
      AA(4*J-1,12)=0.
      AA(4*J , 9)=-BATB*(W(3,I,J+2,K+1)*W(4,I,J+2,K+1)/W(1,I,J+2,K+1)
     1**2)
      AA(4*J , 10)=0.
      AA(4*J ,11)=+BATB*(W(4,I,J+2,K+1)/W(1,I,J+2,K+1))
      AA(4*J ,12)=+BATB*(W(3,I,J+2,K+1)/W(1,I,J+2,K+1))
  116 CONTINUE
      AA(4*J-3,5)=1.
      AA(4*J-3,6)=0.
      AA(4*J-3,7)=0.
      AA(4*J-3,8)=0.
      AA(4*J-2,5)=0.
      AA(4*J-2,6)=1.
      AA(4*J-2,7)=0.
      AA(4*J-2,8)=0.
      AA(4*J-1,5)=0.
      AA(4*J-1,6)=0.
      AA(4*J-1,7)=1.
      AA(4*J-1,8)=0.
      AA(4*J  ,5)=0.
      AA(4*J  ,6)=0.
      AA(4*J  ,7)=0.
      AA(4*J  ,8)=1.
  114 CONTINUE
      DO 207 L=1,2
      DO 208 LL=9,12
```

```
      AA(L  ,LL)= 2.*AA(L  ,LL)
      AA(L+2,LL)=0.
  208 CONTINUE
  207 CONTINUE
      JPP=4*JP
      DO 117 J=5,JPP,4
      DO 188 L=1,4
      DO 189 LL=1,4
      BB(L,LL)=0.
      DO 121 LLL=1,4
      IF (ABS(AA(J+L-1,LLL)) .LT. TMALL) AA(J+L-1,LLL)=0.
      IF (ABS(AA(J+LLL-5,8+LL)) .LT. TMALL) AA(J+LLL-5,8+LL)=0.
  121 BB(L,LL)=BB(L,LL) + AA(J+L-1,LLL)*AA(J+LLL-5,8+LL)
  189 CONTINUE
  188 CONTINUE
      DO 122 L=1,4
  122 AA(J-1+L,5)=AA(J-1+L,5)-BB(L,1)
      DO 123 L=1,3
  123 AA(J,5+L)=(AA(J,5+L)-BB(1,L+1))/AA(J,5)
      IF (J .EQ. (JPP-3)) GO TO 924
      DO 124 L=1,4
  124 AA(J,8+L)=AA(J,8+L)/AA(J,5)
  924 CONTINUE
      DO 125 L=1,3
  125 AA(J+L,6)=AA(J+L,6)-BB(L+1,2)-AA(J+L,5)*AA(J,6)
      DO 126 L=1,2
  126 AA(J+1,6+L)=(AA(J+1,6+L)-BB(2,2+L)-AA(J+1,5)*AA(J,6+L))/AA(J+1,6)
      IF (J .EQ. (JPP-3)) GO TO 127
      DO 128 L=1,4
      AA(J+L+3,2)=AA(J+L+3,2)-AA(J+L+3,1)*AA(J,6)
      AA(J+1,8+L)=(AA(J+1,8+L)-AA(J+1,5)*AA(J,8+L))/AA(J+1,6)
  128 CONTINUE
  127 CONTINUE
      DO 129 L=1,2
  129 AA(J+L+1,7)=AA(J+L+1,7)-BB(2+L,3)-AA(J+L+1,5)*AA(J,7)-
     1AA(J+L+1,6)*AA(J+1,7)
      AA(J+2,8)=(AA(J+2,8)-BB(3,4)-AA(J+2,5)*AA(J,8)-AA(J+2,6)*AA(J+1,8)
     2)/AA(J+2,7)
      IF (J .EQ. (JPP-3)) GO TO 130
      DO 131 L=1,4
      DO 132 LL=1,2
      AA(J+L+3,3)=AA(J+L+3,3)-AA(J+L+3,LL)*AA(J+LL-1,7)
      AA(J+2,8+L)=AA(J+2,8+L)-AA(J+2,4+LL)*AA(J+LL-1,8+L)
  132 CONTINUE
      AA(J+2,8+L)=AA(J+2,8+L)/AA(J+2,7)
  131 CONTINUE
  130 CONTINUE
      AA(J+3,8)=AA(J+3,8)-BB(4,4)-AA(J+3,5)*AA(J,8)-AA(J+3,6)*AA(J+1,8)
     1-AA(J+3,7)*AA(J+2,8)
      IF (J .EQ. (JPP-3)) GO TO 133
      DO 134 L=1,4
      DO 135 LL=1,3
      AA(J+L+3,4)= AA(J+L+3,4)-AA(J+L+3,LL)*AA(J+LL-1,8)
```

```
      AA(J+3,8+L)= AA(J+3,8+L)-AA(J+3,4+LL)*AA(J+LL-1,8+L)
  135 CONTINUE
      AA(J+3,8+L)= AA(J+3,8+L)/AA(J+3,8)
  134 CONTINUE
  133 CONTINUE
      DO 136 L=1,4
      DO 137 LL=1,4
  137 F(L,I,(J+7)/4,K+2)=F(L,I,(J+7)/4,K+2)-AA(J+L-1,LL)*F(LL,I,(J+7)/4
     1-1,K+2)
      LE=L-1
      IF (L .EQ. 1) GO TO 148
      DO 147 LL=1,LE
      F(L,I,(J+7)/4,K+2)=F(L,I,(J+7)/4,K+2)-AA(J+L-1,4+LL)*F(LL,I,(J+7)
     1/4,K+2)
  147 CONTINUE
  148 CONTINUE
      F(L,I,(J+7)/4,K+2)=F(L,I,(J+7)/4,K+2)/AA(J+L-1,5+L-1)
  136 CONTINUE
  117 CONTINUE
      W(4,I,JE,K+2)=F(4,I,JE,K+2)
      W(3,I,JE,K+2)=F(3,I,JE,K+2)-AA(JPP-1,8)*W(4,I,JE,K+2)
      W(2,I,JE,K+2)=F(2,I,JE,K+2)-AA(JPP-2,8)*W(4,I,JE,K+2)
     1-AA(JPP-2,7)*W(3,I,JE,K+2)
      W(1,I,JE,K+2)=F(1,I,JE,K+2)-AA(JPP-3,8)*W(4,I,JE,K+2)
     1-AA(JPP-3,7)*W(3,I,JE,K+2)-AA(JPP-3,6)*W(2,I,JE,K+2)
      DO 138 J=5,JPP,4
      JJ=JPP+5-J-4
      DO 139 L=1,4
      BB(1,L)=0.
      DO 941 LL=1,4
  941 BB(1,L)=BB(1,L)+AA(JJ+1-L,8+LL)*W(LL,I,(JJ+4)/4+1,K+2)
  139 CONTINUE
      W(4,I,(JJ+4)/4,K+2)=F(4,I,(JJ+4)/4,K+2)-BB(1,1)
      W(3,I,(JJ+4)/4,K+2)=F(3,I,(JJ+4)/4,K+2)-BB(1,2)
     1-AA(JJ-1,8)*W(4,I,(JJ+4)/4,K+2)
      W(2,I,(JJ+4)/4,K+2)=F(2,I,(JJ+4)/4,K+2)-BB(1,3)
     1-AA(JJ-2,8)*W(4,I,(JJ+4)/4,K+2)-AA(JJ-2,7)*W(3,I,(JJ+4)/4,K+2)
      W(1,I,(JJ+4)/4,K+2)=F(1,I,(JJ+4)/4,K+2)-BB(1,4)
     1-AA(JJ-3,8)*W(4,I,(JJ+4)/4,K+2)-AA(JJ-3,7)*W(3,I,(JJ+4)/4,K+2)
     2-AA(JJ-3,6)*W(2,I,(JJ+4)/4,K+2)
  138 CONTINUE
  113 CONTINUE
      RETURN
      END



C...THIS SUBROUTINE SERVES THE EXACT SAME PURPOSE AS YIMCRO EXCEPT
C...THAT WE NOW WRITE THE EQUATIONS IMPLICIT IN R.
C...THEREFORE, WE FOREGO DOCUMENTING THIS SUBROUTINE

```

```
1379
1380
1381        SUBROUTINE XIMCRO(K,M,DT,DX,DY,CV,FK,COE,DOE,UN,BATA,BATB,SGO,
1382       1IS,IB,IE,ID,JS,JB,JE,JD,C,IP,JP,TMALL)
1383
1384        DIMENSION PSI(21,22,2),B1(21,22,2),B2(21,22,2),XI(21,22,2),
1385       1C1(21,22,2),C2(21,22,2),C3(21,22,2),T(21,22,2),
1386       2W(4,21,22,3),F(4,21,22,3),EI(21,22,2),B3(21,22,2),SR(21),
1387       4GA(21,22),GB(21,22),GC(21,22),GD(21,22),CN(21,22,2),
1388       5AA(100,12),BB(4,4)
1389        LCM (T2)
1390        COMMON/T2/ PSI,B1,B2,B3,XI,C1,C2,C3,T,W,F,SR
1391       1,GA,GB,GC,GD,CN,EI,AA,BB
1392
1393        K=1
1394        K1=1
1395        K2=3
1396        K3=1
1397
1398        DO 41 J=JB,JE
1399        DO 42 I=IB,IE
1400        F(1,I,J,K2)=W(1,I,J,K1)
1401       2-BATB*(W(3,I,J+1,K3)-W(3,I,J-1,K3))
1402       3+(F(1,I,J,K)+F(1,I,J,K+1))
1403       6+0.5/4.*0.5*DT/DX*(ABS(W(2,I+1,J,K)/W(1,I+1,J,K)-W(2,I,J,K)
1404       7/W(1,I,J,K))*(W(1,I+1,J,K)-W(1,I,J,K))-ABS(W(2,I,J,K)/W(1,I,J,K)
1405       8-W(2,I-1,J,K)/W(1,I-1,J,K))*(W(1,I,J,K)-W(1,I-1,J,K)))
1406       6+0.5/4.*0.5*DT/DY*(ABS(W(3,I,J+1,K)/W(1,I,J+1,K)-W(3,I,J,K)
1407       7/W(1,I,J,K))*(W(1,I,J+1,K)-W(1,I,J,K))-ABS(W(3,I,J,K)/W(1,I,J,K)
1408       8-W(3,I,J-1,K)/W(1,I,J-1,K))*(W(1,I,J,K)-W(1,I,J-1,K)))
1409        F(2,I,J,K2)=W(2,I,J,K1)
1410       4-BATB*(W(2,I,J+1,K3)*W(3,I,J+1,K3)
1411       5/W(1,I,J+1,K3)-W(2,I,J-1,K3)*W(3,I,J-1,K3)/W(1,I,J-1,K3))
1412       6+(F(2,I,J,K)+F(2,I,J,K+1))
1413       6+0.5/4.*0.5*DT/DX*(ABS(W(2,I+1,J,K)/W(1,I+1,J,K)-W(2,I,J,K)
1414       7/W(1,I,J,K))*(W(2,I+1,J,K)-W(2,I,J,K))-ABS(W(2,I,J,K)/W(1,I,J,K)
1415       8-W(2,I-1,J,K)/W(1,I-1,J,K))*(W(2,I,J,K)-W(2,I-1,J,K)))
1416       6+0.5/4.*0.5*DT/DY*(ABS(W(3,I,J+1,K)/W(1,I,J+1,K)-W(3,I,J,K)
1417       7/W(1,I,J,K))*(W(2,I,J+1,K)-W(2,I,J,K))-ABS(W(3,I,J,K)/W(1,I,J,K)
1418       8-W(3,I,J-1,K)/W(1,I,J-1,K))*(W(2,I,J,K)-W(2,I,J-1,K)))
1419        F(3,I,J,K2)=W(3,I,J,K1)
1420       3-BATB*((W(3,I,J+1,K3)**2/W(1,I,J+1,K3)+
1421       4(FK-1.)*W(1,I,J+1,K3)*EI(I,J+1,K ))-(W(3,I,J-1,K3)**2/
1422       5W(1,I,J-1,K3)+(FK-1.)*W(1,I,J-1,K3)*EI(I,J-1,K )))
1423       6+(F(3,I,J,K)+F(3,I,J,K+1))
1424       6+0.5/4.*0.5*DT/DX*(ABS(W(2,I+1,J,K)/W(1,I+1,J,K)-W(2,I,J,K)
1425       7/W(1,I,J,K))*(W(3,I+1,J,K)-W(3,I,J,K))-ABS(W(2,I,J,K)/W(1,I,J,K)
1426       8-W(2,I-1,J,K)/W(1,I-1,J,K))*(W(3,I,J,K)-W(3,I-1,J,K)))
1427       6+0.5/4.*0.5*DT/DY*(ABS(W(3,I,J+1,K)/W(1,I,J+1,K)-W(3,I,J,K)
1428       7/W(1,I,J,K))*(W(3,I,J+1,K)-W(3,I,J,K))-ABS(W(3,I,J,K)/W(1,I,J,K)
1429       8-W(3,I,J-1,K)/W(1,I,J-1,K))*(W(3,I,J,K)-W(3,I,J-1,K)))
1430        F(4,I,J,K2)=W(4,I,J,K1)
1431       3-BATB*(W(3,I,J+1,K3)*W(4,I,J+1,K3)
```

```
     4/W(1,I,J+1,K3)-W(3,I,J-1,K3)*W(4,I,J-1,K3)/W(1,I,J-1,K3))
     5+(F(4,I,J,K)+F(4,I,J,K+1))
     6+0.5/4.*0.5*DT/DX*(ABS(W(2,I+1,J,K)/W(1,I+1,J,K)-W(2,I,J,K)
     7/W(1,I,J,K))*(W(4,I+1,J,K)-W(4,I,J,K))-ABS(W(2,I,J,K)/W(1,I,J,K)
     8-W(2,I-1,J,K)/W(1,I-1,J,K))*(W(4,I,J,K)-W(4,I-1,J,K)))
     6+0.5/4.*0.5*DT/DY*(ABS(W(3,I,J+1,K)/W(1,I,J+1,K)-W(3,I,J,K)
     7/W(1,I,J,K))*(W(4,I,J+1,K)-W(4,I,J,K))-ABS(W(3,I,J,K)/W(1,I,J,K)
     8-W(3,I,J-1,K)/W(1,I,J-1,K))*(W(4,I,J,K)-W(4,I,J-1,K)))
  42 CONTINUE
  41 CONTINUE
     DO 153 J=JB,JE
     F(2,2,J,K+2)=F(2,2,J,K+2)+(FK-1.)*W(1,IS,J,K+1)*EI(IS,J,K+1)
     1*BATA*SR(IS)/SR(2)
     F(2,IE,J,K+2)=F(2,IE,J,K+2)-(FK-1.)*W(1,ID,J,K+1)*EI(ID,J,K+1)
     1*BATA*SR(ID)/SR(IE)
     DO 154 I=IS,IP
     IF (I .EQ. IS) GO TO 155
     AA(4*I-3,1)=0.
     AA(4*I-3,2)=-BATA*SR(I)/SR(I-1)
     AA(4*I-3,3)=0.
     AA(4*I-3,4)=0.
     AA(4*I-2,1)=-BATA*SR(I)/SR(I-1)*((FK-1.)*EI(I,J,K+1)
     1-(W(2,I,J,K+1)/W(1,I,J,K+1))**2)
     AA(4*I-2,2)=-BATA*SR(I)/SR(I-1)*(2.*W(2,I,J,K+1)/
     1W(1,I,J,K+1))
     AA(4*I-2,3)=0.
     AA(4*I-2,4)=0.
     AA(4*I-1,1)= BATA*SR(I)/SR(I+1)*(W(2,I,J,K+1)*W(3,I,J,K+1)
     1/W(1,I,J,K+1)**2)
     AA(4*I-1,2 )=-BATA*SR(I)/SR(I+1)*(W(3,I,J,K+1)/W(1,I,J,K+1))
     AA(4*I-1,3 )=-BATA*SR(I)/SR(I+1)*(W(2,I,J,K+1)/W(1,I,J,K+1))
     AA(4*I-1,4 )=0.
     AA(4*I  ,1)= BATA*SR(I)/SR(I+1)*(W(2,I,J,K+1)*W(4,I,J,K+1)
     1/W(1,I,J,K+1)**2)
     AA(4*I  ,2)=-BATA*SR(I)/SR(I+1)*(W(4,I,J,K+1)/W(1,I,J,K+1))
     AA(4*I  ,3)= 0.
     AA(4*I  ,4)=-BATA*SR(I)/SR(I+1)*(W(2,I,J,K+1)/W(1,I,J,K+1))
 155 CONTINUE
     IF (I .EQ. IP) GO TO 156
     AA(4*I-3,9)=0.
     AA(4*I-3,10)=+BATA*SR(I+2)/SR(I+1)
     AA(4*I-3,11)=0.
     AA(4*I-3,12)=0.
     AA(4*I-2,9)=+BATA*SR(I+2)/SR(I+1)*((FK-1.)*EI(I+2,J,K+1)
     1-(W(2,I+2,J,K+1)/W(1,I+2,J,K+1))**2)
     AA(4*I-2,10)=BATA*SR(I+2)/SR(I+1)*(2.*W(2,I+2,J,K+1)/
     1W(1,I+2,J,K+1))
     AA(4*I-2,11)=0.
     AA(4*I-2,12)=0.
     AA(4*I-1,9)=-BATA*SR(I+2)/SR(I+1)*(W(2,I+2,J,K+1)*W(3,I+2,J,K+1)
     1/W(1,I+2,J,K+1)**2)
     AA(4*I-1,10)=+BATA*SR(I+2)/SR(I+1)*(W(3,I+2,J,K+1)/W(1,I+2,J,K+1))
     AA(4*I-1,11)=+BATA*SR(I+2)/SR(I+1)*(W(2,I+2,J,K+1)/W(1,I+2,J,K+1))
```

```
      AA(4*I-1,12)=0.
      AA(4*I  ,9)=-BATA*SR(I+2)/SR(I+1)*(W(2,I+2,J,K+1)*W(4,I+2,J,K+1)
     1/W(1,I+2,J,K+1)**2)
      AA(4*I  ,10)=+BATA*SR(I+2)/SR(I+1)*(W(4,I+2,J,K+1)/W(1,I+2,J,K+1))
      AA(4*I  ,11)= 0.
      AA(4*I  ,12)=+BATA*SR(I+2)/SR(I+1)*(W(2,I+2,J,K+1)/W(1,I+2,J,K+1))
  156 CONTINUE
      AA(4*I-3,5)=1.
      AA(4*I-3,6)=0.
      AA(4*I-3,7)=0.
      AA(4*I-3,8)=0.
      AA(4*I-2,5)=0.
      AA(4*I-2,6)=1.
      AA(4*I-2,7)=0.
      AA(4*I-2,8)=0.
      AA(4*I-1,5)=0.
      AA(4*I-1,6)=0.
      AA(4*I-1,7)=1.
      AA(4*I-1,8)=0.
      AA(4*I  ,5)=0.
      AA(4*I  ,6)=0.
      AA(4*I  ,7)=0.
      AA(4*I  ,8)=1.
  154 CONTINUE
      IPP=4*IP
      DO 165 I=5,IPP,4
      DO 166 L=1,4
      DO 167 LL=1,4
      BB(L,LL)=0.
      DO 168 LLL=1,4
      IF (ABS(AA(I+L-1,LLL)) .LT. TMALL) AA(I+L-1,LLL)=0.
      IF (ABS(AA(I+LLL-5,8+LL)) .LT. TMALL) AA(I+LLL-5,8+LL)=0.
  168 BB(L,LL)=BB(L,LL) + AA(I+L-1,LLL)*AA(I+LLL-5,8+LL)
  167 CONTINUE
  166 CONTINUE
      DO 169 L=1,4
  169 AA(I-1+L,5)=AA(I-1+L,5)-BB(L,1)
      DO 170 L=1,3
  170 AA(I,5+L)=(AA(I,5+L)-BB(1,L+1))/AA(I,5)
      IF (I .EQ. (IPP-3)) GO TO 971
      DO 171 L=1,4
  171 AA(I,8+L)=AA(I,8+L)/AA(I,5)
  971 CONTINUE
      DO 172 L=1,3
  172 AA(I+L,6)=AA(I+L,6)-BB(L+1,2)-AA(I+L,5)*AA(I,6)
      DO 173 L=1,2
  173 AA(I+1,6+L)=(AA(I+1,6+L)-BB(2,2+L)-AA(I+1,5)*AA(I,6+L))/AA(I+1,6)
      IF (I .EQ. (IPP-3)) GO TO 191
      DO 174 L=1,4
      AA(I+L+3,2)=AA(I+L+3,2)-AA(I+L+3,1)*AA(I,6)
      AA(I+1,8+L)=(AA(I+1,8+L)-AA(I+1,5)*AA(I,8+L))/AA(I+1,6)
  174 CONTINUE
  191 CONTINUE
```

```
      DO 175 L=1,2
  175 AA(I+L+1,7)=AA(I+L+1,7)-BB(2+L,3)-AA(I+L+1,5)*AA(I,7)-
     1AA(I+L+1,6)*AA(I+1,7)
      AA(I+2,8)=(AA(I+2,8)-BB(3,4)-AA(I+2,5)*AA(I,8)-AA(I+2,6)*AA(I+1,8)
     2)/AA(I+2,7)
      IF (I .EQ. (IPP-3)) GO TO 190
      DO 176 L=1,4
      DO 177 LL=1,2
      AA(I+L+3,3)=AA(I+L+3,3)-AA(I+L+3,LL)*AA(I+LL-1,7)
      AA(I+2,8+L)=AA(I+2,8+L)-AA(I+2,4+LL)*AA(I+LL-1,8+L)
  177 CONTINUE
      AA(I+2,8+L)=AA(I+2,8+L)/AA(I+2,7)
  176 CONTINUE
  190 CONTINUE
      AA(I+3,8)=AA(I+3,8)-BB(4,4)-AA(I+3,5)*AA(I,8)-AA(I+3,6)*AA(I+1,8)
     1-AA(I+3,7)*AA(I+2,8)
      IF (I .EQ. (IPP-3)) GO TO 180
      DO 178 L=1,4
      DO 179 LL=1,3
      AA(I+L+3,4)= AA(I+L+3,4)-AA(I+L+3,LL)*AA(I+LL-1,8)
      AA(I+3,8+L)= AA(I+3,8+L)-AA(I+3,4+LL)*AA(I+LL-1,8+L)
  179 CONTINUE
      AA(I+3,8+L)= AA(I+3,8+L)/AA(I+3,8)
  178 CONTINUE
  180 CONTINUE
      DO 181 L=1,4
      DO 182 LL=1,4
      IF (ABS(AA(I+L-1,LL)).LT.TMALL) AA(I+L-1,LL)=0.
      IF (ABS(F(LL,(I+7)/4-1,J,K+2)) .LT. TMALL)
     1F(LL,(I+7)/4-1,J,K+2)=0.
  182 F(L,(I+7)/4,J,K+2)=F(L,(I+7)/4,J,K+2)-AA(I+L-1,LL)*F(LL,(I+7)/4-1
     1,J,K+2)
      LE=L-1
      IF (L .EQ. 1) GO TO 184
      DO 183 LL=1,LE
      F(L,(I+7)/4,J,K+2)=F(L,(I+7)/4,J,K+2)-AA(I+L-1,4+LL)*F(LL,(I+7)/4
     1,J,K+2)
  183 CONTINUE
  184 CONTINUE
      F(L,(I+7)/4,J,K+2)=F(L,(I+7)/4,J,K+2)/AA(I+L-1,5+L-1)
  181 CONTINUE
  165 CONTINUE
      W(4,IE,J,K+2)=F(4,IE,J,K+2)
      W(3,IE,J,K+2)=F(3,IE,J,K+2)-AA(IPP-1,8)*W(4,IE,J,K+2)
      W(2,IE,J,K+2)=F(2,IE,J,K+2)-AA(IPP-2,8)*W(4,IE,J,K+2)
     1-AA(IPP-2,7)*W(3,IE,J,K+2)
      W(1,IE,J,K+2)=F(1,IE,J,K+2)-AA(IPP-3,8)*W(4,IE,J,K+2)
     1-AA(IPP-3,7)*W(3,IE,J,K+2)-AA(IPP-3,6)*W(2,IE,J,K+2)
      DO 192 I=5,IPP,4
      II=IPP+5-I-4
      DO 193 L=1,4
      BB(1,L)=0.
      DO 194 LL=1,4
```

```
      IF (ABS(AA(II+1-L,8+LL)) .LT. TMALL) AA(II+1-L,8+LL)=0.
      IF (ABS(W(LL,(II+4)/4+1,J,K+2)) .LT. TMALL)
     1W(LL,(II+4)/4+1,J,K+2)=0.
  194 BB(1,L)=BB(1,L)+AA(II+1-L,8+LL)*W(LL,(II+4)/4+1,J,K+2)
  193 CONTINUE
      W(4,(II+4)/4,J,K+2)=F(4,(II+4)/4,J,K+2)-BB(1,1)
      W(3,(II+4)/4,J,K+2)=F(3,(II+4)/4,J,K+2)-BB(1,2)
     1-AA(II-1,8)*W(4,(II+4)/4,J,K+2)
      W(2,(II+4)/4,J,K+2)=F(2,(II+4)/4,J,K+2)-BB(1,3)
     1-AA(II-2,8)*W(4,(II+4)/4,J,K+2)-AA(II-2,7)*W(3,(II+4)/4,J,K+2)
      W(1,(II+4)/4,J,K+2)=F(1,(II+4)/4,J,K+2)-BB(1,4)
     1-AA(II-3,8)*W(4,(II+4)/4,J,K+2)-AA(II-3,7)*W(3,(II+4)/4,J,K+2)
     2-AA(II-3,6)*W(2,(II+4)/4,J,K+2)
  192 CONTINUE
  153 CONTINUE
      RETURN
      END



C...THIS SUBROUTINE REDUCES A TRI-DIAGONAL MATRIX USING THE CROUT
C...METHOD.



      SUBROUTINE CROUT(M,K,IB,IE,JB,JE,IP,JP,GA,GB,GC,GD,PSI,JD,ID)

      LCM (CROUT)
      DIMENSION AA(21, 3),E(21),X(21),GA(21,22),GB(21,22),GC(21,22),
     1GD(21,22),PSI(21,22,2)

      SMALL=0.10E-22
      IF (MOD(M,2) .EQ. 1) GO TO 3
      GO TO 2
    3 CONTINUE
      JS=1
      DO 123 I=IB,IE
      DO 122 J=JS,JP
      E(J)=GD(I,J+1)
      AA(J,2)=GB(I,J+1)
      IF (J .EQ. JP) GO TO 124
      IF (J .EQ. JS) GO TO 125
      AA(J,3  )=-GA(I,J+1)
      GO TO 125
  124 E(JP)=GD(I,JP+1)+GA(I,JP+1)*PSI(I,JP+2,2)
  125 CONTINUE
      IF (J .EQ. JS) GO TO 126
      AA(J,1  )=-GC(I,J+1)
      GO TO 127
  126 AA(JS,3)=-(GA(I,JS+1)+GC(I,JS+1))
  127 CONTINUE
```

```
  122 CONTINUE
      AA(JS,3   )=AA(JS,3   )/AA(JS,2 )
      E(JS)=E(JS)/AA(JS,2 )
      DO 130 J=JB,JP
      IF (ABS(AA(J,  1)) .LE. SMALL) AA(J,  1)=0.
      IF (ABS(AA(J-1,3)) .LE. SMALL ) AA(J-1,3)=0.
      AA(J,2)=AA(J,2)-AA(J,1  )*AA(J-1,3)
      IF (ABS(E(J-1)) .LE. SMALL) E(J-1)=0.
      E(J)=(E(J)-AA(J,  1)*E(J-1))/AA(J,2)
      IF (J .EQ. JP) GO TO 131
      AA(J,3  )=AA(J,3  )/AA(J,2)
  131 CONTINUE
  130 CONTINUE
      X(JP)=E(JP)
      JQ=JP-1
      DO 133 J=JS,JQ
      KK=JQ+JS-J
      IF (ABS(AA(KK,3  )) .LE. SMALL) AA(KK,3  )=0.
      IF (ABS(X(KK+1)) .LE. SMALL) X(KK+1)=0.
      X(KK)=E(KK)-AA(KK,3  )*X(KK+1)
  133 CONTINUE
      DO 128 J=JS,JP
      PSI(I,J+1,2)=X(J)
      IF (ABS(PSI(I,J+1,2)) .LT. SMALL) PSI(I,J+1,2)=0.
  128 CONTINUE
  123 CONTINUE
      GO TO 4
    2 CONTINUE
      IS=1
      DO 23 J=JB,JE
      DO 22 I=IS,IP
      E(I)=GD(I+1,J)
      AA(I,2)=GB(I+1,J)
      IF (I .EQ. IP) GO TO 24
      AA(I,3  )=-GA(I+1,J)
      GO TO 25
   24 E(IP)=GD(IP+1,J)+GA(IP+1,J)*PSI(IP+2,J,2)
   25 CONTINUE
      IF (I .EQ. IS) GO TO 26
      AA(I,  1)=-GC(I+1,J)
      GO TO 27
   26 CONTINUE
      E(IS)=GD(IS+1,J)+GC(IS+1,J)*PSI(IS,J,2)
   27 CONTINUE
   22 CONTINUE
      AA(IS,3   )=AA(IS,3   )/AA(IS,2 )
      E(IS)=E(IS)/AA(IS,2 )
      DO 30 I=IB,IP
      IF (ABS(AA(I,  1)) .LE. SMALL) AA(I,  1)=0.
      IF (ABS(AA(I-1,3)) .LE. SMALL) AA(I-1,3)=0.
      AA(I,2)=AA(I,2)-AA(I,  1)*AA(I-1,3)
      IF (ABS(E(I-1)) .LE. SMALL) E(I-1)=0.
      E(I)=(E(I)-AA(I,  1)*E(I-1))/AA(I,2)
```

```
      IF (I .EQ. IP) GO TO 31
      AA(I,3  )=AA(I,3  )/AA(I,2)
   31 CONTINUE
   30 CONTINUE
      X(IP)=E(IP)
      IQ=IP-1
      DO 33 I=IS,IQ
      KK=IQ+IS-I
      IF (ABS(AA(KK,3  )) .LE. SMALL) AA(KK,3  )=0.
      IF (ABS(X(KK+1)) .LE. SMALL) X(KK+1)=0.
      X(KK)=E(KK)-AA(KK,3  )*X(KK+1)
   33 CONTINUE
      DO 28 I=IS,IP
      PSI(I+1,J,2)=X(I)
      IF (ABS(PSI(I+1,J,2)) .LT. SMALL) PSI(I+1,J,2)=0.
   28 CONTINUE
   23 CONTINUE
    4 CONTINUE
      RETURN
      END



C...PLOTTING SUBROUTINE.


      SUBROUTINE PLOT1(P,CRS,SR,ID,JD,M,RO)

      LCM (PLOT1)
      DIMENSION P(6,21),SR(21),PP(21),P1(12),P2(12),CRS(2,21,22)
     1,C(20),P3(4),P4(12),CRS1(21,22),RO(21,22),XX(21,22),YY(21,22)

      DATA P1/"TEMPERAT","URE","DENSITY"," ","CURRENT.",
     1"DENSITY","POLOIDAL"," FIELD","TOROIDAL"," FIELD","PRESSURE",
     2" "/,P2/"KELVIN"," ","NORMALIZ","ED","STATAMPS","/CM**2",
     3"GAUSS"," ","GAUSS"," ","DYNES/CM","**2"/
      DATA P3/"POLOIDAL","  FLUX","TOROIDAL"," CURRENT"/
      DATA P4/"0.5 USEC","1.0 USEC","1.5 USEC","2.0 USEC","2.5 USEC",
     1"3.0 USEC","3.5 USEC","4.0 USEC","4.5 USEC","5.0 USEC","5.5 USEC",
     2"6.0 USEC"/
 1001 FORMAT(2A8)
      DO 1 I=1,6
      AMAX=0.
      AMIN=0.
      DO 2 J=1,ID
      PP(J)=P(I,J)
      AMAX=AMAX1(PP(J),AMAX)
      AMIN=AMIN1(PP(J),AMIN)
2     CONTINUE
      CALL MAPS(2.,4.,AMIN,AMAX,.1,1.,.3,1.)
      CALL TRACE(SR,PP,ID)
      CALL SETCH(20.,5.,0,0,3,0)
```

```
      CALL CRTBCD("NORMALIZED RADIUS")
      CALL SETCH(2.,20.,0,0,3,1)
      WOT 100,1001,P1(2*I-1),P1(2*I)
      CALL SETCH(2.,1.,0,0,2,0)
      CALL CRTBCD("Z=0;  VESSEL HALF-WIDTH=7.5 CM")
      CALL SETCH(2.,3.,0,0,2,0)
      CALL CRTBCD("UNITS=")
      CALL SETCH(10.,3.,0,0,2,0)
      WOT 100,1001,P2(2*I-1),P2(2*I)
      CALL SETCH(2.,2.,0,0,2,0)
      CALL CRTBCD("TIME=")
      CALL SETCH(10.,2.,0,0,2,0)
      IF (M .LT. 250) CALL CRTBCD("INITIAL CONDITIONS")
      IF (M .LT. 250) GO TO 3
      WOT 100,1001,P4(M/250)
3     CALL FRAME
1     CONTINUE
      DO 4 N=1,2
      AMAX=0.
      AMIN=0.
      DO 5 I=1,ID
      DO 5 J=1,JD
      AMAX=AMAX1(CRS(N,I,J),AMAX)
      AMIN=AMIN1(CRS(N,I,J),AMIN)
      CRS1(I,J)=CRS(N,I,J)
5      CONTINUE
      K1=-20
      K2=0
      C(1)=AMAX
      C(2)=AMIN
      CALL MAPS(1.,21.,1.,22.,.25,1.,.25,1.)
      CALL ACONTR(K1,C,K2,CRS1,21,1,21,1,1,22,1)
      CALL SETCH(26.,3.,0,0,3,0)
      CALL CRTBCD("RADIAL GRID")
      CALL SETCH(2.,2.,0,0,2,0)
      WOT 100,1001,P3(2*N-1),P3(2*N)
      CALL SETCH(2.,1.,0,0,2,0)
      CALL CRTBCD("TIME=")
      CALL SETCH(10.,1.,0,0,2,0)
      IF (M .LT. 250) CALL CRTBCD("INITIAL CONDITIONS")
      IF (M .LT.250) GO TO 6
      WOT 100,1001,P4(M/250)
6     CALL SETCH(1.,20.,0,0,3,1)
      CALL CRTBCD("VERTICAL GRID    ")
      CALL FRAME
4     CONTINUE
      NX=21
      NXD=NX
      NY=22
      CALL PICTURE(RO,XX,YY,NX,NY,NXD,21.,22.,60.,60.,60.,0.,5.,2.,
     1-2,2,0,1,NX,1,NY,.1,1.,.2,1.)
      CALL SETCH(3,2,0,0,3,0)
      CALL CRTBCD(" DENSITY")
```

```
1803        CALL FRAME
1804        RETURN
1805        END
```

```
C...CODE:  ONE-DIMENSIONAL DIFFUSION
C...WRITTEN BY:  R. IZZO AND G. ERLEBACHER
C...LANGUAGE:  FORTRAN
C...COMPILER:  CDC 7600


C...SINGLE-FLUID, RESISTIVE MHD EQUATIONS WITHOUT INERTIAL TERMS
C...ARE SOLVED IN ONE DIMENSION.  A CORONAL EQUILIBRIUM IS ASSUMED
C...FOR RADIATIVE LOSSES.

C...VARIABLES ARE DEFINED AS WE ENCOUNTER THEM IN THE CODE.


C**************PROGRAM BEGINS**************

*SELECT PRINTLOG=LOGD
*FILE NAME=DIF

      COMMON/C2/AA(101),BB(101),CC(101),EE(101)
      COMMON/PLT/P1(8),P5(12),P6(12),P7(12)
      COMMON/PL1/RLO,NB,TT1

      DIMENSION P(101),XI(101),V(101),S(101),D1(101),D2(101),D3(101),
     1D5(101),D6(101),CHI(101),RS1(101),RS2(101),R1(101),Q1(101)
     2,BT(101),BP(101),RN(101),R(101),T(101),PSI(101),RS3(101),D4(101)
      DIMENSION WR(101),Z(2),RJT(101),RK(101),TDERIV2(101),
     1RN1(101),RJP(101),PR(4,101),PA(4,6,101),XLZ(4,101),PERC(2)

      DATA P1/"TIME  "," SEC","RADIUS","TIME STEP"," NO ",
     1"CHAR. ","LENGTH  = "," CM"/,P5/2*("CHAR. FI","ELD   = "),
     2"CHAR. CU","RRENT = ","CHAR. TE","MPER. = ","CHAR. DE",
     3"NSITY = ","CHAR. PR","ESSURE = "/,P6/2*(" GAUSS ","       "),
     4" STAT/ ","CM(2) "," KELVI","N     "," CM(-3",")     ",
     5" DYNES","/CM(2)"/,P7/"POLOIDAL"," FIELD  ","TOROIDAL",
     6" FIELD  ","TOROIDAL"," CURRENT","TEMPERAT","URE     ",
     7"DENSITY ","         ","PRESSURE","        "/

      CALL DROPFILE(0)
      CALL OPEN(10,"DATA",0,LEN)
      CALL CREATE(12,"OUT1",3,-1)

C...TTT:  TOTAL TIME ELAPSED
C...NB:  CYCLE NUMBER
      TTT=0.
      NB=0

      CALL KEEP80(1,2)
      CALL DD80ID(9HDIFFUSION,1)
      CALL KEEP80(8HDIFGRAPH,2)
      CALL DDERS(0)

```

```
C...N:  NUMBER OF GRID SPACES
C...R(1):  RADIUS OF INNER WALL (CM)
C...R(N+1):  RADIUS OF OUTER WALL (CM)
C...TT1:  TIME STEP
C...TMX:  MAXIMUM SIMULATION TIME
C...ZZ:  ION MASS/HYDROGEN MASS
C...Z(I):  ATOMIC NUMBER OF IMPURITY I
C...TO:  CHARACTERISTIC TEMPERATURE
C...RLO:  CHARACTERISTIC LENGTH
C...BO:  CHARACTERISTIC FIELD
C...RNO:  CHARACTERISTIC NUMBER DENSITY
      READ(10,480) N
      READ(10,481) R(1),R(N+1),TT1,TMX,ZZ,(Z(I),I=1,2)
      READ(10,482) TO,RLO,BO,RNO

C...IMPURITY 1 (OXYGEN) AS A PERCENTAGE OF HELIUM NUMBER DENSITY
C...IMPURITY 2 (SILICON) AS A PERCENTAGE OF HELIUM NUMBER DENSITY
      PERC(1)=.005
      PERC(2)=.005

480   FORMAT(I3)
481   FORMAT(E13.6/E13.6/E13.6/E13.6/F6.4/F6.4/F6.4)
482   FORMAT(E13.6/E13.6/E13.6/E13.6)
 483  FORMAT(1H1,"THE TEMPERATURE HAS EXCEEDED   ",E13.6)

C...NN:  NUMBER OF GRID POINTS
C...CLT: SPEED OF LIGHT IN VACUUM
C...BLZ:  BOLTZMAN'S CONSTANT
C...PO:  CHARACTERISTIC PRESSURE
C...BETA: HALF THE STANDARD PLASMA BETA
C...RJO:  CHARACTERISTIC CURRENT DENSITY
C...XLAMO:  CHARACTERISTIC COULOMB LOGARITHM
C...RKO:  CHARACTERISTIC THERMAL CONDUCTIVITY
C...ZEFF: PLASMA Z-EFFECTIVE
C...SO:  CHARACTERISTIC ELECTRICAL CONDUCTIVITY
C...TBO:  MAGNETIC DIFFUSION TIME
C...THO: CHARACTERISTIC THERMAL DIFFUSION TIME
C...RMGDIF: RATIO OF CHARACTERISTIC TIME TO MAGNETIC DIFFUSION TIME
C...TTO: CHARACTERISTIC TIME SCALE
C...VO:  CHARACTERISTIC VELOCITY
C...THDIF: RATIO OF CHARACTERISTIC TIME TO THERMAL DIFFUSION TIME
C...GAM: RATIO OF SPECIFIC HEATS MINUS ONE
      NN=N+1
      PI=3.1415927
      CLT=3.E10
      BLZ=1.38E-16
      PO=BLZ*RNO*TO
      BETA=4*PI*PO/BO**2
      RJO=CLT*BO/(4*PI*RLO)
      XLAMO=6.2E3*SQRT(TO*TO*TO/2./RNO)
      XLNLO=ALOG(XLAMO)
      RKO=29.6E-18*XLNLO*RNO*RNO/BO/BO/SQRT(TO)
      ZEFF=2.
```

```
      SO=2.E7*(TO**1.5)/ZEFF/XLNLO
      TBO=4*PI*SO*(RLO/CLT)**2
      THO=1.5*RNO*BLZ*RLO**2/RKO
      RMGDIF=1.
      TTO=TBO
      VO=RLO/TTO
      THDIF=TTO/THO
      GAM=2./3.
      DELTA=GAM*RMGDIF/BETA

C...SOME RADIATION PARAMETERS
C...PRO: NORMALIZATION FACTOR FOR RADIATED POWER LOSS.
C...TO AND TS:  TEMPERATURE RANGES FOR DIFFERENT POLYNOMIAL FITS
C...            TO OXYGEN AND SILICON COOLING CURVES.
      PRO=PO/TTO/GAM
      TO1=5.*11600./TO
      TO2=20.*11600./TO
      TO3=200.*11600./TO
      TS1=20.*11600./TO
      TS2=200.*11600./TO
      TS3=2000.*11600./TO
C...H:  NORMALIZED GRID SPACING
C...TAU:  NORMALIZED TIME STEP
C...TBT:  DECAY TIME OF TOROIDAL FIELD
C...TBP1:  DECAY TIME OF INNER TOROIDAL CURRENT
C...TBPNN:  DECAY TIME OF OUTER TOROIDAL CURRENT
C...RLAM:  A FREQUENTLY APPEARING NUMBER
      H=(R(N+1)-R(1))/(RLO*N)
      TAU=TT1/TTO
      TBT=2.E-1
      TBP1=10.E-5
      TBPNN=4.E-5
      RLAM=2*H**2/TAU

C...DISCRETIZING THE RADIAL COORDINATE
      R(1)=R(1)/RLO
      DO 105 J=2,N+1
      R(J)=R(J-1)+H
105   CONTINUE

C***************INITIAL CONDITIONS***************
C...PW:  PLASMA WIDTH
C...RNPK:  PEAK PLASMA NUMBER DENSITY
C...RLOW:  CUTOFF DENSITY TO AVOID VACUUM REGION
C...JP:  INITIAL PEAK PLASMA GRID POINT
C...XRN:  DENSITY SHAPE FACTOR (LINEAR)
      PW=6./RLO
      RNPK=1.0E15/RNO
      RLOW=.01
      JP=59
      JPW=PW/H
      JPS=JP - JPW/2
      JPE=JP + JPW/2
```

```
      XRN=1.

C...TW:  TEMPERATURE AT THE WALL
C...TPK:  PEAK PLASMA TEMPERATURE
C...JT:  GRID POINT OF PEAK
C...JTS:  START OF NON-LINEAR TEMPERATURE PROFILE
C...JTE:  END OF NON-LINEAR TEMPERATURE PROFILE
C...XTL AND XTR:  TEMPERATURE SHAPE FACTORS
      TPK=75.E4/TO
      TW=1.0E4/TO
      JT=JP
      JTS=JPS
      JTE=JPE
      XTL=2
      XTR=2

C...PCURR:  PLASMA CURRENT
C...PH:  PLASMA HEIGHT
C...JJ:  LOCATION OF PEAK CURRENT DENSITY
C...JJS AND JJE:  BEGINNING AND END OF CURRENT DISTRIBUTION
C...XJL AND XJR:  CURRENT DENSITY SHAPE FACTORS
C...BP(NN):  Z-COMPONENT OF MAGNETIC FIELD AT OUTER WALL
C...PSI1:  FLUX THROUGH HOLE OF TORUS
C...XO:  INITIAL VACUUM POLOIDAL CURRENT FUNCTION
C...PWELL:  DEPTH OF TOROIDAL FIELD WELL
C...JBT,JBTS,JBTE:  LOWEST POINT OF WELL, START AND END OF DEVIATION
C.....                FROM VACUUM BEHAVIOR FOR THE TOROIDAL FIELD
C...XBTL,XBTR:  TOROIDAL FIELD SHAPE FACTORS
      PCURR=-3.E9*25.E3
      PH=12.
      JJS=JPS-5
      JJ=JP
      JJE=JPE+5
      XJL=1.5
      XJR=1.5
      BP(NN)=1500./BO
      PSI(1)=1.5E5/BO/RLO/RLO
      PSI1=PSI(1)
      XO=82.5E3/RLO/BO
      PWELL=.10
      JBTS=JPS
      JBT=JP
      JBTE=JPE
      XBTL=1
      XBTR=1

C...COMPUTE INITIAL PLASMA DENSITY PROFILE
      DO 106 J=1,NN
      IF ((J .LT. JPS) .OR. (J .GT.JPE)) RN(J)=RLOW
      IF ((J .GE. JPS) .AND. (J .LE. JPE)) RN(J)= RLOW +
     1RNPK*(1. -(ABS((R(J)-R(JP))/(R(JPS)-R(JP))))**XRN)
  106 CONTINUE

```

```
      DO 106 J=JT,JTE
      TDERIV2(J)=TDERIV3*((R(J)-R(JT))/(R(JTE)-R(JT)))**XTR
  108 CONTINUE
      T(1)=TW
      DO 109 J=2,NN
      IF (J .LE. JTS) T(J)=T(J-1) + TDERIV1*H
      IF ((J .GT. JTS) .AND. (J .LE. JT)) T(J)=T(J-1) +
     1H/2.*(TDERIV2(J) + TDERIV2(J-1))
      IF ((J .GT. JT) .AND. (J .LE. JTE)) T(J)=T(J-1) +
     1(TDERIV2(J) + TDERIV2(J-1))*H/2.
      IF (J .GT. JTE) T(J)=T(J-1) + TDERIV3*H
  109 CONTINUE

C...COMPUTE TOROIDAL CURRENT DENSITY PROFILE AS DESCRIBED IN THESIS
      RJPK=PCURR/PH/RLO/RJO/((R(JJ)-R(JJS))/(XJL+1.) +
     1(R(JJE)-R(JJ))/(XJR+1.))
      DO 110 J=1,NN
      IF ((J .LE. JJS) .OR. (J .GE. JJE)) RJT(J)=0.
      IF ((J .GT. JJS) .AND. (J .LE. JJ)) RJT(J)=RJPK*((R(J)-R(JJS))
     1/(R(JJ)-R(JJS)))**XJL
      IF ((J .GT. JJ) .AND. (J .LE. JJE)) RJT(J)=RJPK*((R(JJE)-R(J))
     1/(R(JJE)-R(JJ)))**XJR
  110 CONTINUE

C...INTEGRATE TOROIDAL CURRENT DENSITY TO GET Z-COMPONENT OF MAGNETIC
C...FIELD.
      DO 111 J=2,NN
      K=NN+1-J
      BP(K)=BP(K+1)+H/2.*(RJT(K+1)+RJT(K))
  111 CONTINUE
      BP1=BP(1)
      BPNN=BP(NN)

C...INTEGRATE FIELD TO GET POLOIDAL FLUX
      DO 112 J=2,NN
      PSI(J)=PSI(J-1)+H*(R(J)*BP(J)+R(J-1)*BP(J-1))/2.
  112 CONTINUE
C...COMPUTE INITIAL TOROIDAL MAGNETIC FIELD
      DO 113 J=1,NN
      IF ((J .LE. JBTS) .OR. (J .GE. JBTE)) BT(J)=XO/R(J)
      IF ((J .GT. JBTS) .AND. (J .LE. JBT)) BT(J)=
     1XO*(1.-((R(J)-R(JBTS))/(R(JBT)-R(JBTS)))**XBTL*PWELL)/R(J)
```

```
276 17500 FORMAT(//1H ,"CHARACTERISTIC VALUES OF INITIAL AND DIMENSIONLESS"
277      1," PARAMETERS"//5H BO= ,E11.4," GAUSS"/5H TO= ,E11.4,
278      2" KELVIN"/5H RNO= ,E11.4," CM(-3)"/
279      35H RLO= ,E11.4," CM"/5H SO= ,E11.4," SEC(-1)"/5H RKO= ,
280      4E11.4," ERG/(CM SEC K)"/5H PO= ,E11.4," DYNES/CM(2)"/5H RJO= ,
281      5E11.4," STATAMP/CM(2)"/6H VO= ,E11.4," CM/SEC"/7H BETA= ,
282      6E11.4/6H TTO= ,E11.4, "SEC")
283 27500 FORMAT(/6H TBO= ,E11.4," SEC"/5H THO= ,E11.4," SEC"/
284      18H RMGDIF= ,E11.4/8H THDIF= ,E11.4/6H GAM= ,E11.4/8H DELTA= ,
285      2E11.4/4H N= ,I2/4H H= ,E11.4/6H TAU= ,E11.4/6H RLAM= ,E11.4///)
286
287 C...MW:  TIME STEPS BETWEEN OUTPUT
288       MW=100
289 C     SGA=(T(1))**1.5
290  1    NB=TTT/TT1
291       M=NB+1
292       RNAVG=1.
293
294 C...
295 C...CALCULATE INITIAL PRESSURE, ELECTRICAL CONDUCTIVITY, THERMAL
296 C...CONDUCTIVITY, POLOIDAL FLUX AND COULOMB LOGARITHM.  ALSO,
297 C...COMPUTE SOME GEOMETRIC FACTORS THAT ARE OFTEN USED IN LATERR
298 C...CALCULATIONS.
299       DO 10 J=1,N+1
300       XLAM=6.2E3*SQRT((T(J)*TO)**3/(2.*RN(J)*RNO))
301       XLNL=ALOG(XLAM)
302       RK(J)=XLNL/XLNLO*RNAVG*RNAVG/SQRT(T(J))/(BT(J)*BT(J)+BP(J)*BP(J))
303       P(J)=RN(J)*T(J)
304       S(J)=XLNLO/XLNL*T(J)**1.5
305       CHI(J)=R(J)*BT(J)
306       D2(J)=(GAM+1)*BETA*P(J)+BP(J)**2+BT(J)**2
307       RS1(J)=R(J)/S(J)
308       RS2(J)=1./(R(J)*S(J))
309       RS3(J)=R(J)*S(J)
310 C...SET RESISTIVITY HIGH IN LOW DENSITY REGIONS.
311 C     IF ((J .EQ. 1) .OR. (J .EQ. NN)) GO TO 10
312 C     RO=(RN(J-1)+RN(J)+RN(J+1))/3.
313 C     IF (RO .LE. .25) S(J)=SGA
314 10    CONTINUE
315 C     S(1)=SGA
316 C     S(NN)=SGA
317
318 C EVALUATION OF RADIATION PARAMETERS AS PER POST, ET AL,.
```

```
      DO 11 J=1,N+1
      IF ((T(J) .GE. T01) .AND. (T(J) .LE. T02)) GO TO 15
      IF ((T(J) .GT. T02) .AND. (T(J) .LE. T03)) GO TO 16
      IF (T(J) .LT. T01) GO TO 11
      IF (T(J) .GT. T03) WRITE (12,483) T03
      GO TO 1995
15    PA(1,1,J)=652.374
      PA(1,2,J)=1835.499
      PA(1,3,J)=1984.266
      PA(1,4,J)=1059.846
      PA(1,5,J)=280.0476
      PA(1,6,J)=29.33792
      GO TO 11
16    PA(1,1,J)=-55.15118
      PA(1,2,J)=-154.3956
      PA(1,3,J)=-248.992
      PA(1,4,J)=-180.8154
      PA(1,5,J)=-57.64175
      PA(1,6,J)=-6.149181
11    CONTINUE
      DO 12 J=1,N+1
      IF ((T(J) .GE. TS1) .AND. (T(J) .LE. TS2)) GO TO 13
      IF ((T(J) .GT. TS2) .AND. (T(J) .LE. TS3)) GO TO 14
      IF (T(J) .LT. TS1) GO TO 12
      IF (T(J) .GT. TS3) WRITE (12,483) TS3
      GO TO 1995
13    PA(2,1,J)=-52.75519
      PA(2,2,J)=-134.613
      PA(2,3,J)=-208.2753
      PA(2,4,J)=-159.1874
      PA(2,5,J)=-59.89162
      PA(2,6,J)=-8.684849
      GO TO 12
14    PA(2,1,J)=-19.54323
      PA(2,2,J)=.0499481
      PA(2,3,J)=-5.726766
      PA(2,4,J)=-2.710884
      PA(2,5,J)=30.75145
      PA(2,6,J)=26.89966
12    CONTINUE

C...COMPUTE THE POWER RADIATED BY OXYGEN AT GRID POSITION J (PR(1,J))
C...AND THAT RADIATED BY SILICON AT THE SAME POSITION (PR(2,J)).
      DO 17 I=1,2
      DO 18 J=1,N+1
      XXLZ=PA(I,1,J)
      XLOG=ALOG10(T(J)*TO/11600./1000.)
      DO 19 K=1,5
      XLOGK=(ABS(XLOG))**K
      IF ((XLOG .LT. 0.) .AND. (MOD(K,2) .EQ. 1)) XLOGK=-XLOGK
      XXLZ=XXLZ+ PA(I,K+1,J)*XLOGK
19    CONTINUE
      XLZ(I,J)=10.**XXLZ
```

```
      IF (T(J) .LT. T01) XLZ(1,J)=0.
      IF (T(J) .LT. TS1) XLZ(2,J)=0.
      IF ((J .EQ. 1) .OR. (J .EQ. NN)) GO TO 181
      RO=(RN(J-1)+RN(J)+RN(J+1))/3.
      IF (RO .LT. RLOW) RO =RLOW
      IF (RO .GT. .25) GO TO 181
      PR(I,J)=2.*RN(J)*.005/RO*RN(J)*XLZ(I,J)*RNO*RNO/PRO
      GO TO 18
  181 PR(I,J)=2.*RN(J)*PERC(I)*RN(J)*XLZ(I,J)*RNO*RNO/PRO
   18 CONTINUE
   17 CONTINUE

C...  EVALUATION OF DIFFUSION SPEED
C... RJT,RJP:  TOROIDAL AND POLOIDAL CURRENT DENSITY
      DO 20 J=2,N
      RJT(J)=-(BP(J+1)-BP(J-1))/(H*2.)
      RJP(J)=(CHI(J+1)-CHI(J-1))/(2.*H*R(J))
      D1(J)=R(J)*(D2(J+1)/R(J+1)-D2(J-1)/R(J-1))/(2.*H)
      D3(J)=-BT(J)*((BT(J+1)/R(J+1))-(BT(J-1)/R(J-1)))/H
      R1(J)=(RS1(J+1)+RS1(J))*BP(J+1)-(RS1(J+1)+2*RS1(J)+
     1RS1(J-1))*BP(J)+(RS1(J-1)+RS1(J))*BP(J-1)
      R1(J)=R1(J)*RMGDIF/(2.*R(J)*H**2)
      Q1(J)=(RS2(J+1)+RS2(J))*CHI(J+1)-(RS2(J+1)+2*RS2(J)+
     1RS2(J-1))*CHI(J)+(RS2(J-1)+RS2(J))*CHI(J-1)
      Q1(J)=Q1(J)*RMGDIF/(2.*H**2)
      RKGRAD=R(J)*(RK(J+1)-RK(J-1))/2.
      RN1(J)=THDIF/2./R(J)/H/H*(T(J+1)*(RK(J)*(R(J+1)+R(J))
     1+RKGRAD) - T(J)*RK(J)*(R(J+1)+2.*R(J)+R(J-1)) +
     2T(J-1)*(RK(J)*(R(J)+R(J-1)) - RKGRAD)) +
     2DELTA*(RJP(J)**2+RJT(J)**2)/S(J)  -PR(1,J) -PR(2,J)
   20 CONTINUE
      DO 40 J=3,N-1
      D6(J)=(BP(J+1)*R1(J+1)-BP(J-1)*R1(J-1))*R(J)/(2.*H)
     1+(Q1(J+1)*CHI(J+1)*R(J+1)-Q1(J-1)*CHI(J-1)*R(J-1))
     2/(R(J)*2.*H)+BETA*R(J)*(RN1(J+1)-RN1(J-1))/(2.*H)
   40 CONTINUE
      D6(2)=R(2)*(BP(3)*R1(3)-BP(2)*R1(2))/H
     1+(Q1(3)*CHI(3)*R(3)-Q1(2)*CHI(2)*R(2))/(R(2)*H)
     2+BETA*R(2)*(RN1(3)-RN1(2))/H
      D6(N)=R(N)*(BP(N)*R1(N)-BP(N-1)*R1(N-1))/H
     1+(Q1(N)*CHI(N)*R(N)-Q1(N-1)*CHI(N-1)*R(N-1))/(H*R(N))
     2+BETA*R(N)*(RN1(N)-RN1(N-1))/H

C...WE NOW USE THE ABOVE COEFFICIENTS TO SET UP AN EQUATION OF THE
C...FORM A*X(J-1) + B*X(J) + C*X(J+1) = D
      DO 50 J=2,N
      AA(J)=2.*D2(J)-D1(J)*H
      BB(J)=2.*H**2*D3(J)-4.*D2(J)
      CC(J)=D1(J)*H+D2(J)*2
      EE(J)=2.*D6(J)*H**2
   50 CONTINUE
      XI(1)=0.
      XI(N+1)=0.
```

```
425
426 C...SOLVE THE SIMULTANEOUS EQUATIONS AT ALL GRID POINTS BY A DOUBLESWEEP
427 C...METHOD.  OBTAIN THE VARIABLE (VELOCITY*R) AT THE NEW TIME STEP.
428       CALL DBLSWP(XI,N)
429
430 C...COMPUTE THE DIFFUSION VELOCITY
431       DO 55 J=1,N+1
432       V(J)=XI(J)/R(J)
433 55    CONTINUE
434
435 C...OUTPUT INITIAL CONDITIONS AND/OR NEW TIME STEP RESULTS
436       IF (MOD(M,MW) .NE. 1) GO TO 95
437       NBB=NBB+1
438       WRITE(12,9000)NB
439 9000  FORMAT(1H1,"TIME STEP NUMBER ",I4/)
440       WRITE(12,10000)
441       WRITE(12,20000)(R(J),BT(J),BP(J),RJT(J),RJP(J),T(J),RN(J),
442      1V(J),PSI(J),J=1,N+1)
443       PPROL=0.
444       PPROH=0.
445       PPRSL=0.
446       PPRSH=0.
447       DO 56 J=1,N+1
448       IF (RN(J) .GT. 0.1) GO TO 57
449       PPROL=PPROL + PR(1,J)*R(J)
450       PPRSL=PPRSL + PR(2,J)*R(J)
451       GO TO 56
452  57   PPROH=PPROH + PR(1,J)*R(J)
453       PPRSH=PPRSH + PR(2,J)*R(J)
454  56   CONTINUE
455       PPROL=PPROL*PRO*2.*PI*RLO*RLO*PH*H*1.E-13
456       PPRSL=PPRSL*PRO*2.*PI*RLO*RLO*PH*H*1.E-13
457       PPROH=PPROH*PRO*2.*PI*RLO*RLO*PH*H*1.E-13
458       PPRSH=PPRSH*PRO*2.*PI*RLO*RLO*PH*H*1.E-13
459       WRITE (12,5600)PPRSL
460       WRITE (12,5601)PPROH
461       WRITE (12,5602)PPRSL
462       WRITE (12,5603)PPRSH
463  5600 FORMAT(1H,"THE POWER RADIATED BY OXYGEN IN THE LOW DENSITY
464      1  REGION IS (MW)  ",E11.4)
465  5601 FORMAT(1H,"THE POWER RADIATED BY OXYGEN IN THE HIGH DENSITY
466      1  REGION IS (MW)  ",E11.4)
467  5602 FORMAT(1H,"THE POWER RADIATED BY SILICON IN THE LOW DENSITY
468      1  REGION IS (MW)  ",E11.4)
469  5603 FORMAT(1H,"THE POWER RADIATED BY SILICON IN THE HIGH DENSITY
470      1  REGION IS (MW)  ",E11.4)
471
472       CALL PLOT(R,BP,BO,NN,1)
473       CALL PLOT(R,BT,BO,NN,3)
474       CALL PLOT(R,RJT,RJO,NN,5)
475       CALL PLOT(R,T,TO,NN,7)
476       CALL PLOT(R,RN,RNO,NN,9)
477       CALL PLOT(R,P,PO,NN,11)
```

```
478
479 10000 FORMAT(//1H ,"R",13X,"BT",12X,"BP",12X,"RJT",12X,"RJP",12X,
480      1"T",12X,"N",12X,"V",12X,"PSI"/)
481 20000 FORMAT(1H ,9(E11.4,3X))
482
483 95     TTT=TTT+TT1
484        IF(TTT.GT.TMX)GOTO 1995
485
486 C...   EVALUATION OF PLASMA NUMBER DENSITY
487        DO 60 J=2,N
488        AA(J)=-XI(J-1)*H/R(J)
489        BB(J)=RLAM
490        CC(J)=XI(J+1)*H/R(J)
491        EE(J)=RLAM*RN(J)
492 60     CONTINUE
493        RN(1)=RN(2)
494        RN(N+1)=RN(N)
495        CALL DBLSWP(RN,N)
496        DO 61 J=1,N+1
497        IF (RN(J) .LT. RLOW) RN(J)=RLOW
498  61    CONTINUE
499
500 C...   EVALUATION OF POLOIDAL FIELD BP
501        DO 70 J=2,N
502        AA(J)=-V(J)*H*R(J-1)/R(J) - RMGDIF/R(J)*(RS1(J)+RS1(J-1))
503        BB(J)=RLAM+H*(V(J+1)-V(J-1)) + RMGDIF/R(J)*(RS1(J+1)+2.*RS1(J)
504       1+RS1(J-1))
505        CC(J)=V(J)*R(J+1)*H/R(J) - RMGDIF/R(J)*(RS1(J+1)+RS1(J))
506        EE(J)=BP(J)*RLAM
507 70     CONTINUE
508 C      BP(1)=BP1*EXP(-TTT/TBP1)
509        BP(1)=BP(2)
510 C      BP(N+1)=BPNN*EXP(-TTT/TBPNN)
511        BP(NN)=BP(N)
512        CALL DBLSWP(BP,N)
513
514 C...EVALUATION OF POLOIDAL FLUX FUNCTION PSI
515        DO 75 J=2,N
516        PSI(J)=PSI(J-1)+H*(R(J)*BP(J)+R(J-1)*BP(J-1))/2.
517  75    CONTINUE
518
519 C...   EVALUATION OF TOROIDAL FIELD BT
520        DO 80 J=2,N
521        AA(J)=-H*V(J)-RMGDIF*R(J-1)*(RS2(J)+RS2(J-1))
522        BB(J)=RLAM +H*(V(J+1)-V(J-1))+RMGDIF*R(J)*(RS2(J+1)+RS2(J-1)
523       1+2.*RS2(J))
524        CC(J)=H*V(J)-RMGDIF*R(J+1)*(RS2(J+1)+RS2(J))
525        EE(J)=RLAM*BT(J)
526 80     CONTINUE
527        BT(1)=BTIN*EXP(-TTT/TBT)
528        BT(N+1)=BTOUT*EXP(-TTT/TBT)
529        CALL DBLSWP(BT,N)
530        DO 84 J=1,NN
```

```
      CHI(J)=R(J)*BT(J)
 84   CONTINUE

C...  EVALUATION OF NEW CURRENTS
      DO 85 J=2,N
      RJT(J)=-(BP(J+1)-BP(J-1))/(H*2.)
      RJP(J)=(CHI(J+1)-CHI(J-1))/(2.*H*R(J))
      RO=(RN(J-1)+RN(J)+RN(J+1))/3.
      IF (RO .GT. .25) GO TO 85
      RJT(J)=0.
      RJP(J)=0.
 85   CONTINUE

C...  EVALUATION OF TEMPERATURE T
      DO 90 J=2,N
      RKGRAD=THDIF*(RK(J+1)-RK(J-1))/2./RN(J)
      AA(J)=-(R(J-1)+R(J))*THDIF*RK(J)/(RN(J)*R(J))-H*V(J)+RKGRAD
      BB(J)=RLAM+4.*THDIF*RK(J)/RN(J)+H*GAM*(XI(J+1)-XI(J-1))/R(J)
      CC(J)=H*V(J)-(R(J-1)+R(J))*THDIF*RK(J)/(RN(J)*R(J))-RKGRAD
      D6(J)=(RJP(J)**2+RJT(J)**2)*DELTA/(RN(J)*S(J))
     1-PR(1,J)/RN(J)-PR(2,J)/RN(J)
      EE(J)=RLAM*T(J)+2*D6(J)*H**2
90    CONTINUE
      CALL DBLSWP(T,N)
      GOTO 1
1995  CALL PLOTE
      CALL EXIT(2)
      END



C...THIS SUBROUTINE CONTAINS THE DOUBLESWEEP METHOD.


      SUBROUTINE DBLSWP(X,N)
      COMMON/C2/AA(101),BB(101),CC(101),EE(101)
      DIMENSION DSWL(101),DSWK(101),X(101)
      J=2
      IF(ABS(BB(2)).LT.1.E-20)GOTO 99
      DSWL(J)=-CC(J)/BB(J)
      DSWK(J)=(EE(J)-AA(J)*X(1))/BB(J)
      DO 10 J=3,N
      DEN=BB(J)+AA(J)*DSWL(J-1)
      IF(ABS(DEN).LT.1.E-20)GOTO 99
      DSWL(J)=-CC(J)/DEN
10    DSWK(J)=(EE(J)-AA(J)*DSWK(J-1))/DEN
      DO 20 J=N,2,-1
20    X(J)=DSWL(J)*X(J+1)+DSWK(J)
      GOTO 101
99    WRITE(12,100)J,BB(J)
100   FORMAT(1H ,"B(2) OR DEN IS LESS THAN 1.E-20",10X,
```

```
      1"J= ",I2,5X,/1H ,"THEREFORE THE DOUBLESWEEP METHOD IS ",
     2"NOT APPLICABLE"/8H BB(J)= ,E11.4)
101    RETURN
       END


C...THIS SUBROUTINE CONTAINS PLOTTING ROUTINES


       SUBROUTINE PLOT(R,A,A0,NN,J1)
       COMMON/PLT/P1(8),P5(12),P6(12),P7(12)
       COMMON/PL1/RL0,NB,TT1
       DIMENSION R(101),A(101)
       TIME9=NB*TT1
       AMX=A(1)
       AMN=A(1)
       DO 10 J=1,NN
       AMX=AMAX1(A(J),AMX)
       AMN=AMIN1(A(J),AMN)
10     CONTINUE
       AMX=1.01*AMX
       IF(AMN)1,2,2
1      AMN=AMN*1.01
       GOTO 3
2      AMN=AMN*.99
3      RR1=.99*R(1)
       RRN=1.01*R(NN)
       CALL MAP(0.,160.,0.,160.,0.,1.,0.,1.)
       CALL SETLCH(15.,75.,1,0,3,1)
       WOT 100,1000,P7(J1),P7(J1+1)
       CALL SETLCH(75.,148.,1,0,3,0)
       WOT 100,1001,P1(1),TIME9,P1(2)
       CALL SETLCH(70.,35.,1,0,3,0)
       WOT 100,1002,P1(3)
       CALL SETLCH(20.,28.,1,0,2,0)
       WOT 100,1003,P1(4),P1(5),NB
       WOT 100,1004,P1(6),P1(7),RL0,P1(8)
       WOT 100,1005,P5(J1),P5(J1+1),A0,P6(J1),P6(J1+1)
1000   FORMAT(2A8)
1001   FORMAT(A6,E8.2,A4)
1002   FORMAT(A6)
1003   FORMAT(A9,A4,I4)
1004   FORMAT(A6,A10,E8.1,A3)
1005   FORMAT(2A8,E8.1,2A6)
       CALL MAPS(RR1,RRN,AMN,AMX,.2,.9,.3,.85)
       CALL TRACE(R,A,NN)
       CALL FRAME
       RETURN
       END
```

```
637
638
639
640
641 C...THIS FILE CONTAINS THE NECESSARY INPUT DATA
642
643
644 *FILE NAME=DATA
645 83,
646 15.,
647 30.,
648 2.5E-8,
649 35.1E-6,
650 2.,
651 6.,
652 6.,
653 1.E6,
654 10.,
655 1.E3,
656 1.E15,
657 *CHATR I=DIF,LIB=('T','F'),X=CONTROL,D=SYMBOL,GO
```